



**HAL**  
open science

# Descriptors for deciphering the deactivation phenomena of vacuum distillate hydrocracking catalysts

July Carolina Vivas Baez

► **To cite this version:**

July Carolina Vivas Baez. Descriptors for deciphering the deactivation phenomena of vacuum distillate hydrocracking catalysts. Catalysis. Université de Lyon, 2021. English. NNT : 2021LYSE1079 . tel-03324233

**HAL Id: tel-03324233**

**<https://theses.hal.science/tel-03324233>**

Submitted on 23 Aug 2021

**HAL** is a multi-disciplinary open access archive for the deposit and dissemination of scientific research documents, whether they are published or not. The documents may come from teaching and research institutions in France or abroad, or from public or private research centers.

L'archive ouverte pluridisciplinaire **HAL**, est destinée au dépôt et à la diffusion de documents scientifiques de niveau recherche, publiés ou non, émanant des établissements d'enseignement et de recherche français ou étrangers, des laboratoires publics ou privés.



N°d'ordre NNT: 2021LYSE1079

## **THESE de DOCTORAT DE L'UNIVERSITE DE LYON**

opérée au sein de  
**l'Université Claude Bernard Lyon 1**

**Ecole Doctorale N° 206**  
**Ecole doctorale de Chimie de Lyon**

**Spécialité de doctorat** : Chimie  
**Discipline** : Catalyse

Soutenue publiquement le 06/05/2021, par:  
**July Carolina VIVAS BAEZ**

---

# **Descriptors for deciphering the deactivation phenomena of vacuum distillate hydrocracking catalysts**

---

Devant le jury composé de:

ANCHEYTA, Jorge  
PINARD, Ludovic  
ARMAROLI, Tiziana  
COPPENS, Marc-Olivier  
POUILLOUX, Yannick  
TAYAKOUT, Méla  
DUBREUIL, Anne-Claire  
PIRNGRUBER, Gerhard  
SERVIA, Alberto  
PEREZ MARTINEZ David

Professeur  
Maître de Conférences  
Responsable Industriel  
Professeur des Universités  
Professeur  
Professeur des Universités  
Ingénieure de recherche  
Chercheur  
Ingénieur de Recherche  
Ingénieur de Recherche

Mexican Petroleum Institute  
Université de Poitiers  
Eurecat France  
University College London  
Université de Poitiers  
Université Lyon 1  
IFPEN  
IFPEN  
IFPEN  
ECOPETROL

Rapporteur  
Rapporteur  
Examinatrice  
Examineur  
Examineur  
Examinatrice  
Examinatrice  
Directeur de thèse  
Invité  
Invité

# Université Claude Bernard – LYON 1

Président de l'Université	M. Frédéric FLEURY
Président du Conseil Académique	M. Hamda BEN HADID
Vice-Président du Conseil d'Administration	M. Didier REVEL
Vice-Président du Conseil des Etudes et de la Vie Universitaire	M. Philippe CHEVALLIER
Vice-Président de la Commission de Recherche	M. Jean-François MORNEX
Directeur Général des Services	M. Pierre ROLLAND

## COMPOSANTES SANTE

Département de Formation et Centre de Recherche en Biologie Humaine	Directrice : Mme Anne-Marie SCHOTT
Faculté d'Odontologie	Doyenne : Mme Dominique SEUX
Faculté de Médecine et Maïeutique Lyon Sud - Charles Mérieux	Doyenne : Mme Carole BURILLON
Faculté de Médecine Lyon-Est	Doyen : M. Gilles RODE
Institut des Sciences et Techniques de la Réadaptation (ISTR)	Directeur : M. Xavier PERROT
Institut des Sciences Pharmaceutiques et Biologiques (ISBP)	Directrice : Mme Christine VINCIGUERRA

## COMPOSANTES & DEPARTEMENTS DE SCIENCES & TECHNOLOGIE

Département Génie Electrique et des Procédés (GEP)	Directrice : Mme Rosaria FERRIGNO
Département Informatique	Directeur : M. Behzad SHARIAT
Département Mécanique	Directeur M. Marc BUFFAT
Ecole Supérieure de Chimie, Physique, Electronique (CPE Lyon)	Directeur : Gérard PIGNAULT
Institut de Science Financière et d'Assurances (ISFA)	Directeur : M. Nicolas LEBOISNE
Institut National du Professorat et de l'Education	Administrateur Provisoire : M. Pierre CHAREYRON
Institut Universitaire de Technologie de Lyon 1	Directeur : M. Christophe VITON
Observatoire de Lyon	Directrice : Mme Isabelle DANIEL
Polytechnique Lyon	Directeur : Emmanuel PERRIN
UFR Biosciences	Administratrice provisoire : Mme Kathrin GIESELER
UFR des Sciences et Techniques des Activités Physiques et Sportives (STAPS)	Directeur : M. Yannick VANPOULLE
UFR Faculté des Sciences	Directeur : M. Bruno ANDRIOLETTI

quienes son mi centro: Dios, Mi papá, mi linda  
mamita, mi manito, toda mi familia y mi motor  
y cómplice de sueños, Jhon. Ustedes me han  
enseñado las diferentes caras del amor.

Tengo a un país atravesado en la garganta, que no deja que me vaya acostumbrando a la distancia.

(Martha Gómez-Cantautora Colombiana)

Ces travaux de thèse ont été réalisés au sein de la Direction Expérimentation Procédés, Département Intensification de l'expérimentation d'IFP Energies Nouvelles (Solaize) en collaboration avec ECOPETROL Colombie. Je tiens à remercier le directeur Denis Guillaume, ainsi que le chef de département Hervé Cauffriez pour leur accueil au sein de son équipe et pour les moyens mis à disposition pour le bon déroulement de la thèse.

Je souhaiterais également remercier les membres du jury de thèse soient mes rapporteurs MM. Ludovic Pinard et Jorge Ancheyta, ainsi que Mmes. Tiziana Armaroli, Mélaz Tayakout, et MM. Marc-Olivier Coppens et Yannick Pouilloux.

Je tiens à exprimer ma plus profonde gratitude à mes superviseurs Gerhard, Alberto et Anne-Claire. Merci pour leur confiance et la grande liberté qu'ils m'ont laissée pour réaliser ce travail. Son esprit scientifique, ses conseils et sa disponibilité ont été essentiels à la bonne réalisation de cette thèse. Grâce à vous, je peux faire la transition parfois difficile entre le monde de l'ingénierie et celui des scientifiques.

Je remercie particulièrement Thierry-cito, Alain-cito, qui m'ont formé au fonctionnement de l'unité pilote et qui étaient là quand j'en avais besoin. Laëtitia Jacquet pour m'avoir appris les bases de la préparation et de l'analyse des catalyseurs ainsi que tant d'expressions populaires de la langue française. Michael Grenouiller et Cedric Nubois de m'avoir aidé lorsque je peinais avec mon unité. Amaury Donnette pour m'avoir fourni les résultats d'activité. Je dois également remercier l'équipe de Direction du R05, Jeremy Ponthus, Alexandra Berlioz-Barbier, Olivier Delpoux, Cedric Plassais, Marine Colluadin, Florian Reynaud, Cristophe Rouillet, Bertrand Fanget, Leslie Joguet, Romain Renaud, Anne-Lise Taleb et Carole Bobin pour toutes les analyses, mais surtout pour leur gentillesse et leur volonté de discuter des résultats. Je remercie tous les techniciens des départements R153 pour m'avoir accueilli avec chaleur durant ces trois ans. Ce fut un grand plaisir de travailler avec vous tous.

Au-delà de la bulle thésards/ex-thésards IFPEN et notamment les thésards R151 que je remercie tous, je pense particulièrement à Esther, Izabel, Larissa, Rick, Carmen et Santiago pour votre amitié et votre soutien. Un grand merci à la communauté hispanophone Juan, Raquel, María, Gabriel, Luis, David et Deisy pour tant de rires partagés.

Finalmente agradezco de todo corazón a mi familia por su diaria presencia tácita y por todas las celebraciones y juegos virtuales con que ese vínculo inquebrantable traspasó fronteras. A Jhon por siempre saltar conmigo y por ayudarme a develar sueños que eran desconocidos aun para mí misma.

## Descriptors for deciphering the deactivation phenomena of vacuum distillate hydrocracking catalysts.

This work aimed to understand the activity loss of a hydrocracking catalyst during the processing of vacuum gasoil (VGO) at typical operating conditions. First, a representative accelerated deactivation procedure was developed. Experiments were performed in an up-flow fixed-bed pilot plant unit with a VGO feed. The catalyst consisted of nickel-molybdenum sulfide dispersed on a USY zeolite carrier. The impact of operating conditions on catalyst deactivation rate was first studied. The variables with the strongest impact on conversion loss were temperature and space velocity. Based on these results, conditions for an accelerated (30 days) deactivation protocol were selected. The aged catalysts showed comparable properties to industrial spent catalysts. By this procedure, it was found that the organic nitrogen content of the feedstock is crucial since it determines the ratio between the available metal and acid sites. In turn, this ratio determines the coking reactions that take place and the type of coke produced. Subsequently, the impact of feedstock properties on deactivation was studied. Two real feeds from different origins were used. The experiments considered two times on stream (6 or 30 days) to assess the evolution of the catalyst as a function of time. Both the content and type of organic nitrogen and aromatics of the feedstock have a key role on the deactivation rate, even more than the end boiling point of the feed. The organic nitrogen dictates the ratio between available metal and acid sites. The aromatics generate coke precursors on the available acid sites. Both factors play a coupled role that promotes coke deposition on the catalyst surface, leading to an increase in the deactivation rate. Finally, the effect of the metal content on the deactivation rate was examined. Two bifunctional catalysts with different metal oxide contents were submitted to the accelerated deactivation conditions. It was found that in hydrocracking of feedstocks with high nitrogen content, the decrease of the metal content causes a lower deactivation rate.

**Keywords:** deactivation, hydrocracking, coking, nitrogen poisoning, vacuum gasoil.

## A la recherche des descripteurs pour la compréhension de la désactivation de catalyseurs d'hydrocraquage de distillats sous vide.

Ce travail visait à comprendre la perte d'activité d'un catalyseur d'hydrocraquage pendant le traitement de distillats sous vide (DSV) dans des conditions typiques d'opération. Les expériences ont été réalisées dans une unité pilote à lit fixe en flux ascendant. La charge injectée est un distillat sous vide. Le catalyseur est constitué de sulfure de nickel-molybdène dispersé sur un support zéolithique à base de zéolite USY. Dans un premier temps l'impact des conditions opératoires sur le taux de désactivation du catalyseur a été étudié. Les variables ayant l'impact le plus fort sur la perte de conversion sont la température et la vitesse spatiale horaire. Ces résultats ont permis de mettre au point un protocole de désactivation accélérée (30 jours), représentatif d'une désactivation à l'échelle industrielle. En effet, les catalyseurs vieillis selon ce protocole ont montré des propriétés comparables à celles de catalyseurs déchargés d'unités industrielles. Dans un deuxième temps, les phénomènes de désactivation ont été étudiés à l'aide du protocole de désactivation accélérée. La teneur en azote organique de la charge est cruciale puisqu'elle détermine le rapport entre les sites métalliques et acides disponibles pour les réactions. A son tour, ce rapport détermine les réactions de cokage qui ont lieu et la nature du coke produit. Ensuite, l'impact des propriétés de la charge sur la désactivation a été étudié, pour deux temps sous charge (6 et 30 jours). Deux charges réelles d'origine et de propriétés différentes ont été utilisées. La teneur et le type d'azote organique et d'aromatiques de la charge jouent un rôle clé, plus encore que son point d'ébullition final. L'azote organique impose le rapport entre les sites métalliques et acides disponibles. Les aromatiques génèrent des précurseurs de coke sur les sites acides disponibles. Ces deux facteurs jouent un rôle couplé qui favorise le dépôt de coke sur la surface du catalyseur, ce qui augmente le taux de désactivation. Enfin, l'effet de la teneur en métal du catalyseur sur le taux de désactivation a été examiné. Deux catalyseurs bifonctionnels avec différentes teneurs en oxyde métallique ont été soumis aux conditions de désactivation accélérée. Il a été constaté que lors de l'hydrocraquage de charges à forte teneur en azote, la diminution de la teneur en métal entraîne un taux de désactivation plus faible.

**Mots-clés:** désactivation, hydrocraquage, cokage, empoisonnement à l'azote, distillat sous vide.

## RESUME SUBSTANTIEL

Parmi les mesures prises par les raffineurs de pétrole pour répondre aux besoins du marché, l'hydrocraquage des distillats sous vide (DSV) est devenu le principal procédé de production de diesel, tout en répondant aux spécifications plus strictes sur les produits.

L'hydrocraquage des distillats sous vide est un procédé de raffinage qui consiste à convertir des produits lourds en distillats moyens (kérosène et diesel), via la rupture de liaisons carbone-carbone, accompagnée d'une hydrogénation simultanée ou séquentielle. Dans la plupart des procédés d'hydrocraquage, la charge est préalablement soumise à un hydrotraitement dans le même réacteur ou dans un réacteur différent. L'hydrocraquage utilise un catalyseur bifonctionnel, composé de nanoparticules de sulfure métallique (pour la fonction hydrogénante) déposées sur un support acide (pour la fonction d'isomérisation et de craquage). Ce catalyseur se désactive en continu en présence de charges d'hydrocarbures dans les conditions de fonctionnement typiques du procédé. La durée des cycles peut varier de quelques mois à un ou deux ans.

La compréhension des phénomènes de désactivation est fondamentale pour la conception de catalyseurs plus stables. Cependant, il existe peu de travaux de recherche sur la désactivation de catalyseurs d'hydrocraquage de DSV, encore moins en conditions réelles. Les différentes causes de désactivation sont néanmoins bien documentées dans la littérature pour ce type de charges, à savoir l'empoisonnement par des composés azotés et la formation de coke. L'objectif de ce travail est alors de dissocier le rôle individuel de chaque phénomène de désactivation, et déterminer l'impact de leur synergie sur la perte d'activité du catalyseur dans des conditions de fonctionnement représentatives. Le catalyseur étudié est constitué de particules de sulfure de nickel-molybdène dispersées sur un support zéolithique à base de zéolite USY. Les expériences ont été réalisées dans une unité pilote à lit fixe en flux ascendant, avec un distillat sous vide comme charge.

La première étape de la thèse a consisté en un criblage de variables opératoires: celles ayant le plus d'impact sur la désactivation sont la température et la vitesse spatiale horaire. La température accélère la formation des précurseurs de coke qui désactivent les catalyseurs par dépôt de carbone. La diminution du temps de séjour conduit à une diminution de la conversion des composés azotés et de l'hydrogénation des aromatiques, et donc à une augmentation de la concentration en ces précurseurs de coke (qui sont également des inhibiteurs). Ces résultats ont permis de mettre au point un protocole de désactivation accélérée (30 jours), et qualitativement représentatif d'une désactivation à l'échelle industrielle. En effet, les catalyseurs vieillis selon ce protocole présentent des propriétés texturales, des quantités et natures de coke ainsi que des activités résiduelles comparables à celles des catalyseurs déchargés d'unités industrielles.

Dans la deuxième partie de cette thèse, ce protocole de désactivation accélérée est utilisé pour évaluer de manière représentative, rapide et approfondie les phénomènes de désactivation des catalyseurs d'hydrocraquage des DSV. Les sites acides (assurant les fonctions isomérisante et craquante) présentent une perte d'activité beaucoup plus importante que les sites métalliques (assurant la fonction hydrogénante). La désactivation des sites acides est provoquée par l'adsorption des composés organiques azotés de la charge (en raison de leur caractère basique). Cette inhibition initiale se transforme en une désactivation irréversible car ces composés organiques azotés, restant adsorbés sur la surface du catalyseur dans un premier temps, conduisent à la formation de coke avant d'être désorbés dans un deuxième temps. Au contraire, ces composés organiques azotés n'ont qu'un effet inhibiteur sur la fonction hydrogénante et la désactivation permanente de la fonction métallique provient principalement de la dépromotion des feuilletts de sulfure de molybdène. Ainsi, la teneur de la charge en ces composés organiques azotés est un facteur clé puisqu'il détermine le rapport entre les sites métalliques et acides disponibles pour les réactions, ce qui oriente les réactions de cokage et la nature du coke formé.

L'effet des propriétés de la charge sur la désactivation a été étudié à l'aide de deux charges réelles d'origines différentes, un DSV hydrotraité, et un mélange hydrotraité plus léger à base de DSV, de gazole de cokéfaction (HCGO-Heavy coker gasoil) et de gazole de craquage catalytique (LCO-Light cycle oil), présentant une concentration en aromatiques plus élevée et une teneur en azote plus faible. Contrairement à ce qu'on attendrait d'après son poids moléculaire et sa plage de températures d'ébullition, cette deuxième charge est la plus désactivante; sa plus faible teneur en azote et sa forte teneur en aromatiques conduit à un déséquilibre plus important du rapport entre les sites métalliques et acides accessibles aux réactions et à une hydrogénation plus faible des espèces insaturées, précurseurs de coke, produites sur les sites acides, qui subissent des réactions de polymérisation et de condensation conduisant à la formation de coke à la surface du catalyseur. La nature des composés organiques azotés est aussi un facteur clé; les composés azotés les plus réfractaires à la déazotation, comme le carbazole, le benzocarbazole ou l'acridine ainsi que les composés azotés de haut poids moléculaire et de degré de substitution élevé, sont les plus désactivants. En ce qui concerne les aromatiques, plus les structures aromatiques sont condensées, plus la formation de coke à la surface du catalyseur est élevée.

Nous constatons que la teneur et la nature du coke évoluent le long du lit catalytique. En effet, le rapport entre les sites métalliques et acides disponibles pour les réactions diminue entre l'entrée et la sortie du lit catalytique (en raison d'une concentration en azote moindre et donc d'une inhibition/désactivation moindre), ce qui conduit à une quantité de coke plus élevée, présentant une structure plus aromatique, en sortie du lit catalytique. La composition élémentaire du coke, en termes de rapport N/C, suggère aussi que le rôle des composés aromatiques dans la formation du coke devient plus important vers la sortie du lit catalytique.

En outre, la désactivation du catalyseur évolue avec le temps, avec une désactivation rapide pendant les premiers jours de fonctionnement qui s'atténue ensuite. Ce comportement suit l'évolution classique du dépôt de coke, qui est principalement produit au début des essais. L'aromaticité du coke augmente

également avec le vieillissement du catalyseur car, lorsque les réactions de formation du coke progressent, une déshydrogénation se produit. Enfin, l'activité résiduelle du catalyseur vieilli dans des réactions modèles d'hydrogénation du toluène et d'hydroconversion du n-heptane, permet d'accéder à la localisation du dépôt de coke. Sur les sites métalliques, le dépôt de coke se forme dès les premiers jours de fonctionnement et n'évolue plus ensuite. Au contraire, le dépôt de coke sur les sites acides semblent évoluer continuellement au cours du temps.

Enfin, l'effet de la teneur en métal du catalyseur sur le taux de désactivation a été examiné. Deux catalyseurs bifonctionnels avec différentes teneurs en oxyde métallique ont été soumis aux conditions de désactivation accélérée. Il a été constaté que lors de l'hydrocraquage de charges à forte concentration en azote, la diminution de la teneur en métal entraîne une augmentation substantielle des composés azotés dans le lit catalytique. Cette augmentation détermine la performance du catalyseur en réduisant significativement les sites acides disponibles. Il y a donc une augmentation du rapport entre les sites métalliques et les sites acides, ce qui a, pour conséquence, un dépôt de coke et un taux de désactivation plus faibles qu'avec le catalyseur avec une teneur en métal plus élevée.

En ce qui concerne les perspectives de ce travail, une meilleure compréhension du rôle des composés azotés pourrait être obtenue en utilisant des charges à plus faible teneur en azote. Dans cette étude, les mécanismes de désactivation ont été dominés par la forte teneur en azote, ce qui rend difficile le découplage de l'impact des précurseurs de coke aromatique sur la désactivation. Il pourrait également être judicieux de comparer la désactivation dans des conditions d'iso-conversion. Cela pourrait fournir une évaluation plus précise car le type de molécules auxquelles le catalyseur serait soumis serait similaire. En outre, la réalisation d'essais de désactivation en faisant varier de manière plus significative la teneur en composés azotés et aromatiques permettrait de mieux comprendre l'effet de ces propriétés de la charge sur la désactivation. Cela permettrait de concevoir un mécanisme plus spécifique de désactivation par ces composés. Il serait intéressant d'évaluer l'effet de la diminution de la taille des pores sur la désactivation. Cela renforcerait, a priori, la formation de

coke et la désactivation ultérieure. Enfin, toutes ces propositions devraient converger vers la construction d'un modèle de désactivation prédictive qui pourrait être intégré dans les modèles existants du procédé d'hydrocraquage afin d'orienter la conception des futures formulations catalytiques et d'optimiser le fonctionnement de l'installation industrielle en prolongeant la durée de vie du catalyseur.

GENERAL INTRODUCTION .....	1
CHAPTER 1-LITERATURE REVIEW .....	6
1. RESEARCH CONTEXT .....	6
2. THE HYDROCRACKING PROCESS .....	8
2.1. Generalities.....	8
2.2. Main process configurations [9,10,13] .....	12
2.3. Chemical reactions.....	13
2.3.1. Hydrodesulfurization reactions (HDS) .....	13
2.3.2. Hydrodenitrogenation reactions (HDN).....	15
2.3.3. Aromatics hydrogenation reactions (HDA).....	19
2.3.4. Hydrocracking reactions (HCK) .....	23
2.3.4.1. Types of isomerization and $\beta$ -scission mechanisms [9,11,51] .....	26
2.3.5. Kinetics Modeling .....	27
2.3.5.1. Hydrodesulfurization Reactions (HDS) .....	29
2.3.5.2. Hydrodenitrogenation Reactions (HDN) .....	29
2.3.5.3. Aromatics Hydrogenation Reactions (HDA).....	30
2.3.5.4. Hydrocracking Reactions (HCK).....	30
2.4. Hydrocracking Catalysts.....	32
2.4.1. (De)/Hydrogenation Function .....	32
2.4.2. Acid Function .....	36
2.4.3. The balance between metal and acid sites.....	37

## Table of Contents

---

2.4.4. The distance “intimacy” between metal and acid sites.....	41
3. HYDROCRACKING CATALYSTS DEACTIVATION.....	43
3.1. Main deactivation mechanisms.....	44
3.1.1. Catalyst Poisoning .....	45
3.1.1.1. Inhibition Vs. Poisoning .....	45
3.1.1.2. Nitrogen Poisoning.....	47
3.1.2. Deactivation by coke .....	50
3.1.3. Deactivation by modification of the active phase .....	53
3.2. Effect of different operating parameters on deactivation.....	58
3.2.1. Effect of operating conditions .....	58
3.2.2. Effect of feedstock on deactivation.....	61
3.3. Approaches for catalyst deactivation study.....	62
4. LITERATURE REVIEW CONCLUSION .....	65
CHAPTER 2-INSIGHTS IN THE PHENOMENA INVOLVED IN DEACTIVATION OF INDUSTRIAL HYDROCRACKING CATALYSTS THROUGH AN ACCELERATED DEACTIVATION PROTOCOL.....	69
1. INTRODUCTION.....	70
2. EXPERIMENTAL SECTION.....	75
2.1. Pilot unit description and operating procedure.....	75
2.1.1. Pilot unit description .....	75
2.1.2. Procedure for the pilot plant experiments .....	77
2.1.3. Verification of Isothermal and plug-flow behavior .....	78

## Table of Contents

---

2.1.4.	Pilot unit validation .....	80
2.2.	Materials .....	81
2.2.1.	Feed Oil .....	81
2.2.2.	Catalysts .....	82
2.3.	Methods .....	83
2.3.1.	Screening of operating variables .....	83
2.3.2.	Accelerated deactivation protocol.....	84
2.3.3.	Catalyst loading and unloading procedures.....	84
2.3.4.	Catalyst characterization .....	85
2.4.	Data interpretation: kinetic laws, deactivation parameter and hydrogen consumption .	88
3.	RESULTS.....	91
3.1.	Variables screening experiment .....	91
3.1.1.	Evolution of the reaction rate coefficients with time for the whole system .....	94
3.1.1.1.	Reactivity .....	96
3.1.2.	Deactivation .....	97
3.1.3.	Evolution of the reaction rate coefficients with time for the first reactor.....	100
3.1.3.1.	Reactivity .....	100
3.1.3.2.	Deactivation .....	100
3.2.	Accelerated deactivation protocol.....	102
3.2.1.	Evolution of net conversion and reaction rate coefficients over time.....	102
3.2.2.	Spent catalysts characterization.....	104

## Table of Contents

---

3.2.2.1.	Elemental analysis .....	104
3.2.2.2.	Textural analysis .....	105
3.2.2.3.	TGA analysis.....	107
3.2.2.4.	Raman analysis.....	108
3.2.2.5.	TEM/EDX analysis .....	109
3.2.2.6.	Model molecule experiments.....	110
4.	RESULTS DISCUSSION.....	113
5.	CONCLUSIONS.....	116
CHAPTER 3-IMPACT OF FEEDSTOCK PROPERTIES ON THE DEACTIVATION OF A VACUUM GASOIL HYDROCRACKING CATALYST.....		120
1.	INTRODUCTION.....	121
2.	EXPERIMENTAL SECTION.....	125
2.1.	Feedstocks.....	125
2.2.	Catalyst.....	129
2.3.	Experimental set-up .....	129
2.4.	Experimental procedure .....	130
2.5.	Data interpretation: kinetic laws, deactivation parameter and hydrogen consumption	130
2.6.	Samples Characterization .....	133
3.	RESULTS.....	134
3.1.	Reaction rate coefficients .....	134
3.2.	Hydrogen consumption .....	141
3.3.	Activity loss rate coefficients.....	142

## Table of Contents

---

4. DISCUSSION.....	150
4.1. Evolution with time .....	150
4.2. Impact of the feed .....	153
5. CONCLUSIONS.....	157
CHAPTER 4-IMPACT OF METAL CONTENT ON THE DEACTIVATION OF A BIFUNCTIONAL HYDROCRACKING CATALYST .....	160
1. INTRODUCTION.....	160
2. CATALYST PREPARATION AND CATALYTIC TESTS WITH MODEL MOLECULES.....	160
2.1. Catalyst preparation .....	160
2.2. Model molecules tests for fresh catalysts with different MoO <sub>3</sub> contents. ....	161
3. DEACTIVATION EXPERIMENTS WITH CATALYSTS AT DIFFERENT METAL CONTENTS. ....	164
3.1. Evolution of the reaction rate coefficients with time on stream.....	165
3.1.1. Activity loss rate coefficients.....	168
3.2. Spent catalysts characterization.....	169
3.2.1. Elemental analysis .....	169
3.2.2. Textural Analysis.....	172
3.2.3. Thermo-gravimetric Analysis .....	173
3.2.4. Model molecule tests.....	175
4. DISCUSSION.....	178
5. CONCLUSIONS.....	182
GENERAL CONCLUSIONS AND PERSPECTIVES.....	185

## Table of Contents

---

• References.....	191
APPENDICES.....	218

# Table of Figures

FIGURE 1. SIMPLIFIED FLOW DIAGRAM OF A REFINERY.....	7
FIGURE 2. GENERAL FLOW DIAGRAM OF A HYDROCRACKING UNIT. (SINGLE STAGE WITH RECYCLE).....	10
FIGURE 3. THIOPHENE REACTION PATHWAYS.....	14
FIGURE 4. SUGGESTED REACTION NETWORK FOR THE HDS REACTION OF DIBENZOTHIOPHENE; A) HYDROGENATION STEPS; B) C-S BOND- BREAKING STEPS.....	15
FIGURE 5. EXAMPLES OF BOTH FAMILIES OF NITROGEN COMPOUNDS IN PETROLEUM FRACTIONS.....	16
FIGURE 6. REACTIVITY OF NITROGEN COMPOUNDS ACCORDING TO THE WORK OF SCHULZ ET AL.....	17
FIGURE 7. PROPOSED QUINOLINE HDN-REACTION NETWORK.....	19
FIGURE 8. REACTION NETWORKS FOR BENZENE AND BIPHENYL. THE NUMBERS OVER THE ARROWS ARE PSEUDO-FIRST-ORDER RATE CONSTANTS IN L/S*G OF CATALYST AT 325°C.....	21
FIGURE 9. REACTION NETWORKS FOR NAPHTHALENE HYDROGENATION AND 2-PHENYL-NAPHTHALENE. THE NUMBERS OVER THE ARROWS ARE PSEUDO-FIRST-ORDER RATE CONSTANTS IN L/S*G OF CATALYST AT 325°C.....	22
FIGURE 10. REACTION PATHWAY FOR ANTHRACENE HYDROGENATION AND HYDROCRACKING.....	23
FIGURE 11. CLASSICAL MECHANISM OF ISOMERIZATION AND HYDROCRACKING OF AN N-ALKANE ON A BIFUNCTIONAL CATALYST.....	25
FIGURE 12. SKELETAL ISOMERIZATION MECHANISMS.....	26
FIGURE 13. B-SCISSION MECHANISMS.....	27
FIGURE 14. INITIAL SELECTIVITY FOR HYDROGENOLYSIS, CRACKING AND ISOMERIZATION REACTIONS AS A FUNCTION OF THE Ni/(Ni+Mo) ATOMIC RATIO OF THE NiMo/USY CATALYST IN N-HEPTANE HYDROCRACKING.....	33
FIGURE 15. SCHEMATIC DRAWING SHOWING Co(Ni)-Mo-S AND OTHER Co(Ni) SULFIDE STRUCTURES ON ALUMINA AND Co(Ni) IN THE ALUMINA.....	34
FIGURE 16. STM IMAGES OF Co-Mo-S (A), MoS <sub>2</sub> (C), Ni-Mo-S (D) AND BALL MODEL OF SINGLE LAYER Co-Mo-S (B) ADAPTED FROM REFERENCES.....	35
FIGURE 17. ORGANIZATION OF Si AND Al TETRAHEDRA IN ZEOLITES NETWORK. Si, Al, O, AND Na <sup>+</sup> ATOMS ARE INDICATED IN THE FIGURE . .....	37
FIGURE 18. HYDROISOMERISATION AND HYDROCRACKING OF N-DECANE OVER PTHFAU CATALYSTS. REACTION SCHEME FOR (A) A LOW VALUE OF THE HYDROGENATION/ACID BALANCE ( $C_{PT}/C_A < 0.03$ ); (B) A HIGH VALUE OF THIS BALANCE ( $C_{PT}/C_A \geq 0.17$ ). .....	39

# Table of Figures

FIGURE 19. TYPICAL CATALYST DEACTIVATION CURVES AND OPERATING CYCLE LIMITS OF HYDROPROCESSING APPLICATIONS .....	44
FIGURE 20. ACTIVITY TIME PROFILES FOR (A) REVERSIBLE AND (B) IRREVERSIBLE POISONING .....	46
FIGURE 21. PROPOSED MECHANISM OF COKE FORMATION BY CONDENSATION REACTIONS.....	51
FIGURE 22. MECHANISM OF POLYMERIZATION INVOLVING CARBOCATIONS.....	52
FIGURE 23. THE CONCENTRATION OF COKE DEPOSITED ON EACH CATALYTIC FUNCTION AS A FUNCTION OF TIME IN COMMERCIAL OPERATION .....	53
FIGURE 24. SULFIDED CATALYST LIFE CYCLE .....	54
FIGURE 25. EFFECT OF TEMPERATURE ON COKE DEPOSITION (VGO, CoMo/Al <sub>2</sub> O <sub>3</sub> ) .....	58
FIGURE 26. EFFECT OF TEMPERATURE ON CATALYST COKE .....	59
FIGURE 27. CATALYST CARBON CONTENT AS A FUNCTION OF HYDROGEN PRESSURE (NiMo/Al <sub>2</sub> O <sub>3</sub> , 430°C). .....	61
FIGURE 28. EFFECT OF THE FEED CONTENT OF PNA ON THE AMOUNT OF COKE ON THE CATALYST . .....	62
FIGURE 29. PILOT UNIT FLOW DIAGRAM. ....	77
FIGURE 30. THERMAL PROFILES OF THE FIRST AND SECOND REACTORS .....	79
FIGURE 31. THE SEQUENCE OF CHANGES MADE DURING THE SCREENING OF THE OPERATING CONDITIONS. ....	93
FIGURE 32. NET CONVERSION AS A FUNCTION OF TIME ON STREAM, AT THE DIFFERENT OPERATING CONDITIONS SPECIFIED IN TABLE 6....	93
FIGURE 33. EFFECT OF NITROGEN CONTENT IN THE FEEDSTOCK. GLOBAL NET CONVERSION EVOLUTION WITH TIME ON STREAM AND NITROGEN CONTENT AT THE OUTLET OF THE REACTORS AT THE END OF THE EXPERIMENT.....	94
FIGURE 34. REACTION RATE COEFFICIENTS A) FOR CRACKING REACTIONS, B) FOR HYDRODENITROGENATION REACTIONS, C) FOR AROMATICS HYDROGENATION REACTIONS, D) FOR HYDRODESULFURIZATION REACTIONS AT REFERENCE CONDITIONS AND FOR EACH VARIABLE CHANGE SPECIFIED IN TABLE 6.....	95
FIGURE 35. CORRELATION BETWEEN HYDRODENITROGENATION AND CRACKING REACTION RATE COEFFICIENTS. ....	96
FIGURE 36. REACTION RATE COEFFICIENTS OF A) CRACKING REACTIONS B) HDN REACTIONS AT REFERENCE CONDITIONS BEFORE AND AFTER EACH VARIABLE CHANGE. FULL SYMBOLS=WHOLE REACTOR SYSTEM, OPEN SYMBOLS=FIRST REACTOR.....	101
FIGURE 37. EVOLUTION OF THE GLOBAL AND FIRST REACTOR NET CONVERSION WITH TIME ON STREAM WITH THE ACCELERATED DEACTIVATION PROTOCOL (T=418°C, P=14 MPa, LHSV=3H-1, H <sub>2</sub> /HC= 1500 NL/L). FULL SYMBOLS=TOTAL EFFLUENT, OPEN SYMBOLS=FIRST REACTOR EFFLUENT. ....	103

## Table of Figures

FIGURE 38. EVOLUTION OF REACTION RATE COEFFICIENTS WITH TIME ON STREAM DURING THE DEACTIVATION TEST, A) FOR CRACKING REACTIONS, B) FOR HYDRODENITROGENATION REACTIONS. FULL SYMBOLS=WHOLE REACTOR SYSTEM, OPEN SYMBOLS=FIRST REACTOR.....	104
FIGURE 39. CATALYST PORE DISTRIBUTION (NITROGEN DESORPTION ISOTHERM). .....	106
FIGURE 40. TGA PROFILES OF BED INLET AND BED OUTLET SAMPLES FROM THE DEACTIVATION TEST.....	107
FIGURE 41. RAMAN SPECTRA OF SPENT CATALYSTS FROM THE REFERENCE TEST, THE DEACTIVATION TEST AND INDUSTRIAL CYCLES.....	109
FIGURE 42. CATALYTIC ACTIVITY EVALUATED BY MODEL MOLECULES CATALYTIC TESTS FOR THE REFERENCE AND THE DEACTIVATION TESTS SAMPLES AND SOME SPENT INDUSTRIAL CATALYSTS. A) HYDROGENATION OF TOLUENE, B) ISOMERIZATION/CRACKING OF N-HEPTANE AT 360°C. ....	111
FIGURE 43. N-HEPTANE HYDROCONVERSION EXPERIMENT. SELECTIVITY TO I-C <sub>7</sub> VS. CONVERSION N-C <sub>7</sub> . ....	113
FIGURE 44. CUT YIELDS FOR FEEDSTOCKS A AND B. ....	126
FIGURE 45. AROMATICS TYPE OF FEED A AND B.....	127
FIGURE 46. CONCENTRATION OF REPRESENTATIVE FAMILIES BY DBE IN (A) BASIC AND (B) NEUTRAL NITROGEN, DETERMINED BY FT-ICR/MS ANALYSIS FOR BOTH FEEDS. ....	128
FIGURE 47. CARBON NUMBER DISTRIBUTION CURVES OF THE TOTAL NITROGEN CONTENT IN THE FEEDS BY FT-ICR/MS ANALYSIS. ....	129
FIGURE 48. NET CONVERSION EVOLUTION WITH TIME ON STREAM DURING LONG TESTS WITH FEED A AND FEED B. FULL SYMBOLS=TOTAL EFFLUENT, OPEN SYMBOLS=FIRST REACTOR EFFLUENT.....	134
FIGURE 49. SIMULATED DISTILLATION CURVE OBTAINED FOR THE FEED, FIRST REACTOR OUTLET, SECOND REACTOR OUTLET WITH A) FEED A, B) FEED B FOR THE LONG-TERM TESTS. DOTTED LINE=FIRST REACTOR EFFLUENT, CONTINUOUS LINE=TOTAL EFFLUENT. ....	136
FIGURE 50. GLOBAL AND FIRST REACTOR REACTION RATE COEFFICIENTS EVOLUTION WITH TIME ON STREAM FOR CRACKING REACTIONS. A) FEED A AND B) FEED B. OPEN SYMBOLS=FIRST REACTOR EFFLUENT, FULL SYMBOLS=TOTAL EFFLUENT. ....	138
FIGURE 51. GLOBAL AND FIRST REACTOR REACTION RATE COEFFICIENTS EVOLUTION WITH TIME ON STREAM FOR HDN REACTIONS. A) FEED A AND B) FEED B. OPEN SYMBOLS=FIRST REACTOR EFFLUENT, FULL SYMBOLS=TOTAL EFFLUENT.....	139
FIGURE 52. GLOBAL AND FIRST REACTOR REACTION RATE COEFFICIENTS EVOLUTION WITH TIME ON STREAM FOR HDS REACTIONS. OPEN SYMBOLS=FIRST REACTOR EFFLUENT, FULL SYMBOLS=TOTAL EFFLUENT.....	140

## Table of Figures

---

FIGURE 53. GLOBAL AND FIRST REACTOR REACTION RATE COEFFICIENTS EVOLUTION WITH TIME ON STREAM FOR HDA REACTIONS. OPEN SYMBOLS=FIRST REACTOR EFFLUENT, FULL SYMBOLS=TOTAL EFFLUENT.....	140
FIGURE 54. CARBON CONTENT OF THE SPENT CATALYSTS. SAMPLES TAKEN AT DIFFERENT REACTOR LOCATIONS. FULL BARS=30 DAYS TESTS, OPEN BARS=6 DAYS TESTS. ....	144
FIGURE 55. HYDROGEN/CARBON RATIO OF THE SPENT CATALYSTS. SAMPLES TAKEN AT DIFFERENT REACTOR LOCATIONS. FULL BARS=30 DAYS TESTS, OPEN BARS= 6 DAYS TESTS.....	144
FIGURE 56. N/C RATIO OF THE SPENT CATALYSTS. SAMPLES TAKEN AT DIFFERENT REACTOR LOCATIONS. FULL BARS=30 DAYS TESTS, OPEN BARS= 6 DAYS TESTS. ....	145
FIGURE 57. RESIDUAL CATALYTIC ACTIVITY EVALUATED BY MODEL MOLECULES CATALYTIC TESTS A) HYDROGENATION OF TOLUENE, B) ISOMERIZATION/CRACKING OF N-HEPTANE AT 360°C. SAMPLES TAKEN AT DIFFERENT REACTOR LOCATIONS. FULL BARS=30 DAYS TESTS, OPEN BARS= 6 DAYS TESTS. ....	149
FIGURE 58. TEST N-HEPTANE. SELECTIVITY TO I-C <sub>7</sub> Vs. CONVERSION N-C <sub>7</sub> . OPEN SYMBOLS= 6 DAYS TESTS, FULL SYMBOLS=30 DAYS TESTS. ....	150
FIGURE 59. RELATION BETWEEN THE A) HYDROGENATION ACTIVITY AND B) N-C <sub>7</sub> CRACKING ACTIVITY OF THE SPENT CATALYSTS AND THE AMOUNT OF COKE. ....	153
FIGURE 60. CATALYTIC ACTIVITIES EVALUATED BY MODEL MOLECULES CATALYTIC TESTS FOR FRESH DRIED CATALYST SAMPLES WITH DIFFERENT MOO <sub>3</sub> CONTENTS A) HYDROGENATION OF TOLUENE IN THE PRESENCE OF ANILINE, B) ISOMERIZATION/CRACKING OF N-HEPTANE AT 360°C. ....	162
FIGURE 61. SELECTIVITY TO I-C <sub>7</sub> Vs. CONVERSION N-C <sub>7</sub> FOR FRESH DRIED CATALYST SAMPLES WITH DIFFERENT MOO <sub>3</sub> CONTENTS.....	163
FIGURE 62. NET CONVERSION EVOLUTION WITH TIME ON STREAM FOR CATALYSTS WITH DIFFERENT METAL CONTENTS. OPEN SYMBOLS=FIRST REACTOR EFFLUENT, FULL SYMBOLS=TOTAL EFFLUENT.....	165
FIGURE 63. GLOBAL AND FIRST REACTOR REACTION RATE COEFFICIENTS EVOLUTION WITH TIME ON STREAM FOR CRACKING REACTIONS FOR CATALYSTS WITH DIFFERENT METAL CONTENTS. OPEN SYMBOLS=FIRST REACTOR EFFLUENT, FULL SYMBOLS=TOTAL EFFLUENT. ....	167
FIGURE 64. GLOBAL AND FIRST REACTOR REACTION RATE COEFFICIENTS EVOLUTION WITH TIME ON STREAM FOR HDN REACTIONS FOR CATALYSTS WITH DIFFERENT METAL CONTENTS. OPEN SYMBOLS=FIRST REACTOR EFFLUENT, FULL SYMBOLS=TOTAL EFFLUENT. ....	167

## Table of Figures

---

FIGURE 65. GLOBAL REACTOR REACTION RATE COEFFICIENTS EVOLUTION WITH TIME ON STREAM FOR HDA REACTIONS FOR CATALYSTS WITH DIFFERENT METAL CONTENTS. ....	168
FIGURE 66. CARBON CONTENTS OF THE SPENT CATALYSTS WITH DIFFERENT METAL CONTENTS. SAMPLES TAKEN AT DIFFERENT REACTOR LOCATIONS. ....	170
FIGURE 67. N/C RATIO OF THE SPENT CATALYSTS WITH DIFFERENT METAL CONTENTS. SAMPLES TAKEN AT DIFFERENT REACTOR LOCATIONS. ....	170
FIGURE 68. NITROGEN CONTENT OF THE SPENT CATALYSTS WITH DIFFERENT METAL CONTENT. SAMPLES TAKEN AT DIFFERENT REACTOR LOCATIONS. ....	171
FIGURE 69. HYDROGEN/CARBON RATIO OF THE SPENT CATALYSTS WITH DIFFERENT METAL CONTENT. SAMPLES TAKEN AT DIFFERENT REACTOR LOCATIONS. ....	172
FIGURE 70. TGA PROFILES OF BED INLET AND BED OUTLET SAMPLES FROM THE SPENT CATALYST WITH DIFFERENT METAL CONTENT. DOTTED LINE=FIRST REACTOR EFFLUENT, CONTINUOUS LINE=TOTAL EFFLUENT. ....	174
FIGURE 71. RESIDUAL CATALYTIC HYDROGENATION ACTIVITY OF THE SPENT CATALYSTS RELATIVE TO THE FRESH CATALYSTS, EVALUATED BY TOLUENE HYDROGENATION. SAMPLES TAKEN AT DIFFERENT REACTOR LOCATIONS. ....	176
FIGURE 72. RESIDUAL CATALYTIC HYDROGENATION ACTIVITY OF THE SPENT CATALYSTS RELATIVE TO THE FRESH CATALYST, EVALUATED BY ISOMERIZATION/CRACKING OF N-HEPTANE AT 360°C. SAMPLES TAKEN AT DIFFERENT REACTOR LOCATIONS. ....	177
FIGURE 73. SELECTIVITY TO I-C <sub>7</sub> VS. CONVERSION N-C <sub>7</sub> , OBTAINED BY N-HEPTANE HYDROCONVERSION AT DIFFERENT TEMPERATURES. .	178

# Table of Tables

TABLE 1. VGO AVERAGE COMPOSITION FOR DIFFERENT SOURCES [11].....	11
TABLE 2. PARAMETERS IDEAL BEHAVIOR FBR .....	79
TABLE 3. FEEDSTOCK PROPERTIES FOR THE REFERENCE TEST.....	80
TABLE 4. OPERATING CONDITIONS OF THE REFERENCE TEST. ....	81
TABLE 5. FEEDSTOCK PROPERTIES FOR THE DEACTIVATION EXPERIMENTS.....	81
TABLE 6. OPERATING CONDITIONS FOR THE VARIABLES SCREENING EXPERIMENT. ....	83
TABLE 7. OPERATING CONDITIONS OF THE CATALYTIC TESTS WITH MODEL MOLECULES.....	88
TABLE 8. IMPACT OF VARIABLES ON DEACTIVATION: EXTENT OF DEACTIVATION CAUSED BY EACH VARIABLE CHANGE.....	97
TABLE 9. IMPACT OF VARIABLES ON THE DEACTIVATION RATE FOR CRACKING REACTIONS. ....	99
TABLE 10. HYDROGEN CONSUMPTION AND REACTION RATE COEFFICIENTS FOR CRACKING REACTIONS. ....	100
TABLE 11. CHARACTERIZATION OF SPENT CATALYSTS: SURFACE AREA (S), TOTAL PORE VOLUME (V), MICROPORE VOLUME ( $\mu V$ ) AND HYSTERESIS AREA OF THE SPENT CATALYST RELATIVE TO THE FRESH CATALYST AND CARBON CONTENT OF THE SPENT CATALYSTS. ....	105
TABLE 12. ESTIMATION OF CO <sub>2</sub> MASS LOSS AND H/C RATIO OF THE COKE DEPOSIT FROM RATIO I18/I44 FROM TGA PROFILES FOR DIFFERENT SPENT CATALYSTS.....	108
TABLE 13. AVERAGE SLAB LENGTH AND DISPERSION MEASURED BY TEM AND Ni/MO RATIO IN MoS <sub>2</sub> PARTICLES MEASURED BY EDX. .	110
TABLE 14. FEEDSTOCKS PROPERTIES. ....	125
TABLE 15. SAMPLES PREPARATION CONDITIONS FOR FTC-IR-MS ANALYSIS. ....	133
TABLE 16. HYDROGEN CONSUMPTION AND APPARENT CRACKING REACTION RATE COEFFICIENT FOR BOTH TESTS AT DIFFERENT TIMES. ....	142
TABLE 17. DEACTIVATION COEFFICIENTS CALCULATED WITH AN EXPONENTIAL DECAY MODEL. ....	142
TABLE 18. CHARACTERIZATION OF SPENT CATALYST: SURFACE AREA (S) AND TOTAL PORE VOLUME (V) OF THE SPENT CATALYST RELATIVE TO THE FRESH CATALYST AND RATIO OF HYSTERESIS AREA (HA) OF THE SPENT CATALYST COMPARED TO THE FRESH CATALYST. ....	146
TABLE 19 AVERAGE STACKING SIZE AND DISPERSION MEASURED BY TEM AND Ni/MO RATIO IN MoS <sub>2</sub> PARTICLES MEASURED BY EDX. .	147
TABLE 20. ACTIVITY LOSS RATE COEFFICIENTS (A) AND RESIDUAL ACTIVITIES (c), CALCULATED WITH AN EXPONENTIAL DECAY MODEL FOR CATALYSTS WITH DIFFERENT METAL CONTENTS. ....	169
TABLE 21. CHARACTERIZATION OF SPENT CATALYSTS WITH DIFFERENT METAL CONTENTS: SURFACE AREA (S), TOTAL PORE VOLUME (V) AND THE RATIO OF HYSTERESIS AREA (HA) OF THE SPENT CATALYST RELATIVE TO THE FRESH CATALYST. ....	173

TABLE 22. ESTIMATION OF CO<sub>2</sub> MASS LOSS OF THE COKE DEPOSIT AND MAXIMUM PEAK TEMPERATURE FROM TGA PROFILES FOR SPENT

CATALYSTS WITH DIFFERENT METAL CONTENT ..... 175

## GENERAL INTRODUCTION

Nowadays, the oil refining industry faces significant challenges. The crude oil available is becoming heavier and heavier except for the United States and some parts of Europe. Even though diesel demand is declining in some places like Europe, demand growth remains strong in developing areas. Fuels quality, even bunker fuels, has increasingly stringent standards. For instance, in many regions, specifications for sulfur contents in gasoline and diesel of less than 50 ppm are not uncommon. The response of oil refiners to remain competitive includes technologies for eliminating barrel bottoms, increasing diesel production and fuel quality upgrading. The hydrocracking of vacuum gas oils (VGO) in fixed-bed reactors has emerged as the primary diesel producer in many refinery configurations and also is one of the tools to meet the new tightened product specifications.

Hydrocracking is a refining process for converting heavy, high-boiling feedstock molecules into smaller, lower-boiling products through carbon-carbon bond breaking, accompanied by simultaneous or sequential hydrogenation. Most hydrocracking processes use fixed bed down-flow reactors operating at high pressure, 8.5-20 MPa, and temperatures between 350-450°C, to promote hydrocracking reactions. Low values of LHSV, 0.5-2.5 h<sup>-1</sup> and hydrogen to oil ratio (H<sub>2</sub>/HC) ranging from 500-1700 NL/L are used, depending on feedstock complexity. In most hydrocracking processes, the feedstock is submitted to hydrotreating before hydrocracking in the same or different reactors. Hydrotreating is a pretreatment that partially hydrogenates unsaturated hydrocarbons and removes hetero atoms from the feedstock, which have a deleterious effect on the hydrocracking catalyst. Therefore, the initial reactions in the hydrocracking process are hydrodesulfurization (HDS), hydrodenitrogenation (HDN), hydrodeoxygenation (HDO), olefin hydrogenation, and partial aromatics hydrogenation (HDA).

## General Introduction

---

Subsequently, the hydrocracking reactions are carried out. This work focused on the deactivation phenomena related to hydrocracking catalysts.

Vacuum gasoil (VGO) hydrocracking employs bifunctional catalysts, hence composed of metal sulfide nanoparticles (de/hydrogenation function) deposited on an acidic support (isomerization and cracking function). This catalyst is continuously deactivated in the presence of hydrocarbon feedstocks under typical process operating conditions, which affects process cycle lengths. Cycle lengths can vary between a few months and up to one or two years. It is known that in the hydrocracking of vacuum gasoils (VGO), the formation of coke and quasi-irreversible poisoning by heavy nitrogen molecules are the primary reasons for catalyst deactivation. The coke formation is related to polymerization precursors like polynuclear aromatics and cyclic molecules containing heteroatoms. Hydrocracking catalysts lose metal sites due to sintering and de-promotion of the sulfide nanoparticles and coke deposition. In contrast, loss of acid sites is due to the strong adsorption (almost irreversible) of nitrogen compounds that can act as temporary poisons, as well as coke precursors.

Deactivation is a problem of great concern in industrial catalytic processes. The costs of catalyst replacement and process shutdown amount to billions of dollars per year. Catalyst deactivation is inevitable, but it can be slowed down. Understanding the deactivation phenomena is fundamental for the design of more stable catalysts. However, there are not many research works on bifunctional hydrocracking catalysts deactivation for vacuum gasoils, even more with real feedstocks. Therefore, this work aims to understand the loss of activity of a hydrocracking catalyst during the processing of VGO at representative operating conditions.

To accomplish this, an accelerated deactivation protocol for hydrocracking catalysts was developed to assess the deactivation phenomenon in a short period compared to the one related to the industrial unit. For developing this protocol, many variables can be set to favor the catalyst

deactivation. Hence, the first part of the thesis consisted of an operating conditions screening. This screening was carried out in a continuous pilot unit, with two sequential up-flow fixed bed reactors dedicated to study the hydrocracking reactions. The fresh catalyst consisted of nickel-molybdenum sulfide particles dispersed on a carrier containing USY zeolite and the feedstock was a hydrotreated VGO. The variables evaluated were temperature, space velocity, hydrogen/hydrocarbon ratio and organic nitrogen content. The goal was to determine the variables with the most significant impact on deactivation. This impact was determined by tracking the kinetic performance for the main hydrocracking reactions (Cracking, HDN, HDS y HDA) during time on stream.

Based on the variables screening results, the operating conditions for the accelerated protocol were defined. The qualitative validation of the protocol representativeness was determined after comparing the textural properties, amount and nature of coke deposits, and residual activity between the deactivated samples from the pilot unit and some industrial spent catalysts. Thus, all subsequent tests were carried out by following this experimental procedure to get more insight into the deactivation phenomena. In order to understand the impact on catalyst deactivation of the feedstock properties, i.e., the role of nitrogen and aromatic content and the boiling range, the catalyst was submitted to the accelerated deactivation protocol using two real feeds from different origins. Feed A consisted of a hydrotreated VGO, whereas Feed B was a lighter hydrotreated mixture containing heavy coker gasoil (HCGO) and light cycle oil (LCO) in addition to VGO (71%). Finally, the effect of the catalyst metal content on the deactivation rate was examined. Two bifunctional catalysts with different metal oxide contents were submitted to the accelerated deactivation conditions.

This report is divided into five parts. The first part (Chapter 1) consists of a brief literature review on the hydrocracking process, including the typical used catalysts and the main deactivation

## General Introduction

---

mechanisms during VGO hydrocracking. Chapters two and three are written as scientific publications, in which a specific bibliographic background is presented as an introduction to the subject addressed. Each chapter also provides details on the experimental methodology.

The second chapter emphasizes results obtained during the variables screening and the accelerated deactivation protocol development. Chapter three deals with the impact of the feedstock properties on catalyst deactivation. Chapter four covers the effect of the metal content on the deactivation of a bifunctional catalyst. Finally, a general conclusion is provided as an overview of the main results of this work. Some of the perspectives envisioned to continue this study are proposed.

# **CHAPTER 1**

# **Literature Review**

---

### CHAPTER 1-LITERATURE REVIEW

This literature review aims to assess what is known about the hydrocracking of vacuum gas oils and to synthesize the literature studies on the hydrocracking catalysts' deactivation phenomena.

The basic principles of hydrocracking, such as process generalities and related kinetics and catalysts, are first introduced. The literature works on the main deactivation mechanisms of hydrocracking catalysts are discussed secondly. Some of the strategies used to study the deactivation of hydroprocessing catalysts are included in this second section. A state-of-the-art conclusion, which contains the main objectives of this work, is presented at the end of the chapter.

#### 1. RESEARCH CONTEXT

Petroleum in the crude state is of limited value, and refining is required to produce products suitable for the market [1]. A refinery is essentially a group of manufacturing plants designed to produce fuels, for example, gasoline, jet fuel and diesel. To carry out this, the crude oil is subjected to a series of operations and processes [2]. A simplified flow diagram of a refinery operation is shown in Figure 1.

The refining industry has been subject to different drivers that have accelerated its development, as the increasing supply of lower quality, heavy oils [3] and more stringent environmental regulations (demand for clean and ultra-clean fuels) [4]. To handle these challenges, refinery technology had to undergo inevitable changes. It has led to a shift away from conventional means of refining heavy feedstocks using (typically) carbon rejection technologies (visbreaking, delayed coking) to more innovative processes, including hydrogen management, that produce the required liquid fuels from feedstock and keep emissions within the limits of environmental

legislation [4]. Thus, the industry is likely to be more involved in the deep conversion of heavy feedstocks, has higher hydrocracking and hydrotreating capacity, and uses more efficient processes. The hydrocracking process has emerged as the primary diesel producer in many refinery configurations. Hydrocrackers are one of the tools available to refiners to meet new product specifications, as environmental regulations on transportation fuels continue to tighten [5].

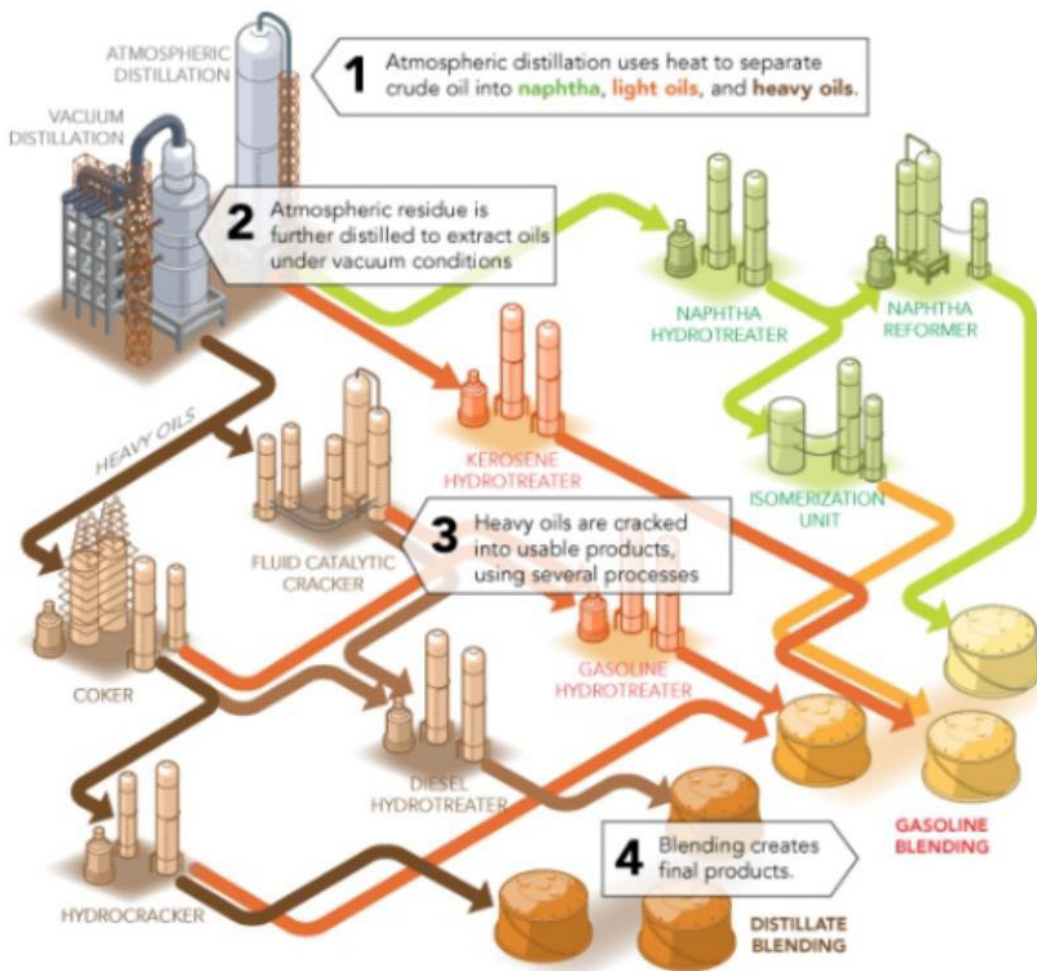


**Figure 1. simplified flow diagram of a refinery.**

<http://heatexchanger-design.com/2011/10/06/heat-exchangers-6/>

The VGO hydrocracking is a hydrogen treatment process; it is explained in detail in the next section. Unlike other processes where catalyst deactivation is slow, and therefore an industrial

cycle easily takes three to four years, the hydrocracking catalysts undergo a continuous deactivation, which, depending on the feedstock, can take from a few months up to two years [5–7]. After this, the catalyst must be replaced. Therefore, the deactivation of the catalyst plays an essential role in the operation and profitability of the industrial process. Although a lot of research on hydrocracking has been published, the study of deactivation phenomena with real feedstocks has not received much attention [8]. Therefore, this work aims to understand the loss of activity of a hydrocracking catalyst during the processing of vacuum gasoils at representative operating conditions.

## 2. THE HYDROCRACKING PROCESS

Extensive literature has been devoted to the study of the hydrocracking process. This section presents a brief overview of the main aspects of vacuum gasoil hydrocracking.

### 2.1. Generalities

Hydrocracking is a refining process for converting heavy, high-boiling feedstock molecules into smaller, lower-boiling products through carbon-carbon bond breaking, accompanied by simultaneous or sequential hydrogenation [9]. This process also has considerable flexibility because it allows the conversion of a wide range of feedstocks to a wide variety of products [9]. Hydrocracking processes are designed to upgrade petroleum feedstocks, such as straight run, vacuum and coker gasoils, deasphalted oils, fluid catalytic cracking cycle oils, straight run and cracked naphthas, by adding hydrogen and cracking to the desired boiling range [9]. Modern hydrocracking processes were initially developed for converting refractory feedstocks to gasoline and jet fuel [10]. Process and catalyst improvements have made it possible to yield products like liquefied petroleum gas (LPG), light and heavy naphtha, jet fuel, diesel, heating oil, petrochemical feedstocks, catalytic cracking feedstock, ethylene cracker feedstock, and lube oil

base stock [1]. In this work, the focus is on the hydrocracking of vacuum gasoils to produce middle distillates (Diesel and kerosene).

Industrial feedstocks treated in hydrocracking processes are complex mixtures of hydrocarbons and heterocompounds containing sulfur, nitrogen, or even metals such as nickel and vanadium in the case of residue feedstocks [9,10]. The hydrocracking process is carried out in two consecutive stages (Figure 2) due to the deleterious effect of the previously described compounds on hydrocracking catalysts: (i) in the first stage (hydrotreating), the feedstock is hydrotreated and partially hydrogenated on a hydrotreating catalyst. The main chemical reactions for hydrotreating and hydrogenating the feedstock are hydrodesulfurization (HDS), hydrodenitrogenation (HDN), hydrodeoxygenation (HDO), olefin hydrogenation and partial aromatics hydrogenation(HDA). (ii) in the second stage (hydrocracking), the hydrotreated feed is hydrocracked (HCK) on a hydrocracking catalyst [9,11]. The hydrocracking unit can be configured in several ways to carry out the mentioned stages; it is discussed in section 2.2. This work focuses on the deactivation phenomena of hydrocracking catalysts.

The fixed-bed reactor technology is preferred for the hydrocracking process due to its low capital cost and easy operation. These reactors are operated in the down-flow mode to limit the operating costs related to hydrogen compression. Most hydrocracking reactors are operated at high pressure, 8.5-20 MPa and moderate temperature, 350-450°C, to promote hydrocracking reactions. A large excess of hydrogen, 500-1700 NL/L hydrogen to oil ratio ( $H_2/HC$ ), is fed to the reactor to improve liquid yield and limit catalyst deactivation. Low values of LHSV, 0.5-2.5  $h^{-1}$ , are required depending on feed nature and complexity [11,12].

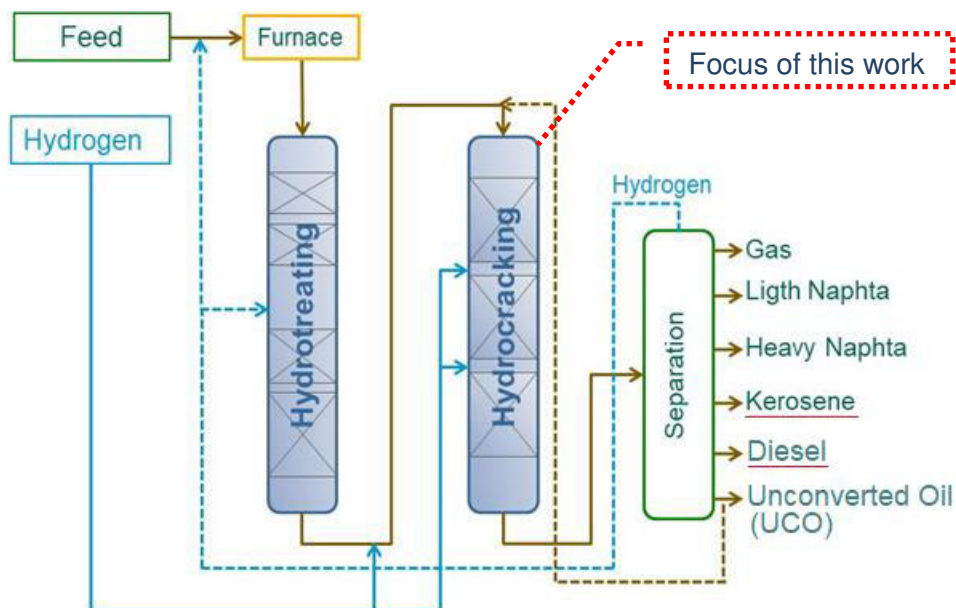


**Figure 2. General flow diagram of a hydrocracking unit. (Single stage with recycle).**

The most common feedstocks treated in hydrocracking are straight-run vacuum gasoils (SR-VGO's). However, a wide variety of feeds coming from different sources can be processed [11], such as:

- Crude oils from different geographic origins after distillation.
- A mix of vacuum gas oils (VGO) from the vacuum distillation with other VGO's from a different process like coking, visbreaking, or hydroconversion. A mix with an HCGO (Heavy Coker Gas Oil) is often injected in the process.
- A mix of SR-VGO with deasphalted oil (DAO).
- 100 % of VGO coming from a conversion process such as coking, visbreaking, or hydroconversion in a fixed or ebullated bed.

The main characteristics of typical VGO's are shown in Table 1. Usually, the heavier the feedstock, the higher the asphaltenes content and consequently the higher the tendency to form coke. For that reason, limits are often set for these compounds, as well as that of metals, to

make a feedstock acceptable for hydrocracking. For VGO's obtained by direct distillation of crude oils, the content of harmful compounds such as nitrogen, sulfur and metals is lower than in the blends with streams from other processes dealing with heavy cuts, which may contain traces of these compounds. These compounds must be eliminated during the hydrotreatment to minimize catalyst poisoning.

**Table 1. VGO average composition for different sources [11].**

	Type		SR-VGO	VGO+Coker	VGO+DAO
<b>Overall analyses</b>	Density 15/4	g/cc	0.900-0.960	0.900-0.960	0.900-0.960
	Refractive Index at 70°C	-	1.48-1.53	1.48-1.53	1.48-1.53
	Distillation range	°C	380-550	380-550	380-700+
	Bromine number	wt %	-	10 - 200	100 – 600
	Molecular weight	g/mol	416	335	400
	Asphaltenes	ppmw	<100	<50	100-1000
	Resins	wt %	1.0-1.5	1.0-1.5	1.0-1.5
<b>Elemental Analyses</b>	Sulfur	wt %	0.1-2	1.5-5	1.5-5
	Nitrogen	ppmw	300-2000	1500-3500	1500-3500
	Basic nitrogen	ppmw	440	830.3	567
	Hydrogen	wt %	12.4	11.7	11.5
	Vanadium	ppmw	<0.5	0.5-2	>2
Nickel	ppmw	<0.5	0.5-2	>2	

Carbon type	Aromatic carbon	wt %	30-70	30-70	30-70
	Paraffinic carbon	wt %	30-60	30-60	30-60
	Naphtenic carbon	wt %	10-30	10-30	10-30

## 2.2. Main process configurations [9,10,13]

The hydrocracking unit can be configured in numerous ways, but there are two main categories: single-stage and two-stage. The simplest configuration consists of a single-stage with a single catalyst in one or two reactors in series. In the single-stage recycle configuration, the fresh feed combined with unconverted oil (UCO) goes down through the catalyst bed in the presence of hydrogen. The effluent from the reactor goes through high- and low-pressure separators, where hydrogen is recovered. The separated hydrogen, together with fresh makeup hydrogen, is recycled to the reactor. The liquid product is sent to fractionation, where the final products are separated from unconverted oil.

Another single-stage process configuration employs two catalysts in the same reactor or different serial reactors (Figure 2). In this case, the first catalyst is a hydrotreating catalyst that pretreats the feedstock to remove the hetero compounds and partially hydrogenate the aromatics. In this configuration, the products from the first reactor pass over a hydrocracking catalyst in the second reactor, where most hydrocracking occurs. Many of the units designed to maximize diesel products utilize this configuration.

A widely used hydrocracking process configuration is the two-stage process, which allows handling higher feed rates than the single-stage process. In the two-stage scheme, hydrotreatment and part of the hydrocracking occur in the first reactor; then, the effluent is separated, and the unconverted oil is fed to the second reactor. A typical two-stage configuration consists of three reactors. This configuration is widely used because it allows processing a wide

range of feeds. This work is centered on the section/reactor in which hydrocracking is carried out.

### 2.3. Chemical reactions

The reaction scheme related to the hydrocracking of petroleum fractions involves numerous compounds and a complex network of chemical reactions. Understanding how these reactions are carried out is fundamental to explain the possible changes in the progress of these reactions during catalyst deactivation.

Transformation of a petroleum vacuum distillate into naphtha, kerosene and diesel occurs according to different chemical reactions that can be grouped into two main classes [14]:

- Hydrotreating reactions: This set of reactions aims to remove unwanted heteroatoms such as sulfur (hydrodesulfurization, HDS), nitrogen (hydrodenitrogenation, HDN), oxygen (hydrodeoxygenation, HDO) and metals (hydrodemetalation, HDM), or to saturate a high variety of unsaturated hydrocarbons [15].
- Hydrocracking reactions such as C-C bonds splitting and C-C rearrangement reactions, also called hydroisomerization reactions.

#### 2.3.1. Hydrodesulfurization reactions (HDS)

Hydrodesulfurization (HDS) is the chemical reaction between the sulfur atom of a given hydrocarbon molecule and hydrogen to produce H<sub>2</sub>S, according to Equation 1. These chemical reactions are carried out on solid catalysts under quite severe conditions of temperature and pressure [11,15]:



A wide variety of sulfur-containing compounds, ranging from thiols to thiophenes, are present in petroleum and refinery fractions [15]. Hydrodesulfurization reactivity strongly depends on the

molecular size and the structure of the sulfur-containing compound. Thiols, sulfides and disulfides can be easily removed, whereas other compounds, like thiophenes, benzothiophenes and especially dibenzothiophenes, are more refractory due to their aromatic character [15]. The following order in terms of desulfurization rates has been reported for thiophenic families [16]: thiophene>benzothiophene>dibenzothiophene. For bigger analogs of the dibenzothiophene, e.g., benzonaphthothiophene, hydrogenation of one of the aromatic rings precedes HDS. Hydrogenated analogs are more easily desulfurized than the corresponding thiophenic compounds [17,18].

Two parallel pathways have been proposed in the literature for the HDS of thiophene-based molecules: the so-called direct desulfurization (DDS) [19] and hydrogenation (HYD) [20–22]. The DDS route consists of the C-S bond cleavage, i.e., direct S-extrusion [23–25], whereas the hydrogenation mechanism implies the prehydrogenation and saturation of the molecule before sulfur scission, as illustrated in Figure 3 for the HDS of thiophene [26]. A similar mechanism has been proposed for dibenzothiophene, as shown in Figure 4 [27].

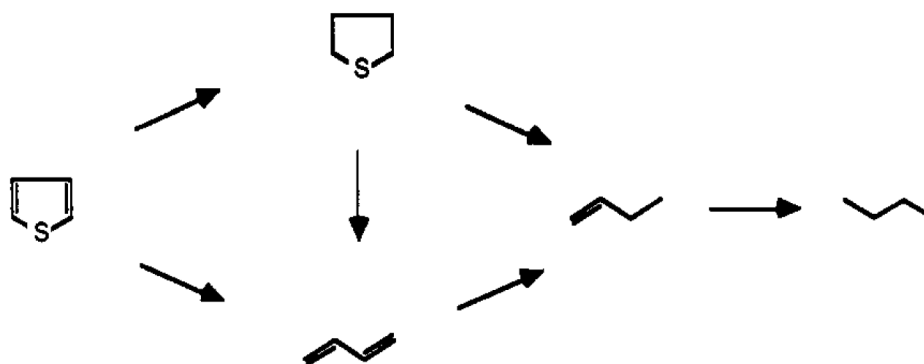
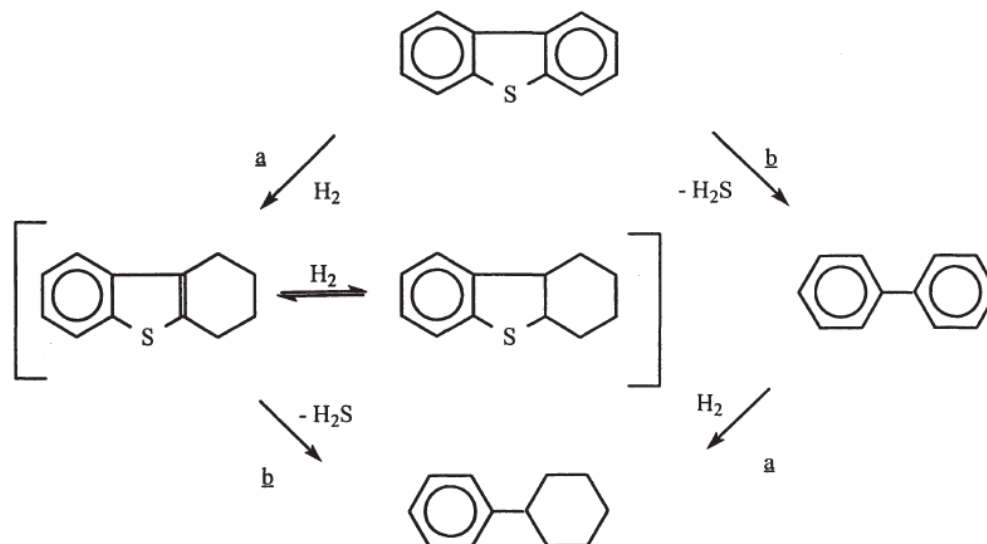


Figure 3. Thiophene reaction pathways [26].

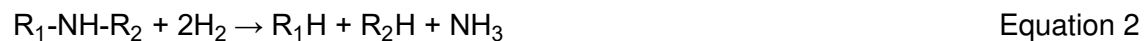


**Figure 4. Suggested reaction network for the HDS reaction of dibenzothiophene; a) hydrogenation steps; b) C-S bond-breaking steps [27].**

Both pathways can occur depending on the nature of the S compound. The prehydrogenation mechanism becomes more predominant for larger S-containing ring systems such as benzonaphthothiophene [28,29]. When electronic density delocalization applies for the S-containing ring, the DDS mechanism is predominant. The prehydrogenation mechanism becomes essential when the delocalization of the electronic density is found within the rings placed at the extremities of the S-containing ring (as for benzothiophene and larger ring systems) [30].

### 2.3.2. Hydrodenitrogenation reactions (HDN)

Hydrodenitrogenation (HDN) represents the removal of nitrogen from organonitrogen compounds by reaction with hydrogen over a solid catalyst to yield ammonia and hydrocarbon(s), according to Equation 2 [31,32].



The type of N-compounds and the total amount of nitrogen vary from feed to feed (Figure 5) [33]. The predominant structures in VGO's feedstocks are the five- and six-membered N-rings, classified as non-basic or "neutral" and basic N-compounds, respectively. In the non-basic N-compounds family, such as pyrrole, indole and carbazole derivatives [11,33], the lone-pair electrons of the nitrogen atom are delocalized around the aromatic ring and are, thus, unavailable for an acid [34]. In the basic heterocyclic N-compounds family, constituted by alkylamines, aniline derivatives, quinoline, acridine and their heavier derivatives with further attached benzene rings, the free electron pair of the nitrogen is available to react with an acid [11,35]. However, this distinction may be less critical under hydroprocessing conditions since the non-basic N-compounds are rapidly hydrogenated to basic N-compounds [35,36].

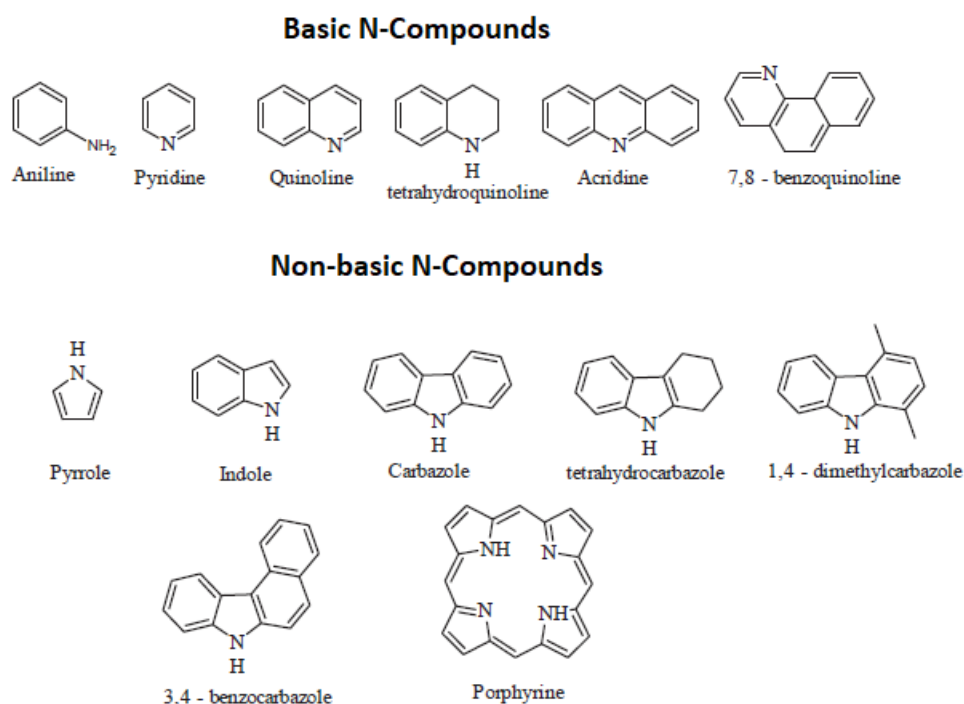


**Figure 5. Examples of both families of nitrogen compounds in petroleum fractions [11,33,35].**

The reactivity of nitrogen-containing compounds depends on their structure, including the alkyl substitution. The conjugation of the free electron pair on nitrogen in the aromatic ring, which strongly affects basicity, plays an important role in reactivity [15,37]. The more easily degraded classes are the non-aromatic N-compounds, mainly amines and nitriles. Conversely, the most highly refractory molecules are the families deriving from the basic pyridine (Py) and the less-basic pyrrole (Pyr) structures. These include bicyclic quinolines (Q) and indoles (In), with one or several short-chain alkyl substituents, as well as higher polycyclic homologs [15].

Schulz et al. [38] established the following order of decreasing reactivity of hydrodenitrogenation for the following molecules:

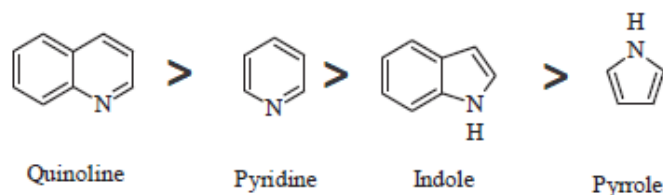


**Figure 6. Reactivity of nitrogen compounds according to the work of Schulz et al. [38].**

Neutral nitrogen compounds were more refractory than basic compounds due to the preferential adsorption of the later compounds on acid sites [39]. Carbazoles and benzocarbazoles type compounds belonging to the neutral class were quite refractory. Regarding the basic N-compounds family, quinoline-type compounds were the most refractory. Benzocarbazoles type compounds are easier to convert than carbazoles. Moreover, further investigation on the carbon number distribution showed that short-alkyl chain nitrogen compounds were probably more reactive than long alkyl chain nitrogen compounds towards the HDN reactions. This suggested that steric hindrance effects may play a role in the HDN of big molecules [40].

Due to the higher C=N bond strength, 147 Kcal/mol vs. 114-128 Kcal/mol for C=S bonds [41] and the smaller atomic radius of N, 0.75 Å vs. 1.09 Å for S, removing nitrogen from heteroatomic

molecules is indeed considerably more difficult than HDS of the sulfur molecules. Consequently, required operating conditions to perform HDN reactions are more severe than in the case of HDS [15]. HDN is essential for ensuring the level of sulfur required by fuel specifications, as nitrogen strongly inhibits HDS due to its preferential adsorption on catalytic sites [42].

Studies concerning the HDN of various N-heterocyclic compounds have shown that the major pathway involves: (i) hydrogenation of the N ring; (ii) cleavage of one C-N bond, resulting in an amine intermediate and (iii) hydrogenolysis of the amine to produce ammonia [15,22]. This is illustrated in Figure 7 for quinoline, one of the most frequently used model molecules for HDN mechanistic studies. Hydrogenation of the N-ring in quinoline is very rapid, whereas hydrogenation of the aromatic ring is considerably slower. It is generally accepted that prehydrogenation of, at least, the N-heterocycle is mandatory for C-N bond cleavage. This is in contrast to the case of HDS, where prehydrogenation of the S-ring is a possible pathway but not a prerequisite for C-S bond scission. The reaction can be considered thermodynamically irreversible. It is exothermic and kinetically favored at high temperature and high hydrogen pressures [11].

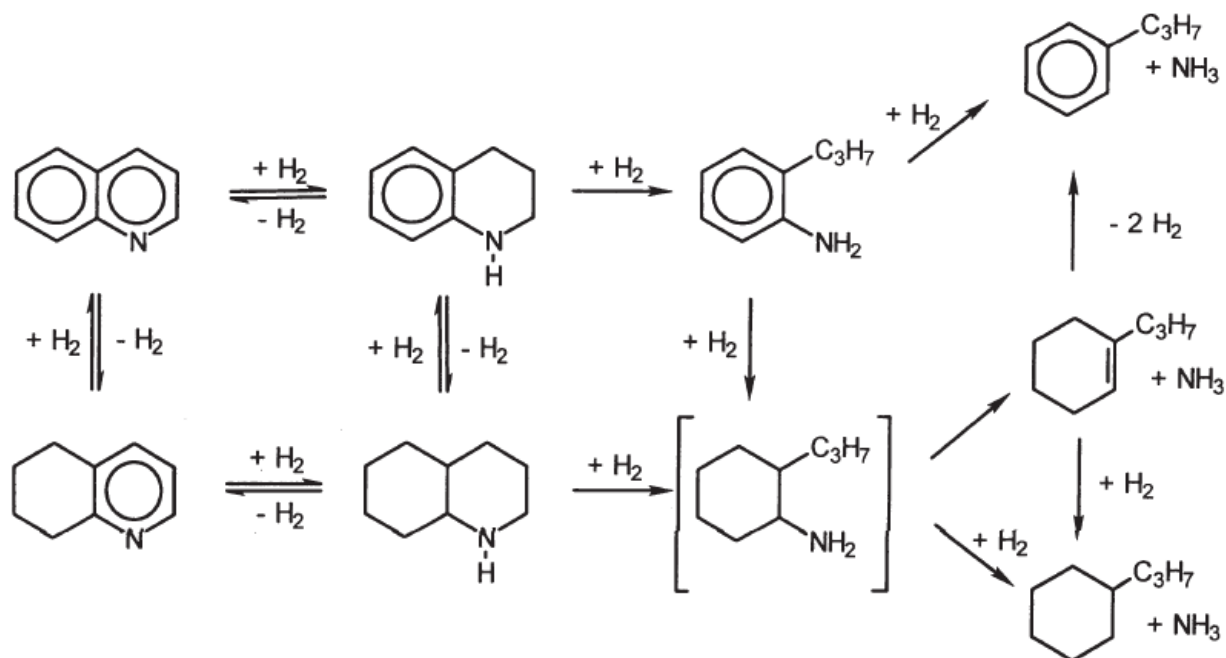
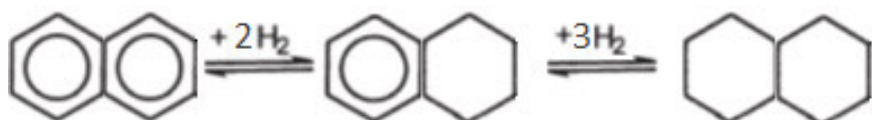


Figure 7. Proposed quinoline HDN-reaction network [43].

### 2.3.3. Aromatics hydrogenation reactions (HDA)

These reactions take place before cracking of the saturated cyclic hydrocarbons. This is because aromatic compounds cannot be cracked under typical hydrocracking conditions. HDA reactions hydrogenate the aromatic rings of aromatic or naphtheno-aromatic compounds to convert them into naphthenes. The naphthenes are readily cracked under the same conditions. A standard aromatic hydrogenation reaction is presented in Equation 3 [11]:



Equation 3

The aromatic hydrogenation reactions are reversible under hydrocracking conditions. Hydrogenation is thermodynamically favored by high pressures and low temperatures, whereas high hydrogen pressures and high temperatures kinetically favor it. A compromise must,

therefore, be found for the temperature to maximize hydrogenation [11,22]. This compromise is located between 380 and 410°C, depending on the chemical structures present. Beyond these temperatures, the thermodynamic limitation overtakes kinetics.

The order of increasing activity of a sulfided NiMo/Al<sub>2</sub>O<sub>3</sub> catalyst for the hydrogenation of one ring of a series of multi-aromatic model compounds was as follows: benzene < phenanthrene < naphthalene < anthracene [44]. Thus, in a homologous series, the hydrogenation rate generally increases with the number of aromatic rings present and is particularly low for benzene [45,46]. Differences in reactivity can be observed, even for molecules presenting the same number of aromatic rings. For instance, phenanthrene is much less reactive than anthracene, even though they both have three aromatic rings. This is probably explained by a difference in the electron density, which is lower in the phenanthrene case, probably leading to a lower adsorption strength. This is supported by Neurock and van Santen [47], who found a good correlation between hydrogenation rate constants and electron densities. Substituents in the benzene ring also increase hydrogenation activity, as indicated as follows [48,49]: benzene < toluene = o-xylene = p-xylene < ethylbenzene.

Sapre and Gates [46] proposed the reaction networks shown in Figure 8 for the hydrogenation of the monoaromatics benzene and biphenyl. This network accounts for the reversibility, which was confirmed by biphenyl presence during experiments with cyclohexylbenzene as a reactant.

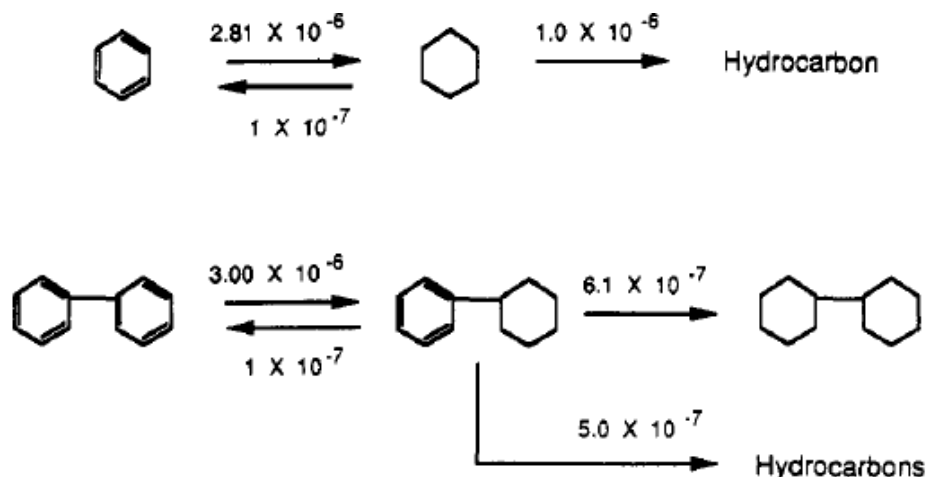


**Figure 8. Reaction networks for benzene and biphenyl. The numbers over the arrows are pseudo-first-order rate constants in L/s\*g of catalyst at 325°C [46].**

Considering the hydrogenation of aromatics with two fused rings, quantitative reaction networks have been reported for the naphthalene hydrogenation (Figure 9). Hydrogenation is sequential, with the hydrogenation rate of tetralin being approximately equal to the one related to benzene and an order of magnitude less than the naphthalene hydrogenation reaction rate. The reversibility of naphthalene hydrogenation was confirmed by using tetralin as reactant. The dehydrogenation rates of the two decalins are negligible.

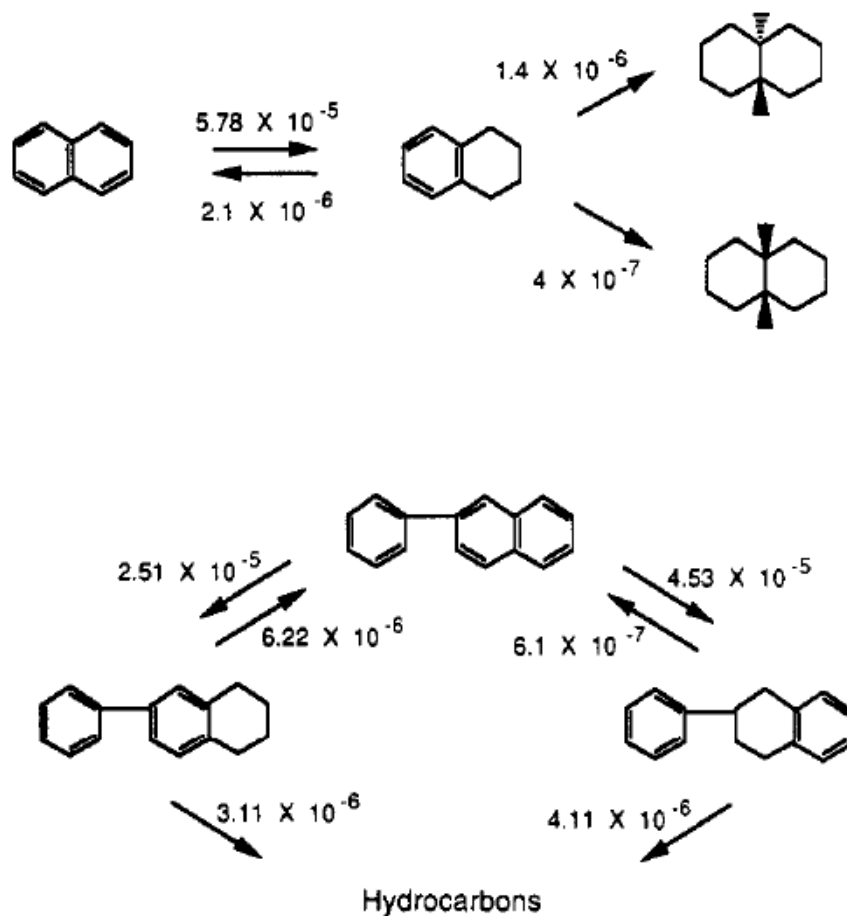
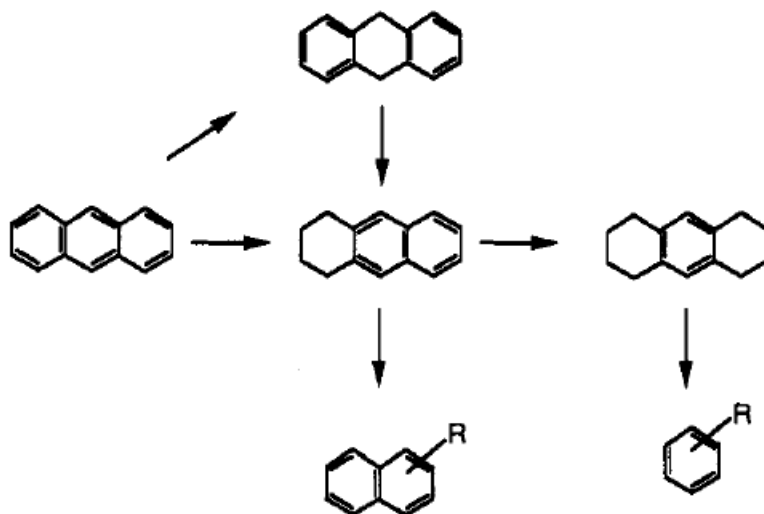


Figure 9. Reaction networks for naphthalene hydrogenation and 2-phenyl-naphthalene. The numbers over the arrows are pseudo-first-order rate constants in L/s\*g of catalyst at 325°C [46].

Hydrogenation activity of compounds with three fused rings, anthracene and phenanthrene, has been investigated, but quantitative reaction networks have not been reported. The suggested reaction pathways for anthracene are shown in Figure 10.



**Figure 10. Reaction pathway for anthracene hydrogenation and hydrocracking [50].**

For a condensed aromatic compound, hydrogenation of the first outer ring is the fastest, the remaining rings becoming more resistant to hydrogenation [45]. The reason for decreasing reactivity is that the resonance stabilization of a ring in a condensed, multi-ring molecule is lower than in smaller molecules like benzene [17].

#### 2.3.4. Hydrocracking reactions (HCK)

Hydrocracking provokes a reduction in the average molecular weight of the feed. In hydrocracking reactions, both the (de)hydrogenation and the acid functions of the catalyst play an important role [11]. The reactions that occur during hydrocracking have been studied extensively. These studies have shown that hydrocracking can take place through three main routes [9,51]:

- Non-catalytic thermal cleavage of C-C bonds via hydrocarbon radicals formation, with hydrogen addition (hydropyrolysis). It occurs at temperatures around 500 to 600°C and elevated hydrogen pressures.

- Monofunctional C-C bond cleavage followed by hydrogenation of the fragments over hydrogenation components consisting of metals (Pt, Pd, Ni), oxides, or sulfides (hydrogenolysis).
- Bifunctional C-C bond cleavage with hydrogen addition over bifunctional catalysts consisting of a hydrogenation/dehydrogenation component dispersed on a porous, acidic support.

The term "ideal hydrocracking" was attributed to catalytic systems, where the main function of the metal is to dehydrogenate saturated reactant molecules to alkenes and to hydrogenate olefinic intermediates desorbed from the acid sites. There, skeletal rearrangements and carbon-carbon bond scissions occur. Mass transfer between both types of sites is considered to occur by alkenes diffusion [51]. With the ideal hydrocracking catalyst, the carbon number distribution of cracked products is fully symmetrical and centered at around half of the original molecule [52].

The classical mechanism for the conversion of an n-alkane on a bifunctional catalyst is represented in Figure 11. The reactant is initially dehydrogenated on the metal sites to produce an n-alkenes,  $n\text{-C}_i\text{H}_{2i}$ . After desorption from the metal site, this alkene diffuses to a Brønsted acid site where it is protonated to yield secondary an alkylcarbenium ion,  $n\text{-C}_i\text{H}_{2i+1}^+$ . Carbenium ions are reactive intermediates that are chemisorbed on acid sites and can suffer different transformations, such as skeletal rearrangements and carbon-carbon bond rupture ( $\beta$ -scission). The products of  $\beta$ -scission are a smaller alkylcarbenium ion and an alkene. In the case of a  $n\text{-C}_i\text{H}_{2i+1}^+$   $\beta$ -scission, a primary carbenium ion would be formed, which is energetically unfavorable. Thus n-alkylcarbenium ions undertake skeletal rearrangements to form monobranched alkylcarbenium ions,  $\text{iso-C}_i\text{H}_{2i+1}^+$ . If there is an efficient desorption mechanism from the acid sites, monobranched alkenes,  $\text{iso-C}_i\text{H}_{2i}$ , are released and diffuse to metal sites to

be hydrogenated into monobranched alkanes,  $\text{iso-C}_i\text{H}_{2i+2}$ . These are the primary products observed at low conversions.

Consecutive reactions occur on the acid sites as conversion increases, particularly a second branching rearrangement leading to dibranched  $\text{iso-C}_i\text{H}_{2i+1}^+$ . These molecules can be desorbed again as dibranched iso-alkenes and appear, upon hydrogenation at the metal sites, as dibranched iso-alkanes  $\text{iso-C}_i\text{H}_{2i+2}$  in the product. Further increase of conversion implies the formation of tribranched alkylcarbenium ions on the acid sites. As the rate of  $\beta$ -scission strongly increases with the degree of branching, these tribranched cations  $\text{iso-C}_i\text{H}_{2i+1}^+$  are not desorbed. Thus, even in ideal bifunctional catalysis, they instead undergo  $\beta$ -scission into an alkylcarbenium ion  $\text{C}_j\text{H}_{2j+1}^+$  and an alkene  $\text{C}_{(i-j)}\text{H}_{2(i-j)}$ .  $\text{C}_1$  and  $\text{C}_2$  hydrocarbons are not produced since the related primary carbenium ions  $\text{CH}_3^+$  and  $\text{C}_2\text{H}_5^+$ , respectively, are energetically unfavorable.

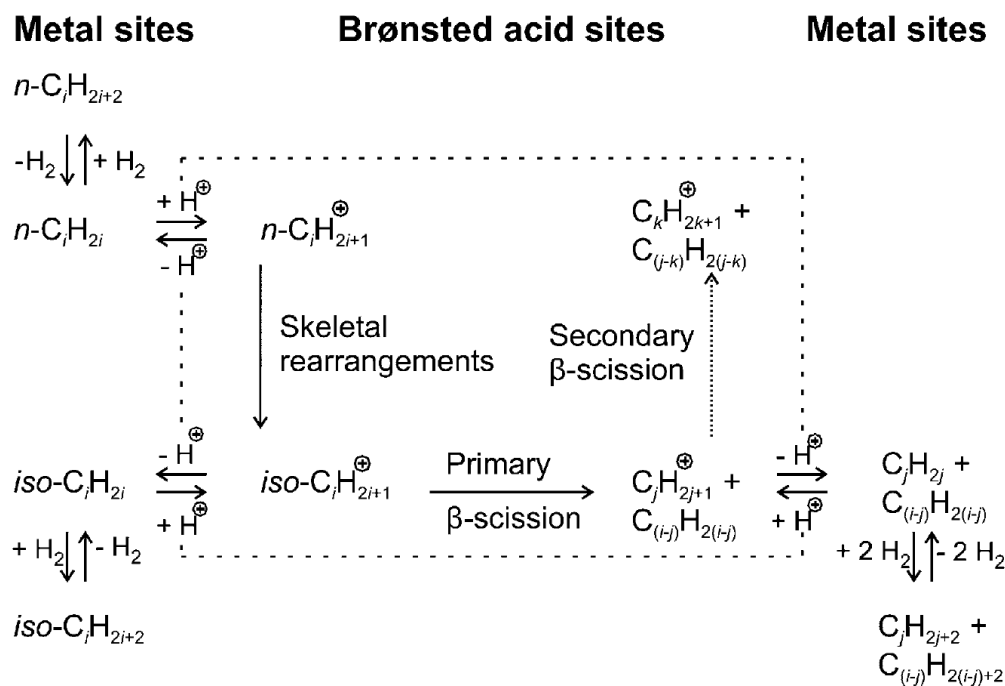


**Figure 11. Classical mechanism of isomerization and hydrocracking of an n-alkane on a bifunctional catalyst [51].**

2.3.4.1. *Types of isomerization and  $\beta$ -scission mechanisms [9,11,51]*

The carbenium ion isomerization reactions can be classified into two categories. The first one is type A isomerization, in which a secondary alkylcarbenium ion is transformed into another secondary carbenium ion through an alkyl shift. A modification of the position of the branch is produced without changing the amount of branching of the molecule. In the second type, named B, the secondary alkylcarbenium ion leads to a tertiary alkylcarbenium ion (branching) through the formation of a protonated cyclopropane (PCP) intermediary. In this type of rearrangement, the amount of branching changes, as illustrated in Figure 12. The isomerization reaction rate is higher for type A isomerization.

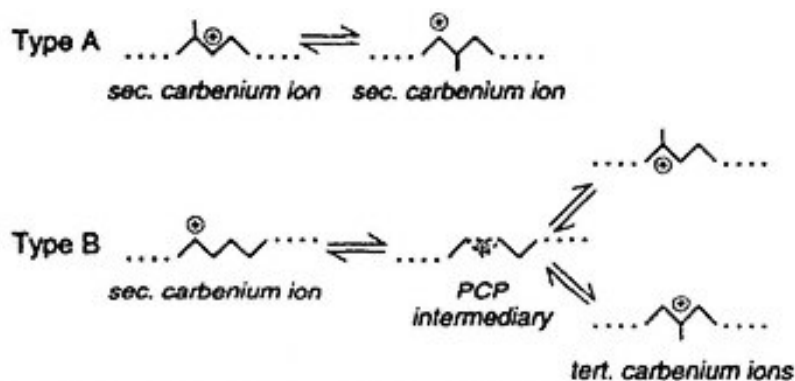


**Figure 12. Skeletal Isomerization mechanisms.**

The proposed  $\beta$ -scission mechanisms, presented in Figure 13, suggest that the n-paraffins submitted to hydrocracking may undergo several isomerizations until a configuration favorable to  $\beta$  scission is achieved.

For large carbenium ions, the cracking by  $\beta$  scission is more likely to occur with dibranched and tribranched isomers than with monobranched ones [6]. Furthermore, lower molecular weight paraffins cracking via  $\beta$ -scission is less likely to occur, which explains their high yields even at high conversions.

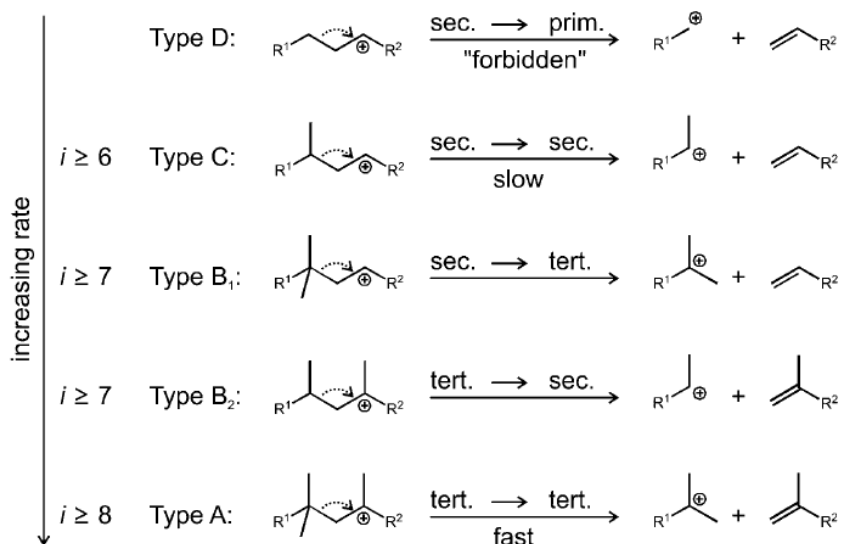


**Figure 13.  $\beta$ -scission mechanisms [51].**

### 2.3.5. Kinetics Modeling

Kinetic studies provide valuable information for comparing, selecting and optimizing catalysts, assessing feeds reactivity and reactor modeling and design [12]. The reaction rates determine the key properties of a hydrocracking catalyst: initial activity, selectivity, stability and product quality [9].

The initial activity is measured by the temperature required to obtain the desired product specification at the start of the run. In general, catalyst activity is a measure of the relative rate of feedstock conversion. In hydrocracking of VGO, activity is defined as the temperature required to obtain a given 370°C<sup>+</sup> cut conversion under certain process conditions. Conversion for the main reactions occurring in hydrocracking is usually defined as:

$$\% \text{Net Conversion} = \left( \frac{\text{mass}_{x \text{ feed}} - \text{mass}_{x \text{ product}}}{\text{mass}_{x \text{ feed}}} \right) * 100 \quad \text{Equation 4}$$

Where  $x$  is either the 370+ mass, the nitrogen the sulfur, or the aromatics content in the liquid phase.

Kinetic studies considering each compound and all the possible reactions are complicated due to the vast number of hydrocarbons involved in the system. However, they permit a mechanistic description of hydrocracking based on the detailed knowledge of the mechanism related to the different reactions. Most of the time, applying this method to hydrocracking of real feeds is difficult due to the analytical complexity and computational limitations. The more compounds a model includes, the more kinetic parameters need to be estimated; consequently, more experimental information is required [53].

So far, detailed characterizations of feeds and products to identify and quantify components and/or groups of components were only achieved for lighter feeds. For heavy feeds such as VGO and heavy gasoil (HGO), the kinetic studies focus essentially on HDS, HDN, HDA and HCK reactions. These chemical reactions are described either with a single power-law expression or with the Langmuir-Hinshelwood (LH) equation (Equation 5).

$$r_i = \frac{k_i P_i}{(1 + \sum K_j P_j)^n} f(P_H) \quad \text{Equation 5}$$

Where  $r_i$  is the conversion rate of reactant  $i$ ,  $k_i$  the reaction rate constant,  $P_i$  the partial pressure (concentrations may be used for liquids).  $P_j$ , are the partial pressure of all the adsorbed species,  $K_j$  is their adsorption constant on the corresponding active site and  $n$  is the number of adsorbed species in the rate-determining step.

The reaction between the adsorbed organic species and the adsorbed hydrogen species is generally considered as the rate-limiting step for hydrotreating reactions. In the hydrocracking mechanism, the carbenium ion C-C bond cleavage is often considered as the rate-limiting step. The  $f(P_H)$  term in Equation 5 refers to a function of the hydrogen pressure,  $P_H$ . In literature, first-order behavior is usually assumed for hydrogen in hydrotreating reactions. In that case, this function can be substituted by the product  $(K_{H_2} P_{H_2})^a$ , in which the parameter  $a$  is equal to 1. In some cases, the  $H_2$  adsorption is dissociative, and consequently, the parameter  $a$  is equal to 0.5. If hydrogen and the organic reactant adsorb on different types of active site, then equation 5 is given by the following general expression:

$$f(P_H) = \frac{(K_H P_H)^a}{1 + (K_H P_H)^a} \quad \text{Equation 6}$$

The constant  $a$  can have values of 1/2 or 1 depending on whether hydrogen is adsorbed dissociative or associated, respectively. Finally, since  $H_2$  does not participate in the limiting step of the hydrocracking reactions,  $f(P_H)=1$ .

### 2.3.5.1. *Hydrosulfurization Reactions (HDS)*

For HDS reactions, the reaction rate form given in Equation 5 has been used to correlate HDS kinetics for thiophene [54], benzothiophene [55] and dibenzothiophene [56,57]. The L-H model can account for the observed strong inhibition by both the S-compound and  $H_2S$ . The  $f(P_H)$  function is often given by Equation 6, which is based on the assumption that  $H_2$  and the S-containing compound are adsorbed on different active sites.

### 2.3.5.2. *Hydrodenitrogenation Reactions (HDN)*

In the case of HDN reactions, strong adsorption of heterocyclic N compounds on molybdenum sulfide catalysts leads to a severe inhibition of the corresponding active sites that are further inhibited by ammonia. A complete description of the HDN global kinetics is complex, as shown

by Satterfield and Yang [58]. These authors considered ten individual steps with inhibition terms for the description of the quinoline HDN. Although a model molecule was used, several assumptions with respect to the adsorption strengths of the various components present were needed. The kinetics of quinoline HDN have been satisfactorily correlated with L-H type equations [58,59]. In these studies, the rate constants for each step of the whole reaction pathway were evaluated using a common denominator adsorption term. The hydrogenation of quinoline to 1,2,3,4-tetrahydroquinoline was found to be essentially at equilibrium under the reaction conditions employed. A similar kinetic treatment for indole HDN has been recently reported by Massoth et al. [60]. Again, the equilibrium for the first hydrogenation step to dihydroindole was observed.

### *2.3.5.3. Aromatics Hydrogenation Reactions (HDA)*

The kinetics related to the hydrocracking of polycyclic aromatics over amorphous catalysts was investigated by Qader [61]. The author concluded that the kinetic data obtained were compatible with the dual-site mechanism of Langmuir–Hinshelwood.

Kinetic data for the hydrogenation of different aromatics over different catalysts were obtained by Dufresne et al. [49]. The relative rate constants of the hydrogenation reactions carried out over catalysts containing sulfided group VI metals show that polyaromatic molecules are rapidly hydrogenated if the thermodynamic conditions are satisfied. However, when catalysts with group VIII metals (Pt, Ni) are used, monoaromatics are more easily hydrogenated.

### *2.3.5.4. Hydrocracking Reactions (HCK)*

Kinetic models have been developed for hydroisomerization and hydrocracking of model compounds, such as n-heptane [62], n-octane [63], n-decane and n-dodecane [64] over zeolite or amorphous catalysts. Bernardo and Trimm [65] postulated an L-H kinetic model for describing

the hydrocracking of light hydrocarbons. Froment et al. [63,64] also assume a Langmuir–Hinshelwood expression for chemisorption and use a Langmuir isotherm to estimate the catalyst surface hydrocarbon concentration. Several studies have been published regarding the kinetics of hydrocracking of diesel and vacuum distillate [61,66]. From these studies, it was concluded that the rate of hydrocracking is of first order with respect to the feed concentration.

From the kinetic studies described above, one can conclude that although the hydrocracking kinetics of model molecules can be described satisfactorily using Langmuir–Hinshelwood models. Nevertheless, such models require a considerable amount of experimental data for parameters estimation, which was not available in this study. Hence, in the interest of simplicity, the present work uses conventional power-law kinetic expressions in agreement with other studies performed on similar reaction systems with acceptable results [67–69]. A first-order [70, 71] kinetics was assumed for VGO conversion, HDN and HDA [35] (Equation 7). The first-order rate law does not account for inhibition effects but allows correcting, albeit approximately, for the impact of depleting reactant concentration on the reaction rates. For HDS, an apparent reaction order of 1.2 ( Equation 8) was used; from our experience, this reaction order allows accounting for the fact that S-species converted at low conversions are more reactive than the refractory species left over at high conversions. These expressions result from a mass balance in the reactor, combined with the reaction kinetics, considering that the reactor behaves as a plug-flow ideal reactor. The verification of ideal behavior is shown in Chapter 2, section 2.

$$k = \text{LHSV} \cdot \ln \left( 1 - \frac{\% \text{Net Conversion}}{100} \right) \quad \text{Equation 7}$$

$$k_i = \frac{\text{LHSV}}{n-1} \left( \frac{1}{(C_s^{\text{out}})^{n-1}} - \frac{1}{(C_s^{\text{in}})^{n-1}} \right) \quad \text{Equation 8}$$

Here  $n=1.2$ ,  $C_s^{\text{in}}$ , and  $C_s^{\text{out}}$  are the feed and product sulfur contents in percentage wt%.

### 2.4. Hydrocracking Catalysts

Hydrocracking catalysts are bifunctional solids that combine an acid function and a (de)/hydrogenation function. The acid function promotes the cracking and isomerization reactions and is provided by an acidic support, whereas the (de)/hydrogenation function is provided by metals [71]. Different materials can provide these functions with different strengths. Their choice depends on the type of feedstock, the conversion level and the desired products [11]. This section gives an overview of the hydrocracking catalysts used in vacuum gasoil (VGO) hydroconversion.

#### 2.4.1. (De)/Hydrogenation Function

The metals providing the (de)/hydrogenation function can be noble (palladium, platinum) or non-noble metal like sulfides from group VIA (molybdenum, tungsten) and group VIIIA (cobalt, nickel) [72]. These metals catalyze the hydrogenation of the feedstock, making it more reactive for cracking and heteroatom removal. This function reduces the coking rate and initiates cracking by producing a reactive olefin intermediate via dehydrogenation [9].

Noble metals such as Pt and Pd present quite high hydrogenation activities. Nevertheless, these metals are rarely used with heavy oil fractions due to their high costs compared to other metals [52,73] and their strong sensitivity to sulfur poisons [74]. Consequently, mainly sulfided NiW, NiMo and CoMo catalysts are applied in most industrial hydrocracking processes [75,76].

The (de)/hydrogenation activity is determined by the type and the amount of metal. Regarding the amount of non-noble metals, the average content in industrial catalysts is around 3-8 wt% of cobalt or nickel oxides and 10-30 wt% of molybdenum or tungsten oxides [9]. An optimal Ni or Co loading can be determined based on the catalyst activity and isomer selectivity. For both

criteria, a Ni/(Ni+Mo) atomic ratio between 0.4 and 0.5 was found, as presented in Figure 14 [77]. Additionally, a higher dispersion implies better accessibility of the metal for the olefinic intermediates. As time on-stream increases, the hydrogenation activity of the hydrocracking catalyst decreases, due in part to metal agglomeration [78]. The most straightforward strategy to increase the metal dispersion is to select smaller support particles containing sufficient mesoporosity [79].

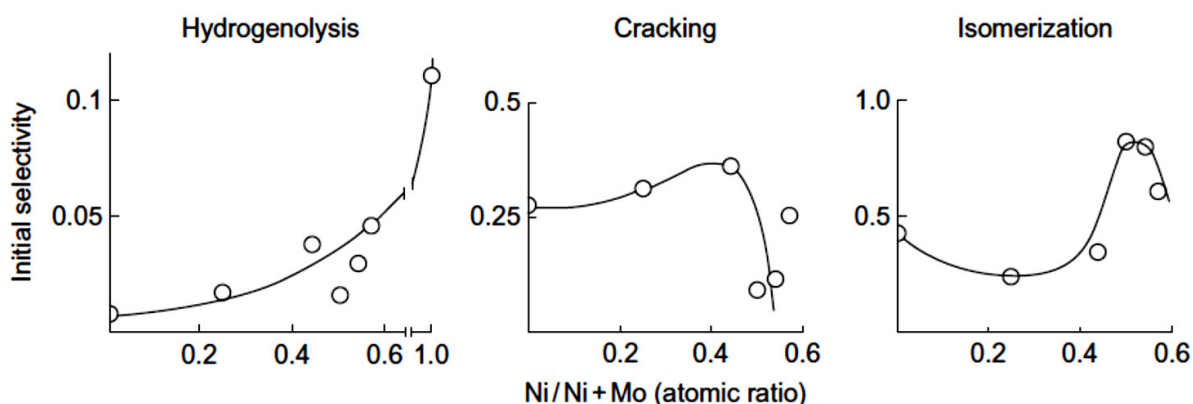


**Figure 14. Initial selectivity for hydrogenolysis, cracking and isomerization reactions as a function of the Ni/(Ni+Mo) atomic ratio of the NiMo/USY catalyst in n-heptane hydrocracking [77].**

Concerning the active metal forms in catalysis, the first studies allow to identify Co-Mo-S structures and their key role in promoting catalytic activity [31,80–82]. Later, several works showed that the building blocks of Co-Mo-S were small MoS<sub>2</sub>-like domains or nanocrystals dispersed on the support. The promoter atoms are located at the edges of the MoS<sub>2</sub> layers or as separate promoter sulfide structures [31,80]. Based on these findings, the most accepted model for the Ni(Co)-Mo-S structures was developed and is shown in Figure 15.

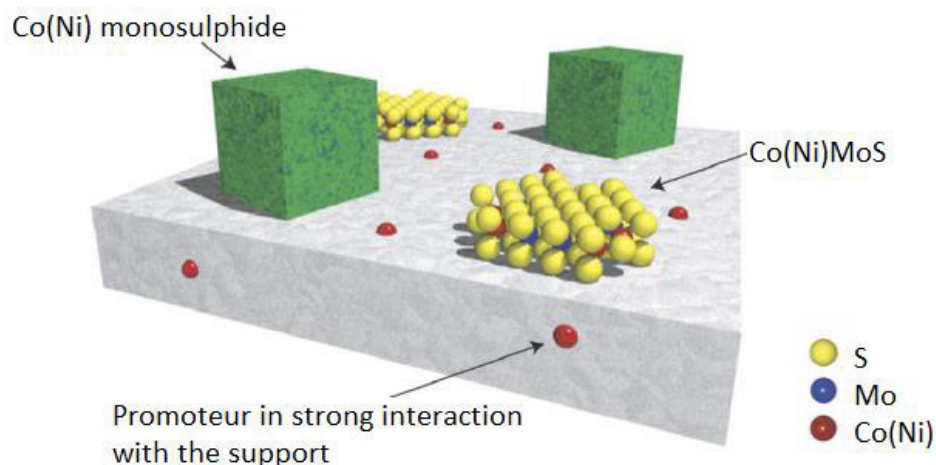


**Figure 15. Schematic drawing showing Co(Ni)–Mo–S and other Co(Ni) sulfide structures on alumina and Co(Ni) in the alumina [83].**

Sulfur vacancies have been typically suggested as active sites [25,84]. Such sites are expected to bind  $\text{H}_2\text{S}$ . The competition between  $\text{H}_2\text{S}$  and reactants for the active sites has been proposed as the main mechanism to explain the  $\text{H}_2\text{S}$  inhibition found in several studies [12,15,35]. The existence of both direct (DDS) and pre-hydrogenation (HYD) desulfurization routes, mentioned previously, is well known. There is an agreement concerning the fact that DDS involves sulfur vacancies [85]; however, the nature of the HYD sites is still controversial [22,86,87]. Hydrogenation reactions were assumed to be catalyzed by acidic SH groups [88]. Nonetheless, more recent scanning tunneling microscopy (STM) studies of Co-Mo-S structures [89] showed, as illustrated in Figure 16, that the small sulfide clusters may have unusual sites with metallic-like character. These so-called brim sites, which appear bright in the STM images, are adjacent to the edges.

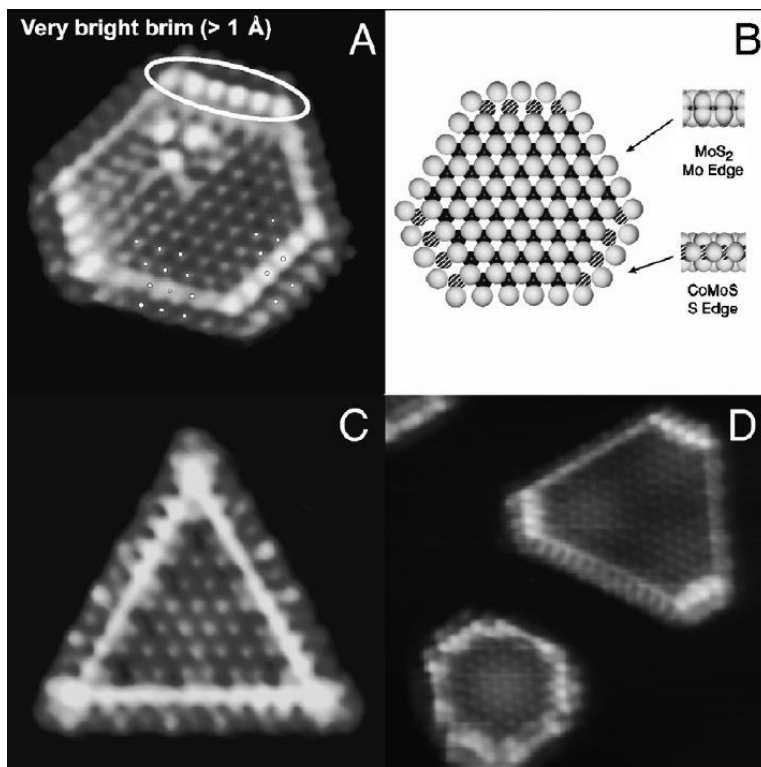


**Figure 16. STM images of Co-Mo-S (A), MoS<sub>2</sub> (C), Ni-Mo-S (D) and ball model of single layer Co-Mo-S (B) adapted from references [89–91].**

The STM images also provided detailed insight into the location of the Co and Ni promoter atoms in the Co-Mo-S and Ni-Mo-S structures. The results confirmed the earlier proposals regarding the location of the promoter atoms at the edges. However, the STM results gave much more detailed insight, and it was found that the promoter atoms prefer to occupy particular types of edge sites (the so-called S edges). STM studies [92] have also delivered direct images of how the HDS reactions can proceed. It was found that the brim sites, due to their metallic character, may bind the sulfur-containing reactants. Furthermore, when hydrogen is available at the neighboring edge sites in the form of SH groups, hydrogen transfer reactions may take place. It should be noted that the STM technique requires the study of model systems, which may differ in many ways from industrial catalysts.

### 2.4.2. Acid Function

Zeolites are the primary solids used as acid function in hydrocracking catalysts [76]. They combine relatively high activity with high resistance to coking and deactivation by heteroatom-containing compounds [93]. Moreover, they exhibit good regeneration performances and their morphology can be optimized in order to improve product selectivity through molecular shape selectivity [72,94]. For zeolite-containing catalysts, the concentration and strength of acid sites have a significant influence on activity and selectivity [95]. Ding et al. [96] have shown that activity in hydrocracking of hexadecane increases with the increasing acidity of the zeolite. Nowadays, ultra-stable zeolites Y are widely used as acidic components of commercial hydrocracking catalysts [97].

Zeolites are crystalline aluminosilicates with the general formula  $M_{2/n}O \cdot Al_2O_3 \cdot zSiO_2$ . According to Loewenstein's rule,  $n$  is the valency of the cation  $M$  whereas  $z$  can vary from 2 to infinity in the previous formula [98]. Structurally, zeolites are constituted by aluminum ( $AlO_4$ )<sup>-</sup> or silicon ( $SiO_4$ ) tetrahedral blocks linked by their oxygen atoms to form sub-units and ultimately large networks consisting of identical units [11], as shown in Figure 17. Since Al is a trivalent element, the  $AlO_4$  tetrahedra of the zeolite framework provide a negative charge. An  $M^+$  cation compensates this negative charge, also called compensating cation, whose nature can vary ( $Na^+$ ,  $K^+$ ,  $H^+$ , organic cations, etc.). These compensation metals can be easily exchanged by other cations, like in the particular case of Brønsted acid sites (BAS), created through the exchange with a proton  $H^+$ . Thus, each tetrahedron centered in an aluminum atom corresponds potentially to a BAS.

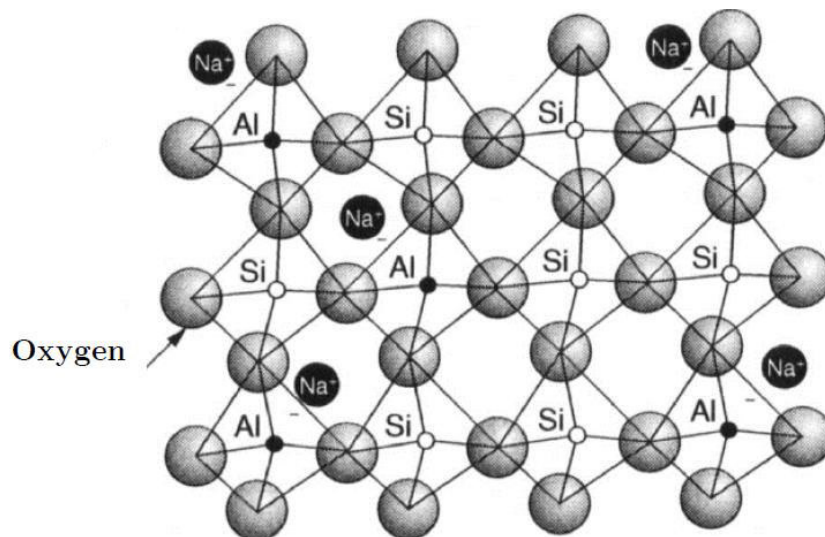


**Figure 17. Organization of Si and Al tetrahedra in zeolites network. Si, Al, O, and Na<sup>+</sup> atoms are indicated in the figure [99].**

The acidity of zeolites is intrinsically related to the density of BAS and their strength. The BAS concentration increases with the decrease of the zeolite framework Si/Al ratio. The strength of the sites is associated with their tendency to donate a proton. This property depends on the interaction between the proton and the zeolite framework, the length of the tetrahedron bonds (Si-OH-Al), and the zeolite structure [100]. Zeolite porosity has a considerable effect on catalyst properties in hydroconversion. Shape selectivity and diffusion limitations in the zeolite pores can affect activity by limiting access to the active sites and/or selectivity by causing products to be retained in the pores, leading to secondary reactions [11].

#### 2.4.3. The balance between metal and acid sites

The hydrocracking rate depends on the balance between the acid and metal functions, defined as the metal-to-acid strength ratio (M/A). This parameter is governed by the number and intrinsic strength related to both sites. Catalyst activity and selectivity strongly depend on whether the

rate-limiting step of the global reaction mechanism is a metal- or an acid-catalyzed reaction [103]. This balance affects the activity, stability, and selectivity of the catalyst.

In a catalyst where the (de)/hydrogenation function is more active than the acid one, the limiting stages are those which are catalyzed by the acid sites. The carbenium ions adsorbed on the acid sites have a minimal residence time. Therefore, the secondary cracking phenomenon can be strictly limited and the reaction products from primary cracking are favored. The activity and the primary product selectivity are optimal and the catalyst is considered to be “well balanced” or “ideal” [11,51].

In a catalyst in which the acid function is stronger than the metal function, the reactions catalyzed by the acid sites are very fast, and the (de)/hydrogenation stages are the limiting ones. It is said that the catalyst is “poorly balanced”. The metal sites cannot provide enough olefins to compete with the carbocations for being adsorbed on the acid sites. Therefore, the carbocations have a longer residence time on the acid sites. It leads to secondary cracking, and as a consequence, the selectivity of the primary(desired) cracking products decreases [11,51,71].

For bifunctional catalysts based on a noble metal (Pt) supported on HY zeolite, Guisnet et al. [101] have characterized the balance between the two functions through the ratio between the number of metal sites and the number of acid sites ( $C_{Pt}/C_A$ ). The bifunctional reactions studied were the hydroisomerization and hydrocracking reactions of n-heptane [102,103] and n-decane [104]. For low ( $C_{Pt}/C_A$ ) values, there is a limitation of the bifunctional process by the (de)/hydrogenation steps. According to the authors [101], the intermediate olefins encounter several acid sites during diffusion between two metal sites, leading to an increase in the cracking products and coke formation. Thus, the mono (M), bi (Bi) and tri (Tri) branched isomers as well as  $C_3$ – $C_7$  cracking products (C) appear as the primary reaction products, i.e., those produced at

low conversion levels. The catalyst activity is low, and the cracking selectivity is more significant than the isomerization selectivity. This mechanism is illustrated in Figure 18 (a) for the n-decane transformation.

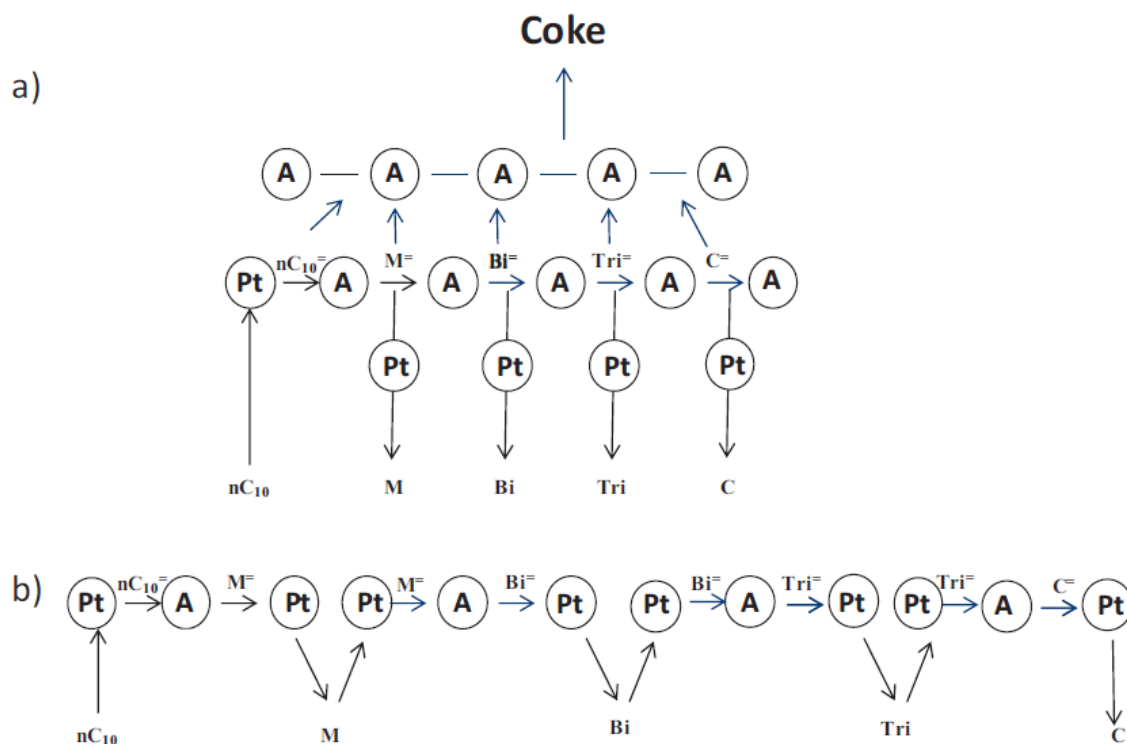


**Figure 18. Hydroisomerisation and hydrocracking of n-decane over PtHFAU catalysts. Reaction scheme for (a) a low value of the hydrogenation/acid balance ( $C_{Pt}/C_A < 0.03$ ); (b) a high value of this balance ( $C_{Pt}/C_A \geq 0.17$ ) [104].**

For intermediate values of  $C_{Pt}/C_A$  values, the metal sites supply enough olefins to the acid sites for the activity to be maximum. However, the reaction intermediates can still undergo several transformations before encountering a hydrogenation site. This means that the selectivity in isomerization and the stability are not optimal. The monobranched and multibranched isomers appear as primary reaction products when compared to the cracking products.

For high  $C_{Pt}/C_A$  values, the reaction intermediates encounter fewer acid sites before encountering a hydrogenation site. Hence, the reaction scheme is sequential (Figure 18b) and

corresponds to the well-known ideal bifunctional hydrocracking mechanism. No deactivation was observed in that particular case.

Some studies have focused on acidity modification to study the impact of the metal/acid (M/A) sites ratio variation on product distribution. Denayer JT et al. [105] found a reduction in activity with an increase of the (M/A) obtained by reducing the number of acid sites. The reduction in activity is related to the decrease in acidity and consequently in cracking power. Meanwhile, the isomer selectivity remains constant [11,106]. In some cases, a change in selectivity is observed, but this is generally due to the modification of other zeolite properties, such as porosity and selective poisoning, rather than to a variation in acidity. These modifications are difficult to distinguish, making it difficult to determine the contribution of the variation of acidity to the catalyst performance [11].

Selective poisoning of active sites by nitrogen, sulfur, or polynuclear aromatics also modifies the hydrogenation/cracking ratio and changes the product yields and quality. For example, the presence of nitrogen compounds in the feedstock can result in selective poisoning of catalyst acid sites, thus increasing the hydrogenation/cracking ratio of the catalyst. This results in a higher liquid product ( $C_5^+$ ) yield, a decrease in the light naphtha octane number and an increase of the middle-distillate yield [107].

The preferential adsorption of polynuclear aromatics on catalytic sites alters the hydrogenation/cracking activity ratio by blocking some of the acid sites of the support. Although most catalyst poisons preferentially affect one catalyst function, they may also affect the other. The relative strengths of adsorption of various species on acid and sulfided metal sites determined by Sullivan et al. are [108]:

- On acid sites: asphaltenes > resins > N-compounds > NH<sub>3</sub> > olefins ≥ thiophenic-compounds > aromatics > H<sub>2</sub>O > H<sub>2</sub>S >> paraffins.
- On sulfide active metals: asphaltenes > resins > H<sub>2</sub>S > S compounds > olefins ≥ N-compounds > aromatics >> paraffins. [109]

In conclusion, the hydrocracking catalysts' performance is dictated by the features of both related functions on the one hand and by their relative strength on the other hand. This is fundamental to interpret the evolution of the catalyst performance during its deactivation, as the rate of activity loss might not be the same for each function.

#### 2.4.4. The distance “intimacy” between metal and acid sites

Besides the balance between the hydrogenating and the acid sites, the distance between them also plays an important role in the catalyst behavior [101,110,111]. In Figure 11 is noted that if the distance between two different sites is too large and diffusivity is too low, concentration gradients develop, and catalytic activity decreases [112]. The intimacy criterion proposed by Weisz has dictated the maximum distance between the two site types, beyond which catalytic activity decreases [110]. Different studies have established that, even more importantly, selectivity might also be affected by intimacy [111,113,114] if the distances between metal and acid sites are large, iso-alkenes might undergo secondary reactions, giving rise to gas and coke.

According to previous studies [93,115–117], some effects of enhanced proximity are a higher partial pressure of olefin near the acid sites, shortening the diffusion paths for olefinic intermediates between the acid and the hydrogenating active sites and the formation of activated hydrogen near the acid sites, which could spill over between the two active sites. Positive impact on conversion by increasing the olefin partial pressure, which would ensure a faster turnover on the acid sites, and by a decrease of coke formation because of the hydrogenation of

the coke precursors by spill over hydrogen. Secondary reactions and, thus, middle distillates selectivity, were shown to be directly related to the average lifetime of carbenium ions intermediates on the acid sites [32].

The criterion by Weisz has often been interpreted simply as the closer the better for positioning metal and acid sites [93,110]. However, some recent studies [112,118] pointed out that, in the past, the intimacy criterion for bifunctional catalysts has been studied at the micron scale because of a lack of synthesis and material characterization methods with nanometre precision. Therefore, the impact of intimacy between metal and acid sites at the nanoscale and on product selectivities is still not described well.

Regarding intimacy at the nanoscale, Höchtl et al. reported that the distance between acid and metal sites has only a minor influence on the hydroisomerization of n-heptane as long as metal and zeolite are in direct contact [112,118]. In contrast, Zecevick et al. [112] studied the hydroconversion of C<sub>10</sub>–C<sub>19</sub> paraffins over bifunctional catalysts containing zeolite Y and an alumina binder, with platinum metal controllably deposited either within the zeolite crystals or on the binder. They found that the platinum-on-binder catalyst offered higher isomerization selectivity and lowered cracking selectivity than the platinum-in-zeolite catalyst. Subsequently, Samad et al. [11] reported that atomic-scale proximity between metal and acid sites was not required to reach a good bifunctionality in isomerization reactions, while catalysts with the two functional sites at a nanoscale distance performed better. Cheng et al. studied the effect of nanoscale intimacy on the hydroisomerization of light alkanes over bifunctional catalysts. They found that the Pt-on-binder catalyst provides a nanoscale proximity between platinum particles and acid sites, while the catalyst with platinum sites inside the zeolite crystals offers the closest proximity. The catalysis results suggest that embedding the platinum particles imposes undesired cracking reactions inside the narrow micropore channels, so the closest proximity

between platinum and acid sites is detrimental to product selectivity. The extent of the influence of the platinum location is strongly dependent on the dimensionality of the zeolite, the size of the molecules, and the reaction conditions.

In conclusion, the initial concept that metal sites should be as close as possible to acid sites is being revised and redefined thanks to new analytical and synthesis techniques.

### 3. HYDROCRACKING CATALYSTS DEACTIVATION

Catalyst deactivation is a physical and/or chemical process that decreases the activity of a given catalyst. Quantitative measurement of deactivation is performed by comparing activity data obtained for the deactivated and corresponding active (or fresh) catalysts. Such data can be provided as follows [9]:

- The temperature required for a given conversion (industrial practice).
- Conversion obtained by a set temperature and space velocity.
- Space velocity required for a given conversion and temperature.
- Reaction rates under differential conversion conditions.
- Rate constants determined from kinetic studies.

The type of application strongly influences the hydroprocessing catalyst life cycle. Figure 19 shows typical catalyst deactivation curves for different classes of feeds. The processing of heavier feeds requires higher operating temperatures (and pressures), which is generally accompanied by a faster catalyst deactivation rate. This results in a shorter cycle length, although the higher pressure somewhat alleviates deactivation [119].

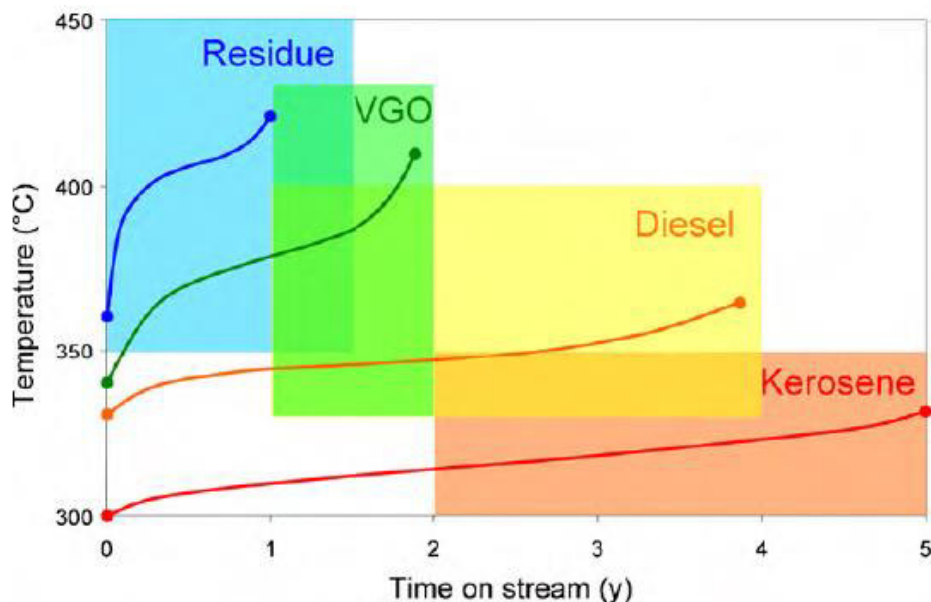


Figure 19. Typical catalyst deactivation curves and operating cycle limits of hydroprocessing applications [119].

### 3.1. Main deactivation mechanisms

There are four primary catalyst deactivation mechanisms: poisoning, coking, sintering and phase transformation [120]. Other deactivation mechanisms encountered in catalysis are pore-blocking via coke or metal deposition in the catalyst pores (or at the pore mouths); volatilization of the catalytically active component; destruction of active sites and reaction between the active component and support with formation of an inactive form [9].

For VGO feeds, catalyst deactivation is dominated by the poisoning involving organic nitrogen compounds and coke deposition. The contribution of metals to deactivation becomes important with heavier feedstocks, such as deasphalted oils, atmospheric and vacuum residues. The relative contribution of coke and metals to catalyst deactivation depends on several factors, such as the origin of feed, type of catalyst, operating conditions, flow configuration, and catalyst position within the fixed bed [33,121].

### 3.1.1. Catalyst Poisoning

#### 3.1.1.1. *Inhibition Vs. Poisoning*

Poisoning refers to the strong chemisorption of reactants, products, or impurities on active sites that would normally be available for catalysis [120,122,123]. This mechanism can be divided into two different categories depending on chemisorption strength: inhibition or poisoning. Inhibition results from reversible adsorption of the "poison", which, in that case, should be rather called inhibitor, as the catalyst regains its original activity after its removal [124]. An inhibitor is not a real poison since it only temporarily competes for active sites [33]. An actual poison is not desorbed; its bonding to the active site is so strong that its desorption rate is negligible under reaction conditions [33,120,123]. The poison gradually neutralizes the catalytic sites along the catalyst bed. In vacuum gasoil hydrocracking, two types of nitrogen molecules can be distinguished: ammonia produced by the hydrodenitrogenation (HDN) reactions and residual organic nitrogen compounds. The residual organic nitrogen compounds in hydrocracking feedstocks can be divided into two families: low-basicity or "neutral" nitrogen compounds, such as pyrrole homologues and basic nitrogen compounds such as pyridine homologues and amines [12,125]. The lightest basic or neutral nitrogen derivatives are readily decomposed into ammonia, which acts as an inhibitor of the cracking reaction. The more basic compounds are cataloged as poisons as they are strongly adsorbed on the acid sites of the catalyst [126]. Furimsky and Masoth [33] identified the inhibition (reversible) and poisoning (irreversible) phenomena, as is showed in Figure 20.

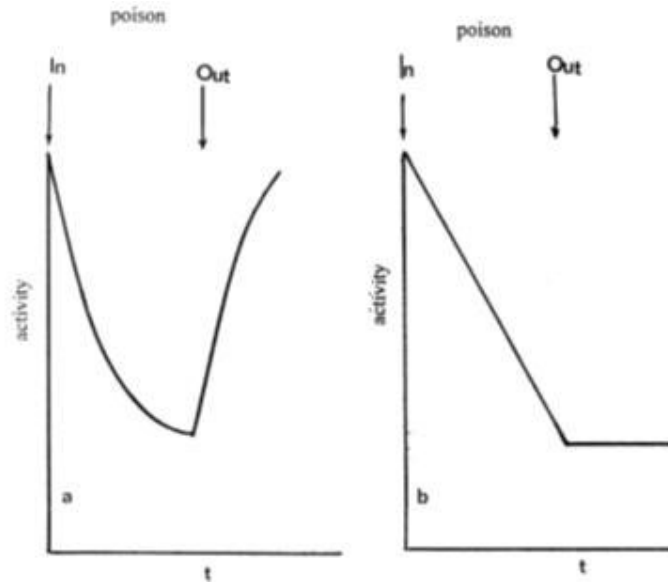


**Figure 20. Activity time profiles for (a) reversible and (b) irreversible poisoning [33].**

In the case of an inhibitor, its effect is transitory and appears in the adsorption (denominator) term of the typical Langmuir-Hinshelwood rate expression given below for a specific reactant A [33].

$$r_A = \frac{k_A f(C_A)}{(1 + K_p C_p + \sum K_i C_i)^n} \quad \text{Equation 9}$$

Where:

- $k_A$  is the rate constant.
- $C_A$  the concentration of A.
- $f(C_A)$ : A particular rate form.
- $K_p$ : the adsorption constant of the poison.
- $C_p$ : poison concentration.
- $K_i$  the adsorption constant of all other adsorbed species on the active sites related to the rate-determining step.
- $C_i$ : concentrations of all other adsorbed species.
- $n$ : Number of active sites involved in the rate-limiting step.

Thus, the main reaction rate is affected by the adsorption strength of all species under the given conditions. Since the effect of the  $K_i C_i$  term is inherent to the reaction, it is always present

(although some or all of the  $K_i$ 's may be sufficiently small to consider their effect as negligible). The presence of a reversible poison further lowers the main reaction rate. Its effect depends upon its concentration and adsorption strength.

As mentioned before, a poison permanently poisons some active sites, resulting in a lower number of active sites available. Thus, it effectively lowers the rate constant rather than appearing in the inhibition term. The rate constant in Equation 9 includes the total number of active sites within the catalyst to transform the reactant A [33].

### *3.1.1.2. Nitrogen Poisoning*

As already stated, the residual organic nitrogen compounds in hydrocracking feedstocks can be divided into two families: low-basicity or "neutral" nitrogen compounds, such as pyrrole homologues and basic nitrogen compounds, such as pyridine homologues and amines [12,125]. The lightest basic or neutral nitrogen derivatives are readily decomposed into ammonia, which acts as an inhibitor in hydroconversion [127]. The more basic compounds are cataloged as poisons as they are strongly adsorbed on the acid sites of the catalyst [126]. The work of Park et al. [128] indicated that, when adsorbed on catalytic sites, N-compounds hinder the adsorption of other reactants and slow down the hydrogen activation process. The availability of active surface hydrogen [129] for the other hydroprocessing reactions and the coke formation is thus limited. Studies on model compounds and real feeds indicate that less than 50 ppm of organic nitrogen in the feed can be responsible for the complete poisoning of the catalytic sites [130].

Nitrogen derivatives are also known to be inhibitors of the active sites of metal sulfides. Inhibition is related to the competitive adsorption between nitrogen compounds and sulfur molecules for the catalyst active sites [131–133]. Compared to sulfur compounds, such as dibenzothiophene (DBT) and 4,6-dimethyl-dibenzothiophene (4,6-DMDBT), nitrogen compounds show higher

adsorption constants on NiW/Al<sub>2</sub>O<sub>3</sub> catalyst surfaces [134]. Besides, the nitrogen inhibiting effect on HDS is related mainly to the concentration and the type of nitrogen compounds in the feedstock. The adsorption energies on the metal sites of a NiMoS catalyst decrease in the following order aza-arene compounds > ammonia > pyrrole derivatives. Thus, pyrrole derivatives are weaker from the adsorption point than aza-arene compounds [11]. The HDS of gas oil has been reported to increase around 60% after removing nitrogen compounds from the feedstock [135]. In the case of diesel hydrotreating, neutral nitrogen compounds are the most abundant nitrogen-containing species. These compounds are transformed into basic ones during the hydrotreating process, resulting in a marked inhibition related to the HDS of prehydrotreated distillates [136,137].

It is known that adsorbed N-compounds act as coking precursors; there are several studies about it. On spent hydrotreating catalysts, Furimsky [33,138] observed an increase in the nitrogen content of coke during the time on stream, which suggests preferential deposition of N-containing species. Choi et al. [9] identified a series of quinolines and amides adsorbed on the catalyst surface. Satterfield et al. [139] observed that intermediates formed during HDN of quinoline leave some deposits on the catalyst surface. Wiwel et al. [140] discussed the specific coking from nitrogen-containing compounds during deactivation. Adkins et al. [141] reported that the coke distribution derived from coal processing contains nitrogen. Muegge and Massoth [142] studied the effect of using either a vacuum gas oil or anthracene (AN) on hydrotreating catalyst deactivation. The authors found that hydrodenitrogenation was substantially lower for the VGO-coked catalysts than the AN-coked catalyst, which was partly attributed to the presence of nitrogen on the catalyst surface. All these observations support the fact that a substantial part of the coke deposits originates from N-containing species.

The effect of N-compounds on coke formation is attributed to the strong adsorption of the N-compounds on the catalyst surface compared with other hydrocarbon structures present in the feed. With a longer time on stream, the adsorbed species are converted to coke. Furimsky [33] suggested that in hydrotreating catalysts, the N-compound is initially adsorbed either by the interaction of the nitrogen atom electron pair with a Lewis site or by its ability to remove protons from the catalyst surface. Zeuthen et al. [143,144] have reported two types of nitrogen deposits on the catalyst surface according to their TPO studies: the first one (low-temperature peak) is associated with the reaction between sulfided catalysts and ammonia [121]. The second nitrogen-type deposits (high-temperature peak) were attributed to strongly adsorbed organic-N species. These species consisted of either strongly adsorbed organic-N species. Zeuthen et al. [145] showed that nitrogen adsorbs preferentially during the initial coke laydown. This is also supported by the high N/C ratios observed in the first stages of operation. Absi-Halabi et al. [146] also found that the N/C ratio decreased with time on stream, indicating that nitrogen was strongly adsorbed at the beginning of the experiment.

In vacuum gas oil (VGO) hydrocracking, little information is available in the open literature on the effects of nitrogen compounds on hydrocracking conversion. Sau et al. [8] studied the inhibition effects of nitrogen on VGO hydrocracking at different temperatures. Results showed a rapid drop in hydrocracking conversion as the nitrogen content increases. This drop became less significant as the nitrogen level increases, probably due to the increasing coverage of the active surface. The higher the reaction temperature, the lower the conversion drop at the same nitrogen content because of the higher desorption rate at elevated temperatures. The HDS activity increased by about 60% after the N-compounds were removed from the VGO through adsorption with silica-alumina, which proved the inhibition of the HDS reaction by nitrogen compounds. Kaernbach et al. [147] also observed a higher HDS conversion in the absence of N-compounds from a

Russian crude, confirming their negative impact on the catalyst (de)hydrogenation activity. The important contribution of N-compounds to catalyst deactivation during the hydroprocessing of a VGO was also confirmed by Massoth et al. [148].

Related to the impact of weakly basic organic nitrogen, Celis et al. [149] carried out a work that consisted of studying the hydrocracking of phenanthrene over a conventional Ni–MoS<sub>2</sub>/Y-zeolite–alumina catalyst as a model reaction. Results showed that the weakly basic nitrogen compounds, carbazole and its partially hydrogenated compound tetrahydrocarbazole, affect the catalytic performance by reducing its activity and inhibiting its selectivity to hydrocracking products. Laredo et al. reported that the inhibiting effect of the non-basic compounds, viz., carbazole, quinoline and indole, is strong, even at a low concentration of 5 ppmw [150].

### 3.1.2. Deactivation by coke

When the adsorbed species polymerize or condense into larger units on the catalyst surface, poisoning loses its meaning; these transformations lead to the so-called coke deactivation [33]. Coking or fouling is the formation process of hydrogen-deficient carbonaceous residues on the catalyst surface. Coke formed on the catalyst physically blocks the access of reactants to the active sites. They firstly cover active sites and as accumulation proceeds, they progressively block the porous structure, leading to catalyst deactivation [9]. An increase in the metal/acid ratio in the catalyst increases the hydrogen content of the coke deposits. On the other hand, the hydrogen content of coke decreases with time on-stream. An increase in support acidity increases coke laydown [151].

Coke formation depends on the type of processed feed. For example, aromatic feedstocks produce more coke than aliphatic ones under similar processing conditions as polyaromatic structures are more easily formed from aromatics compounds [152,153]. Coking is more

pronounced with condensed ring systems (e.g., naphthalene, anthracene) than with the corresponding linked systems (biphenyl, terphenyl) [154,155]. Heterocycles produce more coke than hydrocarbon analogs [33]. For alkyl-substituted aromatics, coke deposition increases with the length of the side chains rather than with the number of alkyl substitutions [155].

Two different mechanisms have been proposed to explain coke formation on the metal and the acid sites of bifunctional catalysts. On metal sites, it is presumed that coke results from successive dehydrogenation reactions leading to atomic carbon or partially hydrogenated intermediates that combine to form a graphitic coke [109,156]. It is difficult to suggest an exact mechanism of coke formation via this route because of the difficulty in distinguishing intermediates on a catalyst surface. However, coke builds up on the catalyst surface due to condensation reactions is the generally accepted mechanism to explain this phenomenon on metal sites, as illustrated in Figure 21 [146]. On acid sites, it is accepted that coke results from polymerization of dehydrogenated intermediates generated on the metal sites [157]. Figure 22 illustrates the proposed mechanism of coke formation from polymerization reactions [158].

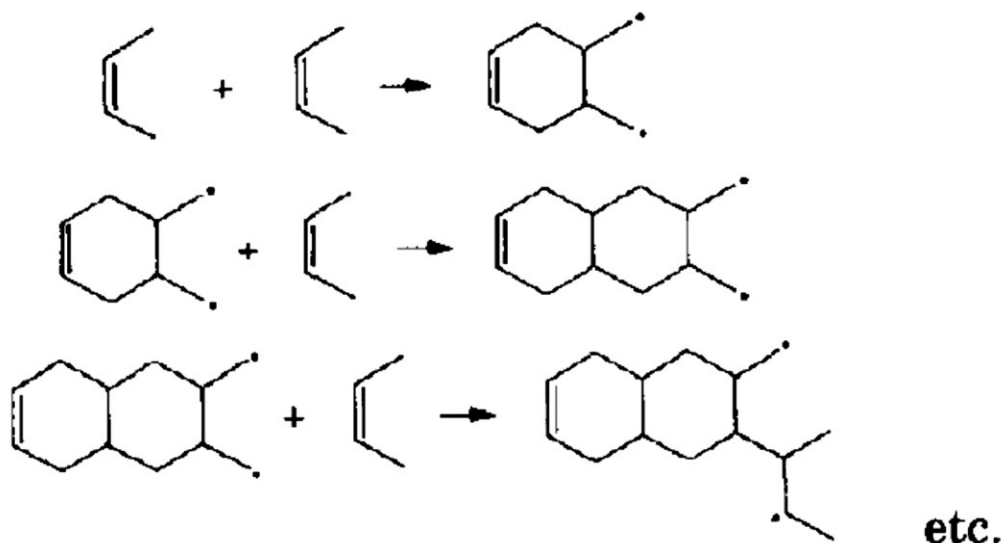


**Figure 21. Proposed mechanism of coke formation by condensation reactions [146].**

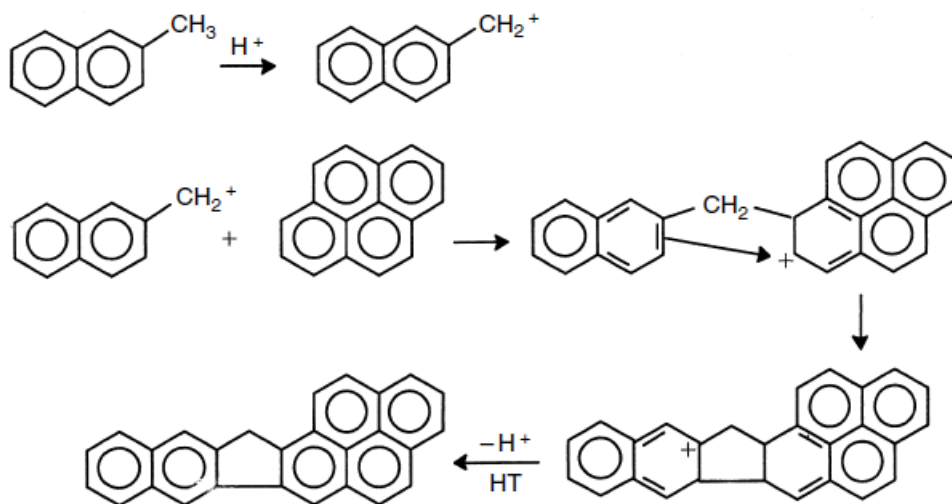


**Figure 22. Mechanism of polymerization involving carbocations [158].**

The deactivation of bifunctional catalysts by coking has been the focus of extensive research. Many of these studies were carried out on reforming catalysts, having a (de)/hydrogenation function (Pt or Pt-Re) and an acid function ( $Al_2O_3$  or chlorinated  $Al_2O_3$ ). Barbier [157] identified two peaks by temperature-programmed combustion of the coke deposits of a spent reforming catalyst, one at around 300°C and the other at around 450°C. According to Barbier, the former was associated with coke on the metallic phase, which accounts for a small portion of the total amount of coke deposited on the whole catalyst. Querini et al. [159] tested an industrial reforming catalyst, Pt/ $Al_2O_3$ , by thermal programmed oxidation (TPO) and reported that coke is firstly deposited on the metal sites and only then on the acid sites. Metal sites coking initially increases with time and then remains constant, while coke on the acid sites increases during the whole run, as illustrated in Figure 23. The coke deposited on the metal function is more dehydrogenated than the coke deposited on the support [160]. Bartholomew [161] claimed that coke precursors might be formed on the metal sites via hydrogenolysis during coke deactivation of reforming catalysts. The unsaturated intermediates then migrate to the support and undergo

polymerization and cyclization reactions, producing larger molecules that can be further dehydrogenated on the metal sites. Finally, they accumulate on the support, causing loss of isomerization activity.

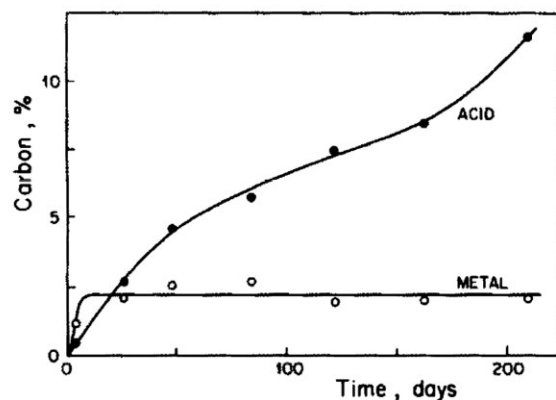


**Figure 23. The concentration of coke deposited on each catalytic function as a function of time in commercial operation [159].**

Regarding studies performed on spent catalysts from VGO hydroprocessing, Sahoo et al. [162] characterized two samples after extraction with dichloromethane. The soluble part was called "soft coke," and its structure corresponds to the heavy components of the VGO used during the runs. The insoluble part, called "hard" coke, was more aromatic. Coke deactivation during the hydroprocessing of atmospheric (ARs) and vacuum residues (VRs) is even harder. Amemiya et al. [163] collected catalyst samples from a VGO hydroprocessing unit after 12 months of operation. These samples were taken from different locations in the axial direction of a single fixed bed. The amount and the graphitic nature of the coke increased toward the end of the bed. Koizumi et al. [164] found an amorphous coke structure on catalyst samples from the bed inlet and a graphitic structure within the bed outlet catalyst.

### 3.1.3. Deactivation by modification of the active phase

The stability of the active phase is essential for maintaining a desirable catalyst lifetime. The temperature seems to be the most important parameter involved in this process [33]. Changes in

catalyst structure have an adverse effect on catalyst activity. These changes are mostly irreversible, thus resulting in a permanent loss of activity [33]. This deactivation can come from the segregation of the promoter and/or sintering of the active phase [165].

Eijsbouts [165] pointed out, as illustrated in Figure 24, the changes of the structure and dispersion of the active phase during the life cycle of a Co-Mo (Ni-Mo)/Al<sub>2</sub>O<sub>3</sub> supported hydrotreating catalyst. In general, after the sulfidation phase, the catalyst in operation evolves. MoS<sub>2</sub> sheets agglomerate and nickel atoms are removed from the active phase to form a separate phase. The detail of the different steps related to the active phase evolution during catalyst lifetime is presented hereinafter.

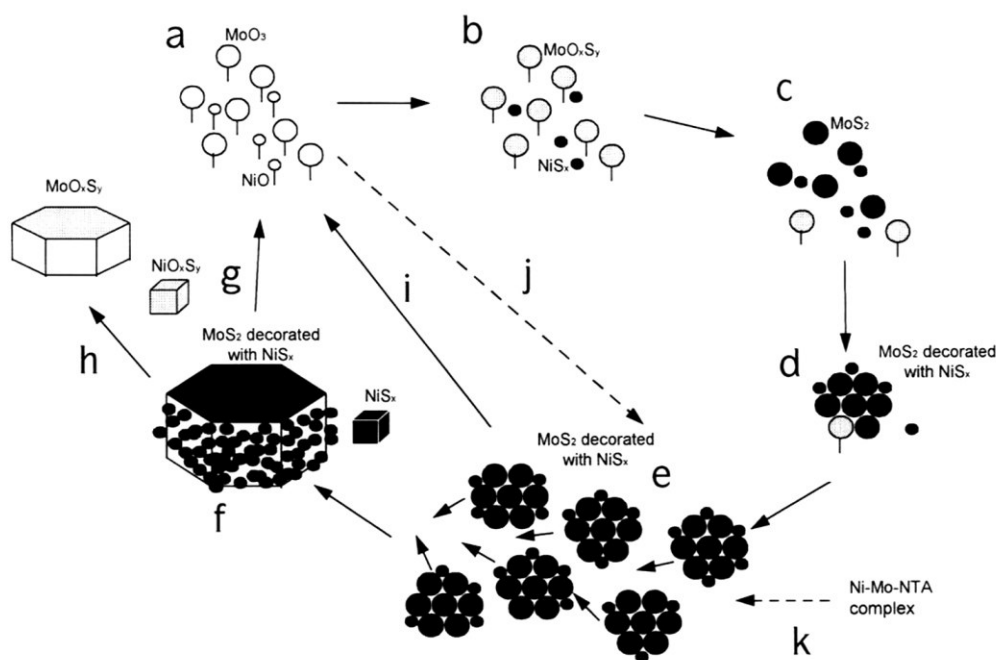


**Figure 24. Sulfided catalyst life cycle [165].**

(a) Oxidic catalyst - oxidic Mo and Ni (or Co) are bound to Al<sub>2</sub>O<sub>3</sub>.

(b) Partly sulfide catalyst - sulfidic Ni (or Co) is no longer linked to Al<sub>2</sub>O<sub>3</sub>, Mo oxysulfide is still bound to Al<sub>2</sub>O<sub>3</sub>.

- (c) Partly sulfided catalyst - part of Mo is no longer bound to  $\text{Al}_2\text{O}_3$ .
- (d) Partly sulfided catalyst - small  $\text{MoS}_2$  slabs decorated with Ni (or Co) is formed; these slabs are still anchored to  $\text{Al}_2\text{O}_3$ .
- (e) Fully sulfided catalyst – Mo gets completely sulfided, so these  $\text{MoS}_2$  slabs decorated with sulfidic Ni (or Co) become mobile.
- (f) Deactivation - small  $\text{MoS}_2$  slabs decorated with sulfidic Ni (or Co) sinter to form larger slabs, stacks and crystals, the edge surface area of these crystals is insufficient to accommodate all of Ni (or Co) so that separate Ni (or Co) sulfide crystals are formed.
- (g) Regeneration -  $\text{MoS}_2$  crystals and some decorating Ni (or Co) sulfide get partly redispersed.
- (h) Regeneration - large Mo  $\text{MoS}_2$  crystals get only oxidized on the surface; Ni (or Co) sulfide crystals cannot redisperse on oxidation.
- (i) Regeneration - small structures get fully oxidized and return nearly to their original state.
- (j) High-temperature sulfidation - Mo gets completely sulfided so rapidly that the intermediate steps can be neglected; (k) NTA preparation route - Ni-Mo-NTA complex gets completely sulfided. No linkages with the support are formed at any stage of the process.

Metal sintering in zeolites is affected by the metal melting point [166]; the higher the melting point of the metal, the lower the mobility of the atoms. For example, under identical conditions and in the same zeolite, the Pd atoms migrate out of a sodalite cage at 200–300°C, compared to 300–600°C in the case of Pt atoms[167]. Sintering is also affected by the nature of the surrounding atmosphere, which may interact with the surface metal atoms, thus increasing their mobility. Pt clusters encaged in the super cages of Y zeolite are stable up to 800°C under vacuum. However, at 320°C in the presence of  $\text{H}_2$  and  $\text{NH}_3$ , migration and sintering are induced [168]. The Mössbauer spectroscopy experimental study carried out by Breysse [151] revealed the loss of part of the mixed-phase of  $\text{CoMo}/\text{Al}_2\text{O}_3$  catalysts in a reducing medium. Nevertheless,

under hydrotreating conditions, the authors did not observe any change in promotion by EXAFS. Thus, the segregation of the promoter seems highly dependent on the operating conditions.

Sintering becomes more important near the end of the cycle when the catalyst is operated at high temperatures [33]. Prolonged exposure at elevated temperatures can lead to irreversible structural changes of the catalyst, causing a permanent activity loss. These may include sintering or segregation of the active phase, diffusion of active metals to the support and/or recrystallization of the metal phases [119,165,169].

High-temperature sulfiding has been employed in laboratory tests [169,170] to obtain information on the structural and morphological changes that may occur during long-term industrial use. The changes in the Co-phase distribution were followed by in-situ Mossbauer emission spectroscopy [169]. The results show that upon increasing the sulfiding temperature, cobalt typically segregates out of the alumina to form  $\text{Co}_9\text{S}_8$  [169,171]. Changes in the amount of Co-Mo-S may also take place during high-temperature sulfiding. This is due to the sintering of  $\text{MoS}_2$  and loss of edge surface area necessary for accommodating the Co edge atoms. After edge saturation has been reached,  $\text{Co}_9\text{S}_8$  may be formed from the remaining Co atoms, which can no longer be accommodated. Consequently, Co-Mo-S concentration depends strongly, among other parameters, on the initial Co edge concentration [169,170]. For high initial Co edge concentrations, Co segregation occurs at lower temperatures (lower extent of sintering of the  $\text{MoS}_2$  phase) than at low Co edge concentrations.

A study published by Makishima et al. [172] attributed the cause of deactivation to a decrease in the Ni/W ratio accompanied by lateral growth of  $\text{WS}_2$  crystallites. Similarly, Eijsbouts et al. [173] reported that lateral growth of  $\text{MoS}_2$ -like structures was one of the main causes of catalyst deactivation with hydrotreating industrial feeds, such as brown coal-derived oils. Upon

regeneration, the large MoS<sub>2</sub>-like structures were found to redisperse to regain the fresh catalyst level [173].

The structural features of the active phases in hydroprocessing vacuum gas oil catalysts have been recently investigated [169]. As the severity of the operation is increased, similar changes as those observed by increasing the sulfiding temperature were noticed [169]. Specifically, the edge dispersion of the MoS<sub>2</sub> phase decreases upon aging of the catalysts, resulting in the release of Co from the edge sites [169].

Guichard et al. [174] analyzed spent (Ni(Co)MoP/Al<sub>2</sub>O<sub>3</sub>) catalysts from gas oils hydrotreatment industrial and pilot plant units and found that the active phase is strongly modified by aging. EXAFS and EDX measurements carried out in this work show a significant decrease in NiMoS sites caused by segregation of the promoter, especially at short lifetimes. They also noted a strong correlation between the promotion rate and the hydrogenation activity, which was not observed in the case of hydrogenolysis.

In summary, most authors agree that deactivation by coke and nitrogen compounds are the most important mechanisms in the deactivation of hydrocracking catalysts when processing complex feedstocks such as VGO. Therefore, to correlate the loss of activity with these mechanisms, it is necessary to evaluate the amount of coke deposited and its nature and composition. It is also essential to have information on the type of nitrogenous molecules within the feed, as these molecules strongly chemisorb on the catalyst active surface, leading to catalyst inhibition and/or deactivation. Finally, for the metallic phase, the phase modification effect must be taken into account since there is an agreement on its particular role on deactivation, especially at high temperatures, as is the case of accelerated protocols in which the catalyst is subjected to more severe operating conditions.

## 3.2. Effect of different operating parameters on deactivation

### 3.2.1. Effect of operating conditions

Coke formation and deposition occur at relatively low rates under typical hydrocracking reaction conditions. However, under unfavorable conditions, high coking rates can lead to catastrophic failure of the catalyst and reactor voids plugging, resulting in unit shut down within hours. Temperature is one key operating variable for accelerating deactivation, as shown by many literature studies [33,123,146] (Figure 25). It is well known that poly-aromatic or even graphitic compounds are formed and deactivate catalysts through the carbonaceous compounds deposition at high temperatures. The coke yield increases with time on-stream. The hydrogen content of coke obtained from aliphatic compounds decreases with increasing reaction temperature<sup>1</sup> and time on-stream. Coke aromaticity follows the inverse order, thus increasing with both temperature and time on stream.

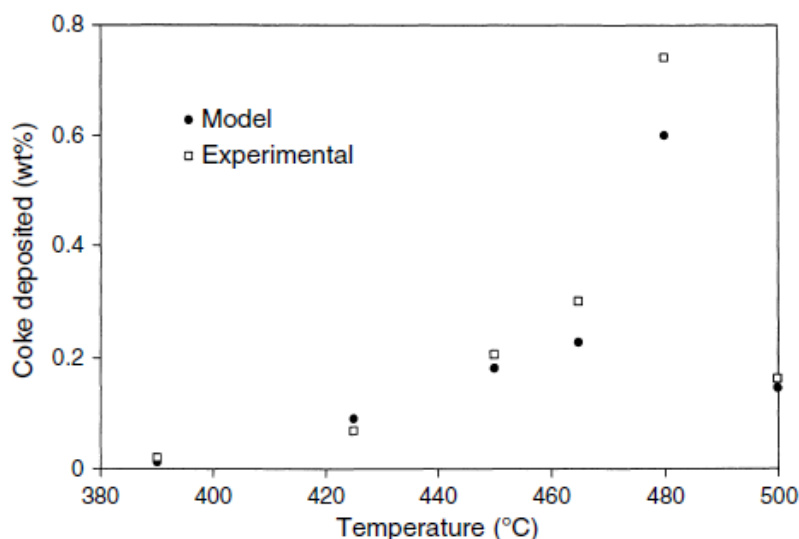


Figure 25. Effect of temperature on coke deposition (VGO, CoMo/Al<sub>2</sub>O<sub>3</sub>) [175].

Dong et al. [148] studied the influence of N-compounds in VGO along with the increase in temperature on catalyst deactivation and observed that the higher the temperature, the higher the coke deposition. This observation can be attributed to a decrease in the coke precursors saturation rate as temperature increases [33]. Figure 26 illustrates the evolution of the coke production rate with temperature. Three main regimes can be identified. The coke build-up below 375°C could be attributed to the slow conversion of heavy species in the feed. Consequently, the residence time of these molecules on the active surface increases, thus increasing the probability of polymerization. Beyond 375°C, the rate of coke precursors hydrogenation becomes comparable with polymerization. Moreover, the residence time of coke precursors on active sites decreases as conversion increases, leading to a global slowing down of the coking rate[176]. Above 440°C, the coke build-up strongly increased, which can be attributed to thermal effects.

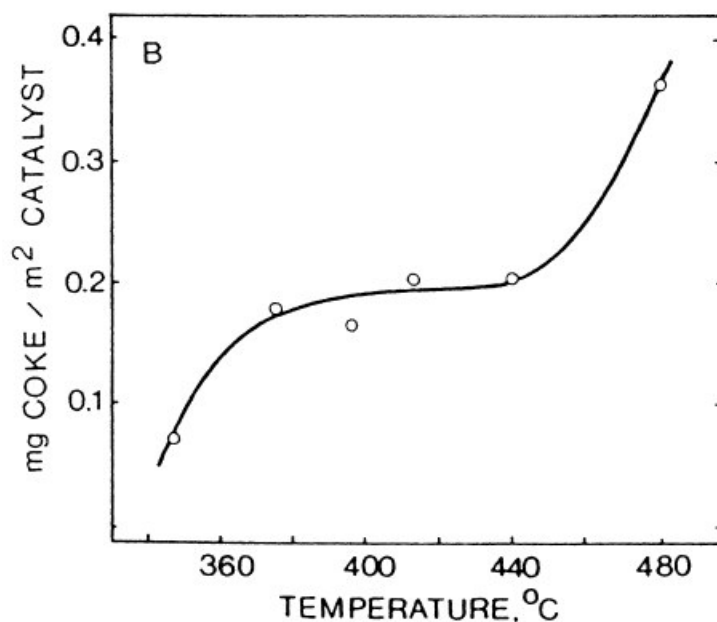


Figure 26. Effect of temperature on catalyst coke [177].

Hydrogen partial pressure directly affects the hydrogenation of the feedstock's unsaturated compounds and the hydrocarbon cracking rate. The hydrogen pressure is another parameter for

controlling coke formation, as suggested by Figure 27 [9]. An increase in hydrogen partial pressure increases the rate of aromatics hydrogenation. Hydrogen partial pressure has a dual effect on catalytic cracking and isomerization. On the one hand, an increase in pressure has a favorable effect due to an enhancement in the hydrogenation of coke precursors and to catalyst surface cleaning. On the other hand, the rate of cracking and isomerization reactions decreases when hydrogen partial pressure increases, thus increasing the residence time of the molecules on the active sites. The relative importance of the previous antagonist effects strongly depends on the processed feedstock [49]. Thus, the first effect becomes crucial when aromatic feedstocks are processed, whereas when processing paraffinic, low-coke-forming feedstock, the second effect predominate.

Richardson et al. [178] used Athabasca bitumen to study the hydrogen pressure effect on the initial coke formation (between 1.5 and 5 h on stream) in an autoclave CSTR reactor using a commercial NiMo/Al<sub>2</sub>O<sub>3</sub> catalyst at 703 K. After a rapid coke build-up during the first hour of operation; the coke formation did not change with an increase on the feed to catalyst ratio. Simultaneously, increasing H<sub>2</sub> pressure from 7 to more than 15 MPa decreased the amount of coke from about 17 to about 11 wt%. Gualda and Kasztelan [179] found that the amount of coke decreased from about 10 to 4 wt% by increasing the H<sub>2</sub> pressure from 2 to 15 MPa during atmospheric residue hydroprocessing. Moreover, the hydrogen pressure was found to have a pronounced effect on the H/C ratio of coke on the catalyst.

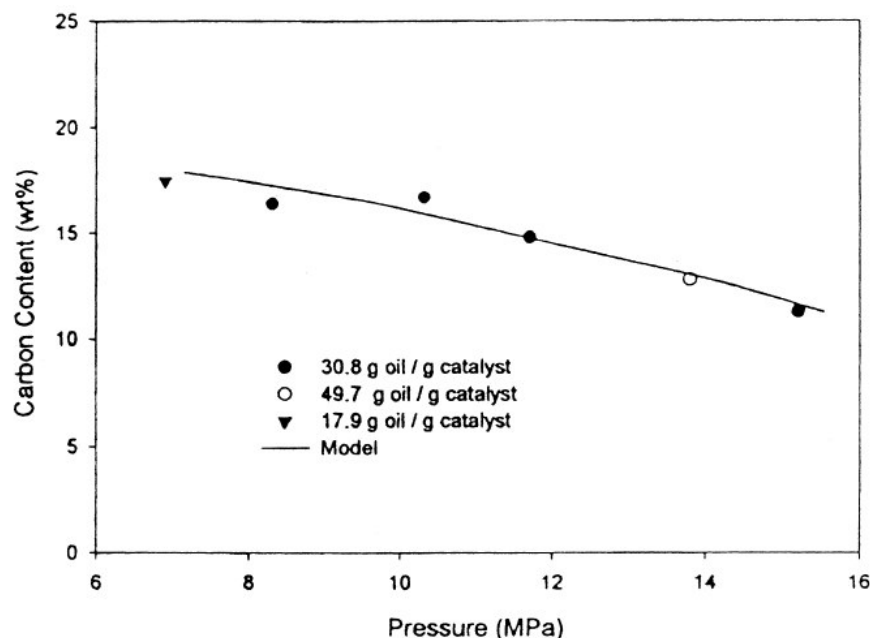


Figure 27. Catalyst carbon content as a function of hydrogen pressure (NiMo/Al<sub>2</sub>O<sub>3</sub>, 430°C).

### 3.2.2. Effect of feedstock on deactivation

The reactivity of a given feedstock for hydrocracking is a strong function of its related composition and properties. Highly paraffinic feeds require high temperatures in hydrocracking as normal paraffins are difficult to crack. However, they do not significantly contribute to catalyst deactivation, as these molecules have a low tendency to form coke. Aromatic feeds tend to deposit coke on the catalyst surface, thus promoting catalyst deactivation [9]. The feedstock composition also affects both coke yield and composition. In general, coking increases with the molecular weight/boiling point of the fraction to be processed [146].

Among the aromatics compounds, polynuclear aromatic compounds (PNAs) are the major coke precursors. The PNAs are polycyclic, condensed hydrocarbons that contain two or more fused aromatic rings. The light PNAs, with two to six rings, are present in straight-run VGO. Their concentration increases during the hydrocracking process [11]. Wiwel et al. [180] obtained a

correlation between the coking propensity of the feed and the PNA content in the feed. This correlation is illustrated in Figure 28.

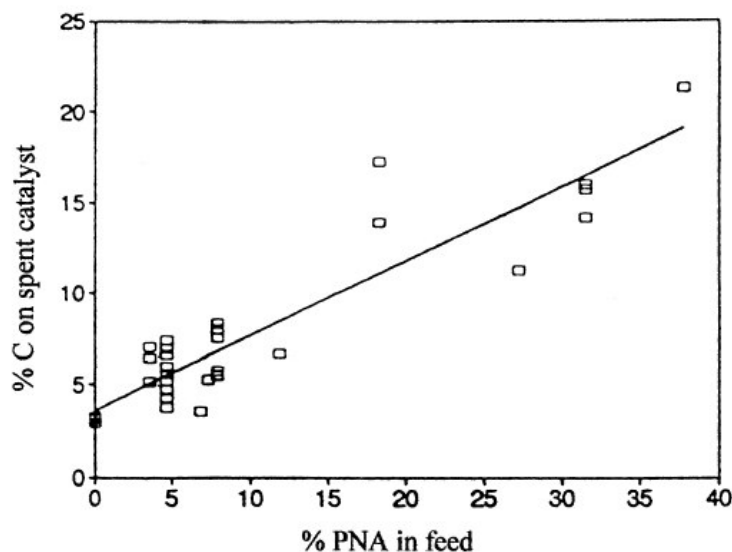


**Figure 28. Effect of the feed content of PNA on the amount of coke on the catalyst [180].**

Olefins, acting as hydrogen acceptors, promote coke formation by removing hydrogen from coke precursors [9]. Furthermore, it has been reported that coke formation occurs more rapidly when a hydrogen acceptor, such as an olefin, is present, in line with the hypothesis of a carbonium ion chemistry during coke formation [33].

### 3.3. Approaches for catalyst deactivation study

The deactivation of hydrocracking and, in general, hydroprocessing catalysts, under typical industrial operating conditions, occurs slowly. Depending on the feed and operation severity, cycle lengths can vary from a few months to as much as one or two years [6,7,181]. Catalyst deactivation is unavoidable; however, it can be retarded [6,182,183]. The comprehension of the deactivation phenomena is fundamental to design more stable catalysts. Ideally, catalyst deactivation should be studied under industrially relevant conditions. However, it is difficult to replicate these conditions in laboratory experiments since, as mentioned, the cycle duration can

be very long [119,184,185]. Hence commonly, there are two main strategies to study catalyst deactivation. The first one consists of examining samples withdrawn from an industrial unit to determine coke and/or metal deposition effects on catalyst properties. This approach has, for instance, been applied to the hydroprocessing of diesel, VGO and vacuum residue [11,186]. However, this method may not give sufficient insight into deactivation phenomena as feed and operating conditions continuously change during industrial operation. Thus, linking these parameters to the degree of deactivation becomes tricky. Besides, as samples are withdrawn once during the cycle length, the deactivation evolution with time on stream cannot be assessed. An alternative approach is to test the catalysts in the laboratory under accelerated conditions [187]. More specifically, this approach consists of submitting the catalyst to reaction conditions that strongly promote catalyst deactivation. The main challenge is to obtain a similar deactivation pattern as the one observed for the catalytic system under typical industrial conditions within a shorter time scale [67,70,188,189]. The accelerated methodology allows a kinetic evaluation [70,83], based on the activity loss between the beginning and the end of the experiment, to be performed. Moreover, spent catalysts detailed characterization can be carried out for evaluating the changes in the catalyst properties [8].

Several authors have investigated the deactivation phenomena based on accelerated protocols using model molecules or real feedstocks. Regarding experiments with model molecules, Muegge et al. [142] studied the effect of the coke produced from a model coke precursor, anthracene, on the physical properties and intrinsic activity of a Ni-Mo catalyst. Zeuthen et al. [143] carried out experiments with model compounds, ethyl carbazole, pyrene and anthracene, for coking NiMoP catalysts. The authors reported different types of nitrogen species within the coke from model molecules and real feeds. In turn, Guichard et al. [83] evaluated some Ni(Co)MoP catalysts aged with anthracene and phenyl-carbazole and found an amount and

aromaticity of coke not representative of industrial spent catalysts. Dujardin evaluated hydrocracking catalysts stability using n-heptane but only identified soft coke in the spent samples [190]. The selection of the model molecules is very complex and hardly represents the performance obtained with real feeds. Therefore, the deactivation mechanisms observed in both cases are different.

Concerning works with real feedstocks, Figoli [191] studied platinum catalysts deactivation. An accelerated deactivation experimental procedure consisting of the following steps was developed for studying naphtha reforming catalyst deactivation: 10 h under typical reforming conditions to obtain a RON of 95, then 10 h at a lower hydrogen pressure to obtain rapid coke deposition, and finally 10 h where the temperature was increased until the RON of the first period was reached. With this protocol, a coke of similar nature to the one produced in a commercial plant was obtained.

Weissman and Edwards [192] exposed commercial NiMo/Al<sub>2</sub>O<sub>3</sub> and CoMo/Al<sub>2</sub>O<sub>3</sub> catalysts to differing cycles length and severity using various naphtha and gas oil feeds. The formed carbon on these catalysts was less condensed than the one related to the deposits collected over a much longer time from similar feeds. Tanaka et al. [183] performed accelerated deactivation tests with a laboratory prepared CoMo/Al<sub>2</sub>O<sub>3</sub> catalyst using a VGO under high severity conditions. They obtained a catalyst with a very high carbonaceous deposition which does not fully represent industrial deactivation. Vogelaar et al. [119] submitted some catalysts used in hydroprocessing of diesel, vacuum gas oil and vacuum residue to more severe conditions to accelerate the deactivation process. Characterization results for spent samples from the accelerated deactivation procedure and normal cycles were compared. The catalyst deactivated more during the normal cycle than during the artificial aging run. This was attributed to the strong

sintering related to the catalyst from the accelerated deactivation, which was the primary cause of deactivation, whereas coking was identified as the main mechanism of catalyst deactivation during the normal cycle.

Ahmed et al. [193] studied catalyst deactivation during vacuum residue hydrocracking at a high temperature to accelerate activity loss. During the test, large quantities of carbon deposited on the catalyst with high aromaticity were identified. This was attributed to the decreased hydrogenation activity of the catalyst due to coke and metal deposition on the sulfide nanoparticles.

More recently, Pacheco et al. [70] applied an accelerated deactivation methodology to study catalyst deactivation by coke deposition on commercial HDT catalysts. This study focused on mimicking the decrease of the kinetic constants for HDS, HDN and HDA reactions as deactivation proceeds. They claimed that the residual catalyst activities were similar to those obtained at the end of industrial cycles and concluded that the accelerated deactivation methodology led to proper representation of actual industrial data. All of these examples illustrate that it is challenging to mimic the industrial life cycle of a catalyst at the laboratory scale, mostly when much more severe conditions are used [119].

#### **4. LITERATURE REVIEW CONCLUSION**

This section aimed to trace the drivers responsible for bifunctional catalysts deactivation during VGO hydroprocessing based on the information from the literature review. It has been found that deactivation related to this type of feed has two leading causes: poisoning by nitrogen compounds and coke deposition. Most authors agree that the change in coke deposition rate is linked to operating conditions and the molecules that give rise to the coke formation. Coke

precursors are mainly nitrogen compounds and aromatics, especially those with two or more rings. Therefore, it is clear that the physicochemical nature of the feed has a significant influence on the coke deposition and hence on catalyst deactivation.

Considering that the performance of hydrocracking catalysts results from the relative strength of both acid and metal functions, the mechanisms of the deactivation for both functions were reviewed. According to different authors, it could be argued that acid function is deactivated mainly by coke deposition and loss of acid sites because of the strong adsorption of nitrogen compounds. Meanwhile, the metal function is deactivated by coke deposition and changes in the active phase. Nitrogen compounds inhibit both functions.

Many works have been carried out on the study of catalyst deactivation using methodologies to accelerate this phenomenon. Some of them used model molecules that do not fully represent the deactivation pattern obtained with a real feed. Therefore, deactivation mechanisms in both cases are expected to be different. Regarding the use of real feeds, the studies presented clearly show the difficulty of reproducing the deactivation of a catalyst in the laboratory in a representative way, especially when the operating conditions used at the pilot level are far from the industrial ones. However, some strategies allowing the deactivation phenomena to be accelerated have been derived from these studies, such as the use of higher temperatures, lower hydrogen pressures, or more complex feedstocks. Most of these studies have been implemented for hydroprocessing catalysts or bifunctional catalysts based on noble metals. No significant information was found in the case of bifunctional catalysts consisting of a sulfide metal.

Therefore, a comprehensive study consisting of developing an accelerated deactivation protocol with real feedstocks to understand the loss of activity of a NiMoP/USY catalyst during VGO hydrocracking is carried out. The application of this protocol with two different feeds allows to

establish the impact of the feed properties on the deactivation of these catalysts. The same experimental protocol was also used to assess the impact of decreasing the catalyst metal content on the deactivation rate. This study contemplates evaluating the kinetic constants evolution of the main hydrocracking reactions with time, as well as the detailed characterization of the spent catalysts in a coupled way.

**CHAPTER 2**  
**Insights in the phenomena**  
**involved in deactivation of**  
**industrial hydrocracking**  
**catalysts through an**  
**accelerated deactivation**  
**protocol**

---

# Chapter 2-Insights in the phenomena involved in deactivation of industrial hydrocracking catalysts through an accelerated deactivation protocol

---

## CHAPTER 2-INSIGHTS IN THE PHENOMENA INVOLVED IN DEACTIVATION OF INDUSTRIAL HYDROCRACKING CATALYSTS THROUGH AN ACCELERATED DEACTIVATION PROTOCOL

Publication accepted in Fuel Journal: <https://doi.org/10.1016/j.fuel.2021.120681>

### ABSTRACT

A representative accelerated experimental deactivation procedure was developed to understand the activity loss of bifunctional vacuum gasoil (VGO) hydrocracking catalysts over time. Experiments were performed in an up-flow fixed-bed pilot unit with a typical vacuum gas oil feedstock. The deactivation was measured by tracking the decrease of VGO conversion ( $370^{\circ}\text{C}^+$ ) with time on stream. The catalyst consisted of nickel-molybdenum sulfide particles dispersed on a carrier containing USY zeolite. The impact of temperature, liquid hourly space velocity (LHSV), hydrogen to hydrocarbon ( $\text{H}_2/\text{HC}$ ) ratio and organic nitrogen ( $\text{N}_{\text{org}}$ ) on the catalyst deactivation rate was first studied. The variables with the most significant impact on conversion loss were temperature and space velocity. Temperature directly influences the production rate of coke precursors, whereas space velocity affects the local concentration of feed contaminants along the reactor. Based on these results, the following operating conditions were selected to establish the final accelerated deactivation experimental protocol:  $T=418^{\circ}\text{C}$ ,  $\text{LHSV}=3\text{ h}^{-1}$ ,  $\text{H}_2/\text{HC}=1500\text{NL/L}$ ,  $P=14\text{ MPa}$ , organic nitrogen content ( $\text{N}_{\text{org}}$ )=150 ppm weight, total nitrogen content=2500 ppm weight and a total time on stream of 30 days. Spent samples from this procedure presented similar properties to some industrial catalysts submitted to cycle lengths between 12 and 18 months. Both types of samples yield similar values of surface area and pore volume loss as well as a similar amount and nature of coke deposits. These results led to the qualitative validation of the protocol representativeness. This experimental procedure was

## Chapter 2-Insights in the phenomena involved in deactivation of industrial hydrocracking catalysts through an accelerated deactivation protocol

---

then used to get more insight into the deactivation phenomenon. It was found that the organic nitrogen content of the feedstock is crucial, as it determines the ratio between available metal and acid sites. This ratio determines the reactions that take place and, therefore, the type of coke produced.

**Keywords:** deactivation, hydrocracking, coking, vacuum gasoil.

### 1. INTRODUCTION

Hydrocracking is one of the most flexible refining processes for converting heavy high-boiling feedstock molecules into smaller lower-boiling products. Hydrocracking processes are operated at high pressure, 8.5-20 MPa, and moderate temperature, 350-450°C, to promote hydrocracking reactions. A large excess of hydrogen, 500-1700 NL/L hydrogen to oil ratio ( $H_2/HC$ ), is fed to the reactor to improve liquid yield and limit catalyst deactivation. Low values of LHSV, 0.5-2.5  $h^{-1}$ , are required depending on feed nature and complexity [125]. The feedstocks used in hydrocracking processes contain sulfur, nitrogen and, in the case of residue feedstocks, metals such as nickel and vanadium [125]. Due to the deleterious effect of these compounds on hydrocracking catalysts, the hydrocracking process is carried out in two consecutive stages: (i) in the first stage, the feedstock is hydrotreated and partially hydrogenated on a hydrotreating catalyst. The main chemical reactions for hydrotreating and hydrogenation of the feedstock are hydrodesulfurization (HDS), hydrodenitrogenation (HDN), hydrodeoxygenation (HDO), olefin hydrogenation and partial aromatics hydrogenation. (ii) In the second stage, the hydrotreated feed is hydrocracked on a hydrocracking catalyst [194]. This work focuses on the deactivation phenomena related to the catalyst of the second stage of a typical hydrocracking process.

## Chapter 2-Insights in the phenomena involved in deactivation of industrial hydrocracking catalysts through an accelerated deactivation protocol

---

Hydrocracking catalyst deactivation under typical industrial operating conditions occurs slowly, depending on feed and operation severity. Cycle lengths can vary between a few months and up to one or two years [6,7,181]. One cycle involves the processing of approximately 5000 tons of feed per ton of catalyst [195]. The loss of activity determines the length of an operation cycle and, consequently, profitability [7]. Catalyst deactivation is inevitable, but it can be slowed down [6,182,183]. Understanding the deactivation phenomena is fundamental for the design of more stable catalysts.

Based on the literature on catalyst deactivation related to several refinery applications such as hydrotreating, heavy oil hydroprocessing, and catalytic reforming, two main approaches for studying this complex phenomenon can be distinguished. The first one is based on the characterization of industrial-spent catalyst samples to link coke or metal deposition to catalyst deactivation. This approach has, for instance, been applied to the hydroprocessing of diesel, vacuum gasoil (VGO) and vacuum residue [11,186]. Understanding deactivation phenomena through this specific approach is limited as feed and operating conditions continuously change during industrial operation. This approach does not allow to link these parameters to the extent of deactivation, as the spent catalyst is characterized only once at the end of the industrial cycle. Another approach could consist of performing experiments at equivalent industrial conditions in the laboratory [67]. This approach can be expensive and time-consuming, as industrial cycle lengths can be up to two years. Hence, the development of accelerated deactivation procedures, which is the second approach for studying deactivation, appears as an instrument capable of providing relevant information on the deactivation phenomena in a reduced time [67,70]. Accelerated deactivation consists of submitting the catalyst to specific reaction conditions that strongly promote deactivation [83]. On the one hand, the accelerated methodology allows

## Chapter 2-Insights in the phenomena involved in deactivation of industrial hydrocracking catalysts through an accelerated deactivation protocol

---

performing a kinetic evaluation [70,83] based on the activity loss between the beginning and the end of the operation. And on the other hand, this methodology includes the detailed characterization of the deactivated catalysts, which is more valuable for assessing the changes in catalyst properties [8].

The specific deactivation mechanisms of vacuum gasoil (VGO) hydrocracking catalysts are now addressed. The industrial catalysts are bifunctional, i.e., composed of metal sulfide nanoparticles (de/hydrogenation function) deposited on an acidic support (isomerization and cracking function). This catalyst is continuously deactivated in the presence of hydrocarbon feedstocks under typical hydrocracking process operating conditions. The primary sources of deactivation are coke formation and quasi-irreversible poisoning by heavy nitrogen molecules [8,12]. These phenomena depend on feedstock, operating conditions and catalyst properties such as catalyst acidity, nature of the sulfide phase and support porosity [119]. The coke formation is related to polymerization precursors like polynuclear aromatics and cyclic molecules containing heteroatoms [8,11]. Both metal sulfide nanoparticles and acid sites are deactivated by coke deposition [8]. Other deactivation mechanisms can also occur as sintering and de-promotion of the sulfide nanoparticles and strong adsorption (almost irreversible) of nitrogen compounds [8,119,125,190] (that can act as temporary poisons [12]) on the acid sites.

Nitrogen compounds can act as inhibitors or poisons, depending on their structure and properties. Poisoning refers to the strong chemisorption of reactants, products, or impurities on active sites that would normally be available for catalysis in the absence of these poison compounds. Inhibition results from the reversible adsorption of a given nitrogen compound. The main difference between both mechanisms is that, in the case of inhibition, the catalyst regains its original activity after inhibitor removal from the feedstock. Thus, an inhibitor is not a real

## Chapter 2-Insights in the phenomena involved in deactivation of industrial hydrocracking catalysts through an accelerated deactivation protocol

---

poison since it only temporarily competes for active sites. An actual poison is not desorbed; its bonding to the active site is so strong that its desorption rate is negligible under reaction conditions [8,11]. The poison gradually neutralizes the catalytic sites along the catalyst bed. In vacuum gasoil hydrocracking, two types of nitrogen molecules can be distinguished: ammonia produced by the hydrodenitrogenation (HDN) reactions and residual organic nitrogen compounds. The residual organic nitrogen compounds in hydrocracking feedstocks can be divided into two families: low-basicity or "neutral" nitrogen compounds, such as pyrrole homologues, and basic nitrogen compounds such as pyridine homologues and amines [12,125]. The lightest basic or neutral nitrogen derivatives are readily decomposed into ammonia, which acts as an inhibitor of the cracking reaction, whereas the more basic compounds are cataloged as poisons as they are strongly adsorbed on the acid sites of the catalyst [126].

Regarding coking, a major part of the studies in literature, for instance, the works of Muegge [196,197], Zeuthen [198], and Guichard [174], was carried out by using model molecules. The selected molecules were not fully representative of the real components of the industrial feed, and the deactivation mechanisms were different from those in real feeds. In the case of hydrocracking catalysts, Dujardin [190] only identified "soft coke" (high H/C ratio) in the spent catalysts as the deactivation experiments were performed with n-heptane.

Concerning works with real feedstocks, Tanaka et al. [183] conducted tests with VGO under high severity conditions to evaluate coke deposition effects on the hydrotreating process. They concluded that a higher temperature and a heavier feed resulted in a serious carbonaceous deposition, which did not fully represent industrial deactivation. Ahmed et al. [193] studied the loss of catalyst activity during the hydrocracking of a vacuum residue under accelerated deactivation conditions. A high reaction temperature was imposed for catalyst accelerated aging,

## Chapter 2-Insights in the phenomena involved in deactivation of industrial hydrocracking catalysts through an accelerated deactivation protocol

---

resulting in large amounts of carbonaceous deposits with high aromaticity. This result was attributed to a decrease in the hydrogenation activity of the catalyst due to coke and metal deposition on sulfide nanoparticles. Figoli [191] studied the deactivation of a Pt-catalyst during naphtha reforming through a protocol that consisted of the three following stages: 10 h under typical reforming conditions to obtain a RON of 95, then 10 h at a lower hydrogen pressure to obtain rapid coke deposition and finally 10 h where the temperature was increased until the RON of the first stage was reached. With this protocol, a coke of similar nature as the one produced in a commercial plant was obtained.

To the best of our knowledge, a representative experimental procedure for studying this phenomenon is missing in that specific case. The first objective of this work was to develop an accelerated deactivation protocol to study the deactivation phenomena under representative conditions of the industrial operation. Aged catalysts from this procedure were characterized for the determination of their porosity, the quantity and nature of coke deposits and the residual activity of their two catalytic functions, acid and metal. The results were compared to the characterization results of industrial spent catalysts for the qualitative validation of the accelerated deactivation procedure. The second and final aim of this study was to get insights into the VGO hydrocracking catalysts deactivation phenomenon itself through this specific experimental procedure.

# Chapter 2-Insights in the phenomena involved in deactivation of industrial hydrocracking catalysts through an accelerated deactivation protocol

---

## 2. EXPERIMENTAL SECTION

### 2.1. Pilot unit description and operating procedure

#### 2.1.1. Pilot unit description

The experiments were carried out in a fixed bed pilot unit with a co-current gas-liquid mixture flowing upwards to ensure complete catalyst wetting. The flow diagram of the unit is shown in Figure 29. The unit consists of a feed, a reaction and separation sections with an online chromatograph for determining the outlet gas stream composition. The feed section consists of a storage tank filled with the process feed and pressurized with nitrogen. The content of this storage tank was transferred to a smaller intermediate tank employing a pump. The feed flow rate was controlled based on the decrease in weight measured by a balance on which the intermediate tank was supported. The feedstock was injected into the reactor using a positive displacement pump. A mass flowmeter-controlled hydrogen flow. Feed and hydrogen were mixed upstream of the reaction section and flowed concurrently in an upflow configuration. The pilot unit has two tubular reactors in series (R1 and R2 in the figure below). Each reactor was placed within a furnace presenting three independent heating zones. Each zone was equipped with internal and external thermocouples to ensure isothermal conditions (the thermal profile was measured at the beginning of the test in which the screening of the operating variables was performed – see section 2.3.1). The two reactors were used for the hydrocracking process; or in other words, the feed used in this work was hydrotreated ex-situ.

Additionally, a sampling system allowing the liquid phase effluent from the first reactor to be collected and analyzed was placed between the two reactors. The samples taken at this point contained some dissolved gases, including hydrogen sulfide and ammonia. Therefore, these

## Chapter 2-Insights in the phenomena involved in deactivation of industrial hydrocracking catalysts through an accelerated deactivation protocol

---

samples were washed with water to eliminate these gases, allowing their properties to be accurately measured. To calculate the net conversion obtained in the first reactor, the gas formation was estimated from the correlation established between both gas and liquid yields. The effluent of the second reactor was then sent to the separation section. This section comprises a high-pressure flash separator for gas/liquid separation. The gas-phase was continuously recovered at the top of the separator under pressure control. The gas effluent was transferred to a gas flowmeter, and a sample was taken for online gas chromatographic analysis. The liquid product was continuously recovered at the bottom of the separator, under level control, and sent to a low-pressure hydrogen stripper. The stripper conditions were adjusted for removing the residual hydrogen sulfide and ammonia dissolved in the products. The stripped product was finally sent to a storage recipient equipped with a balance to quantify the amount of product obtained. Liquid products were characterized by density, refraction index, nitrogen and sulfur content and simulated distillation.

## Chapter 2-Insights in the phenomena involved in deactivation of industrial hydrocracking catalysts through an accelerated deactivation protocol

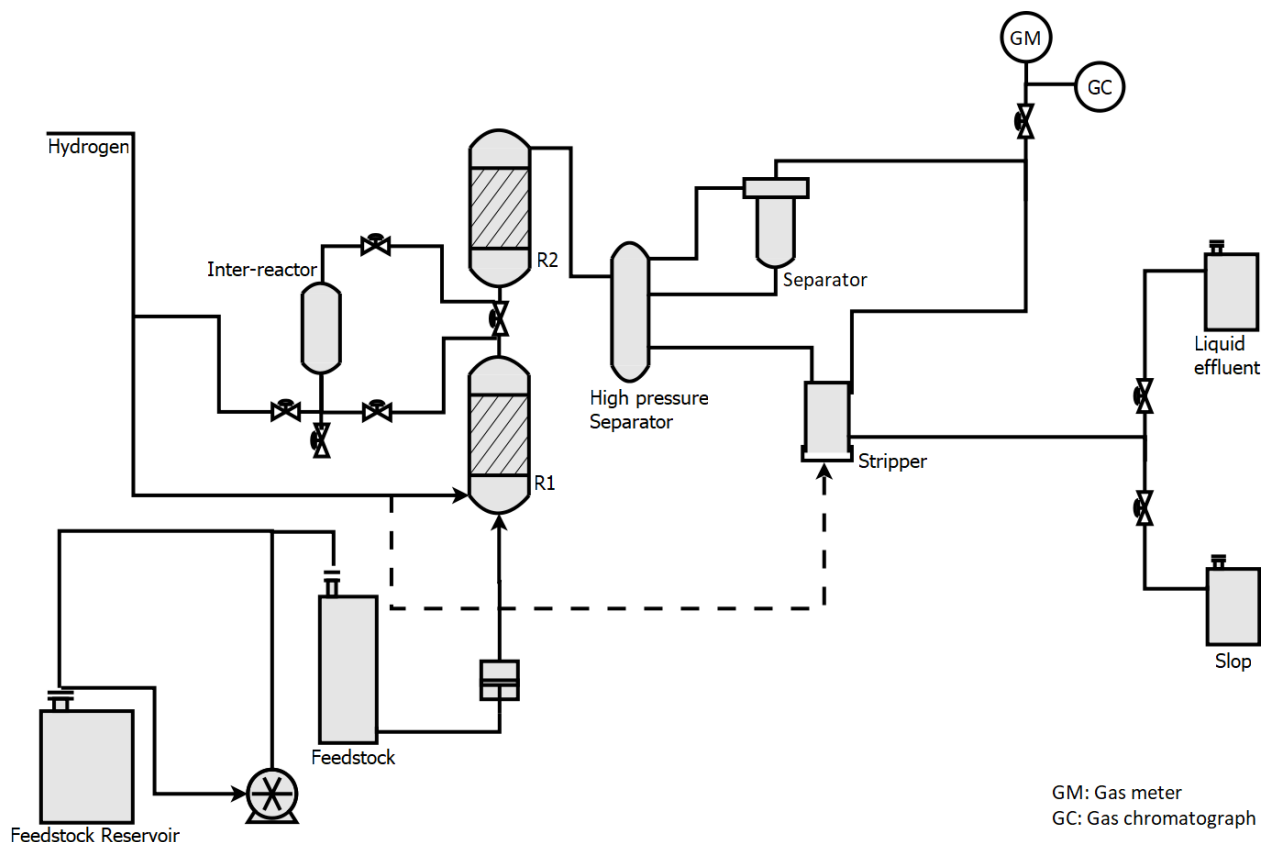


Figure 29. Pilot unit flow diagram.

### 2.1.2. Procedure for the pilot plant experiments

Each experiment started with the in-situ catalyst sulfidation with an atmospheric gasoil ( $d_{15}:0.8491 \text{ g/cm}^3$ ) spiked with 2% wt %/feed. of dimethyl disulfide (DMDS) and 2% wt %/feed. of aniline, at  $350^\circ\text{C}$ . After catalyst sulfidation, the operating conditions were imposed (temperature ranging from 374 to  $418^\circ\text{C}$  and LHSV between  $1.5$  and  $3 \text{ h}^{-1}$  depending on the specific experiment). A mass balance and relevant gas and liquid analysis were carried out after catalyst stabilization for accurate catalyst performance measurement. Unit stabilization was tracked through the monitoring of the liquid effluent density. The performance was considered stable when the density variation was lower than  $0.0010 \text{ g/cm}^3$  for 24 consecutive hours. Once

## Chapter 2-Insights in the phenomena involved in deactivation of industrial hydrocracking catalysts through an accelerated deactivation protocol

---

this condition is reached, the catalyst performance evaluation was launched, and the process continued at the same operating conditions until the desired evaluation time is completed. At the end of the experiment, the temperature was decreased to 350°C, and the feed switched to the atmospheric gasoil to wash both the unit and the catalyst at constant pressure and hydrogen flow. Afterward, the feed flow was stopped, and the catalyst was stripped and dried at a reduced pressure of 2 MPa in the presence of hydrogen. At the end of the experiment, the temperature was reduced to ambient conditions. The unit was purged with nitrogen to ensure inert conditions and then depressurized. The catalyst was finally unloaded by following the specific procedure described in section 2.3.3.

### 2.1.3. Verification of Isothermal and plug-flow behavior

To relate the reactant conversion in laboratory-scale reactors to those found in industrial processes, it is desirable to match the space velocities of large and small reactor [199]. In these reactors, heat and mass transfer effects lead to temperature and concentration gradients, and the presence of these gradients in experimental fixed-bed reactors (FBR) can provoke severe deviations in catalyst's performance in such a way that experimental results are not representing the true (or intrinsic) kinetics of the reaction. To ensure that kinetic data obtained in an experimental reactor reflect only chemical events, gradients must be virtually eliminated. Several criteria based on theoretical and experimental results have been developed for minimizing heat and mass transfer limitations [200], some of these criteria were verified for the pilot unit, as shown in Table 2. In some internal studies, experiments at hydrocracking conditions were carried out with grounded catalysts in a similar experimental set-up to the one used in this work, and no differences in reactivity were observed, which allows us to infer that no external diffusion limitations are present in our system.

## Chapter 2-Insights in the phenomena involved in deactivation of industrial hydrocracking catalysts through an accelerated deactivation protocol

**Table 2. Parameters ideal behavior FBR**

Criterion	Ideal condition	Pilot unit value	Pilot unit value
Interparticle gradients	$LB/d_{pe} \geq 30$	81	ok
Radial Intrareactor temperature gradients	$Radial\ d_{pe}/d_{re} \geq 4$	8	ok
Axial Intrareactor temperature gradients	$Axial\ LB/d_{pe} \geq 30$	81	ok
Axial mass dispersion	$\frac{L_B}{d_{pe}} > \frac{\sqrt{20n}}{Bo} \ln \frac{1}{1-X}$	78	ok

Additionally, the temperature profile along the two reactors length was measured by a sliding axial thermocouple located inside the reactor in order to check that the catalytic bed was isothermal. It was observed that the greatest deviation from the desired temperature value was  $\pm 2\text{ }^\circ\text{C}$  ( Figure 30).

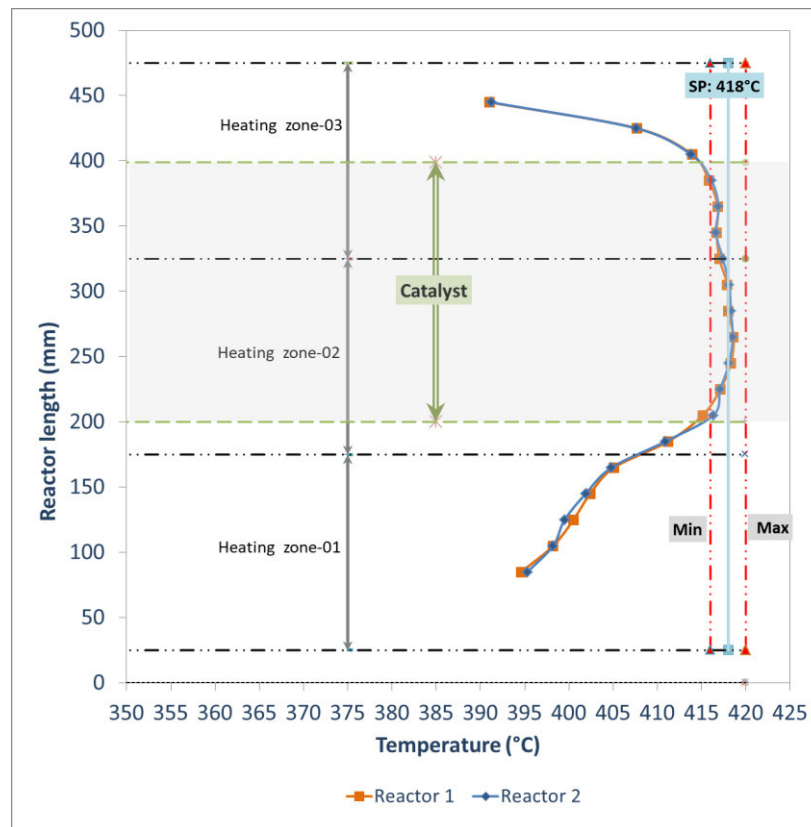


**Figure 30. Thermal profiles of the first and second reactors**

## Chapter 2-Insights in the phenomena involved in deactivation of industrial hydrocracking catalysts through an accelerated deactivation protocol

---

### 2.1.4. Pilot unit validation

Before developing the accelerated deactivation protocol, a reference test was executed to ensure the representative performance of the unit. This test was performed with the fresh catalyst described in section 2.2.2 and a hydrotreated VGO (Table 3)) similar to the one used in the rest of the experimental plan but with lower nitrogen content. The criterion to be fulfilled for pilot plant validation is the performance similarity compared to a more representative unit of 200 cm<sup>3</sup>, which is four times bigger than the fixed bed used in this work in terms of catalyst volume. The reactor diameters are the same for both units, but the catalytic length is around 10 times higher in the bigger unit. The operating conditions for this test are presented in Table 4. The global operation was validated as mass balances (raw data) were respected with deviations lower than 2% weight (Appendix 1). Both units present similar kinetic performances and a deviation between apparent activation energies lower than 2% (Appendix 2). Therefore, the performance of the pilot unit selected for this work can be considered as representative of a bigger unit used for scale-up purposes. The catalyst samples of this validation test were used as references (without deactivation) to compare samples from the deactivation experiment.

**Table 3. Feedstock properties for the reference test.**

<b>Properties</b>	<b>VGO-HDT1</b>	
Density @ 15°C	g/cm <sup>3</sup>	0.8787
Refraction Index @ 70° C		1.4627
Sulfur content	wt%	0.0054
Nitrogen Content	ppm	4.9
Yield of 370°C <sup>+</sup> fraction	wt%	79
Initial boiling point (IBP)	°C	110

## Chapter 2-Insights in the phenomena involved in deactivation of industrial hydrocracking catalysts through an accelerated deactivation protocol

Final boiling point (FBP)	°C	606
---------------------------	----	-----

**Table 4. Operating conditions of the reference test.**

Point	P	T	H <sub>2</sub> /HC	LHSV	Time*
	MPa	°C	NL/L	h <sup>-1</sup>	Days
1	14	374	1000	1.5	11
2	14	380	1000	1.5	4
3	14	388	1000	1.5	5

\*Including stabilization time

## 2.2. Materials

### 2.2.1. Feed Oil

The feedstock consisted of a hydrotreated vacuum gas oil (VGO-HDT2) containing around 150 ppm of organic nitrogen on a mass basis. This content was selected to accelerate catalyst deactivation. The main properties of this feed are shown in Table 5.

**Table 5. Feedstock properties for the deactivation experiments.**

Properties	VGO-HDT2	
Density @ 15°C	g/cm <sup>3</sup>	0.8984
Refraction Index @ 70° C		1.47505
Sulfur	wt%	0.068
Nitrogen	ppm	149
Aromatic carbon	%	10.3
Yield of 370°C+ fraction	wt%	92
Initial boiling point (IBP)	°C	179.8
Final boiling point (FBP)	°C	589.8

## Chapter 2-Insights in the phenomena involved in deactivation of industrial hydrocracking catalysts through an accelerated deactivation protocol

---

Dimethyl disulfide and aniline were added to the hydrotreated VGO to generate the hydrogen sulfide and ammonia partial pressures representative of the VGO mother feed. The mother feed contained a sulfur and a nitrogen content of 1.18 wt% and 0.22 wt%, respectively. The percentage of aromatic carbon was estimated through the n-d-M method according to the standard ASTM D3238. To use this method, the molecular weight was estimated by the Lee-Kesler correlation.

The hydrotreating of the feed was carried out ex-situ to have a homogeneous feed and minimize the influence of its properties variability (due to the hydrotreating catalyst deactivation) on the assessment of the performance of the hydrocracking catalyst. The production of this feed was done by controlling the required nitrogen content by increasing the temperature to compensate for the hydrotreating catalyst deactivation.

### 2.2.2. Catalysts

The fresh catalyst consisted of nickel-molybdenum sulfide particles dispersed on a carrier containing USY zeolite. No additional information on catalyst properties is given for confidentiality reasons.

The industrial spent catalyst samples were obtained from two industrial units processing vacuum gas oils having densities ranging from 0.91 to 0.925 g/cm<sup>3</sup>, sulfur mass percentage from 1 to 2% and nitrogen content from 1000 to 1400 ppm wt. They were unloaded by gravity at the end of the cycle, which lasted between 12 and 18 months to have a range of the variability of spent catalyst properties.

# Chapter 2-Insights in the phenomena involved in deactivation of industrial hydrocracking catalysts through an accelerated deactivation protocol

## 2.3. Methods

### 2.3.1. Screening of operating variables

A screening of the operating variables was carried out to determine which key operating variables had the most impact on deactivation. The selected variables were temperature (T), space velocity (LHSV), hydrogen/hydrocarbon ratio (H<sub>2</sub>/HC) and organic nitrogen (N<sub>org</sub>). At the beginning of this procedure, the catalyst was submitted to the following reference case (RC) conditions: 403°C, 14 MPa, H<sub>2</sub>/HC = 1500 NL/L, LHSV = 2h<sup>-1</sup>, total nitrogen and organic nitrogen content of 2200 ppm and 150 ppm in a mass basis, respectively. These conditions are within the operating window of a typical hydrocracking process. After catalyst stabilization, the temperature was changed and then kept constant for ten days, a period expected to be sufficient for evaluating the influence of each variable on deactivation. Afterward, the reference case conditions were restored and after catalyst stabilization, the loss in net conversion (Equation 11) caused by the variable under study was measured. The deactivating effect of each variable switch was evaluated by the difference between the conversions obtained at the reference conditions immediately before and after each operating variable switch. The procedure was repeated for all the variables mentioned above, as illustrated in Figure 31 and Table 6.

**Table 6. Operating conditions for the variables screening experiment.**

Condition	P	T	H <sub>2</sub> /HC	LHSV	N <sub>org</sub>	N <sub>Total</sub>
	MPa	°C	NL/L	h <sup>-1</sup>	ppm	ppm
<b>1 Reference case (RC)</b>	14	403	1500	2	150	2200
2 Temperature	14	<b>410</b>	1500	2	150	2200
<b>3 RC</b>	14	403	1500	2	150	2200
4 H <sub>2</sub> /HC	14	403	<b>1000</b>	2	150	2200

## Chapter 2-Insights in the phenomena involved in deactivation of industrial hydrocracking catalysts through an accelerated deactivation protocol

---

<b>5 RC</b>	14	403	1500	2	150	2200
6 LHSV	14	403	1500	<b>3</b>	150	2200
<b>7 RC</b>	14	403	1500	2	150	2200
8 Norg	14	403	1500	2	<b>300*</b>	2200
<b>9 RC</b>	14	403	1500	2	150	2200

---

\* The feedstock was spiked with acridine, and carbazole, in a mass proportion of 1:3, respectively.

According to the literature, the sequence selected for the variables evaluation was based on the expected impact of each operating parameter on deactivation rate. Thus, the variables expected to have a more significant impact on deactivation were tested at the beginning of the experiment.

### 2.3.2. Accelerated deactivation protocol

Based on the results obtained during the variables screening experiment, the following set of conditions was selected for the final accelerated deactivation protocol:  $T = 418^{\circ}\text{C}$ ,  $\text{LHSV} = 3 \text{ h}^{-1}$ ,  $\text{H}_2/\text{HC} = 1500\text{NL/L}$ ,  $P = 14 \text{ MPa}$ , with the feedstock spiked with aniline as described in Section 2.2.1 ( $N_{\text{org}} = 150 \text{ ppm wt.}$ , and  $N_{\text{total}} = 2500 \text{ ppm wt.}$ ) and a total time on stream of 30 days. The purpose of this protocol was to obtain a deactivated catalyst with properties similar to those related to industrial spent catalysts, with emphasis on the amount and nature of coke produced, as this is the primary mechanism of hydrocracking catalyst deactivation.

### 2.3.3. Catalyst loading and unloading procedures

Bed dilution is commonly used to minimize axial dispersion and gas-liquid mass transfer effects in pilot reactors [201]. In our case, bed dilution was performed by a direct mixture of the catalyst and inert particles of the same size as the catalyst. The dilution was carried out with silicon

## Chapter 2-Insights in the phenomena involved in deactivation of industrial hydrocracking catalysts through an accelerated deactivation protocol

---

carbide particles of 1 mm diameter, and each reactor was loaded with 12.5 cm<sup>3</sup> of catalyst diluted with 37.5 cm<sup>3</sup> of silicon carbide. The mixture was divided into four small recipients, which were homogenized through manual shaking and then loaded into the reactor. The homogenization quality was previously checked in a glass reactor to ensure that the catalytic bed was uniform.

Catalyst samples taken at the end of each test run were carefully collected to separate the particles from the inlet and outlet of each catalytic bed. Different preliminary trials were carried out with a glass reactor in order to optimize this specific unloading protocol. Accurate catalyst unloading is very important since it allows to assess the evolution of catalyst properties depending on reactor location. The samples were grouped as reactor inlet and outlet for each reactor. These samples were not prevented from contacting air, therefore for the assessment of the residual activity an initial sulfidation was carried out previous to catalytic test.

### 2.3.4. Catalyst characterization

Previous to catalyst characterization, samples were submitted to an extraction with toluene for 7 h in a soxhlet extractor at 250°C to remove the physically adsorbed hydrocarbons on the catalyst and dried under vacuum at 120°C for 12 h. The catalyst was characterized by the following analysis.

Nitrogen adsorption-desorption isotherms were measured in an ASAP 420 Micromeritics apparatus. The sample was submitted to a thermal pretreatment consisting of a temperature increase up to 100°C at 1°C/min, then a step of 30 min and after that, a new increase in temperature up to 500°C at 5°C/min with a step of 6 h under vacuum pressure (100 Pa). The surface area was calculated from the BET equation, using data in the relative pressure range of

## Chapter 2-Insights in the phenomena involved in deactivation of industrial hydrocracking catalysts through an accelerated deactivation protocol

---

$p/p_0=0.05$  to  $0.3$ . The total pore volume was deduced from the  $N_2$  adsorption at the endpoint of the isotherm. Micropore volume was determined from the t-plot method, with the Harkins-Jura formula, in the range from  $0.35$  to  $0.50$ . The uncertainty of surface area and volume measurements is  $5\%$  and  $2.5\%$ , respectively. The pore size distribution was calculated from the desorption branch of the  $N_2$  isotherm using the BJH model.

The carbon and nitrogen contents determination was carried out on a Thermoscientific FlashSmart equipment. Samples were pre-dried in situ at  $290^\circ\text{C}$  under helium flow for 15 minutes for water removal purposes to exclusively quantify the hydrogen directly bound to the coke. The uncertainties of measurement are  $10\%$  for carbon and  $14\%$  for nitrogen.

TGA of the deactivated catalysts was carried out on a thermobalance Mettler Toledo TGA-DSC1 coupled with mass spectroscopy (MS). The analysis has an uncertainty of  $0.1\%$  for the mass loss measurements. The sample was heated under a  $25\text{ cm}^3/\text{min}$  air flow rate using a  $5^\circ\text{C}/\text{min}$  temperature ramp from  $25$  to  $900^\circ\text{C}$ . The effluents were qualitatively analyzed by an online mass spectrometer (Thermostar/Pfeiffer). The mass spectrometer signal recorded as a function of time allowed to qualified the nature of the emitted gas during sample decomposition. For estimating the H/C ratio, as the physisorbed water is eliminated at temperatures lower than  $200^\circ\text{C}$ , only the  $\text{CO}_2$  and the  $\text{H}_2\text{O}$  detected between  $200^\circ\text{C}$  and  $650^\circ\text{C}$  were considered. The mass spectrometer signals of the  $\text{CO}_2$  (44) and  $\text{H}_2\text{O}$  (18) were then integrated between the mentioned temperatures, and the ratio of these areas was considered to be proportional to the H/C atomic ratio of the coke deposit [83].

$$\frac{\text{H}}{\text{C}} \sim \frac{I_{18}}{I_{44}} \quad \text{Equation 10}$$

## Chapter 2-Insights in the phenomena involved in deactivation of industrial hydrocracking catalysts through an accelerated deactivation protocol

---

In the previous equation, I44 represents the area measured for the CO<sub>2</sub> (m/z = 44) signal, and I18 the area corresponding to water (m/z = 18).

The nature of the coke was investigated by Raman spectroscopy. The analysis was performed on a Renishaw Raman spectrometer using an argon-laser focused on the sample by a microscope. Spent catalysts were analyzed in their extrudate form. The sample was cut with a scalpel along the transverse axis to obtain a flat cut that allows the analysis of the solid. Spectra of spent catalysts can often be compared to the spectra of graphite-like coke (peak at 1580 cm<sup>-1</sup>) [202]. There are two graphite-like predominant bands. These bands are identified by group theory at 1580-1600 cm<sup>-1</sup> (band G) and 1350-1400 cm<sup>-1</sup>(band D1) [202]. They result from the vibration of C=C bonds of the coke in both perpendicular and plane directions, respectively.

The MoS<sub>2</sub> sheets were visualized and analyzed by transmission electron microscopy (TEM) with a JEOL JEM 2100F microscope. The samples were prepared in three steps. In the first step, the catalyst was ground to a fine powder. Then it was dispersed in ethanol in an ultrasonic bath, and two drops of the solution were deposited on a copper grid. Finally, the solvent was evaporated, and the sample was introduced into the microscope. The TEM images were recorded in bright field mode. The average dispersion of the MoS<sub>2</sub> particles was calculated from the slab length distribution, assuming a hexagonal shape of the particles [91]. The promoter segregation was investigated by TEM–EDX detection, leading to a Ni/Mo ratio calculated for about 25 particles.

Finally, evaluating the residual activities of the spent catalysts provides essential information on the catalyst deactivation state. In this case, the aim is to evaluate both the hydrogenation and isomerizing/cracking activities. Concerning the hydrogenation function, activity was evaluated via the conversion of toluene to hydrogenated products, following the protocol described elsewhere

## Chapter 2-Insights in the phenomena involved in deactivation of industrial hydrocracking catalysts through an accelerated deactivation protocol

[203]. For the acid function, the isomerizing/cracking activity was assessed via the hydroconversion of n-heptane to isomerization and cracking products using a testing protocol analogous to the one used for toluene hydrogenation. For both cases, the reaction is carried out in a fixed bed reactor in the presence of H<sub>2</sub>S (generated by decomposition of DMDS) under hydrogen pressure. The operating conditions for each experiment are presented in Table 7. Catalyst samples were sulfurized in situ at the beginning of the experiment, with the same feedstock and same operating conditions (T=350°C) as presented in Table 7, for 2 hours.

**Table 7. Operating conditions of the catalytic tests with model molecules.**

		<b>Toluene Hydrogenation</b>	<b>n-Heptane Hydroconversion</b>
Concentration of reactant	wt %/feed	20*	95.15
DMDS concentration	wt %/feed	6	4.85
P	MPa	6	6
LHSV	h <sup>-1</sup>	2	4
T	°C	350	350/360/380
H <sub>2</sub> /HC	NL/L	450	330

\* in cyclohexane as solvent

### 2.4. Data interpretation: kinetic laws, deactivation parameter and hydrogen consumption

Deactivation was assessed by monitoring the evolution of the apparent kinetic constants for the target hydrocracking reactions, i.e., cracking, hydrodenitrogenation (HDN), aromatics hydrogenation (HDA) and hydrodesulfurization (HDS). These equations are based on the conversion of VGO (370°C<sup>+</sup>) for cracking reactions and nitrogen, sulfur and aromatics for HDN, HDS and HDA, respectively. Equation 11 shows the general expression to calculate the conversion. Along with this work, the results are given in terms of either global or first reactor properties. The term “global” is applied to reactor 1 and reactor 2 as a whole. Thus, for instance, the “global net conversion” is determined from the difference between the 370°C<sup>+</sup> cut mass at

## Chapter 2-Insights in the phenomena involved in deactivation of industrial hydrocracking catalysts through an accelerated deactivation protocol

---

the first reactor inlet and the 370°C<sup>+</sup> cut mass at the second reactor outlet. Conversely, the “first reactor net conversion” is calculated through the difference between the 370°C<sup>+</sup> cut mass at the first reactor inlet and the 370°C<sup>+</sup> cut mass at the first reactor outlet. The mass values were calculated after data reconciliation of the experimental mass balances to distribute the losses. Some authors [67,68,204] have used power-law models to calculate these apparent kinetic constants for similar reaction systems. This type of expression was also used in this study for the sake of simplicity, although Langmuir-Hinshelwood-based models would be more appropriate for kinetics determination purposes. A first-order [70] kinetics was assumed for N-containing and aromatic molecules [205], i.e., for HDN and HDA, respectively (Equation 12). An apparent reaction order of 1.2 for the S-containing molecules (Equation 13) was considered in the case of HDS. To determine the apparent HDA kinetic constant, the amount of aromatic carbon was estimated through the n-d-M method according to the standard ASTM D3238.

$$\% \text{Conversion} = \left( \frac{\text{mass}_x \text{ feed} - \text{mass}_x \text{ product}}{\text{mass}_x \text{ feed}} \right) * 100 \quad \text{Equation 11}$$

Where x is either the 370<sup>+</sup> mass, the nitrogen, the sulfur, or the aromatic carbon content.

$$k = \text{LHSV} * \ln(1 - \% \text{Net Conversion} / 100) \quad \text{Equation 12}$$

$$k_i = \frac{\text{LHSV}}{n-1} \left( \frac{1}{(C_s^{\text{out}})^{n-1}} - \frac{1}{(C_s^{\text{in}})^{n-1}} \right) \quad \text{Equation 13}$$

Here  $n=1.2$ ,  $C_s^{\text{in}}$ , and  $C_s^{\text{out}}$  are the feed and product concentration of sulfur in percentage wt%.

Kinetics and deactivation were decorrelated through the fitting of an exponential decay function to the experimental data (Appendix 3). An exponential decay function (Equation 14) was assumed for catalyst deactivation ( $\varphi$ ), which depends on the deactivation constant ( $\alpha$ ) and time on stream (TOS) [6,68]. The deactivation constant was fitted to the experimental data of the

## Chapter 2-Insights in the phenomena involved in deactivation of industrial hydrocracking catalysts through an accelerated deactivation protocol

---

cracking apparent kinetic constant evolution as a function of time. Although to be rigorous the deactivation models must be a function of the agent causing the deactivation (i.e. coke, nitrogen compounds, etc), in this work the information on the evolution of these agents was not available. However, this way of approaching the results allows a comparison of the deactivation rates in a semi-quantitative way.

$$k_{crack} = k_{crack}^{fresh} \exp(-\alpha * TOS) \quad \text{Equation 14}$$

The hydrogen consumption was calculated from the experimental data by performing a global hydrogen balance (Equation 15). It was based on the elemental analysis of liquid streams and gas chromatography. Hydrogen in gas compounds such as H<sub>2</sub>S and light hydrocarbons (C<sub>1</sub> to C<sub>6</sub>) was calculated from molar equivalents and assuming all the hydrocarbons to be paraffins. All the molecules measured by GC were assumed to be uniquely in the gas phase.

$$H_{cons} = H_{Liq}^{out} - H_{Liq}^{in} + H_{Light\ HC}^{out} + H_{H_2S}^{out} \quad \text{Equation 15}$$

H<sub>cons</sub> is the hydrogen consumption, H<sub>Liq</sub><sup>out</sup> is the total amount of hydrogen contained in the hydrocracked liquid product, H<sub>Liq</sub><sup>in</sup> are the total amount of hydrogen contained in the hydrotreated liquid feed and the additives (dimethyl disulfide, aniline), H<sub>Light HC</sub><sup>out</sup> is the amount of the hydrogen contained in light hydrocarbons and H<sub>H<sub>2</sub>S</sub><sup>out</sup> is the amount of hydrogen contained as H<sub>2</sub>S in the gas phase.

## Chapter 2-Insights in the phenomena involved in deactivation of industrial hydrocracking catalysts through an accelerated deactivation protocol

---

### 3. RESULTS

In this section, the results obtained during the screening of the operating conditions are presented first. The results of the final accelerated deactivation protocol are exposed afterward, together with the spent catalysts' characterization.

#### 3.1. Variables screening experiment

The sequence of changes made in the operating conditions and the global net conversion evolution during variables screening are depicted in Figure 31 and Figure 32, respectively. The analysis of Figure 32 can be carried out by considering the influence of the operating conditions on catalyst activity, as well as on catalyst deactivation. In this section, the impact of operating conditions on catalyst activity is first presented. The increase of temperature naturally favors conversion, which increased from 40 to 70%. The decrease of the H<sub>2</sub>/HC ratio had a low impact on conversion, kept at an almost constant level of 30%. An increase of the LHSV translates into a lower residence time, which provoked a decrease in conversion up to 10%. Finally, the increase of the organic nitrogen content had practically no effect on conversion. This result was expected since the literature shows that as nitrogen level increases from zero, the conversion drops sharply until a certain nitrogen concentration, but then the loss of activity becomes less pronounced as nitrogen level increases [8]. During the hydrocracking at 370°C of a hydrotreated VGO at different nitrogen levels, a conversion loss of around 60% was observed when nitrogen increased until 120 ppm. However, a loss of only 15% was observed beyond that concentration up to 600 ppm nitrogen.

From a deactivation point of view, a rapid drop in conversion was observed at the beginning of the experiment, under reference conditions. This result is consistent with the high activity of

## Chapter 2-Insights in the phenomena involved in deactivation of industrial hydrocracking catalysts through an accelerated deactivation protocol

---

fresh catalysts that presented a perfectly clean active surface. The temperature increase had a strong effect on catalyst deactivation, as conversion under reference conditions was reduced from 40 to 30%. The H<sub>2</sub>/HC ratio did not affect catalyst deactivation, as the global net conversion remained at an almost constant value of 30%. LHSV strongly deactivated the catalyst, as conversion dropped to 20% net conversion. Finally, organic nitrogen had no substantial effect on catalyst deactivation. An additional experiment was carried out to validate this result, as a totally deactivated catalyst could have masked the organic nitrogen impact on catalyst deactivation. Acridine and carbazole in a mass proportion of 1:3, respectively, were added to the feedstock (hydrotreated up to 150 ppm of nitrogen) to achieve a total organic nitrogen content of 300 ppm wt. results are depicted in Figure 33. No significant impact of additional organic nitrogen was observed, either in catalyst activity or catalyst deactivation. This observation could be because, beyond 150 ppmw, further increase of the organic nitrogen content does not practically affect activity nor catalyst deactivation. But it may also be related to the lower basicity and/or the lower molecular weight of the added nitrogen molecules blend, compared to the basicity and size of the nitrogen compounds contained in the real feedstock. The former based on that an increase in the nitrogen content of liquid product at the first and second reactors outlets was noticed, suggesting that the added nitrogen compounds were not instantaneously converted into ammonia. However, the observed increase in nitrogen content of the liquid product was not equivalent to the nitrogen concentration increase in the feed; in other words, the added components had a higher reactivity than the nitrogen compounds of the initial feed.

## Chapter 2-Insights in the phenomena involved in deactivation of industrial hydrocracking catalysts through an accelerated deactivation protocol

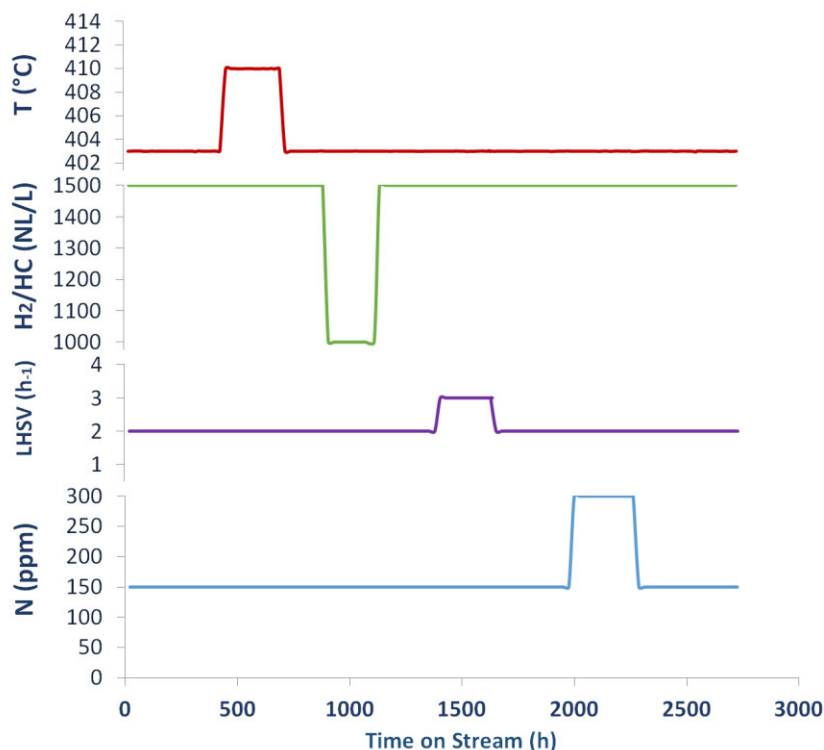
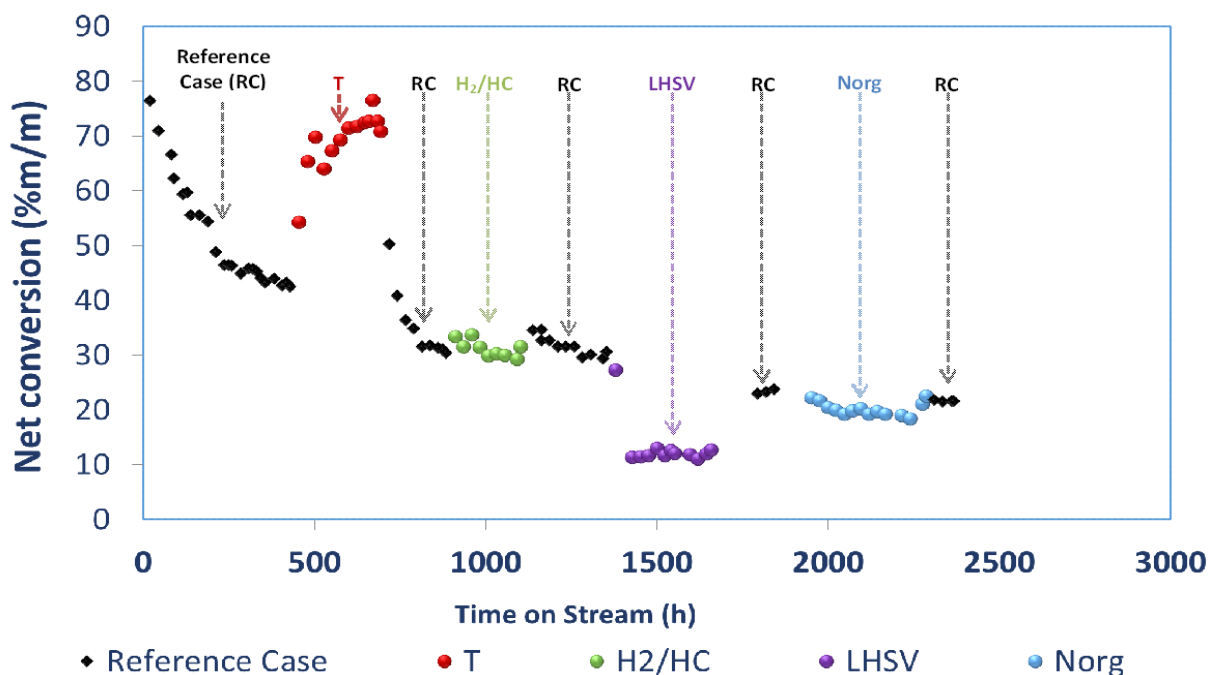
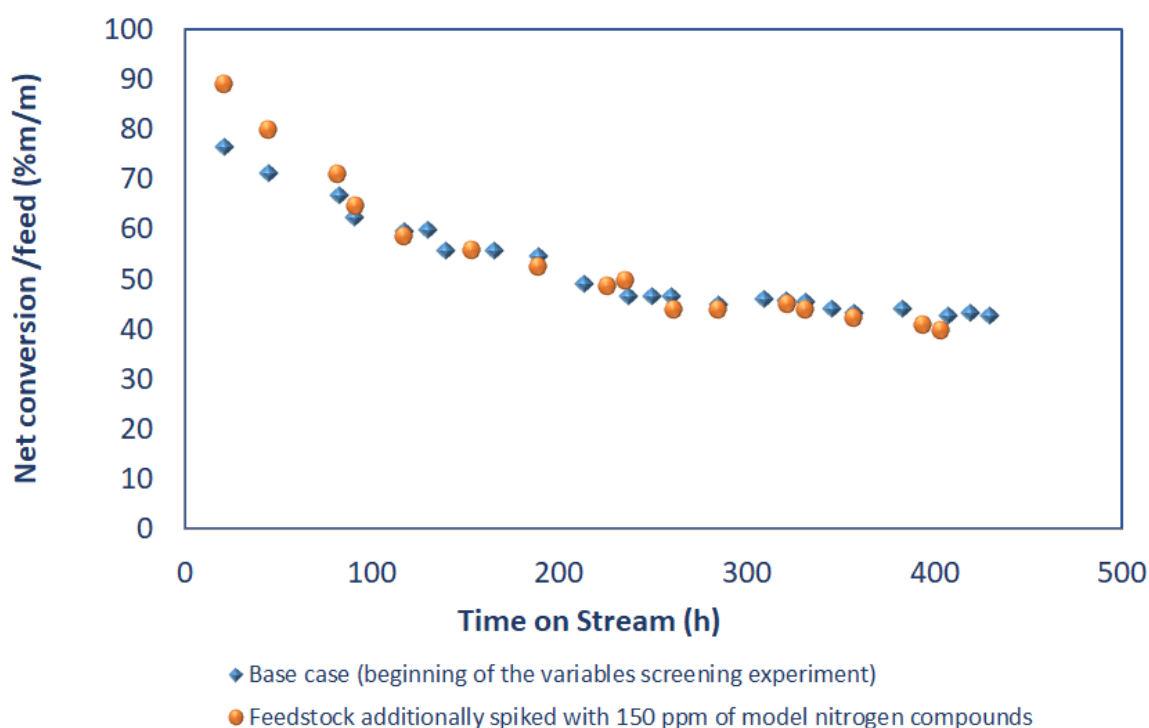


Figure 31. The sequence of changes made during the screening of the operating conditions.



◆ Reference Case      ● T      ● H2/HC      ● LHSV      ● Norg  
 Figure 32. Net conversion as a function of time on stream, at the different operating conditions specified in Table 6.

## Chapter 2-Insights in the phenomena involved in deactivation of industrial hydrocracking catalysts through an accelerated deactivation protocol



**Figure 33. Effect of nitrogen content in the feedstock. Global net conversion evolution with time on stream and nitrogen content at the outlet of the reactors at the end of the experiment.**

The evolution of the apparent reaction rate coefficients of each key chemical reaction with time on stream is presented in the following sections, first for the whole system and then for the first reactor R1. These results quantify the effect of each variable on deactivation separately to define the operating conditions for the accelerated deactivation protocol.

### 3.1.1. Evolution of the reaction rate coefficients with time for the whole system

The evolution of the global reaction rate coefficients of the relevant chemical reactions (cracking, HDN, HDA, and HDS) with time on stream (TOS) is shown in Figure 34.

## Chapter 2-Insights in the phenomena involved in deactivation of industrial hydrocracking catalysts through an accelerated deactivation protocol

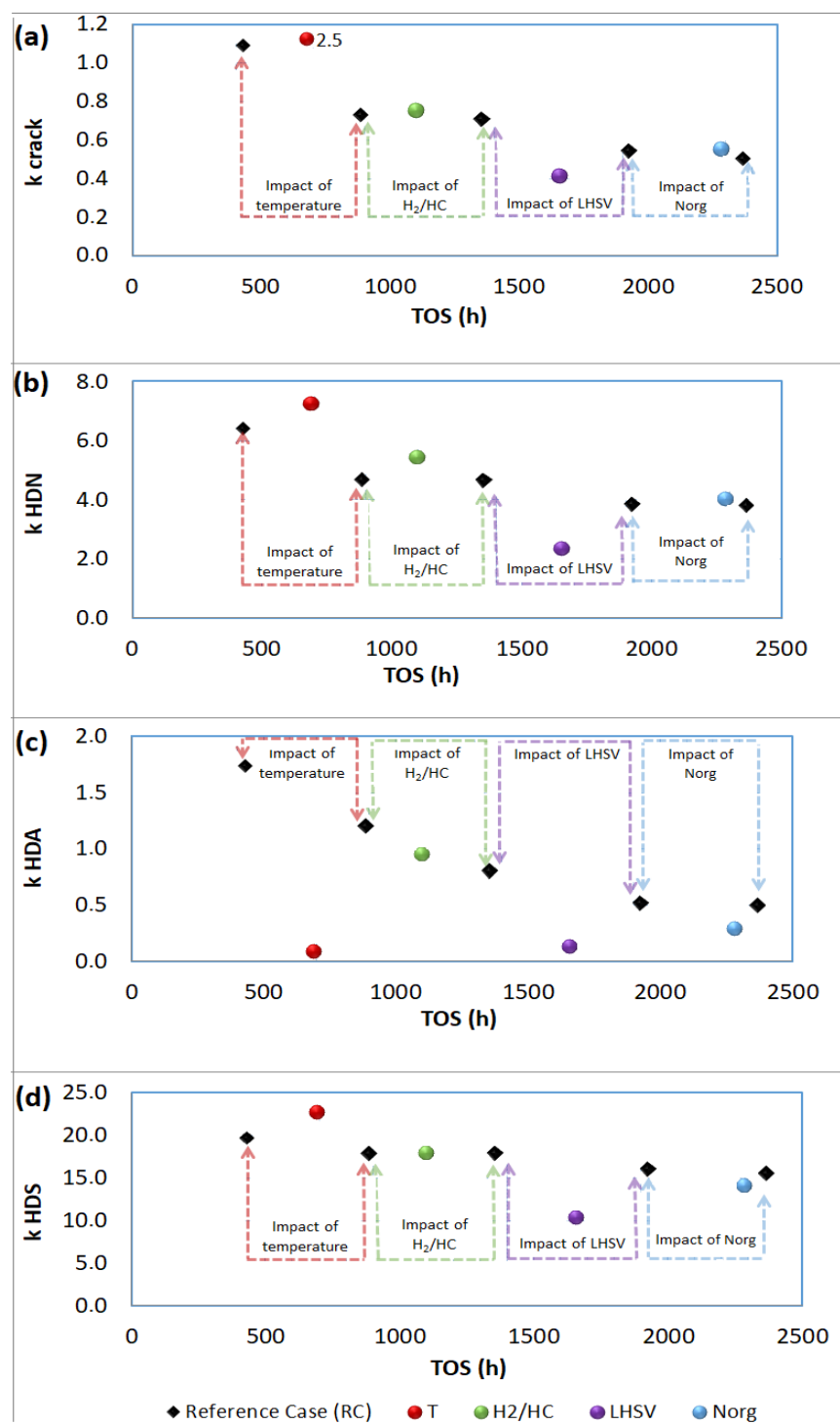


**Figure 34. Reaction rate coefficients a) for cracking reactions, b) for hydrodenitrogenation reactions, c) for aromatics hydrogenation reactions, d) for hydrodesulfurization reactions at reference conditions and for each variable change specified in Table 6.**

## Chapter 2-Insights in the phenomena involved in deactivation of industrial hydrocracking catalysts through an accelerated deactivation protocol

### 3.1.1.1. Reactivity

It is worth to comment on the effect of the operating variables on each chemical reaction rate (i.e., the colored points in Figure 34) before discussing deactivation. The impact of each operating variable on the HDN reaction rate coefficient was very similar to the one observed for the cracking function (Figure 34a vs. b). The correlation between both reaction rate coefficients is shown in Figure 35. HDN reactions determine the residual organic nitrogen content. This has a strong repercussion on the cracking function of the catalyst through its inhibition [206]. Similar behavior was observed for both the HDA and the HDS reaction rate coefficient, except in the case of the effect of an increase of temperature on HDA. In fact, the related reaction coefficient approached zero in that case. This can be attributed to the chemical equilibrium between aromatics and naphthenes, which is unfavorable at high temperatures. This observation is consistent with other works showing that HDA reactions are limited by chemical equilibrium at low pressure and high temperatures [207,208]

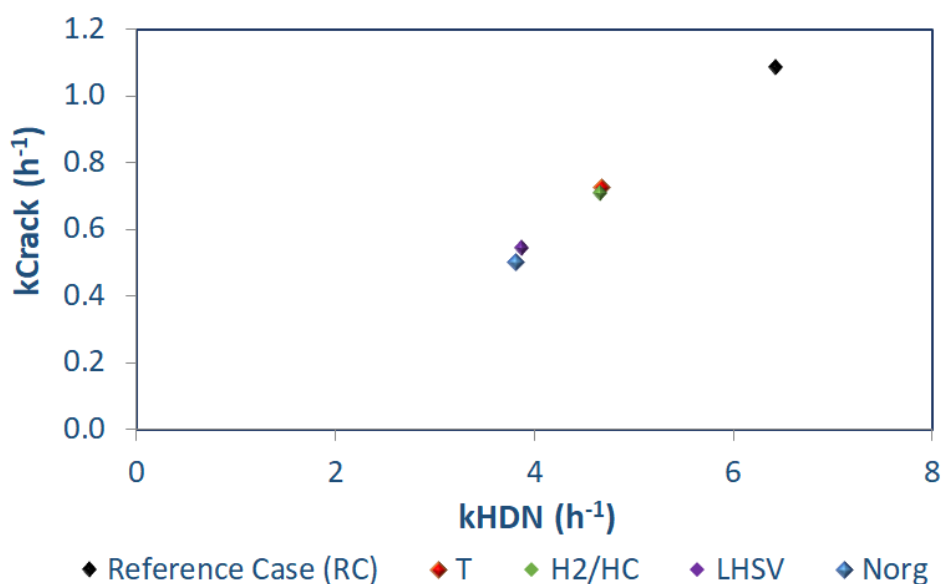


Figure 35. Correlation between hydrodenitrogenation and cracking reaction rate coefficients.

## Chapter 2-Insights in the phenomena involved in deactivation of industrial hydrocracking catalysts through an accelerated deactivation protocol

---

### 3.1.2. Deactivation

Concerning deactivation, i.e., the activity difference at reference conditions after each variable change, the results are presented in Table 8. Temperature and LHSV were, by far, the variables having the strongest impact on catalyst deactivation. The deactivation mainly affected cracking, HDN and HDA reactions. The HDS reaction rate remained almost unchanged.

**Table 8. Impact of variables on deactivation: extent of deactivation caused by each variable change.**

	$100 - \frac{k_{ref\ case\ i}}{k_{ref\ case\ i-1}} * 100$			
	Cracking	HDN	HDA	HDS
	%	%	%	%
Impact of Temperature	33	27	31	9
Impact of H <sub>2</sub> /HC	3	0	33	0
Impact of LHSV	21	17	36	10
Impact of Norg	7	1	3	3

The data show that increasing temperature had the biggest impact on catalyst deactivation for every reaction. This result agrees with several studies in the literature claiming that coke precursors are formed faster and deactivate catalysts through carbonaceous compounds deposition at high temperatures [12,125,126,195,209]. The temperature excursion deactivated cracking, HDN, and HDA reactions to roughly the same extent, whereas HDS was less affected.

Even if a higher hydrogen/hydrocarbon (H<sub>2</sub>/HC) ratio is supposed to retard coke deposition due to the saturation of compounds involved in coke formation [8], the amplitude of the variation of this variable was not sufficient to observe any significant impact on deactivation. After the restoring of the reference conditions, all the reaction rate coefficients remained almost constant, except for HDA, which decreased by 33%.

## Chapter 2-Insights in the phenomena involved in deactivation of industrial hydrocracking catalysts through an accelerated deactivation protocol

---

The variable with the second-highest impact on deactivation was space velocity. A higher space velocity lowers the residence time and, consequently, lowers the conversion of the different reactions. In the case of the HDN reactions, this reduction causes an increase in the nitrogen compounds concentration along the reactor. In contact with the catalyst, these compounds can be adsorbed on the acid sites, thus neutralizing and leaving them unavailable for the VGO molecules to react. The adsorbed organic nitrogen compounds remain on the catalyst surface leading to coke formation due to coking reactions that are faster than the desorption of nitrogen-containing compounds [8]. When returning to the reference case conditions, this coke deposition reduces cracking reactions rate and conversion with respect to the values observed for the previous point made at the same conditions, as illustrated in Figure 31 and Figure 32. There is also a reduction in the HDA reaction rate that increases aromatics concentration along the reactor. According to the mechanisms of carbenium ions proposed by different authors [10,125], when there is weak hydrogenation, aromatics can undergo addition, dehydrogenation, and hydrogen transfer reactions to grow into large polyaromatic molecules, i.e., coke precursors.

The behavior of the HDS reaction rate coefficient is particularly interesting. As mentioned before, the hydrotreating reactions are carried out on metal sulfide particles. However, Figure 32 shows that the HDS reaction rate coefficient remained nearly constant for all the reference points. In contrast, the HDN and HDA coefficients exhibited more important changes with TOS. This behavior can be explained, considering that desulfurization occurs through two different mechanisms, direct desulfurization (DDS) and pre-hydrogenation (HYD) [11,12]. The catalytic sites responsible for each one of these mechanisms are different. Some studies [88,210,211] have established that sulfur vacancies promote the DDS pathway, and hydrogenation is promoted either by the so-called Brim sites [90,210] or by the acidic SH groups [212]. Despite

## Chapter 2-Insights in the phenomena involved in deactivation of industrial hydrocracking catalysts through an accelerated deactivation protocol

---

the current controversy over these sites, there is an agreement concerning the strong inhibition of the HYD pathway by basic nitrogen compounds [90], consistent with the observed decrease of the HDA and HDN reaction coefficients upon deactivation by organic nitrogen compounds in the feed. The existence of an alternative reaction pathway, the DDS, for HDS, allows explaining why this particular chemical reaction is less affected.

The evaluation of the impact of the different operating variables on deactivation allows the following ranking to be established:  $T > \text{LHSV} > \text{H}_2/\text{HC} > \text{N}_{\text{org}}$ . The determination of the deactivation parameters for the cracking function and the hydrogen consumption evolution consolidates this ranking, as shown hereinafter.

The ratio of the deactivation rate coefficients for cracking reactions is presented in Table 9. The results confirm that the variables impact on the deactivation rate at the evaluated conditions, follows the order mentioned previously.

**Table 9. Impact of variables on the deactivation rate for cracking reactions.**

	$\alpha_{ref\ case\ i} / \alpha_{ref\ case\ i-1}$
	Cracking
Impact of Temperature	3.0
Impact of $\text{H}_2/\text{HC}$	0.3
Impact of LHSV	2.3
Impact of $\text{N}_{\text{org}}$	0.0

Finally, Table 10 shows the hydrogen consumption for each point of the variables screening. The data were consistent with the evolution of the cracking reaction rate coefficients. The higher the reaction coefficient, the higher the hydrogen consumption. This result agrees with the hydrocracking stoichiometry, which predicts the consumption of one  $\text{H}_2$  molecule per cracking reaction.

## Chapter 2-Insights in the phenomena involved in deactivation of industrial hydrocracking catalysts through an accelerated deactivation protocol

**Table 10. Hydrogen consumption and reaction rate coefficients for cracking reactions.**

<b>Condition</b>	<b>H<sub>cons</sub></b>	<b>k<sub>Crack</sub></b>
	Nm <sup>3</sup> /m <sup>3</sup>	
Reference Case	60	1.09
Impact of Temperature	47	0.73
Impact of H <sub>2</sub> /HC	45	0.71
Impact of LHSV	41	0.54
Impact of Norg	35	0.50

### 3.1.3. Evolution of the reaction rate coefficients with time for the first reactor

The analysis of the effluent of the first reactor allows pushing the interpretation of the data a little bit further. Figure 36 shows a comparison between the reaction rate coefficients in the first reactor and in the whole system for cracking and HDN reactions. HDA reactions were not considered since the respective reaction coefficients were negligible.

#### 3.1.3.1. Reactivity

The effect of the different operating variables on each reaction rate is not discussed here as it is quite similar to the one observed for the whole system. The reaction rate coefficients of the first reactor were lower than the corresponding global values. This is probably due to the higher organic nitrogen content in the first reactor, which strongly inhibits chemical reactions.

#### 3.1.3.2. Deactivation

The cracking apparent reaction rate coefficient for reactor R1 remained nearly unchanged for all the reference conditions, whereas the global value displayed a decrease, as discussed in the previous section. The HDN reaction rate coefficient of the first reactor followed the same trend as the global HDN constant. The absence of further deactivation of the cracking function in the first reactor, despite a systematic deactivation of HDN, can be explained by the saturation of the

## Chapter 2-Insights in the phenomena involved in deactivation of industrial hydrocracking catalysts through an accelerated deactivation protocol

inhibition effect at high organic nitrogen concentration. This is in agreement with the conclusions from the experiment carried out at a higher organic nitrogen content.

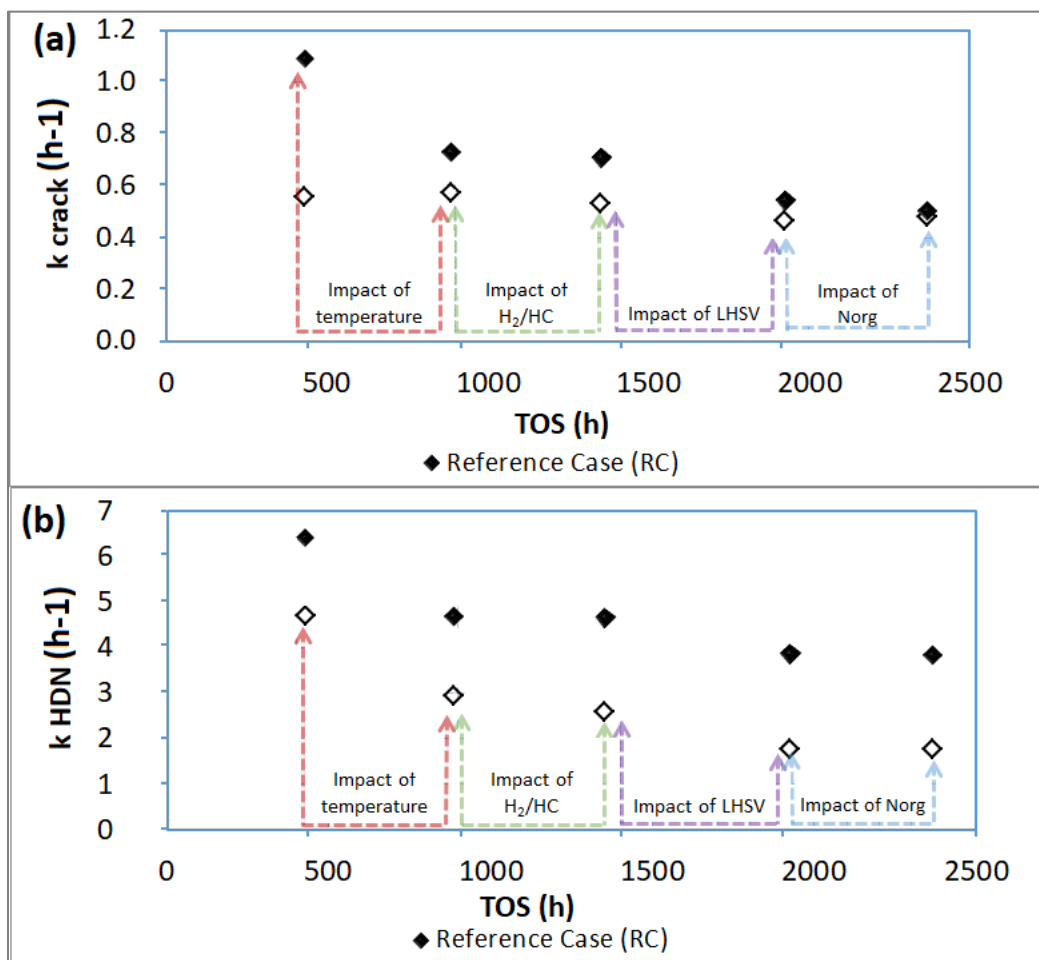


**Figure 36. Reaction rate coefficients of a) Cracking reactions b) HDN reactions at reference conditions before and after each variable change. Full symbols=whole reactor system, open symbols=first reactor.**

In conclusion, the variable screening experiment showed that the two variables, which had the strongest impact on deactivation by far, were temperature and space velocity. Therefore, a high temperature associated with a high space velocity was chosen for the accelerated deactivation protocol. The highest LHSV which was feasible on the testing unit was 3 h<sup>-1</sup>. At this LHSV, the

## Chapter 2-Insights in the phenomena involved in deactivation of industrial hydrocracking catalysts through an accelerated deactivation protocol

---

highest possible temperature, which avoided full conversion of the 370°C<sup>+</sup> fraction, was about 418°C.

### 3.2. Accelerated deactivation protocol

#### 3.2.1. Evolution of net conversion and reaction rate coefficients over time

The catalyst was subjected to the accelerated deactivation conditions for one month. The evolution of the global and first reactor net conversions over time is presented in Figure 37. After the stabilization time, global conversion decreased by about 20%. Industrial conversion losses are considerably lower, i.e., around 5%/month. The main loss of activity occurred in the first 6 days; after this time, the decline rate was lower until conversion reached a pseudo-steady state. The conversion evolution with time on stream followed the trend usually obtained during coke formation on hydroprocessing catalysts [6,8]. During industrial catalyst deactivation through coking, coke is rapidly formed in the initial stages of the operation; then, the coke level reaches a near steady-state [11]. The conversion in the first reactor remained constant after the stabilization time, as already observed during the variables screening experiment.

## Chapter 2-Insights in the phenomena involved in deactivation of industrial hydrocracking catalysts through an accelerated deactivation protocol

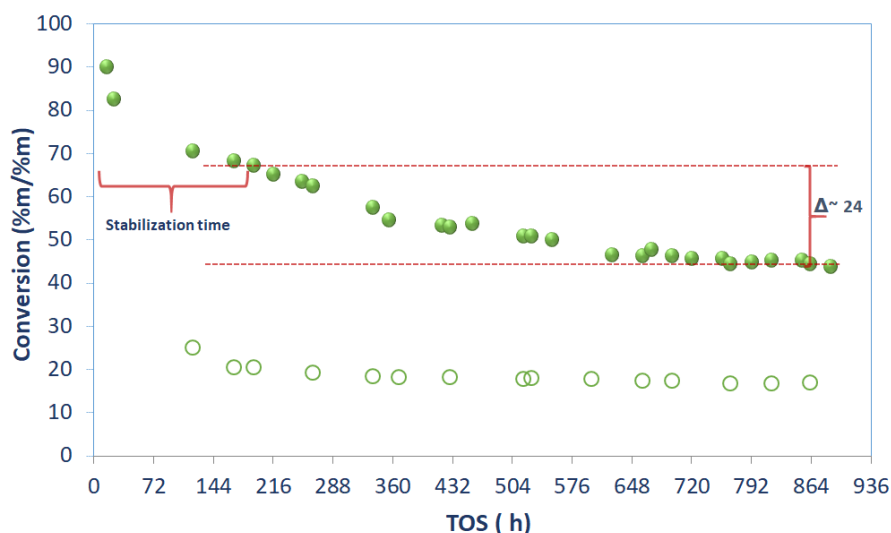


**Figure 37. Evolution of the global and first reactor net conversion with time on stream with the accelerated deactivation protocol ( $T=418^{\circ}\text{C}$ ,  $P=14\text{ MPa}$ ,  $\text{LHSV}=3\text{h}^{-1}$ ,  $\text{H}_2/\text{HC}=1500\text{ NL/L}$ ). Full symbols=Total effluent, open symbols=First reactor effluent.**

The evolution of cracking and HDN reaction rate coefficients over time is presented in Figure 38. The results show a reduction of around 40% and 25% in the global cracking and HDN reaction rates, respectively. Hence, the acid function underwent a higher deactivation than the metal function. The cracking and HDN rate constants in the first reactor remained constant during the whole test, confirming that different mechanisms took place in each reactor.

The obtained results allow us to partially decorrelate the cracking function deactivation from the HDN conversion loss. Indeed, the HDN reaction rate coefficient reached a pseudo-plateau after around 144 h of operation, whereas the cracking coefficients continuously decreased until 500 h of operation. Thus, the cracking activity loss was not entirely explained by inhibition due to a progressive increase in the organic nitrogen content, i.e., an indirect consequence of the deactivation of the HDN activity. Although this indirect effect certainly contributes to the deactivation of cracking, a direct deactivation mechanism of the acid sites must exist in parallel.

## Chapter 2-Insights in the phenomena involved in deactivation of industrial hydrocracking catalysts through an accelerated deactivation protocol

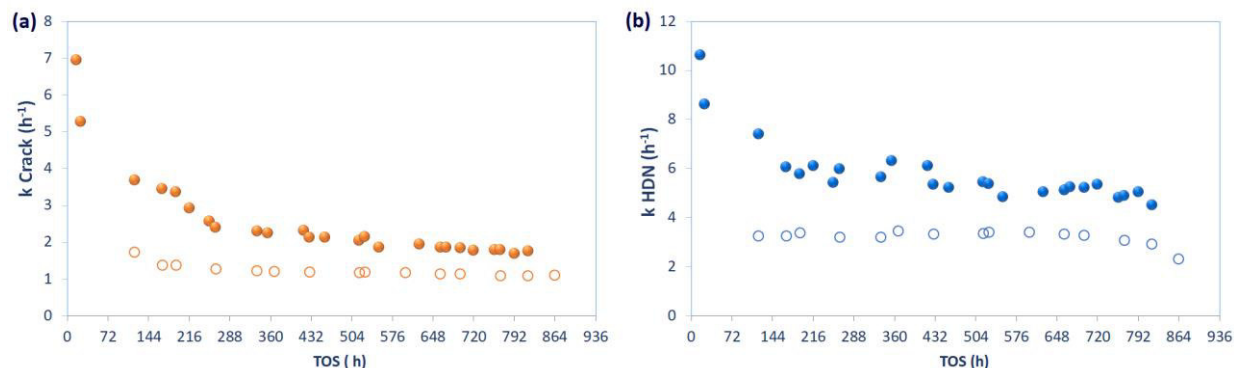


**Figure 38. Evolution of reaction rate coefficients with time on stream during the deactivation test, a) for cracking reactions, b) for hydrodenitrogenation reactions. Full symbols=whole reactor system, open symbols=first reactor.**

### 3.2.2. Spent catalysts characterization

This section presents the characterization results of the spent samples from the accelerated deactivation procedure. Samples were drawn from the first reactor inlet (Bed inlet) and from the second reactor outlet (Bed outlet) to understand the effect of reactor location on deactivation. These results are compared to the characterization results obtained for the samples from the reference test, described in section 2.1.4, to assess the extent of deactivation. Finally, some characterization results related to industrial spent catalysts are exposed for the qualitative validation of the representativeness of the experimental procedure.

#### 3.2.2.1. Elemental analysis

Results from the elemental analysis are shown in Table 11. As expected, the catalyst from the accelerated deactivation experiment had a higher carbon content than the catalyst obtained from the reference test. The carbon content of industrial spent catalysts was even higher. Regarding the effect of reactor location, the carbon content of the spent catalyst at the reactor outlet was higher than at the reactor inlet.

## Chapter 2-Insights in the phenomena involved in deactivation of industrial hydrocracking catalysts through an accelerated deactivation protocol

**Table 11. Characterization of spent catalysts: Surface area (S), total pore volume (V), micropore volume ( $\mu V$ ) and hysteresis area of the spent catalyst relative to the fresh catalyst and carbon content of the spent catalysts.**

Sample	Carbon content*	S/S <sub>fresh</sub>	V/V <sub>fresh</sub>	$\mu V$	$HA_{Spent}$
				$\mu V_{fresh}$	$HA_{Fresh}$
	(% wt)	(%)	(%)	(%)	
Reference Test - Bed In	5.4	92	85	84	1.1
Reference Test - Bed Out	5.7	95	86	87	1.1
Deactivation Test - Bed In	6.6	86	81	65	1.2
Deactivation Test - Bed Out	8.8	71	71	60	1.4
Industrial Spent Catalysts	10 -15	65 – 85	60 - 85	65-78	1.4-1.6

\*Carbon content on fresh-basis

### 3.2.2.2. Textural analysis

The porosity of the spent catalysts from the accelerated deactivation procedure was analyzed via the nitrogen adsorption-desorption isotherms. Coke caused a decrease in pore volume, accompanied by a decrease in surface area (Table 11). The accelerated deactivation procedure provoked higher surface area losses (S) and pore volume (V) than the reference test. These relative losses were within the range typically observed for industrial spent catalysts. A more pronounced decrease of surface and pore volume was observed at the bed outlet, in agreement with the higher carbon content at this location.

The pore size distributions of the different catalyst samples, measured by nitrogen desorption isotherms, are shown in Figure 39. Note that in this figure, the mesopore distribution is the pore distribution of the carrier and not of the USY crystals. The pore size distribution of the deactivated samples always remained similar to the one determined for the fresh catalyst, except for a shift towards smaller pores. This phenomenon was very pronounced for the deactivated solids from the accelerated deactivation protocol and even more for the bed outlet sample, consistent with higher carbon content in this location. Furthermore, the loss of

## Chapter 2-Insights in the phenomena involved in deactivation of industrial hydrocracking catalysts through an accelerated deactivation protocol

micropore volume ( $\mu\text{Vol}$ ) follows the same tendency as global volume loss (Table 11). Both facts suggest that the deposition of coke seems to be homogeneous in all pores.

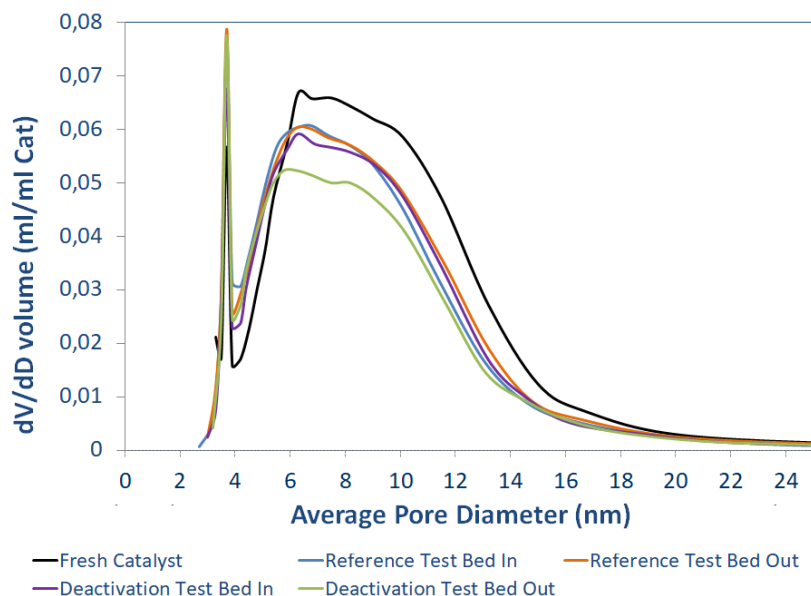


**Figure 39. Catalyst pore distribution (Nitrogen desorption isotherm).**

An approach based on the ratio of the hysteresis area of the spent catalyst with respect to the hysteresis area of the fresh catalyst was developed by Sámano et al. [213]. The authors established this ratio as a semi-quantitative analysis to evaluate the extent of catalyst deactivation. Table 11 indicates that the ratio of areas is higher for samples from the accelerated deactivation test than for samples from the reference test, as expected. Results also showed lower values for the spent samples from the first reactor inlet than for the reactor outlet, in accordance with the previous results. The obtained values for the pilot deactivated samples were close to the magnitude observed for industrial spent catalysts. The curves of the normalized isotherms are shown in Appendix 4.

## Chapter 2-Insights in the phenomena involved in deactivation of industrial hydrocracking catalysts through an accelerated deactivation protocol

### 3.2.2.3. TGA analysis

The spent catalyst samples were characterized by TGA analysis to compare the nature of coke deposits. The first time-derivative of weight loss as a temperature function is illustrated in Figure 40 for bed inlet and bed outlet samples from the deactivation test.

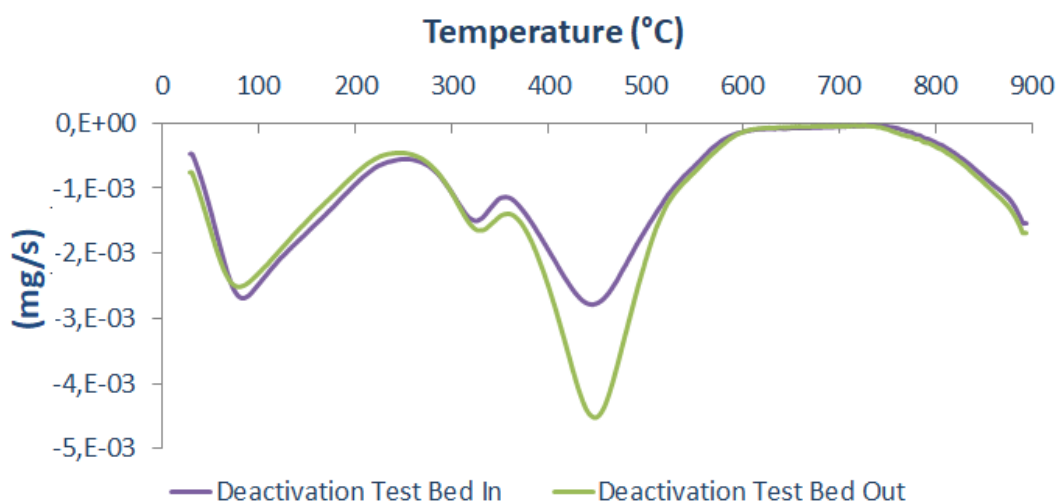


**Figure 40. TGA profiles of bed inlet and bed outlet samples from the deactivation test.**

The first peak around 100°C corresponds to H<sub>2</sub>O desorption, whereas the second one (280-330°C) and the third one (350-550°C) correspond mainly to SO<sub>2</sub> and CO<sub>2</sub> releases, respectively. Consequently, and in agreement with other studies [198,214,215], it is concluded that the deposit on the catalyst is composed mainly of carbon, whereas the SO<sub>2</sub> detected can be attributed to the molybdenum sulfide.

In general, the quantity of coke deposited is related to the intensity of the third peak (350-550°C) [6, 34]. The TGA results (Table 12) confirm the elemental analysis. The coke content was higher for the spent samples coming from the bed outlet of the deactivation test.

## Chapter 2-Insights in the phenomena involved in deactivation of industrial hydrocracking catalysts through an accelerated deactivation protocol

---

The temperature related to the maximum weight loss is an indicator of the nature of coke. The coke structure is expected to be more graphitic, hence more difficult to combust, at higher values of maximum weight loss temperature. The peak temperatures indicate that catalyst samples from the bed outlet (peak at 450°C) contained a slightly more graphitic coke than the spent solids from the bed inlet (peak at 445°C). The coke can be further characterized by determining its H/C ratio, which is proportional to the ratio of the CO<sub>2</sub> (44) and H<sub>2</sub>O (18) mass spectrometer signals, I<sub>18</sub>/I<sub>44</sub>. As was mentioned in section 2.3.4, only the CO<sub>2</sub> and the H<sub>2</sub>O detected between 200°C and 650°C were considered. The lowest I<sub>18</sub>/I<sub>44</sub> ratio of the coke deposited, and then the higher coke aromaticity was found for the industrial samples, followed by the bed outlet and the bed inlet samples from the deactivation test. The reference test samples presented the highest values, that is, the lowest coke aromaticity. Regarding bed location, the aromatic character increased from the first reactor inlet towards the second reactor outlet.

**Table 12. Estimation of CO<sub>2</sub> mass loss and H/C ratio of the coke deposit from ratio I18/I44 from TGA profiles for different spent catalysts.**

Sample	CO <sub>2</sub> mass loss (wt %)	I18/I44
Reference Test-Bed In	8.0	4.3
Reference Test-Bed Out	8.3	4.3
Deactivation Test- Bed In	9.1	3.4
Deactivation Test-Bed Out	11.0	2.1
Industrial Spent Catalysts	13-16	0.5-0.9

### 3.2.2.4. Raman analysis

The differences in aromaticity of the coke produced during the reference and deactivation experiments and some industrial cycles were confirmed by Raman spectroscopy. The spectra are showed in Figure 41. The reference test samples presented high fluorescence, showing very

## Chapter 2-Insights in the phenomena involved in deactivation of industrial hydrocracking catalysts through an accelerated deactivation protocol

noisy spectra. It indicates that the carbonaceous deposit was very poorly organized. In contrast, the spectra for the deactivation test and industrial spent samples were well defined. Hence, the carbonaceous deposit had a more organized structure in these cases. In fact, the two prominent peaks ( $1330\text{ cm}^{-1}$  and  $1600\text{ cm}^{-1}$ ) identified in the spectra are typically found in the case of a graphitic coke-type [24].

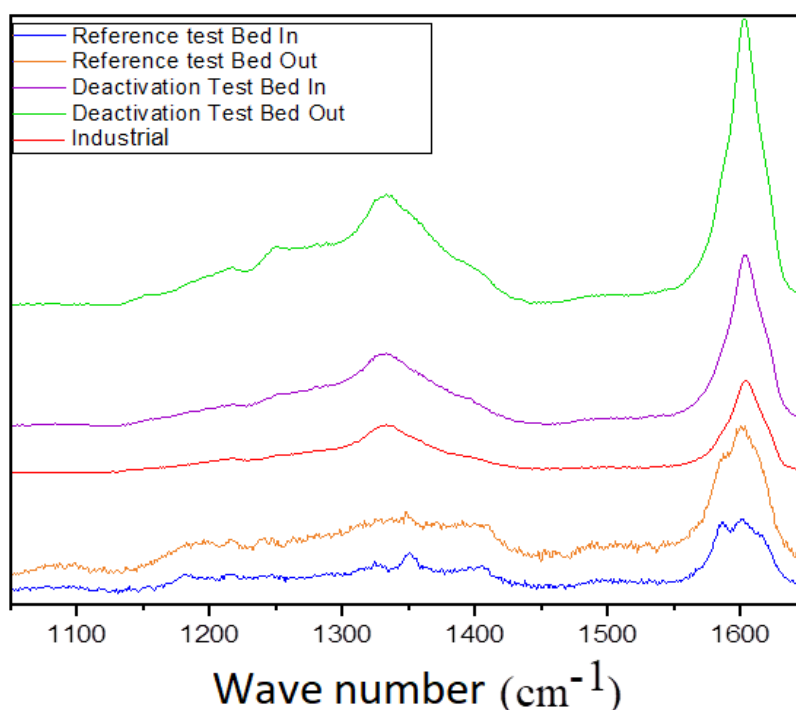


**Figure 41. Raman spectra of spent catalysts from the reference test, the deactivation test and industrial cycles.**

### 3.2.2.5. TEM/EDX analysis

TEM/EDX analysis was performed on spent samples from both the reference and the deactivation experiments. Morphology of the  $\text{MoS}_2$  slabs and Ni/Mo ratio are presented in Table 13. The  $\text{MoS}_2$  slabs for the deactivation test samples were between 10 and 25% longer than the reference test samples, whereas the dispersion values are very close. These results indicate a

## Chapter 2-Insights in the phenomena involved in deactivation of industrial hydrocracking catalysts through an accelerated deactivation protocol

---

slight sintering of the MoS<sub>2</sub> slabs under severe conditions during the deactivation test. Finally, a significant nickel depromotion was observed for the deactivation test samples. The related Ni/Mo ratio was about 40% lower than in the reference test samples.

**Table 13. Average slab length and dispersion measured by TEM and Ni/Mo ratio in MoS<sub>2</sub> particles measured by EDX.**

	Slab length (nm)	Dispersion	Ni/Mo
Reference test bed in	3.7±1.4	0.24	0.37±0.18
Reference test bed out	3.8±1.5	0.23	0.35±0.12
Deactivation test bed in	4.3±1.7	0.22	0.19±0.11
Deactivation test bed out	4.6±2.2	0.18	0.23±0.12

### 3.2.2.6. Model molecule experiments

The residual catalytic activities of the different spent samples were evaluated through specific experiments with model molecules. The hydrogenation of toluene provides information on the residual metal sites of the spent catalysts. The residual activity of the acid function is assessed through the n-heptane hydrocracking. The results are represented in Figure 42, which includes data related to the fresh catalyst. All spent catalysts presented lower metal and acid activities than the fresh catalyst, as expected. The deactivation test samples exhibited similar residual activities compared to the industrial samples and lower residual activities than the reference test samples.

The toluene conversion of the deactivation test samples was around 36% lower than the reference test samples. As mentioned above, the MoS<sub>2</sub> slab depromotion was 40% on average. According to previous works [216], there is a roughly linear correlation between the catalyst promoter content (Ni) and the hydrogenation activity. Hence, the loss of the hydrogenation activity can be mainly attributed to catalyst depromotion in that particular case. Furthermore,

## Chapter 2-Insights in the phenomena involved in deactivation of industrial hydrocracking catalysts through an accelerated deactivation protocol

concerning the location impact on deactivation, spent samples from the second reactor exhibited slightly lower conversions in the hydrogenation of toluene than samples from the first reactor.

The loss of conversion for the fresh catalyst was much more pronounced in the n-heptane hydrocracking case (see Figure 42 b vs. a). Thus, coke deposits seem to be preferentially located on the acid sites of the spent catalysts. Concerning reactor location, samples from the second reactor outlet showed slightly higher conversions than spent solids from the first reactor inlet. Consequently, the acid sites remained more active in the second reactor than in the first one, despite a higher carbon content and a higher aromatic character of the coke.

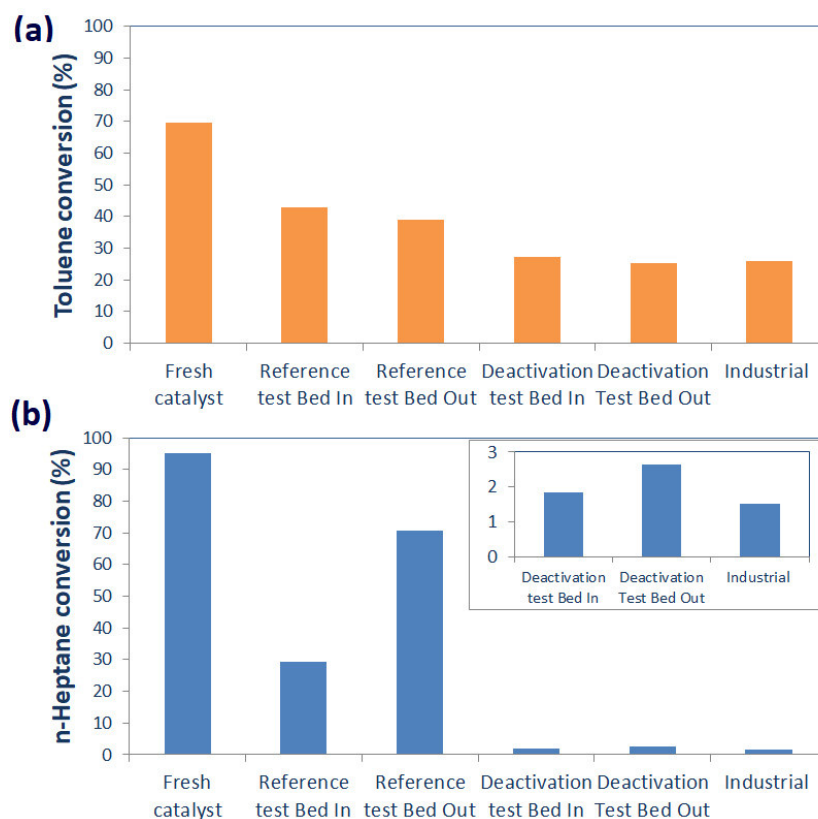


**Figure 42. Catalytic activity evaluated by model molecules catalytic tests for the reference and the deactivation tests samples and some spent industrial catalysts. a) Hydrogenation of toluene, b) Isomerization/cracking of n-heptane at 360°C.**

## Chapter 2-Insights in the phenomena involved in deactivation of industrial hydrocracking catalysts through an accelerated deactivation protocol

---

The selectivity towards i-heptane formation (the primary product) in the n-heptane hydrocracking experiment is illustrated in Figure 43 as an n-heptane conversion function. The selectivity towards the production of cracked products,  $C_3+C_4$ , naturally presents the opposite trend. The i-heptane selectivity, compared at the same conversion level, can be considered as an indicator of the residual metal/acid balance [102,217]. High selectivity is a sign of high hydrogenation activity as compared to the acid sites. A low i-heptane selectivity means that the acid sites are ill-balanced by the hydrogenation sites.

The i-heptane selectivity was higher in the case of the deactivated samples than the samples from the reference test as well as to the fresh catalyst. This is coherent with the previously described toluene hydrogenation and n-heptane hydroconversion activities. Indeed, these results show that the acid function underwent a much more severe deactivation than the hydrogenation function for the deactivated catalysts. This positively influences the metal/acid balance, leading to an increase in the i-heptane selectivity. Regarding reactor location, in agreement with previous considerations, the selectivity to i-heptane was higher for spent samples from the first reactor.

## Chapter 2-Insights in the phenomena involved in deactivation of industrial hydrocracking catalysts through an accelerated deactivation protocol

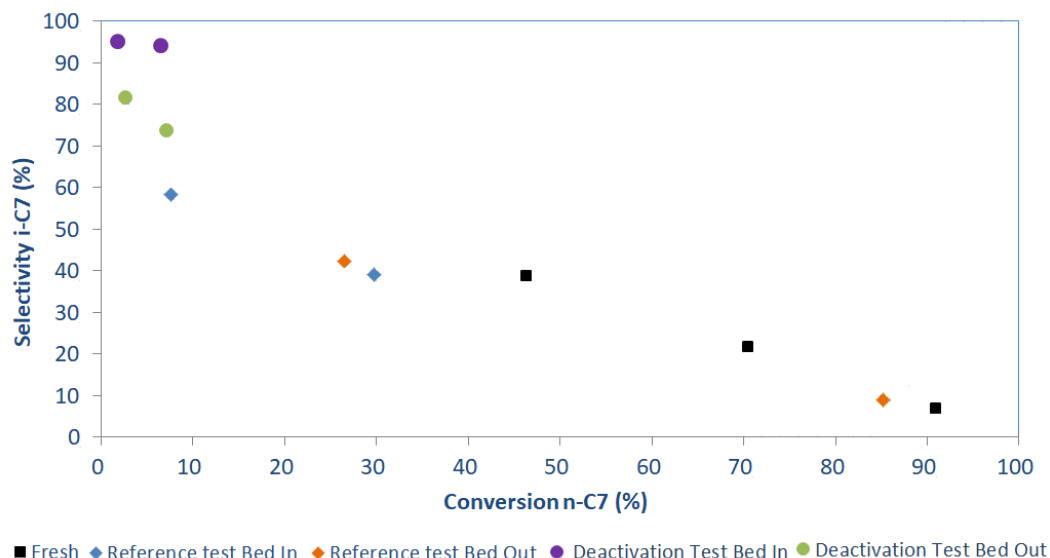


Figure 43. n-heptane hydroconversion experiment. Selectivity to i-C<sub>7</sub> Vs. conversion n-C<sub>7</sub>.

### 4. RESULTS DISCUSSION

Considerations about the deactivation phenomena are given in this section, with a special focus on the main mechanisms leading to hydrocracking catalyst deactivation with real feedstocks.

Organic nitrogen plays a key role in the deactivation phenomena. Organic nitrogen compounds are rapidly adsorbed on the catalyst acid sites [8,194] due to their basic character. This adsorption firstly leads to acid site inhibition through neutralization and, subsequently, to an irreversible deactivation by coke deposits. These deposits are produced by the reaction between adsorbed nitrogen species. This result agrees with the decrease of the coke's N/C ratio along with the system (from 0.035 at the bed inlet to 0.025 at the bed outlet). Both inhibition and coking lead to the loss of cracking activity [10].

One of the issues related to bifunctional catalyst deactivation in this particular case is to decorrelate the cracking function loss of activity from the metal function's deactivation. In fact,

## Chapter 2-Insights in the phenomena involved in deactivation of industrial hydrocracking catalysts through an accelerated deactivation protocol

---

the latter leads to a decrease in the HDN reaction rate. Thus, more nitrogen compounds are available to be adsorbed on the acid sites, resulting in a possible increase in acid function inhibition. Consequently, it is difficult to conclude if the cracking activity loss is simply due to further inhibition due to the increase of the nitrogen species concentration or other mechanisms such as coking by aromatics. The results obtained from the accelerated deactivation protocol (Figure 38) revealed that the cracking reaction rate continuously decreases even if HDN conversion remains almost unchanged. Moreover, the experiments performed with model molecules (Figure 42) showed an almost complete deactivation of the acid sites. Both findings indicate that the deactivation of the cracking function can be attributed to both inhibition by nitrogen species (which increases due to the deactivation of HDN) and coking of the acid sites.

The considerations made in the previous two paragraphs allow concluding on the mechanisms that lead to the deactivation of the acid sites. It is suspected that the very strong interaction of the organic nitrogen compounds with the acid sites may be at the origin of the coke formation. The N/C ratio values of the spent catalyst samples reinforce this hypothesis. These values are 0.035 mol/mol and 0.025 mol/mol for the bed inlet and outlet samples, respectively. This ratio is similar to the one related to typical organic nitrogen compounds in vacuum gas oils (molecules containing 20 to 40 carbon atoms and one nitrogen atom). Thus, an important proportion of coke originates from these nitrogen species, especially in the bed inlet samples. The higher amount of coke with a lower N/C ratio for bed outlet samples suggests that there might also be a contribution of aromatic compounds to the coke generation in the second reactor.

The effect of reactor location on the extent of the catalyst acid function deactivation is, once again, deeply linked to the organic nitrogen concentration evolution along the reactor. The bed inlet (and the first reactor as a whole) is exposed to a high concentration of organic nitrogen,

## Chapter 2-Insights in the phenomena involved in deactivation of industrial hydrocracking catalysts through an accelerated deactivation protocol

---

which leads to an almost full inhibition of the cracking function in R1; the 370°C<sup>+</sup> conversion can be attributed to hydrogenation and dealkylation reactions. This explains why the conversion in R1 remains constant after an initial stabilization period of ~150 h. In the second reactor, where the nitrogen inhibition was lower, a progressive loss of the cracking activity was observed before establishing a pseudo-plateau after ~500 h.

The spent samples characterization results agree well with the explanations given in the previous paragraph. The carbon content of the deactivated catalyst samples increases along the reactor, which is attributed to the inverse trend observed for the organic nitrogen concentration. In fact, the preferential adsorption of nitrogen compounds on acid sites inhibits polymerization of the dehydrogenated intermediates on metal sites, thus reducing the coke production rate. The textural properties show a higher loss in both BET surface and total volume related to spent solids from the second reactor.

The toluene hydrogenation test (Figure 42) showed a slightly higher residual hydrogenation activity for first reactor samples. This is contrary to the trend of the HDN reaction rate coefficients in the pilot experiments, which exhibited a lower value in the first reactor (Figure 36, Figure 38). To explain this behavior, it is important to have in mind that the performance (reaction rate coefficient) reflects both the inhibition and the permanent deactivation taking place over time on stream during the experiments. Model molecule catalytic tests are carried out on spent catalyst samples previously washed (see Section 2.3.4). As a result, these experiments display the residual activity due to the permanent catalyst deactivation exclusively. The extent of metal activity loss was assessed to 65%. This activity loss was mainly attributed to the significant observed Ni depromotion (Table 13). This depromotion reaches a value of 40% in the MoS<sub>2</sub> slabs of the spent catalysts from the accelerated deactivation procedure.

## Chapter 2-Insights in the phenomena involved in deactivation of industrial hydrocracking catalysts through an accelerated deactivation protocol

---

Finally, evaluating the ratio between available metal and acid sites allows concluding on the coke type as a function of reactor location. In fact, a difference in the relative rate at which each function is deactivated along the reactor induces a modification of the metal/acid sites' ratio (M/A). Thus, the ratios related to deactivated and to the fresh catalyst samples are expected to be different, as illustrated via the i-heptane selectivity in Figure 43. According to the i-heptane selectivity, the (M/A) ratio is lower for spent samples at the bed outlet spent samples than for the bed inlet. This can explain the higher amount of coke in the second reactor and its more aromatic character (lower H/C ratio, Table 11 and Table 12). Indeed, since the number of available metal sites is lower in the second reactor, the intermediate unsaturated coke precursors species produced on the acid sites undergo polymerization reactions before being hydrogenated.

### 5. CONCLUSIONS

- An accelerated deactivation protocol at the pilot plant scale was developed to study the hydrocracking catalyst deactivation phenomena in a short period of 30 days. From textural, elemental, thermogravimetry analysis as well as from the evaluation of the residual activities by model molecules tests, it is concluded that this protocol generates spent catalysts, which are very similar to industrial spent catalysts. This methodology allows a representative, fast and insightful way to evaluate the deactivation phenomena for hydrocracking catalysts. It can be used to evaluate the potential of a feedstock or certain operating conditions to coke and deactivate and compare different catalytic formulations from a stability point of view.

## Chapter 2-Insights in the phenomena involved in deactivation of industrial hydrocracking catalysts through an accelerated deactivation protocol

---

- The organic nitrogen content of the feedstock to the hydrocracking process is determinant in catalyst deactivation. The basicity of these compounds explains their strong adsorption on the acid sites (initial inhibitory effect), leading to the formation of coke deposits, which deactivate the catalyst acid function permanently. In contrast, nitrogen compounds have just an inhibitory effect on the metal function. The organic nitrogen impact on the reaction rates follows this order: Cracking>>HDN>HDA>HDS. The HDS activity is less affected as desulfurization can proceed via direct desulfurization (DDS), which does not rely on hydrogenation sites, which are inhibited by nitrogen.
- The deactivation of the metal function is mainly due to nickel depromotion; it reduces the hydrogenation activity by about 40%. The deactivation of the cracking function is much more significant. Due to two different mechanisms, the direct poisoning of the acid sites by the organic nitrogen compounds from the feed and an indirect consequence of the decreased HDN activity leads to a progressive increase of the average organic nitrogen concentration in the reactor during the time on stream. This increase in inhibition is mainly observed at reduced organic nitrogen contents, conditions at which these species do not fully cover the acid active surface.
- The coke composition analysis suggests that an important proportion of the coke originates from the organic nitrogen species. However, as the HDN is carried out along the reactor and nitrogen is removed, other mechanisms, like aromatic coke formation, start to play a more important role in catalyst deactivation.

## Chapter 2-Insights in the phenomena involved in deactivation of industrial hydrocracking catalysts through an accelerated deactivation protocol

---

- The balance in the ratio of the metal/acid sites determines the amount and the type of formed coke. The lower the ratio, the lower the hydrogenation of intermediate unsaturated coke precursors species produced in the acid sites, and consequently, the higher the coke production rate. A lower metal/acid balance also leads to coke presenting a lower hydrogen content and, as a result, a more aromatic (less reactive) structure. Since the metal/acid balance decreases from bed inlet to bed outlet (due to less inhibition by organic nitrogen at the bed outlet), the bed outlet contains a higher amount of coke, which is more aromatic.

**CHAPTER 3**  
**Impact of feedstock properties**  
**on the deactivation of a**  
**vacuum gasoil hydrocracking**  
**catalyst**

---

## Chapter 3-Impact of feedstock properties on the deactivation of a vacuum gasoil hydrocracking catalyst

---

### CHAPTER 3-IMPACT OF FEEDSTOCK PROPERTIES ON THE DEACTIVATION OF A VACUUM GASOIL HYDROCRACKING CATALYST

Publication accepted in Energy & Fuels: <https://doi.org/10.1021/acs.energyfuels.1c00965>

#### ABSTRACT

The aim of this study was to understand the impact of vacuum gas oil (VGO) properties on the deactivation rate of a hydrocracking catalyst (a nickel-molybdenum sulfide dispersed on a carrier containing USY zeolite). For that purpose, two hydrotreated feeds of different density, organic nitrogen (~120-150 ppmw) and aromatic content, were hydrocracked under operating conditions that favor catalyst deactivation, i.e., high temperature ( $T=418^{\circ}\text{C}$ ) and high space velocity ( $\text{LHSV}=3\text{ h}^{-1}$ ). The catalyst performance was followed by measuring the VGO conversion ( $370^{\circ}\text{C}^{+}$  petroleum cut) and determining the reaction rate coefficients for the main hydrocracking reactions (cracking, hydrodenitrogenation, hydrodesulfurization and aromatics hydrogenation). The experiments were stopped after different times on stream (either 6 or 30 days) in order to assess the evolution of the catalyst as a function of time. The spent catalysts, obtained from three different reactor locations, were characterized by elemental and textural analysis and by thermogravimetry to investigate the quantity and nature of the coke formed. Catalytic tests with different model compounds (toluene, n-heptane) were carried out to determine the residual activity of the hydrogenating and acid catalyst functions. It was found that, at the evaluated conditions, both organic nitrogen and aromatics, nature and content of the feedstock, have a determinant role on the deactivation rate. The organic nitrogen determines the ratio between available metal and acid sites. The aromatics generate coke precursors on the available acid

## Chapter 3-Impact of feedstock properties on the deactivation of a vacuum gasoil hydrocracking catalyst

---

sites. Both factors play a coupled role that promotes coke deposition on the catalyst surface, which leads to an increase in the deactivation rate on top of the end boiling point of the feed.

### 1. INTRODUCTION

Catalyst deactivation is a physical and/or chemical process that decreases the activity of a given catalyst [218]. The deactivation is a problem of great concern in the practice of industrial catalytic processes. Costs for catalyst replacement and process shutdown total billions of dollars per year [219]. Deactivation depends on feedstock, operating conditions and catalyst properties [119]. Concerning the feedstocks, it is known that in the hydrocracking of vacuum gasoils (VGO), the formation of coke and quasi-irreversible poisoning by heavy nitrogen molecules are the primary reasons for catalyst deactivation [8,130]. The contribution of metals to deactivation becomes evident with deasphalted oil and increases as the feed becomes heavier, such as with atmospheric and vacuum residues [220].

Carbonaceous deposits (“coke”) on catalysts are gradually formed during the hydrocarbon conversion reactions. Deactivation by coke is due to physical blocking of active sites or because large amounts of coke can lead to pore blocking and prevent reactant molecules from reaching the active sites inside the pores [218]. Coke formation depends on the type of processed feed. For example, aromatic feedstocks form more coke than aliphatic ones under similar processing conditions because polyaromatic structures are more easily formed from aromatics [152]. Coking is more pronounced with condensed ring systems (e.g., naphthalene, anthracene) than with the corresponding linked systems (biphenyl, terphenyl) [154,155]. Heterocycles produce more coke than hydrocarbon analogs [33]. For alkyl-substituted aromatics, coke deposition increases with the length of the side chains rather than with the number of alkyl substitutions [155].

## Chapter 3-Impact of feedstock properties on the deactivation of a vacuum gasoil hydrocracking catalyst

---

Two different mechanisms have been proposed for coke formation on the metal and the acid sites of bifunctional catalysts. On metal sites, it is presumed that coke results from successive dehydrogenations leading to atomic carbon or partially hydrogenated intermediates that combine to form graphitic coke [109,156]. On acid sites, it is accepted that coke results from polymerization of dehydrogenated intermediates generated on the metal sites [157].

Concerning spent catalysts from VGO hydroprocessing, Sahoo et al. [162] characterized two samples after a dichloromethane extraction. The soluble part was termed as “soft coke,” and its structure was similar to those of the VGO heavy components. The insoluble part, named as “hard coke”, was more aromatic. Coke on catalysts deactivated during the hydroprocessing of atmospheric (ARs) and vacuum residues (VRs) is even “harder”. Amemiya et al. [163] took catalyst samples from a VGO hydroprocessing unit after 12 months on stream. These samples were extracted from different locations in the axial direction of a single fixed bed. The amount and the graphitic nature of the coke increased toward the end of the bed. Koizumi et al. [164] also found an amorphous coke structure at the inlet and a graphitic structure at the catalyst bed outlet.

Regarding the deactivation by nitrogen compounds, it is necessary to explain the deactivation mechanism by poisoning. This mechanism corresponds to the strong chemisorption of impurities on active sites preventing the access of reactants to them [161]. Even if the term “poisoning” is used, this mechanism can be divided into two different categories: inhibition or poisoning. Inhibition results from reversible adsorption of the pollutant named inhibitor. The catalyst regains its original activity when it is removed [33]. On the other hand, a poison is not desorbed; its bonding to the active site is so strong that its desorption rate is negligible under reaction conditions. Upon its removal from the feed, the catalyst activity loss is not recovered [33]. The type of N-compounds and the total amount of nitrogen vary from feed to feed [221]. The five and

## Chapter 3-Impact of feedstock properties on the deactivation of a vacuum gasoil hydrocracking catalyst

---

six-membered N-rings, classified as non-basic “neutral” and basic N-compounds, respectively, are predominant structures [222]. The less basic or neutral nitrogen derivatives are readily decomposed into ammonia[35], which acts as an inhibitor of the cracking reaction. The more basic compounds are cataloged as poisons as they are strongly adsorbed on the acid sites of the catalyst [11].

The work of Park et al. [128] indicated that, when adsorbed on catalytic sites, N-compounds hinder the adsorption of other reactants and slow down the hydrogen activation process. The availability of active surface hydrogen [129] for the other hydroprocessing reactions and the coke formation is thus limited. Therefore, at least part of the coke is formed due to the catalyst poisoning by N-compounds. Studies on model compounds and real feeds indicate that less than 50 ppm of organic nitrogen in the feed can poison catalytic sites [130].

Regarding vacuum gas oil (VGO) hydrocracking, little information is available in the open literature on the effects of nitrogen compounds on hydrocracking conversion. Sau et al. [8] studied the inhibition effects of nitrogen on VGO hydrocracking at different temperatures. Results showed a rapid drop in hydrocracking conversion as the nitrogen content increases. The higher the reaction temperature, the lower the conversion drop at the same nitrogen content because of the higher desorption rate at elevated temperatures. The increase of nitrogen level in the feed inhibited the catalyst; thus, the conversion drops rapidly, and the drop becomes less significant as the nitrogen level increases. It is because the adsorption equilibrium might have been reached. The HDS activity increased by about 60% after the N-compounds were removed from the VGO by adsorption with silica-alumina, which evidence the inhibition of the HDS reaction by nitrogen compounds. Kaernbach et al. [147] also observed a higher HDS conversion in the absence of N-compounds from a Russian crude, confirming their negative impact on the

## Chapter 3-Impact of feedstock properties on the deactivation of a vacuum gasoil hydrocracking catalyst

---

catalyst (de)hydrogenation activity. The important contribution of N-compounds to catalyst deactivation during the hydroprocessing of a VGO was also confirmed by Massoth et al. [148].

Related to the impact of weakly basic organic nitrogen, Celis et al. [149] carried out a work that consisted of studying the hydrocracking of phenanthrene as a model reaction over a conventional Ni-MoS<sub>2</sub>/Y-zeolite-alumina catalyst. Results showed that the weakly basic nitrogen compounds, carbazole and its partially hydrogenated compound tetrahydrocarbazole, affect the catalytic performance by reducing its activity and inhibiting its selectivity to hydrocracking products. Laredo et al. reported that the inhibiting effect of the non-basic compounds, viz., carbazole, quinoline and indole, is powerful even at a low concentration of 5 ppmw [150].

In the previous chapter was described the development of an accelerated deactivation procedure for hydrocracking catalysts using real feeds (VGO) at conditions close to typical process conditions. The aged catalysts from this protocol showed comparable properties to some industrial spent catalysts. Through this experimental procedure, it was found that the organic nitrogen content of the feedstock is crucial since it determines the ratio between the available metal and acid sites. In turn, this ratio determines the coking reactions that take place and, therefore, the type of coke produced. This work aims to evaluate the effect of the feedstock properties on the deactivation. For this purpose, the catalyst was submitted to the mentioned protocol using two different VGO's. The reactivity evolution of the main hydrocracking reactions, as well as the deactivation phenomena by coke and nitrogen compounds in a coupled way, were studied.

# Chapter 3-Impact of feedstock properties on the deactivation of a vacuum gasoil hydrocracking catalyst

---

## 2. EXPERIMENTAL SECTION

### 2.1. Feedstocks

Two different feedstocks were used to evaluate the impact of feedstock properties on catalyst deactivation. Feedstock A consisted of a hydrotreated straight-run vacuum gas oil (VGO-HDT); the feedstock B was a hydrotreated blend of 71% vacuum gasoil, 16% coker gasoil and 13% light cycle oil on a weight basis. The main properties of these feeds are shown in Table 14. Both feedstocks have a quite different boiling range, feed A being heavier than feed B. The distillation yields for each one are presented in Figure 44. Dimethyl disulfide and aniline were added to the hydrotreated feeds to generate the hydrogen sulfide and ammonia partial pressures representative of the mother feed containing sulfur and nitrogen contents of 1,18 wt% and 0,25 wt%, respectively.

**Table 14. Feedstocks properties.**

<b>Properties</b>		<b>Feed A</b>	<b>Feed B</b>
Density @ 15°C	g/cm <sup>3</sup>	0.8984	0.8679
Refraction Index @ 70° C		1.4751	1.4791
Sulfur	wt%	0.068	0.016
Nitrogen	ppm	149	120
Aromatics content	wt%	~37	~42
Yield of 370°C+ fraction	wt%	92	64
Initial boiling point (IBP)	°C	179.8	130.5
T50 boiling point	°C	461	397
Final boiling point (FBP)	°C	589.8	554.4

## Chapter 3-Impact of feedstock properties on the deactivation of a vacuum gasoil hydrocracking catalyst

---

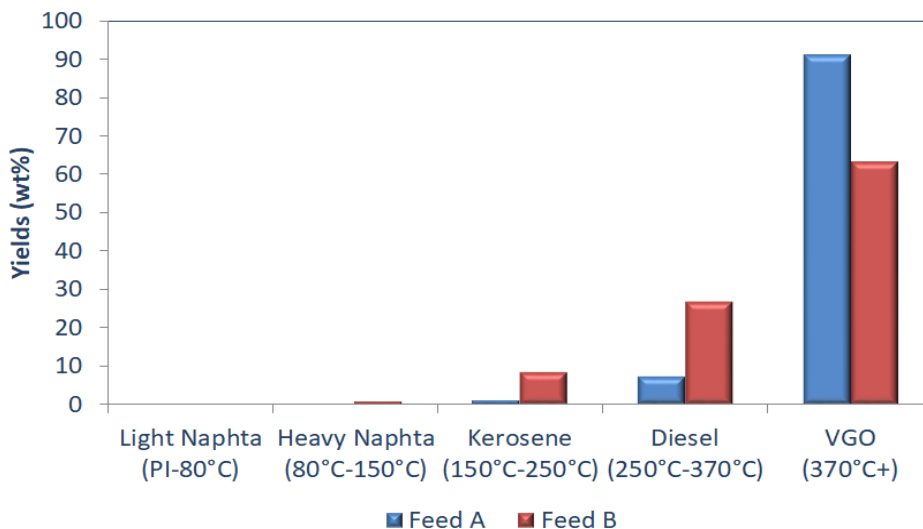


**Figure 44. Cut yields for feedstocks A and B.**

Considering that the main deactivation mechanisms in the deactivation of VGO hydrocracking catalysts are coking deposition and poisoning by nitrogen compounds, more detailed information about the aromatics type and the nitrogen compounds is given in Figure 45 and Figure 46, respectively. The aromatics content was ~37 wt% and ~42 wt% for feed A and feed B, respectively. Monoaromatics were the dominating family within both feeds, followed by diaromatics and triaromatics; the mass fractions of these three families were slightly higher for feed B.

## Chapter 3-Impact of feedstock properties on the deactivation of a vacuum gasoil hydrocracking catalyst

---

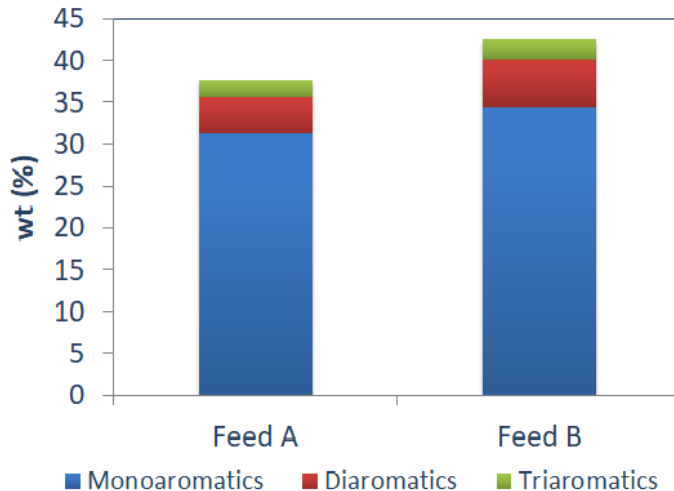


**Figure 45. Aromatics type of Feed A and B.**

These feeds had a different organic nitrogen content: 149 ppm wt. (Basic Nitrogen - 36 ppm wt.) for feed A and 120 ppm (~30 ppm of basic nitrogen) for feed B. Such high nitrogen contents are untypical (usually hydrotreating is pushed to lower nitrogen concentration before entering the hydrocracking reactor) but were deliberately chosen to accelerate catalyst deactivation. To determine the distribution of the different nitrogen families, an analysis by FT-ICR/MS was carried out. The nitrogen families in both feedstocks are shown in Figure 46; feed A contained more acridine (basic nitrogen), carbazoles, benzocarbazoles and dibenzocarbazole (neutral nitrogen) than feed B. Carbazole compounds are usually considered as most refractory for the HDN reactions (they are left over at high HDN conversions) [40].

## Chapter 3-Impact of feedstock properties on the deactivation of a vacuum gasoil hydrocracking catalyst

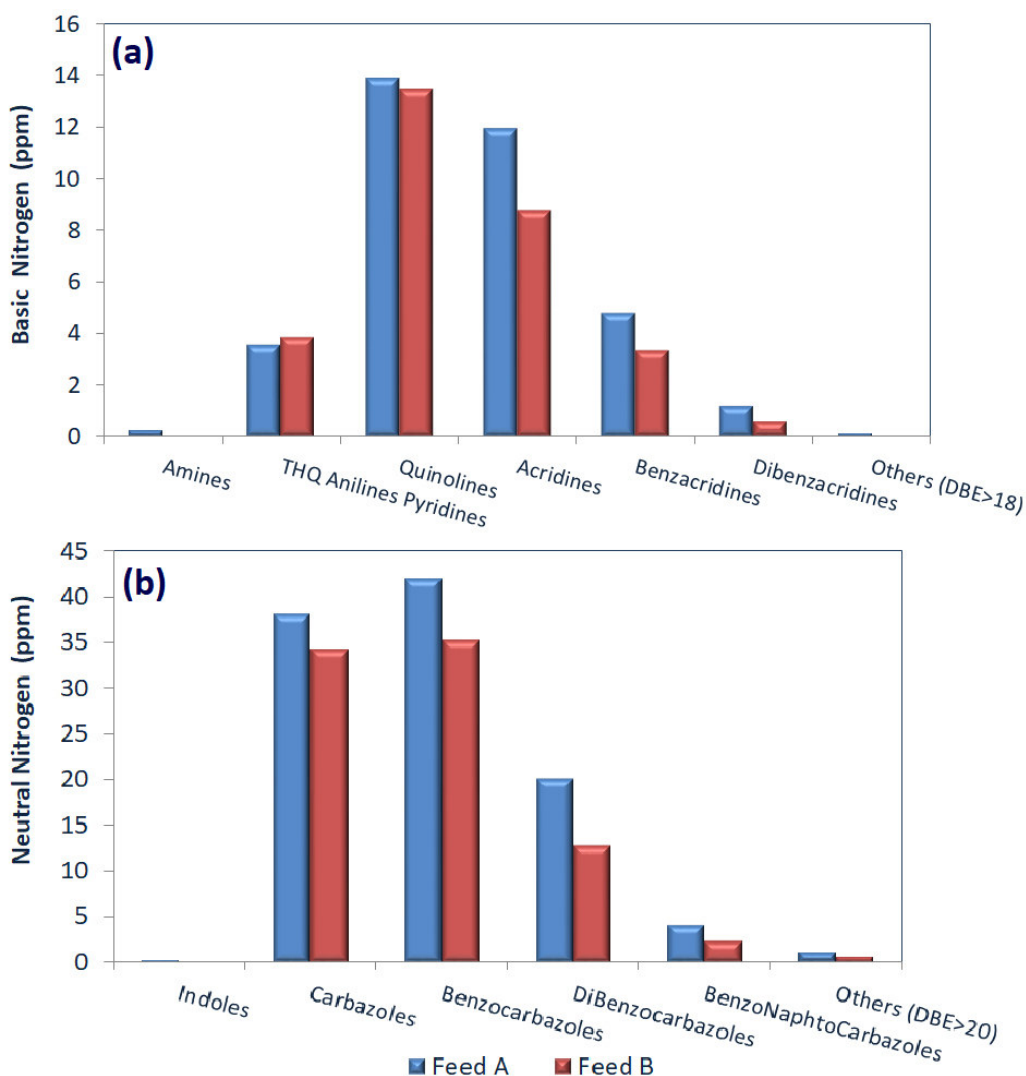


**Figure 46. Concentration of representative families by DBE in (a) basic and (b) neutral nitrogen, determined by FT-ICR/MS analysis for both feeds [223].**

Figure 47 presents the experimental carbon number distributions of the N-containing compounds for the two feeds. These curves are obtained from summing up the ESI(+) and ESI(-) FT-ICR/MS data. The curve for feed B shifted to a lower carbon number with respect to the curve for feed A. The carbon number for feed A is in the range of 15 to 67, whereas for feed B, the carbon number is between C10 and C60. The maximum of the carbon number distribution for feed A is

## Chapter 3-Impact of feedstock properties on the deactivation of a vacuum gasoil hydrocracking catalyst

around 40; meanwhile, for feed B is 33. All the above indicates nitrogen molecules of higher molecular weight for feed A associated with a higher degree of alkyl substitution.

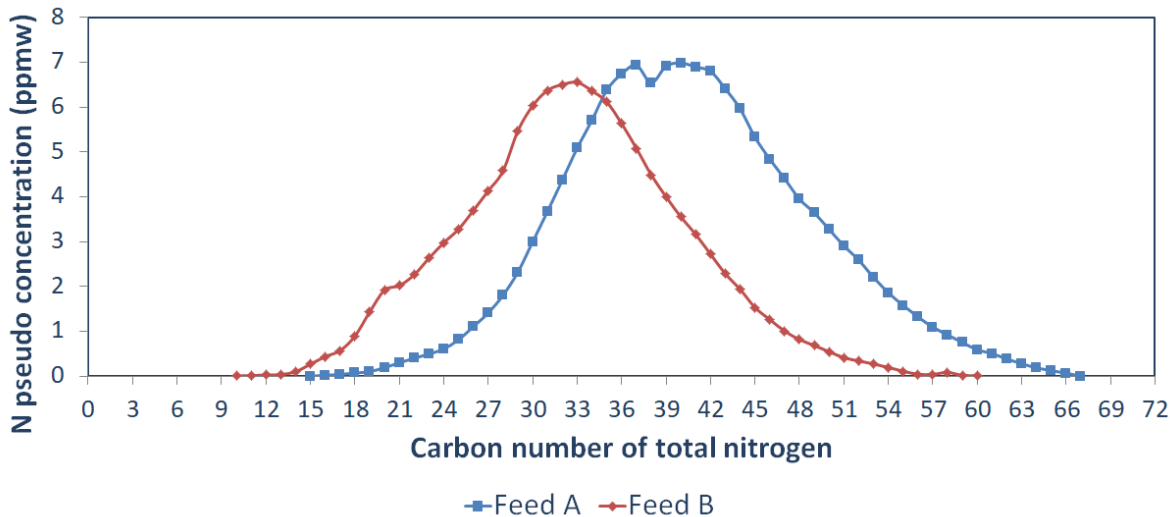


Figure 47. Carbon number distribution curves of the total nitrogen content in the feeds by FT-ICR/MS analysis [223].

### 2.2. Catalyst

The fresh catalyst consisted of nickel-molybdenum sulfide particles dispersed on a carrier containing USY zeolite.

### 2.3. Experimental set-up

The experiments were carried out in a fixed bed pilot unit with a co-current gas-liquid mixture flowing upwards. The detailed information has been reported in the previous chapter, section 2.1. The pilot plant consisted of two isothermal (Figure 30) reactors in series, which were used for the hydrocracking process. The catalyst bed was diluted with inert carborundum (SiC). A liquid sampling system was placed between the two reactors. At the second reactor outlet, a high-pressure separator was installed to separate the gas and liquid phases. The gas effluent was transferred to a gas flowmeter and then analyzed by gas chromatography, whereas the liquid product was sent to a stripper and finally to a storage recipient. Liquid products were

## Chapter 3-Impact of feedstock properties on the deactivation of a vacuum gasoil hydrocracking catalyst

---

characterized by density, refraction index, nitrogen and sulfur content and simulated distillation to monitor the daily performance of the catalyst. At the end of the run time (6 or 30 days), liquid samples were also analyzed to measure the aromatics, carbon and hydrogen contents.

### 2.4. Experimental procedure

The catalyst was activated in situ by sulfidation with an atmospheric gasoil spiked with 2% wt. (%/feed) of dimethyl disulfide (DMDS) and 2% wt. aniline (%/feed) at 350°C and 14MPa. Once sulfidation was completed, the deactivation conditions were applied, i.e., 418°C, LHSV of 3 h<sup>-1</sup>, H<sub>2</sub>/HC = 1500NL/L and P = 14 MPa, with the feedstock spiked with aniline as described in section 2.1 (N<sub>org</sub> = 150 ppm wt., and N<sub>total</sub> = 2500 ppm wt). Under the conditions applied, the catalyst immediately enters a deactivation regime, which does not exhibit stabilization. However, in the analysis of the experimental results, the values of the first two days of the test were not taken into account, since at the beginning, the effects of the system stabilization and the catalyst deactivation may be overlapped. The catalyst remained at the same conditions for 6 or 30 days, depending on the test. At the end of the run, the unit was washed with atmospheric gasoil. The catalyst was stripped and dried with hydrogen before being unloaded. Catalyst samples taken at the end of each experiment were carefully collected to separate the particles from the inlet, middle and outlet of each catalytic bed. More information about specific experimental procedures can be found in chapter 2.

### 2.5. Data interpretation: kinetic laws, deactivation parameter and hydrogen consumption

The catalyst performance was tracked by estimating the VGO conversion (370°C<sup>+</sup>) as well as the hydrodenitrogenation (HDN), aromatics hydrogenation (HDA) and hydrodesulfurization (HDS) conversion (Equation 16). For calculating the HDA conversion, the amount of aromatic carbon was estimated through the n-d-M method according to the standard ASTM D3238. To

## Chapter 3-Impact of feedstock properties on the deactivation of a vacuum gasoil hydrocracking catalyst

---

use this method, the molecular weight was estimated by the Lee-Kesler correlation. Yet, interpreting raw conversion data may be misleading, especially when conversion is high, because the differential reaction rate necessarily decreases when the reactant is depleted at increasing conversion. For a rigorous analysis of reaction rates, a kinetic model should be established, but for the complex VGO reaction network this requires a considerable amount of input data [53], which was not available in our case. Therefore, for the sake of simplicity, power-law models have been employed in this work. Several authors [67–69] have used this type of expression to calculate these constants for similar reaction systems. A first-order [70] kinetics was assumed for VGO conversion, HDN and HDA [205] (Equation 17). The first-order rate law does not account for inhibition effects, but allows correcting, albeit approximately, for the impact of depleting reactant concentration on the reaction rates. For HDS an apparent reaction order of 1.2 (Equation 18) was used; from our experience this reaction order allows accounting for the fact that S-species converted at low conversions are more reactive than the refractory species left over at high conversions.

$$\%Conversion = \left( \frac{mass_x \text{ feed} - mass_x \text{ product}}{mass_x \text{ feed}} \right) * 100 \quad \text{Equation 16}$$

Where x is either the 370+ mass, the nitrogen content, the sulfur content, or the aromatic carbon content.

$$k = LHSV * \ln(1 - \%Conversion/100) \quad \text{Equation 17}$$

$$k_i = \frac{LHSV}{n-1} \left( \frac{1}{(C_s^{out})^{n-1}} - \frac{1}{(C_s^{in})^{n-1}} \right) \quad \text{Equation 18}$$

## Chapter 3-Impact of feedstock properties on the deactivation of a vacuum gasoil hydrocracking catalyst

---

Here  $n=1.2$ ,  $C_s^{in}$ , and  $C_s^{out}$  are the feed and product concentration in percentage of sulfur.

An exponential decay model with three parameters (Equation 19) was assumed to dissociate the deactivation from the kinetic performance. In this model, the catalyst deactivation depends on the deactivation constant and time on stream (TOS) [6,68]. The experimental data of the evolution of the cracking kinetic constant with time was then fitted to this exponential decay function.

$$k_{crack}=A*\exp(-\alpha*TOS)+c \quad \text{Equation 19}$$

Where:  $(A+c)$  corresponds to the kinetic constant of the fresh catalyst at time=0,  $c$ , corresponds to the residual activity of the spent catalyst and  $\alpha$  corresponds to the deactivation rate (1/time).

The hydrogen consumption was calculated from the experimental data by performing a global hydrogen balance [224] (Equation 20). It was based on the elemental analysis of liquid streams and gas chromatography. Hydrogen in gas compounds such as  $H_2S$  and light hydrocarbons ( $C_1$  to  $C_6$ ) was calculated from molar equivalents, assuming that all the light products are paraffins and all is present only in the gas product.

$$H_{cons} = H_{Liq}^{out} - H_{Liq}^{in} + H_{Light\ HC}^{out} + H_{H_2S}^{out} \quad \text{Equation 20}$$

Where  $H_{cons}$  is the hydrogen consumption,  $H_{Liq}^{out}$  is the total amount of hydrogen contained in the hydrotreated liquid product,  $H_{Liq}^{in}$  are the total amount of hydrogen contained in the hydrotreated liquid feed and the additives (dimethyl disulfide, aniline),  $H_{Light\ HC}^{out}$  is the amount of the hydrogen contained in light hydrocarbons and  $H_{H_2S}^{out}$  is the amount of hydrogen contained as  $H_2S$  in the gas phase.

## Chapter 3-Impact of feedstock properties on the deactivation of a vacuum gasoil hydrocracking catalyst

### 2.6. Samples Characterization

Feed and daily liquid products were characterized by a densimeter for determining the density, by chemiluminescence for the nitrogen content, by X-Ray fluorescence spectrometry for the sulfur content and gas chromatography for the simulated distillation. At the end of the test, the product samples were also analyzed by combustion and thermal conductivity detection to measure the carbon and hydrogen contents and by UV spectrometry to identify the different aromatic families.

In the case of the nitrogen compounds families, feed samples were analyzed by Fourier transform ion cyclotron resonance mass spectrometry (FT-ICR/MS). The analyses were carried out using an LTQ FT Ultra Mass Spectrometer FT-ICR/MS (ThermoFisher Scientific, Bremen Germany) equipped with a 7T magnet (Oxford Instruments), electrospray ionization (ESI) ion source in both polarities (ThermoFisher Scientific, Bremen Germany). The ESI+ ionization mode is selective to basic nitrogen compounds, the ESI- mode to neutral nitrogen compounds. Mass range was set to  $m/z$  98-1000. The sample preparation conditions are shown in Table 15.

**Table 15. Samples preparation conditions for FTC-IR-MS analysis.**

		ESI (+)	ESI (-)
Dilution level	(%v/v)	1 Toluene	1 Toluene
Mix of solvents	(%v/v)	75/25 (Toluene/Mehtanol)	75/25 (Toluene/Mehtanol)
Additive added	(%v/v)	1 (Acetic Acid)	1 (Ammonium Hydroxide)

Concerning the spent catalysts, they were characterized by the same analytical methods described in the preceding chapter, section 2.3.4. except by Raman spectroscopy. The residual

## Chapter 3-Impact of feedstock properties on the deactivation of a vacuum gasoil hydrocracking catalyst

activity of the spent catalysts was determined following the methodology detailed in the same section (2.3.4.).

### 3. RESULTS

#### 3.1. Reaction rate coefficients

The global net conversion evolution during the long-term tests for both feeds is represented in Figure 48. The performance for the short-term tests was very close to the corresponding period of the long test, so the related data are not shown. As expected, the curves exhibited a lower conversion for feed A, which was heavier and had a higher organic nitrogen content than feed B. The loss of conversion under the accelerated deactivation protocol conditions was more appreciable for feed A than for feed B. The conversion value in the first reactor for feed A was around 20% and 40% for feed B; this conversion was mainly due to dealkylation and hydrogenation reactions carried out on the metal function.

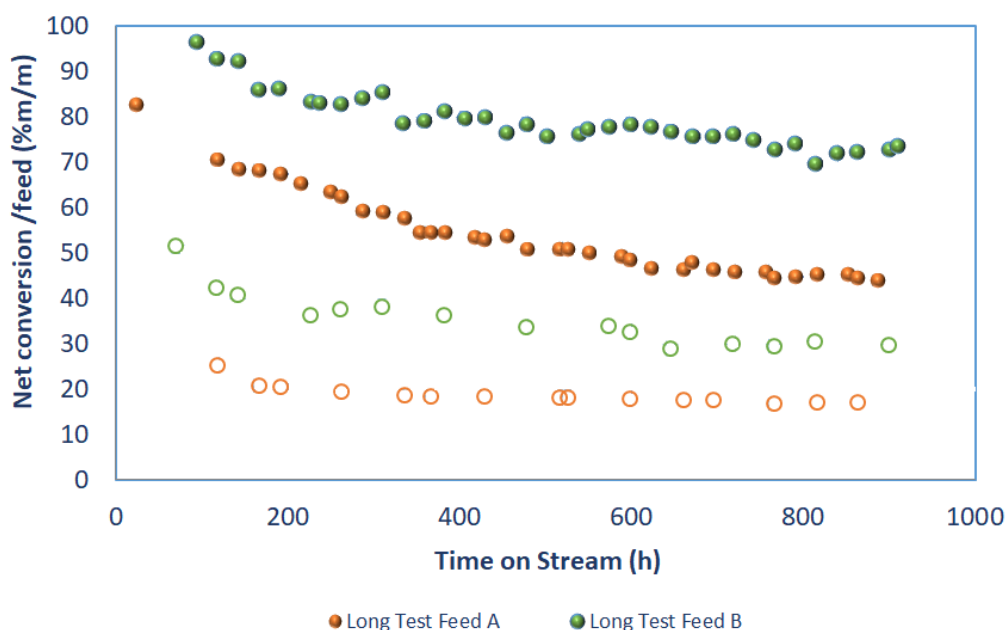


**Figure 48. Net conversion evolution with time on stream during long tests with feed A and feed B. Full symbols=Total effluent, open symbols=First reactor effluent.**

## Chapter 3-Impact of feedstock properties on the deactivation of a vacuum gasoil hydrocracking catalyst

---

The distillation curves of the final effluents of the long-term experiment at the first and second reactor outlets are shown in Figure 49. No significant shift with respect to the related feed was observed for the effluents from the first reactor. This behavior was not observed in the case of the effluents from the second reactor. It suggests that cracking reactions in the first reactor were limited.

## Chapter 3-Impact of feedstock properties on the deactivation of a vacuum gasoil hydrocracking catalyst

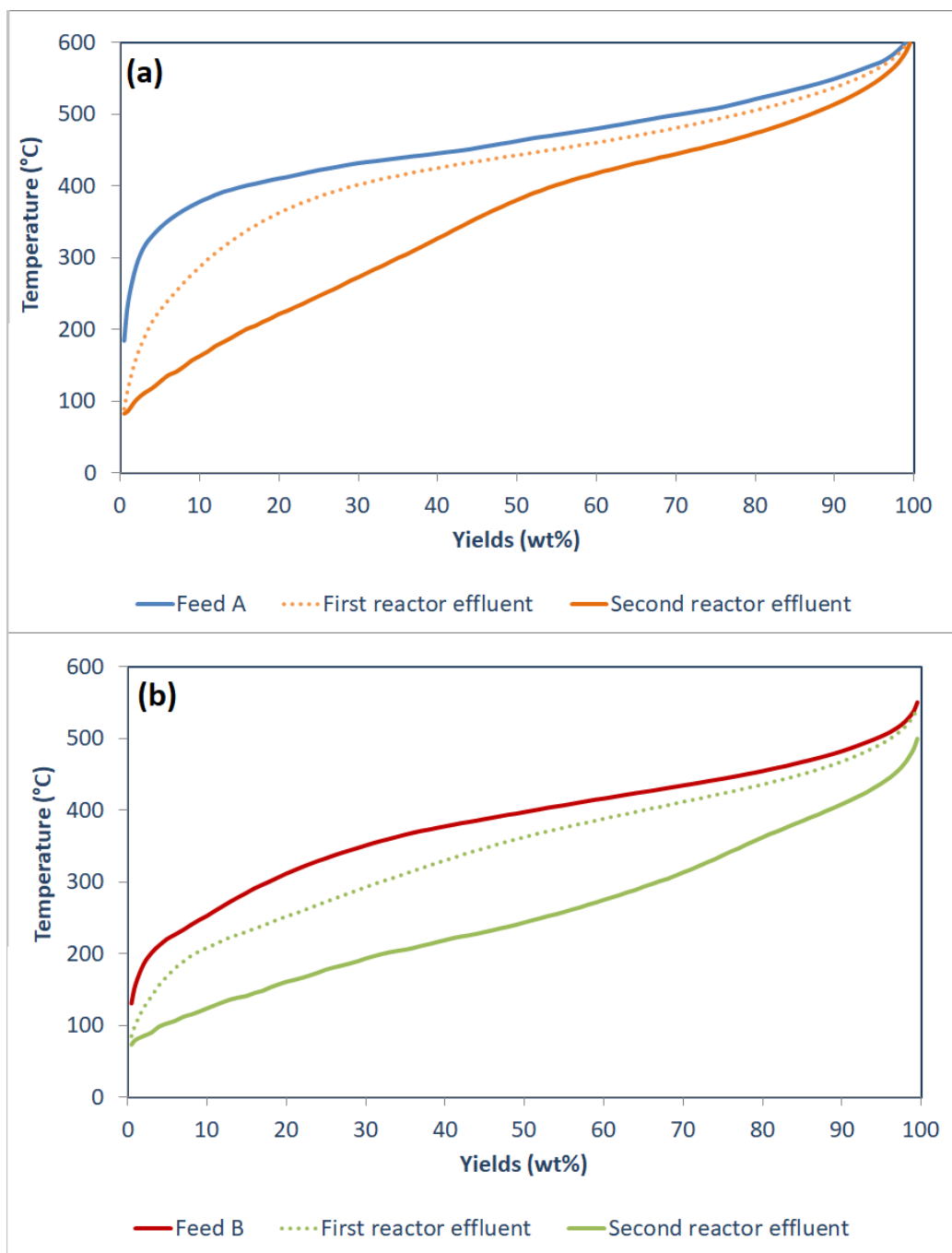


Figure 49. Simulated distillation curve obtained for the feed, first reactor outlet, second reactor outlet with a) feed A, b) feed B for the long-term tests. Dotted line=First reactor effluent, continuous line=Total effluent.

## Chapter 3-Impact of feedstock properties on the deactivation of a vacuum gasoil hydrocracking catalyst

---

The evolution of the reaction rate coefficients of the relevant chemical reactions (cracking, HDN, HDA and HDS) with time on stream (TOS) is shown in the figures below. Both the global performance of the two reactors and the one for the first reactor are presented for the two different feeds during the long-term test.

Regarding the global performance, the data for the cracking constants (Figure 50) showed that, as was foreseeable, feed B was more reactive than feed A. The rate coefficients of the HDN reactions (Figure 51) were also higher for feed B. This can be attributed to the lower amount of carbazole, benzocarbazole and acridine in this feed (Figure 46), identified among the most refractory compounds in the neutral and the basic nitrogen families [225–227]. The higher degree of alkyl substitution (Figure 47) of the nitrogen heterocycles in feed A further reduces their reactivity [223].

## Chapter 3-Impact of feedstock properties on the deactivation of a vacuum gasoil hydrocracking catalyst

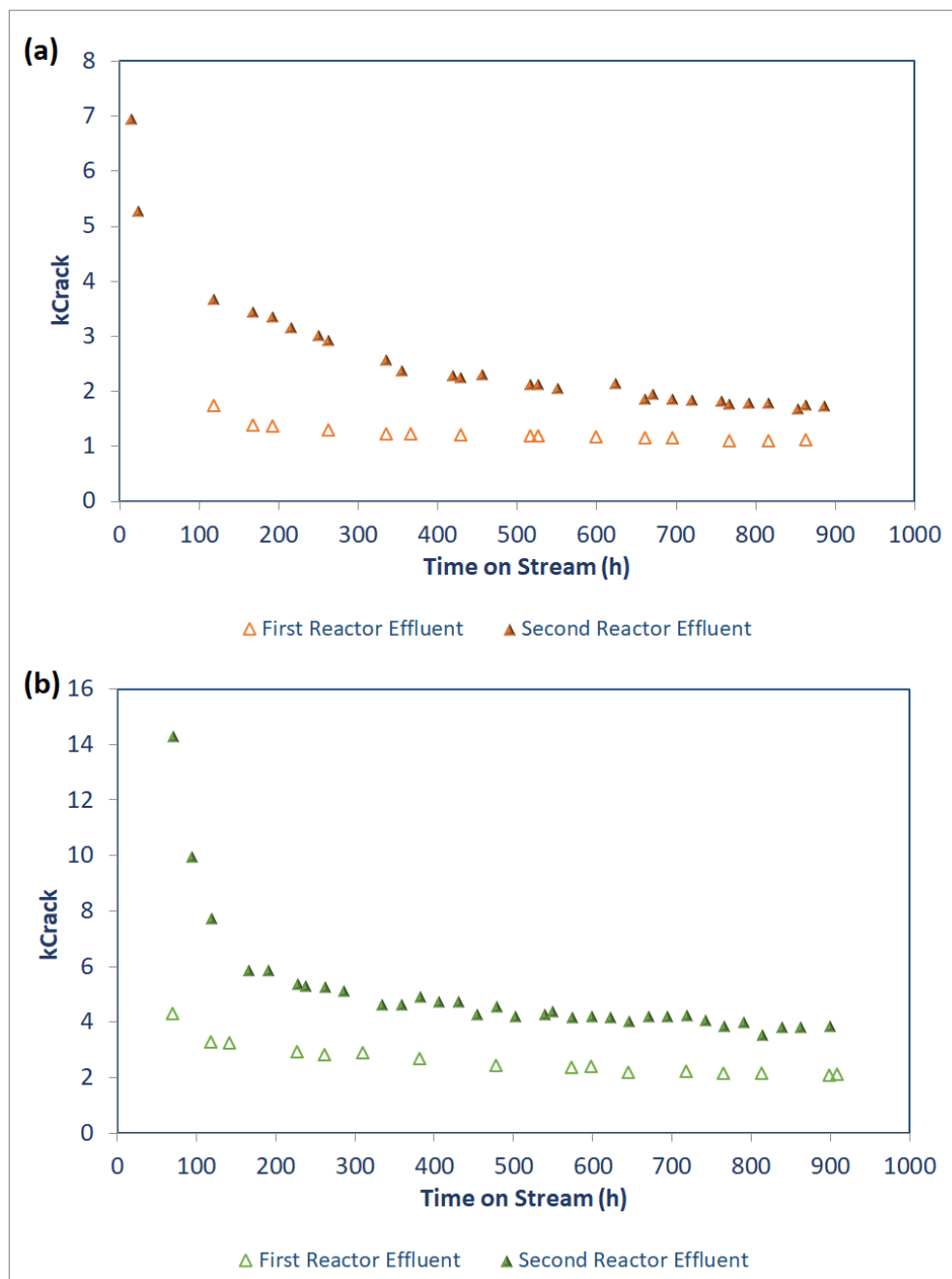
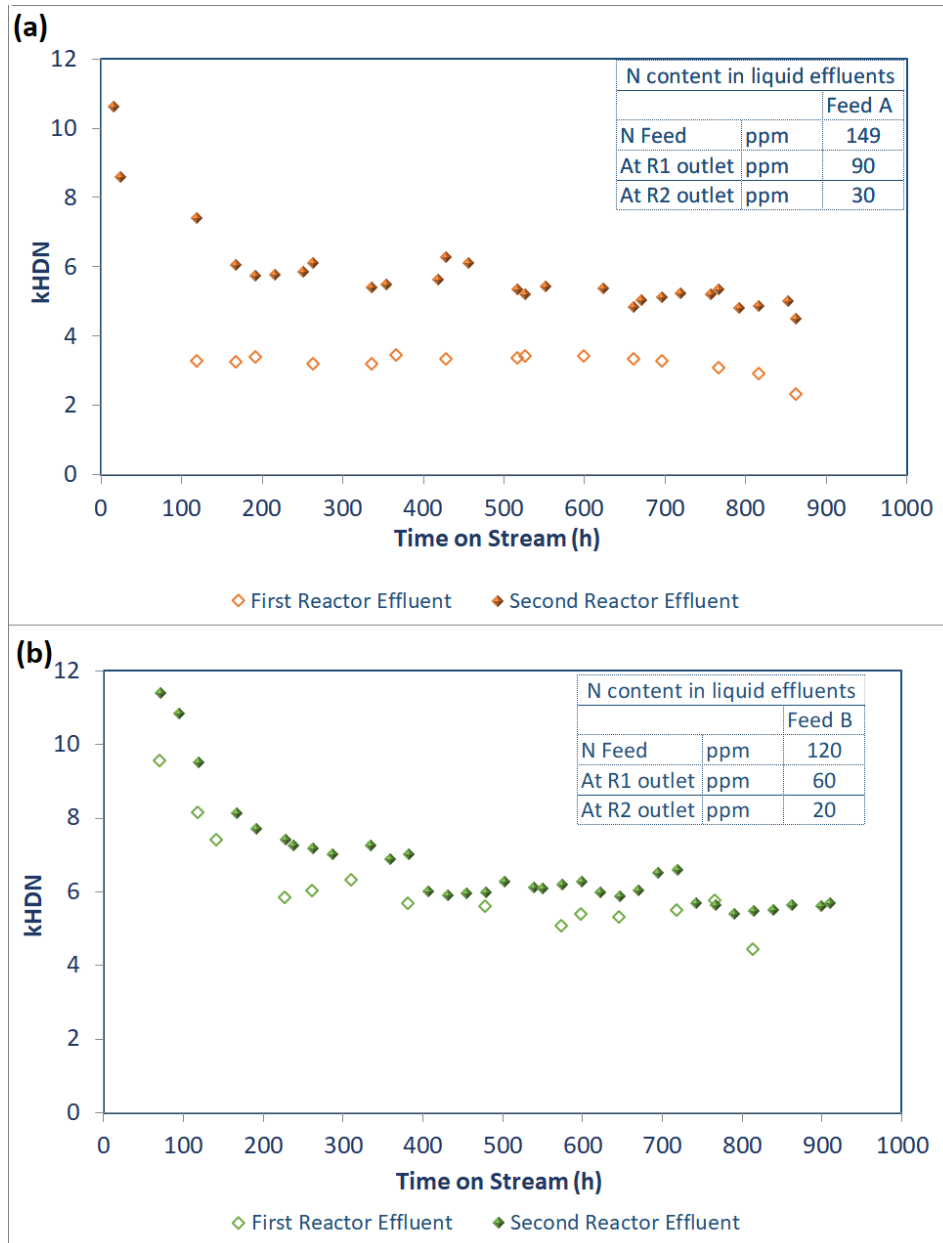


Figure 50. Global and first reactor reaction rate coefficients evolution with time on stream for cracking reactions. a) Feed A and b) feed B. Open symbols=First reactor effluent, Full symbols=Total effluent.

## Chapter 3-Impact of feedstock properties on the deactivation of a vacuum gasoil hydrocracking catalyst



**Figure 51. Global and first reactor reaction rate coefficients evolution with time on stream for HDN reactions. a) Feed A and b) feed B. Open symbols=First reactor effluent, Full symbols=Total effluent.**

Concerning the HDS kinetic coefficients (Figure 52), those remained nearly constant during the tests and had very similar values for both feeds. The HDA reaction rate was lower for feed B (Figure 53). It is related to the origin of feed B, which is composed of streams from processes

## Chapter 3-Impact of feedstock properties on the deactivation of a vacuum gasoil hydrocracking catalyst

that promote the cracking reactions (LCO from fluid catalytic cracking and HCGO from delayed coking), reducing the alkyl chains, therefore, produce more condensed aromatic structures which have a refractory character to the hydrogenation.

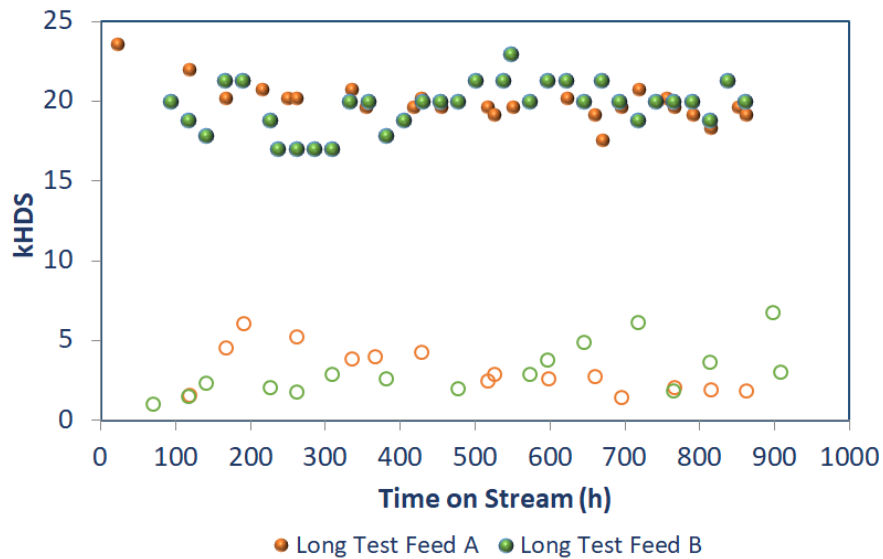


Figure 52. Global and first reactor reaction rate coefficients evolution with time on stream for HDS reactions. Open symbols=First reactor effluent, Full symbols=Total effluent.

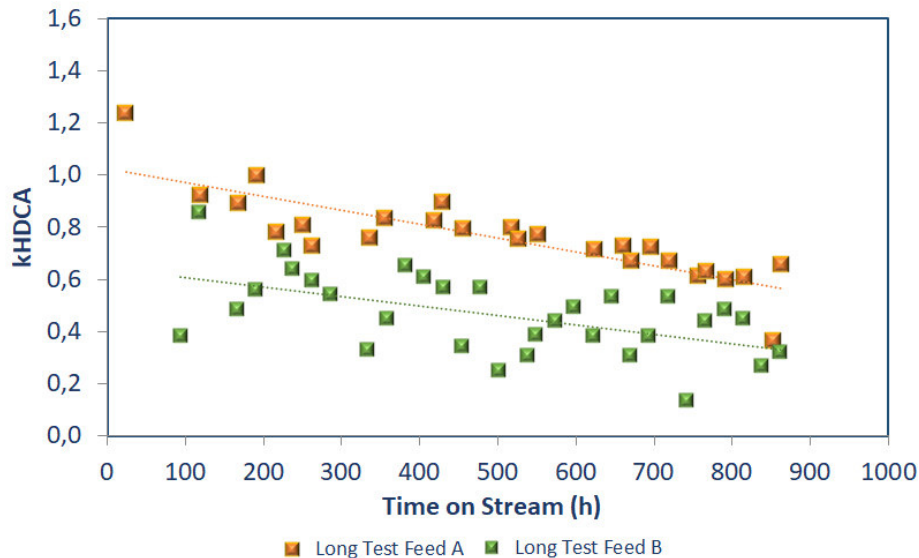


Figure 53. Global and first reactor reaction rate coefficients evolution with time on stream for HDA reactions. Open symbols=First reactor effluent, Full symbols=Total effluent.

## Chapter 3-Impact of feedstock properties on the deactivation of a vacuum gasoil hydrocracking catalyst

---

In the first reactor, all the reaction rate coefficients were lower than in the second reactor. The nitrogen content for both feeds was so high that it provoked an almost total inhibition of the hydrotreating and cracking reactions [130]. The cracking reaction rate was nearly stable for the first reactor with feed A. The inhibition of the acid function was so strong that no additional deactivation was observed. For feed B, the inhibition in the first reactor was lower. This can be explained by the lower nitrogen concentration combined with its lower molecular weight in this feed. As a consequence of the lower inhibition, deactivation could already be observed in the first reactor, related to some coke deposition from aromatics. The values of the HDA coefficients are not shown for the first reactor because they were very low.

During time on stream, the catalysts presented a loss in activity, the reaction rate coefficients for cracking, HDN and HDA reactions decreased for both feeds. The loss in activity was more significant for cracking and HDN than for HDA reactions. The decrease in the reaction rate coefficients was significantly faster at the beginning than at the end of the test.

### 3.2. Hydrogen consumption

Table 16 points out the hydrogen consumption calculated from experimental data for the different feedstocks at the end of all the experiments. The results confirmed the higher reactivity of feed B compared to feed A. More cracking leads to a higher hydrogen consumption because each cracking event consumes one hydrogen molecule. The hydrogen consumption decreased over time which is proportional to the activity loss as time progress.

## Chapter 3-Impact of feedstock properties on the deactivation of a vacuum gasoil hydrocracking catalyst

**Table 16. Hydrogen consumption and apparent cracking reaction rate coefficient for both tests at different times.**

Case	Time on stream	$H_{\text{consumption}}^{\text{End of run}}$	$k_{\text{cracking}}^{\text{fresh catalyst}}$	$K_{\text{cracking}}^{\text{spent catalyst}}$
	Days	$\text{Nm}^3/\text{m}^3$		
Feed A	6	100.5	~7	2.3
Feed A	30	89.6	~7	1.7
Feed B	6	124.53	~27	4.5
Feed B	30	113.2	~27	3.8

### 3.3. Activity loss rate coefficients

As it was stated, the experimental data for the cracking reaction rate coefficient was fitted with an exponential decay function (Appendix 5). Table 17 displays the model parameter value for the activity loss rate,  $\alpha$ , for both feeds during the long-term tests. This coefficient accounts for both inhibition and deactivation during the test run.

**Table 17. Deactivation coefficients calculated with an exponential decay model.**

Case	Time on stream	$\alpha$
	days	(1/day)
Feed A	30	0.15
Feed B	30	0.69

Feed A was heavier than feed B and had a low reactivity for cracking and HDN reactions; it showed a lower deactivation coefficient than in the case of feed B.

We recall that the inspection of the raw conversion data had suggested the opposite trend: the conversion loss as a function of time was higher for feed A (Figure 48). However, as explained in section 2, it may be misleading to look at raw conversion data. For comprehension purposes, the analysis of the evolution of the apparent rate coefficients is more appropriate.

## Chapter 3-Impact of feedstock properties on the deactivation of a vacuum gasoil hydrocracking catalyst

---

### Spent catalysts characterization

Samples from the first reactor inlet (Bed In), second reactor inlet (Middle bed) and second reactor outlet (Bed Out) of the catalytic bed were characterized. The samples obtained from the short-term tests (6 days) and long-term tests (30 days) for both feeds were compared.

Results from the elemental analysis are shown in Figure 54 and Figure 55. The catalysts from the tests with feed B had a higher carbon content (Figure 54) with a slightly lower H/C ratio (Figure 55) than the catalyst obtained from the tests with feed A. The carbon content along the reactor increased from the inlet to the outlet for all the samples. Furthermore, the aromatic character (inverse of ratio H/C) of coke deposits also increased in the same sense. This tendency was confirmed by TGA (Appendix 6).

The coke was readily formed at the start of run for both feeds (Figure 54), but the H/C ratio (Figure 55) diminished with time because of the dehydrogenation of the carbon deposits initially formed. For feed A, the coke deposition increased at the bed outlet (vs. the inlet and middle of the bed); for feed B, the coke deposition increased progressively from bed inlet to bed outlet. The coke gradient from bed inlet to bed outlet can be explained by the inhibition of the coke formation by organic nitrogen, which progressively decreases from bed inlet to bed outlet.

## Chapter 3-Impact of feedstock properties on the deactivation of a vacuum gasoil hydrocracking catalyst



Figure 54. Carbon content of the spent catalysts. Samples taken at different reactor locations. Full bars=30 days tests, open bars=6 days tests.

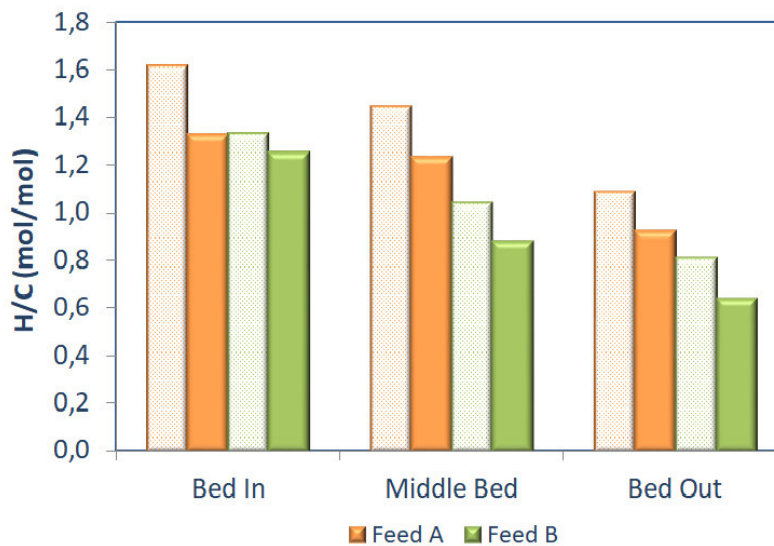


Figure 55. Hydrogen/Carbon ratio of the spent catalysts. Samples taken at different reactor locations. Full bars=30 days tests, open bars=6 days tests.

The N/C ratios of the spent catalyst samples are displayed in Figure 56. The values were similar to the ratio of typical organic nitrogen compounds in vacuum gas oils. The nitrogen proportion in

## Chapter 3-Impact of feedstock properties on the deactivation of a vacuum gasoil hydrocracking catalyst

the deposited coke was higher for the samples from the tests with feed A than for feed B samples. It correlates with the higher nitrogen concentration in feed A. So spent catalyst from the tests with feed B had more deposited coke with a lower nitrogen content than samples from feed A. It means that the contribution of aromatics coke precursors was more significant for feed B, which was related to the higher aromatics content in this feed.

The values of the N/C ratio decreased along the reactor, which agrees with the profile of nitrogen concentration, which shows a maximum at bed inlet. The nitrogen compounds are strongly adsorbed in the acid sites and formed coke because its desorption rate is slow compared to the coke reactions rate. With time on stream, the N/C ratio (Figure 56) decreased.

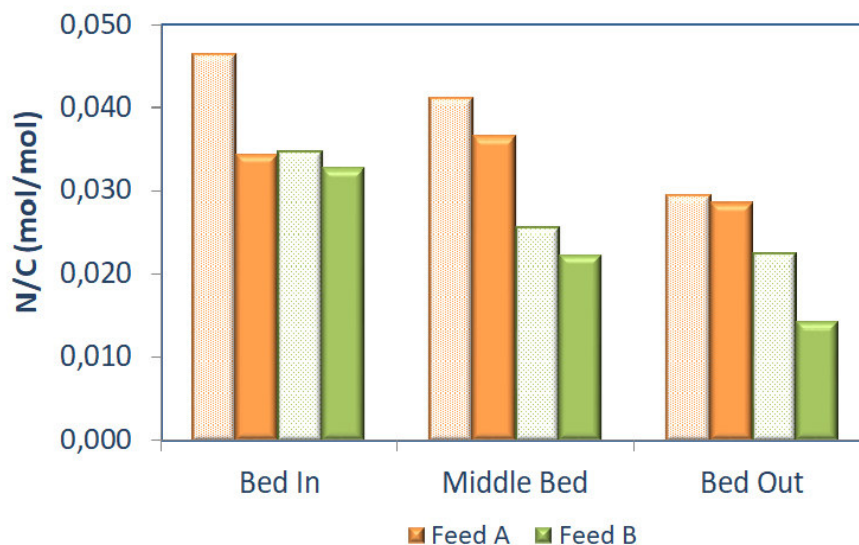


**Figure 56. N/C ratio of the spent catalysts. Samples taken at different reactor locations. Full bars=30 days tests, open bars= 6 days tests.**

The coke deposit influenced the catalyst textural properties since it reduced the available pore volume and the surface area (Appendix 7 and 8). Table 18 shows the losses in surface area (S) and pore volume (V) for the spent samples compared to the fresh catalyst. The samples from

## Chapter 3-Impact of feedstock properties on the deactivation of a vacuum gasoil hydrocracking catalyst

the test with feed B, with the higher carbon content, also produced the highest surface area losses and pore volume. In the same sense, for both feeds, the loss in textural properties was more pronounced for the samples obtained from the second reactor, where the carbon deposition was also enhanced. Surface area and pore volume slightly decreased with time on stream (except for the first reactor with feed A because the coke deposition was controlled by the nitrogen inhibition). The loss of surface and pore volume was proportional to the amount of deposited coke.

**Table 18. Characterization of spent catalyst: Surface area (S) and total pore volume (V) of the spent catalyst relative to the fresh catalyst and ratio of hysteresis area (HA) of the spent catalyst compared to the fresh catalyst.**

Feed	Time on stream	S/S <sub>fresh</sub>		V/V <sub>fresh</sub>		$\frac{HA_{Spent\ Catalyst}}{HA_{Fresh\ Catalyst}}$	
		Bed Inlet	Bed Outlet	Bed Inlet	Bed Outlet	Bed Inlet	Bed Outlet
	days	(%)	(%)	(%)	(%)		
Feed A	6	86	82	80	75	1.10	1.20
Feed A	30	86	78	81	71	1.16	1.38
Feed B	6	85	75	81	70	1.23	1.25
Feed B	30	82	71	78	69	1.33	1.49

Ancheyta et al. [213] proposed a semi-quantitative approach to evaluate catalyst deactivation based on adsorption-desorption isotherms data. They noted that the hysteresis loop tends to increase with the higher blockage of catalyst pores (The normalized isotherms are shown in Appendix 9). Thus, dividing the hysteresis areas of spent and fresh catalysts makes it possible to compare the extent of catalyst deactivation. The higher the value, the higher the deactivation rate. The values of this ratio are presented in Table 18; these data confirmed the faster deactivation rate with feed B even at the lower time on stream. The values for the first reactor

## Chapter 3-Impact of feedstock properties on the deactivation of a vacuum gasoil hydrocracking catalyst

---

samples were also in agreement with the performance observed for the reaction rate coefficients.

TEM/EDX analysis was performed on the spent catalysts to evaluate the morphology of the MoS<sub>2</sub> slabs and their Ni/Mo ratio (Table 19). The results for all the samples were quite similar. Sintering and depromotion are expected to depend mainly on the operating conditions (temperature) but not on the nature of the feed, which is confirmed by Table 19. Depromotion was established by comparing the obtained values of Ni/Mo ratio with the values reported in chapter for a catalyst tested under typical hydrocracking conditions, which were around 0.36 for both inlet and outlet of the catalytic bed. Moreover, there was little evolution between 6 and 30 h, which means that sintering and depromotion took place in the initial stages and then the slab morphology reached a steady state.

**Table 19 Average stacking size and dispersion measured by TEM and Ni/Mo ratio in MoS<sub>2</sub> particles measured by EDX.**

	Time on Stream (days)	Slab length (nm)	Dispersion	Ni/Mo
Feed A Bed In	6	4.7±1.6	0.20	0.24±0.08
Feed A Bed Out	6	4.4±1.6	0.22	0.21±0.12
Feed A Bed In	30	4.3±1.7	0.22	0.19±0.11
Feed A Bed Out	30	4.6±2.2	0.18	0.23±0.12
Feed B Bed In	6	4.5±1.7	0.20	0.19±0.06
Feed B Bed Out	6	4.3±1.6	0.21	0.20±0.07
Feed B Bed In	30	4.6±1.5	0.22	0.14±0.21
Feed B Bed Out	30	4.6±1.7	0.20	0.16±0.08

Catalytic assays evaluated the residual catalytic activity of the spent samples with model molecules, toluene hydrogenation for the (de)hydrogenation function and heptane

## Chapter 3-Impact of feedstock properties on the deactivation of a vacuum gasoil hydrocracking catalyst

---

hydroconversion for the acid function. The fresh catalyst presented a toluene conversion of 70% and an n-heptane conversion of 95%. The obtained results are illustrated in Figure 57. It is clear that there was an activity loss of both functions, even more significantly for the acid function. The solids from the test with Feed A exhibited a higher residual hydrogenation activity but a lower cracking/isomerization activity than the solids from the tests with feed B.

The deactivation of the metal function increased along the catalytic bed; this behavior was more pronounced with feed B samples. However, this loss of activity did not strongly depend on time on stream. Since the depromotion for all the samples under the deactivation conditions was similar, the observed differences between the solids from the tests with both feeds can be related to the carbon deposition on the catalyst. For the acid function, the performance was the opposite. The number of available acid sites in the second reactor was higher than in the first one, despite a higher carbon content. This tendency was more marked with feed B.

The model molecule tests (Figure 57) also showed an activity decrease in hydrogenation and cracking functions with time, especially for the latter. The greatest loss of activity for the two functions with respect to the fresh catalyst occurs in the early stage of the experiment.

## Chapter 3-Impact of feedstock properties on the deactivation of a vacuum gasoil hydrocracking catalyst

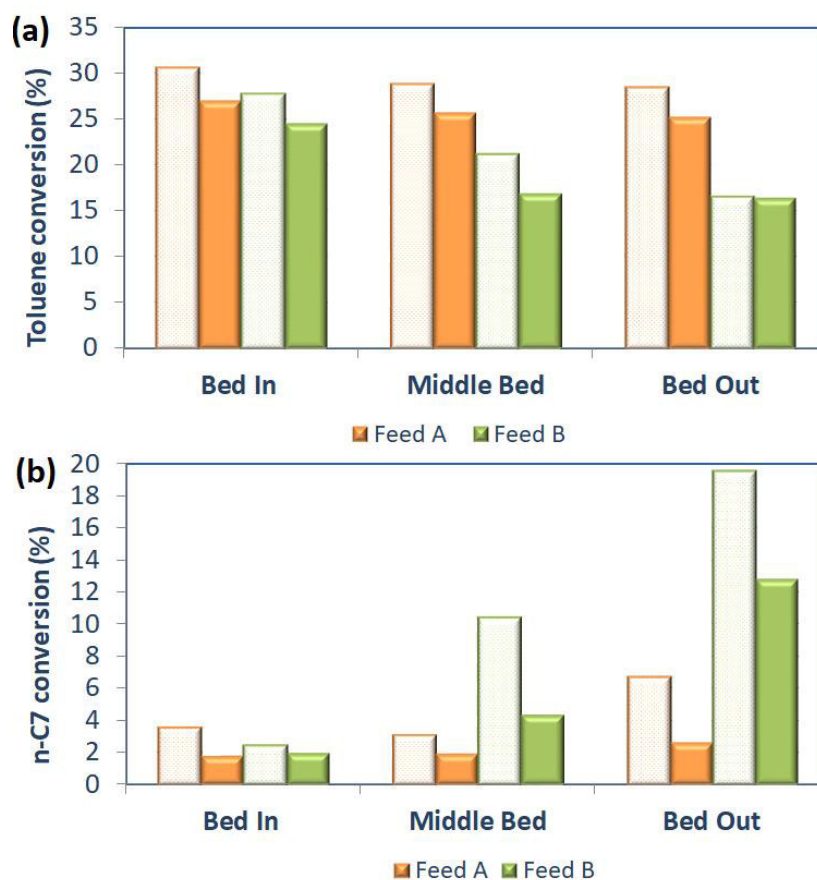


**Figure 57. Residual catalytic activity evaluated by model molecules catalytic tests a) Hydrogenation of toluene, b) Isomerization/cracking of n-heptane at 360°C. Samples taken at different reactor locations. Full bars=30 days tests, open bars= 6 days tests.**

The selectivity to i-heptane (compared at the same conversion level) can be considered as an indicator of the metal/acid balance [102,217]. The higher the selectivity, the higher the hydrogenation activity of the metal sites compared to the activity of the acid sites. In contrast, a low i-heptane selectivity means that the acid sites are not well balanced by the hydrogenation sites. Figure 58 represents the selectivity performance for the samples obtained during the processing of both feeds. Spent materials from runs with feed A showed higher i-heptane selectivity than the ones from feed B. It is in line with the fact that those samples presented the

## Chapter 3-Impact of feedstock properties on the deactivation of a vacuum gasoil hydrocracking catalyst

highest hydrogenation activity and the lowest cracking activity. It reinforces the balance of metal/acid sites and, in this way, the selectivity to i-heptane.

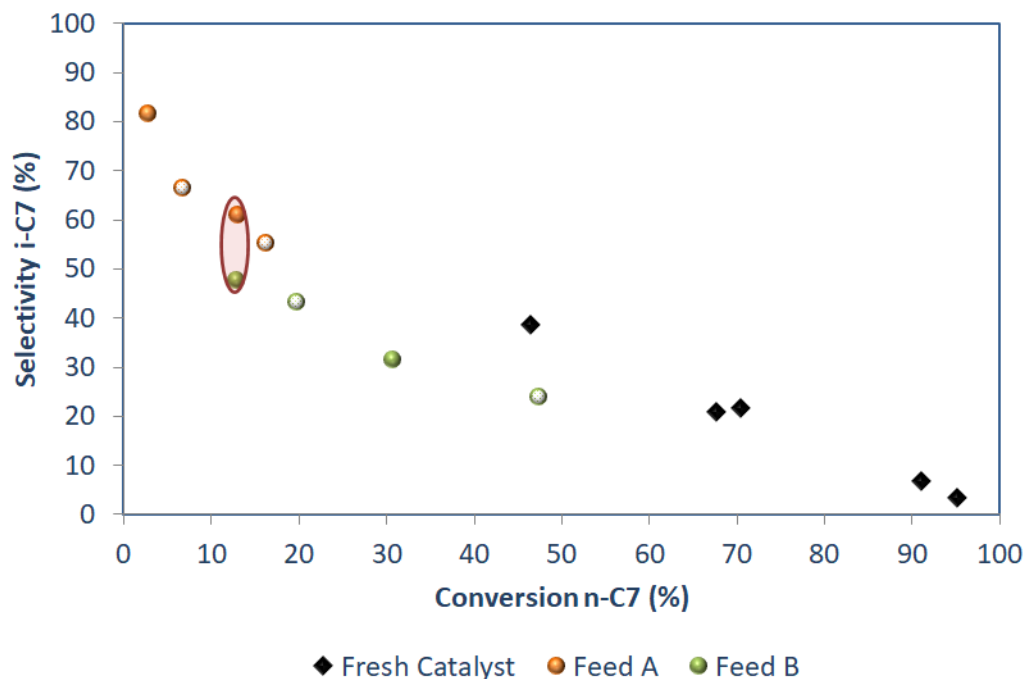


Figure 58. Test n-heptane. Selectivity to i-C<sub>7</sub> Vs. conversion n-C<sub>7</sub>. Open symbols= 6 days tests, full symbols=30 days tests.

## 4. DISCUSSION

### 4.1. Evolution with time

During time on stream, the catalysts presented a loss in activity; the reaction rate coefficients for cracking (Figure 50), HDN and HDA (Figure 53) reactions decreased for both feeds. Actually, during the test with feed A, the HDA had a significant reduction with time compared to the performance with feed B. The loss in activity was accompanied by a decrease in hydrogen consumption (Table 16), so this value also diminished over time. The decrease was slightly more notable for feed A; it may be due to the higher aromatic hydrogenation with this feed

## Chapter 3-Impact of feedstock properties on the deactivation of a vacuum gasoil hydrocracking catalyst

---

compared with feed B. For both feeds, the data based on the nitrogen isotherms (Table 18) pointed out the change in the deactivation rate during the time on stream, which initially exhibited a slower deactivation rate as time progresses. These results agree with different works [123,129] that reported a faster activity decay at the beginning of the run.

Regarding the carbon content evolution with time, the data (Figure 54) indicated that the major part of the coke was formed at the beginning of the tests for both feeds. During the first 6 days on-stream after performance stabilization, between 90 and 95% of total final coke was deposited for feed A and between 80 and 85% for feed B. It is consistent with the literature [123,228,229] that claims that coke deposition initially increases rapidly with time on-stream before a pseudo-stable state is reached. For reforming catalysts, Querini [159] and Absi-Halabi [228] found that coke equivalent to 25% of the weight of the original catalyst is deposited within the first few hours of operation. The increase of the coke deposition was less significant for feed A than for feed B due to the higher inhibition of the coke reactions by nitrogen compounds. The H/C ratio (Figure 55) also decreased with time because as condensation and polymerization reactions to form coke progress, dehydrogenation occurs [129,163,164,230]. This evolution of the coke deposition is at the origin of the observed performance for the deactivation rate. As was expected, textural properties followed the same behavior as coke deposition. Thus, there was no meaningful change in the first reactor for feed A with time on stream because the coke deposition was controlled by the nitrogen inhibition, which was more important than in the second reactor. There was a decrease in the surface area and the pore volume as time progresses for feed B.

The amount of N, which was deposited on the catalyst also did not evolve much any longer after 150 h on stream. On the other hand, the N/C ratio (Figure 56) continued to decrease with time, in agreement with previous works [136], which state that as the catalysts ages, N/C ratios

## Chapter 3-Impact of feedstock properties on the deactivation of a vacuum gasoil hydrocracking catalyst

---

decrease. This may be related to the preferential adsorption of the nitrogen compounds on the acid sites [148,228]. These adsorbed compounds in the early stages form coke precursors with moderate aromaticity (relatively high H/C ratio). Subsequent accumulation of coke results from the condensation/polymerization reactions of the unsaturated intermediates formed preferentially from aromatic structures, which provokes a reduction in the N/C and H/C ratio.

The model molecule tests (Figure 57) allow evaluating the effect of coke formation on the hydrogenation and cracking functions. The hydrogenation activity of the spent catalysts is rather well correlated with the amount of deposited coke (Figure 61a). The residual hydrocracking activity, however, is totally anticorrelated with the amount of coke (Figure 61b). It drops drastically in the initial stage and then continues to decay gradually (even when the total coke content remains almost constant). The bed outlet always maintains a higher residual cracking activity than the bed inlet, despite the lower carbon content of the latter. The concentration of organic nitrogen compounds in the reactor follows the opposite trend: it decreases from reactor inlet to reactor outlet and increases with time due to the deactivation of HDN. We therefore suppose that the acid sites undergo a very specific deactivation due to nitrogen compounds, which is uncorrelated from the global coke build-up.

## Chapter 3-Impact of feedstock properties on the deactivation of a vacuum gasoil hydrocracking catalyst

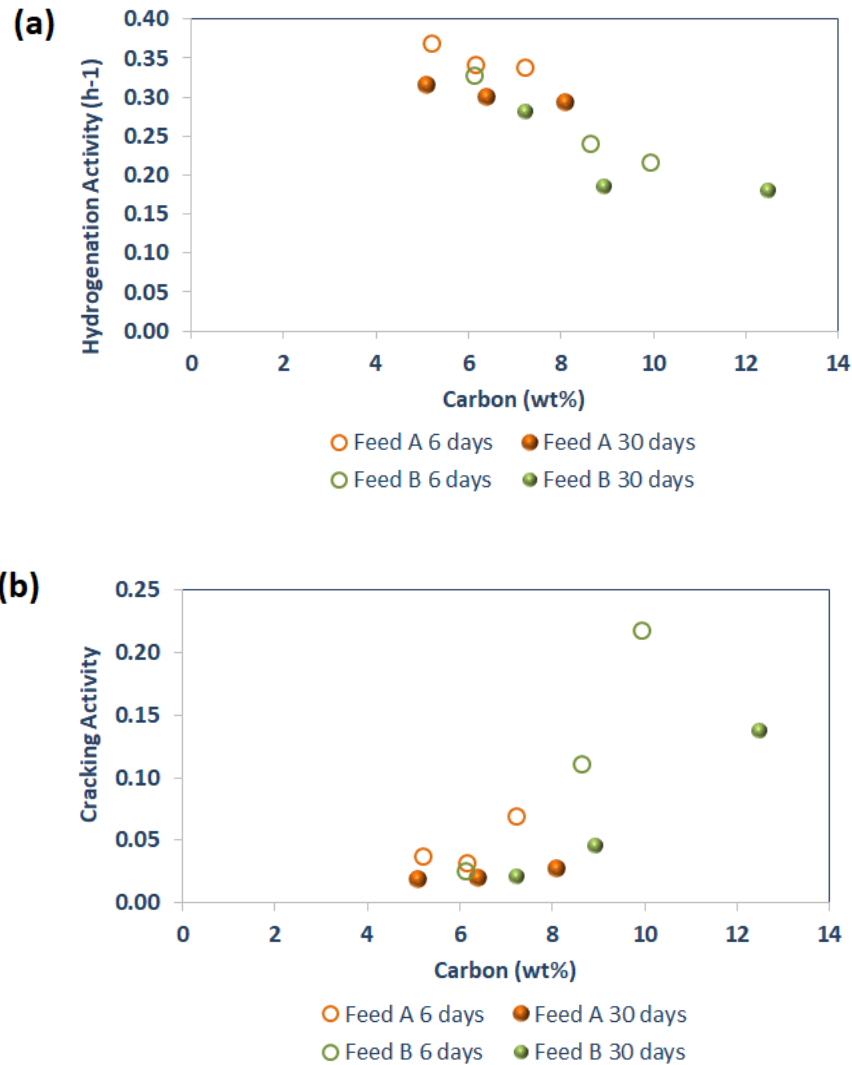


Figure 59. Relation between the a) hydrogenation activity and b) n-C7 cracking activity of the spent catalysts and the amount of coke.

### 4.2. Impact of the feed

The effect of the type of feedstock on catalyst deactivation was studied with a hydrotreated VGO, Feed A, and a lighter mixture, Feed B, which was a hydrotreated mixture containing heavy coker gasoil (HCGO) and light cycle oil (LCO) in addition to VGO (71%). These feeds had a different organic nitrogen content: 149 ppmw (Basic Nitrogen 36 ppmw) for feed A and 120

## Chapter 3-Impact of feedstock properties on the deactivation of a vacuum gasoil hydrocracking catalyst

---

ppmw (~30 ppmw of basic nitrogen) for feed B. The nitrogen families in both feedstocks were similar. However, the distribution of the compounds was different; essentially, feed A contained slightly more acridine (basic nitrogen), carbazoles, benzocarbazoles and dibenzocarbazoles (neutral nitrogen) than feed B. These compounds are the most refractory for the HDN reactions. Additionally, nitrogen compounds of feed A showed higher molecular weight associated with a higher degree of alkyl substitution what decreases the hydrogenation reactivity of these compounds. The aromatics content was ~37 wt% and ~42 wt% for feed A and feed B, respectively. Monoaromatics were the dominating family within both feeds, followed by diaromatics and triaromatics; the mass fractions of these three families were slightly higher for feed B. This feed is composed of streams from processes that promote the cracking, fluid catalytic cracking (LCO), and delayed coking (HCGO), reducing the alkyl chains, therefore producing more condensed aromatic structures that have a refractory character to the hydrogenation.

Both feeds were submitted to the same deactivation conditions during the same time. Results based on the exponential decay function (Table 17) and textural properties of the catalyst (Table 18) showed a lower deactivation rate for feed A. It is consistent with the lower coke deposition on the spent catalysts from the feed A tests (Figure 54). It was unexpected considering the higher molecular weight of feed A and also its higher nitrogen content. However, the obtained results indicate that these are not the determinant factors on the observed catalyst deactivation. It is rather the nature of the coke precursor molecules, i.e., aromatics and nitrogen compounds. As already mentioned, this nature is dictated by the origin of the feedstocks.

As it was mentioned, feed A had a higher nitrogen concentration and more refractory compounds than feed B. Also, a lower HDN rate was observed during the tests with feed A (Figure 50). Thus the nitrogen content was higher for feed A than for feed B at the same reactor

## Chapter 3-Impact of feedstock properties on the deactivation of a vacuum gasoil hydrocracking catalyst

---

location. The organic nitrogen compounds are rapidly adsorbed on the acid sites of the catalyst due to their basic character [119,149,219,231]. This adsorption leads first to the inhibition of these sites by neutralization and then to irreversible deactivation by coke deposits since the adsorbed nitrogen compounds react to form coke before being desorbed. Both mechanisms result in the loss of cracking activity [34] and low coke deposition from aromatics [222]. These effects were less significant for feed B because its nitrogen compounds were more reactive and in a lower proportion than feed A. The model molecules tests (Figure 57) pointed out the bigger loss of cracking activity for the catalyst samples obtained from the runs with feed A compared to feed B, except at the first reactor inlet where the activities were similar and substantially low. However, feed A leads to a lower deactivation rate. As the acid function determines cracking activity, it is concluded that the solids from the tests with feed B had more acid sites available than those from feed A. These sites are poorly balanced by the metal sites as observed in the selectivity results.

In contrast, the toluene hydrogenation test showed a higher activity loss for all the spent catalysts from the experiments with feed B than with feed A, which was attributed to a higher coke build-up with feed B. As a matter of fact, the TEM/EDX analysis shows no significant differences in terms of MoS<sub>2</sub> slab morphology and Ni/Mo ratio related to the spent catalysts in contact with both feeds. The higher hydrogenation activity for feed A might be related to the higher inhibition of the (de)hydrogenation reactions by the nitrogen compounds, which also inhibit the coke deposition on the metal surface.

In summary, spent catalysts from tests with feed A had a higher hydrogenation activity and a lower cracking activity than catalysts from the test with feed B. Accordingly, the balance between

## Chapter 3-Impact of feedstock properties on the deactivation of a vacuum gasoil hydrocracking catalyst

---

metal sites and acid sites (M/A) of the spent catalysts was different for both feeds. The i-heptane selectivity can assess this balance; results were presented in Figure 58. A high selectivity indicates a high number of active metal sites with respect to acid sites. A low selectivity means that there is an imbalance between the acid sites and hydrogenation sites. Hence the (M/A) ratio was lower in spent catalyst obtained with feed B than with feed A. As a consequence of the difference ratio, both quantity and type of deposited coke were also different. Actually, during the test with feed B, since there were more available acid sites, many free radicals and carbocations were formed that undergo polymerization reactions before finding a metal site for being hydrogenated. Therefore, there was an increase in the amount of coke with a lower H/C ratio, indicating a more aromatic character from the tests with feed B (Figure 55). So, after all, although feed A leads to a more substantial deactivation of acid sites, this is not the main parameter explaining deactivation. The metal/acid balance explains the extent of coke formation and the ranking of the deactivation rates.

The formed coke could originate from the organic nitrogen compounds or other coke precursors like aromatic compounds. To estimate the contribution of each one of them, the N/C ratio values of the spent catalyst were measured (Figure 56). Despite the higher quantity of deposited carbon on the catalysts from the test with feed B, the values of the N/C ratio were lower. The former suggests that feed B might have an important contribution from aromatic compounds that may condense and form coke deposits reducing the global activity. It is consistent with the higher amount of aromatics coupled with a lower concentration and refractory character of N-containing compounds in this feed. In contrast, for catalyst samples from the test with feed A, there were lower coke generation and higher values of N/C, which means a major role of nitrogen

## Chapter 3-Impact of feedstock properties on the deactivation of a vacuum gasoil hydrocracking catalyst

---

compounds in coke formation. It is in line with the fact that this feed has a higher nitrogen content and fewer aromatics.

Summing up the higher catalyst deactivation obtained with feed B results from two joint facts: more aromatics with low reactivity and a lower nitrogen content with a less basic character and more reactivity, all of this compared to feed A. Herein constituted a strong synergy to leads to a poor balance in the M/A ratio because the fewer nitrogen leads to more available acid sites where the aromatics can form intermediates that undergo condensation/polymerization reactions rather than saturation due to a hydrogenation function also weakened for the low inhibition of the coke formation by nitrogen.

### 5. CONCLUSIONS

- Combining a feedstock with higher aromatics and a lower nitrogen content creates an imbalance in the ratio M/A, with a low number of metal sites in relation to the acid sites. Consequently, there is poor hydrogenation of the unsaturated coke precursors species produced in the acid sites, which undergo polymerization and condensation reactions forming the coke deposits on the catalyst surface and promoting its deactivation. This combination has an effect that outweighs the effect of differences in molecular weight and boiling range.
- For a similar type of feed with a similar final boiling point, the total nitrogen and aromatics content significantly impacted the resulting catalyst deactivation. Actually, the key parameters are both the content but mostly the type of nitrogen compounds because they are at the origin of the inhibition of hydrogenation and cracking activities, but even more important, they determine the number of acid sites available for the reactions.

## Chapter 3-Impact of feedstock properties on the deactivation of a vacuum gasoil hydrocracking catalyst

---

- Independent of the feed properties, the catalyst was strongly deactivated during the first days on-stream. Then, reaction rate coefficients reached almost constant values. This behavior follows the evolution of coke deposition, which is mainly deposited at the beginning of the test runs. These coke deposits are preferentially formed on the acid sites because of the rapid and strong chemisorption of nitrogen on these sites on one side, and due to condensation and polymerization of aromatics carried out on these sites, on the other side.
- The balance in the metal/acid site ratio determines the amount and type of formed coke. The lower the ratio, the lower the hydrogenation of olefins produced in acid sites, and consequently, the formed coke increases, and its hydrogen content decrease producing a more aromatic (less reactive) coke.
- For the lighter VGO/LCO/HCGO blend cracking, HDS and HDN reaction rate coefficients were higher than for the pure VGO feed. However, the reaction rate coefficient for HDA was lower for the VGO/LCO/HCGO feed. This difference is related to the more condensed aromatic structures of this feed have a refractory character to the hydrogenation because it was composed of streams from processes (fluid catalytic cracking and delayed coking) that promote side-chain cracking.

# **CHAPTER 4**

## **Impact of metal content on the deactivation of a bifunctional hydrocracking catalyst**

---

## CHAPTER 4-IMPACT OF METAL CONTENT ON THE DEACTIVATION OF A BIFUNCTIONAL HYDROCRACKING CATALYST

### 1. INTRODUCTION

Considering that the balance between the metal and acid functions (M/A) determines the hydrocracking catalyst behavior and, consequently, its activity loss, this chapter focuses on studying the impact of the metal oxide ( $\text{MoO}_3$ ) content on the deactivation of a vacuum gasoil hydrocracking catalyst. The preparation of some laboratory catalysts with different metal contents and their performance during model molecule reactions experiments (toluene hydrogenation and n-heptane hydroconversion) are first presented. The results obtained in the pilot unit experiments under deactivation conditions for two catalysts with different metal contents are then reported. Subsequently, the characterization of the spent catalysts obtained in the pilot plant experiments is shown. Finally, a review of the main findings and conclusions is presented.

### 2. CATALYST PREPARATION AND CATALYTIC TESTS WITH MODEL MOLECULES

#### 2.1. Catalyst preparation

The reference catalyst studied is the same as the one used for the experiments carried out so far, consisting of nickel-molybdenum sulfide particles dispersed on a carrier containing USY zeolite. In order to perform a rapid screening of molybdenum content, a series of catalysts with varying metal oxide content at constant Ni/Mo molar ratio was prepared. Their molybdenum oxide contents were 25%, 50% and 75% of the molybdenum oxide content related to the reference catalyst. No modification was made to the zeolitic support.

## Chapter 4-Impact of metal content on the deactivation of a bifunctional hydrocracking catalyst

---

The catalysts were synthesized by incipient wetness impregnation of the zeolitic support in extrudates shape. After 1.5 hours of maturation, the solids were dried at 120°C for 12 hours and then calcined at 450 °C for 2 hours under air.

### **2.2. Model molecules tests for fresh catalysts with different MoO<sub>3</sub> contents.**

Catalytic tests with model compounds were carried out to characterize the activity of both catalytic functions related to the dried catalyst samples. The hydrogenation function activity was evaluated by converting toluene to hydrogenated products in the presence of aniline (0.5 wt %), whereas the cracking function was determined by the hydroconversion of n-heptane to isomerization and cracking products. The used methods are analogous to the one described in chapter 2, experimental section (2.3.4).

## Chapter 4-Impact of metal content on the deactivation of a bifunctional hydrocracking catalyst

---

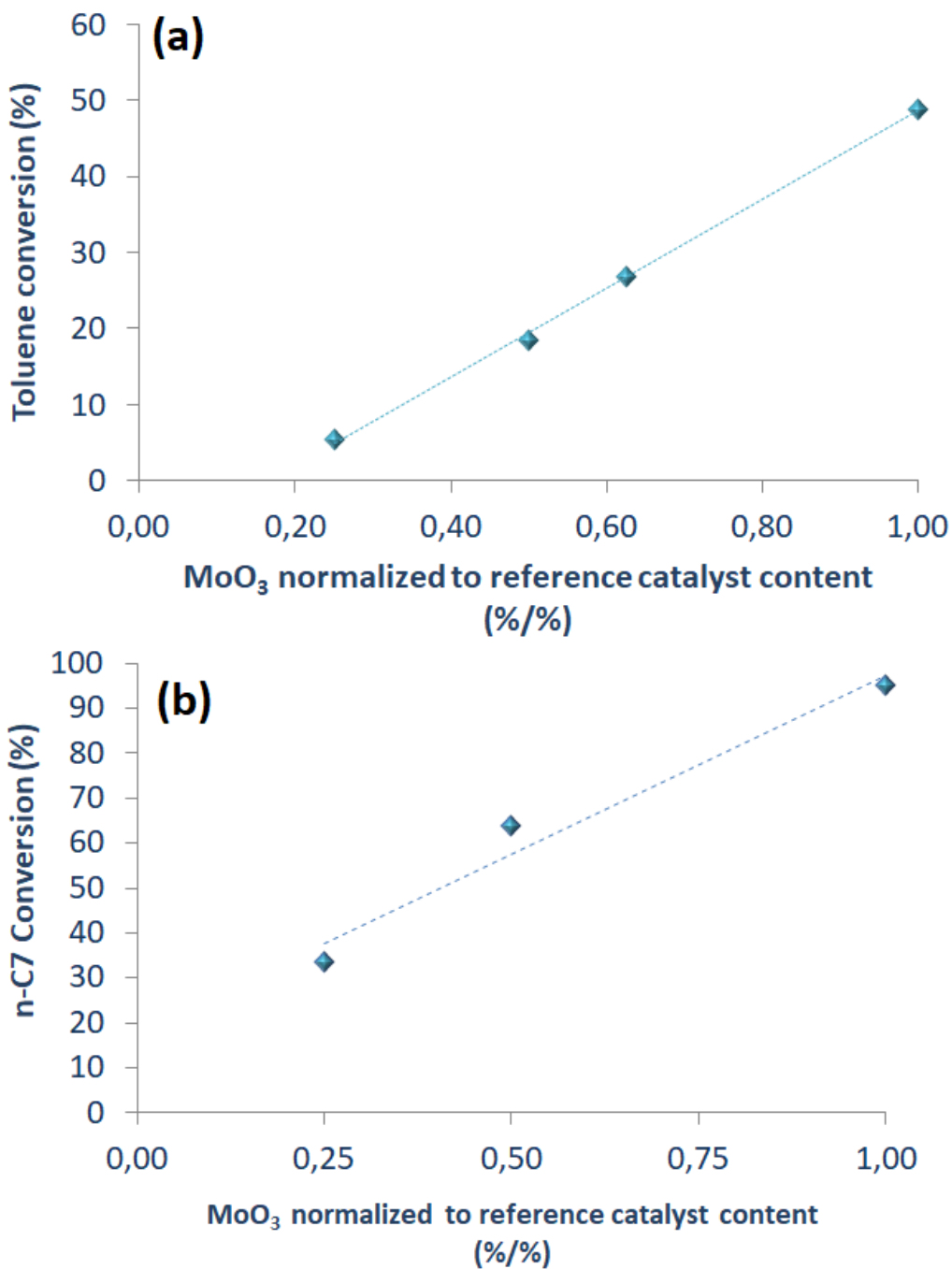


Figure 60. Catalytic activities evaluated by model molecules catalytic tests for fresh dried catalyst samples with different MoO<sub>3</sub> contents a) Hydrogenation of toluene in the presence of aniline, b) Isomerization/cracking of n-heptane at 360°C.

## Chapter 4-Impact of metal content on the deactivation of a bifunctional hydrocracking catalyst

---

The obtained results are illustrated in Figure 60; the hydrogenation activity increases with the metal oxide content, as expected. Concerning the cracking function, the lower the amount of molybdenum, the lower the activity, although no modification was made to the zeolitic support. The strong dependence of the cracking activity on molybdenum loading is quite remarkable because it is more pronounced than reported in previous studies [217,232,233]. This indicates a strong limitation of the bifunctional mechanism by the initial de/hydrogenation steps.

In Figure 61, the selectivity to *i*-heptane is shown. The results indicate that the selectivity increases as the metal oxide increases. This means a better metal/acid (M/A) balance since as the metal content of the catalyst increases, the probability of an intermediate olefin from the acid sites finding a metal site increases.

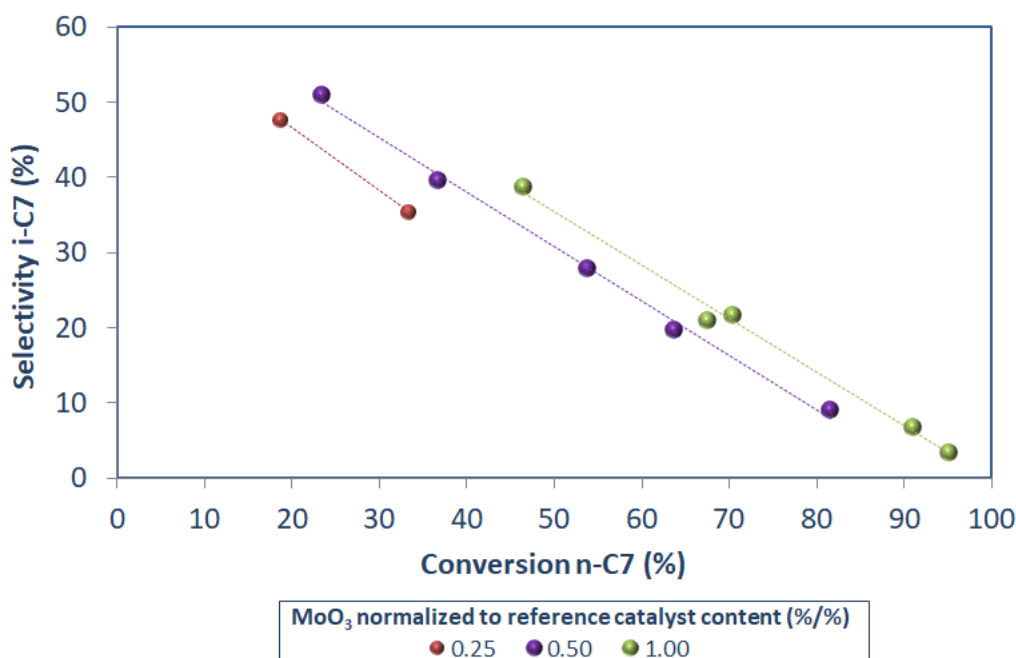


**Figure 61. Selectivity to *i*-C<sub>7</sub> Vs. conversion n-C<sub>7</sub> for fresh dried catalyst samples with different MoO<sub>3</sub> contents.**

Once this simple screening of the molybdenum content was accomplished, the catalyst with 50 % of the metal oxide content of the reference catalyst was selected to evaluate its loss of activity

## Chapter 4-Impact of metal content on the deactivation of a bifunctional hydrocracking catalyst

---

in the pilot unit under accelerated deactivation conditions. With this choice, the goal was to evaluate the impact of an important activity decrease without strongly modifying the M/A ratio, on catalyst deactivation. Otherwise, a huge unbalance of the acid sites could generate results that might be more representative of a purely acid catalyst.

### 3. DEACTIVATION EXPERIMENTS WITH CATALYSTS AT DIFFERENT METAL CONTENTS.

The reference catalyst (designated as “Reference”) and the catalyst with one-half of molybdenum oxide (designated as “0.5 MoO<sub>3</sub>”) were submitted to the following operating conditions  $T=418^{\circ}\text{C}$ ,  $\text{LHSV}=3\text{ h}^{-1}$ ,  $\text{H}_2/\text{HC}=1500\text{NL/L}$ ,  $P=14\text{ MPa}$ , which promote their deactivation (chapter 2). The feedstock consisted of a hydrotreated blend of 71% vacuum gasoil, 16% coker gasoil, and 13% light cycle oil on a weight basis containing around 120 ppmw of organic nitrogen. The feedstock properties are shown in Table 14 (Feed B) of chapter 3 (Section 2.1). The hydrocracking experiments were conducted in a fixed-bed pilot unit. A detailed description of the unit and the experimental procedures was presented in chapter 2 (Section 2). The gas effluent of the unit was analyzed on-line by gas chromatography. The liquid products were characterized by density, refraction index, nitrogen and sulfur contents and simulated distillation to monitor the daily performance of the catalyst. The spent catalysts were characterized by elemental and textural analysis and by thermogravimetry to investigate the quantity and nature of the coke formed. Catalytic tests with different model compounds (toluene, n-heptane) were carried out to determine the residual activity of the hydrogenation and acid catalytic functions. The catalyst performance during the deactivation experiment was followed by measuring the VGO conversion ( $370^{\circ}\text{C}^+$  petroleum cut) and determining the apparent kinetic

## Chapter 4-Impact of metal content on the deactivation of a bifunctional hydrocracking catalyst

constants for the main hydrocracking reactions, i.e. (cracking, hydrodenitrogenation, and aromatics hydrogenation).

In this section, the evolution of the reaction rate coefficients of each key chemical reaction with time on stream is presented first and then the characterization of the spent catalysts.

### 3.1. Evolution of the reaction rate coefficients with time on stream

In the first place, the evolution of the net conversion (Equation 11) with run time is displayed in Figure 62 for both the first reactor and the whole system. The catalyst with the lower molybdenum content presented a lower conversion for both reactors. Independent of the catalyst, the conversion in the first reactor was lower than in the second one.

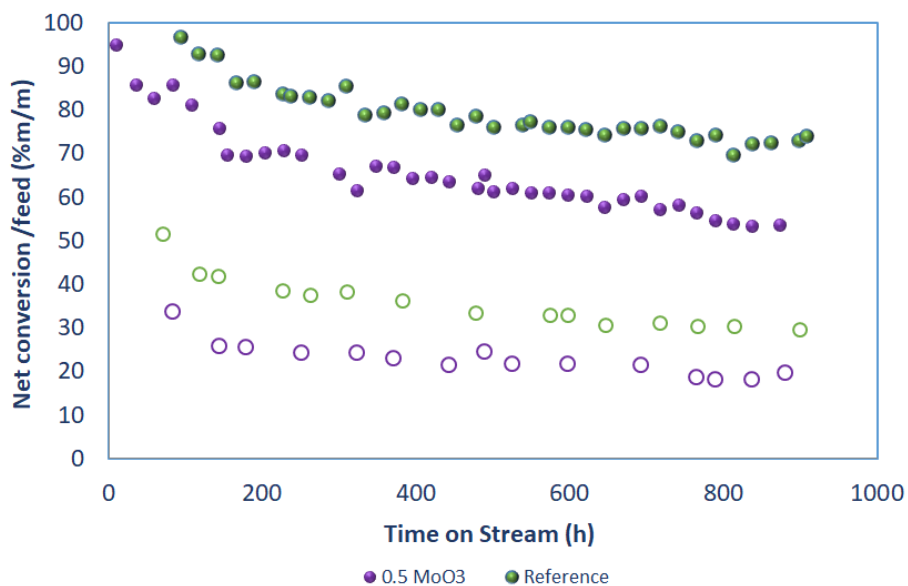


**Figure 62. Net conversion evolution with time on stream for catalysts with different metal contents. Open symbols=First reactor effluent, Full symbols=Total effluent.**

The evolution with time on stream (TOS) of the reaction rate coefficients for cracking, hydrodenitrogenation (HDN), and aromatic hydrogenation (HDA) reactions are shown in Figure

## Chapter 4-Impact of metal content on the deactivation of a bifunctional hydrocracking catalyst

---

63, Figure 64 and Figure 65, respectively. The global performance of the two reactors and the one for the first reactor are presented for the two catalysts.

As was expected, the data indicate that the reduction in the amount of molybdenum (the component responsible for the hydrogenation activity) caused a decrease in the hydrogenation reactions of both aromatics and nitrogen compounds. Furthermore, this reduction impacted the acid function activity, resulting in lower reaction rate coefficients. This is consistent with the preliminary results for fresh catalysts (Figure 60). Thus, as previously stated, this is due to a limitation of the dehydrogenation step, which is the triggering step of the bifunctional catalysis mechanism. The reaction rate coefficients for the mentioned reactions were lower in the first reactor than in the second one (HDA values are not shown since they are negligible). It is because, at the catalytic bed entrance, the concentration of nitrogen compounds was the highest and, therefore, there was a higher inhibition of the cracking and (de)/hydrogenation reactions in the first reactor. The difference between the two reactors was more pronounced for the catalyst with the lower molybdenum content than for the reference catalyst because of its lower hydrogenation rate. This was anticipated considering the higher difference in the HDN reaction coefficients between both reactors with the  $0.5\text{MoO}_3$  catalyst.

# Chapter 4-Impact of metal content on the deactivation of a bifunctional hydrocracking catalyst

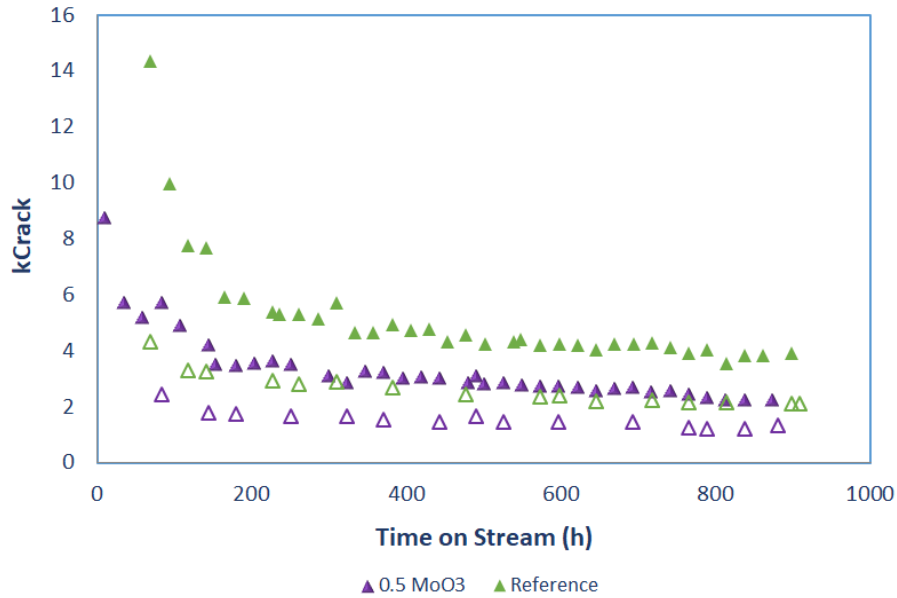


**Figure 63. Global and first reactor reaction rate coefficients evolution with time on stream for cracking reactions for catalysts with different metal contents. Open symbols=First reactor effluent, Full symbols=Total effluent.**

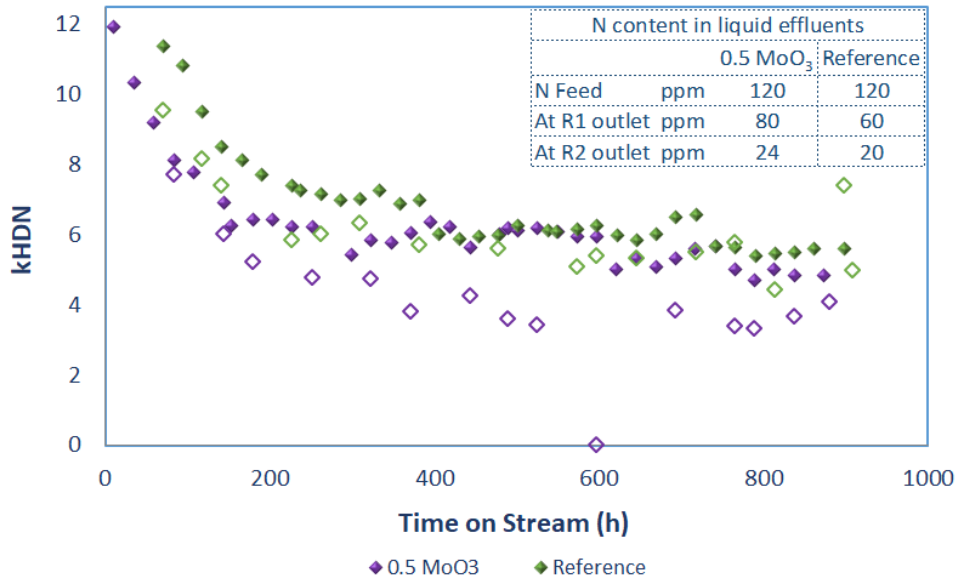


**Figure 64. Global and first reactor reaction rate coefficients evolution with time on stream for HDN reactions for catalysts with different metal contents. Open symbols=First reactor effluent, Full symbols=Total effluent.**

## Chapter 4-Impact of metal content on the deactivation of a bifunctional hydrocracking catalyst

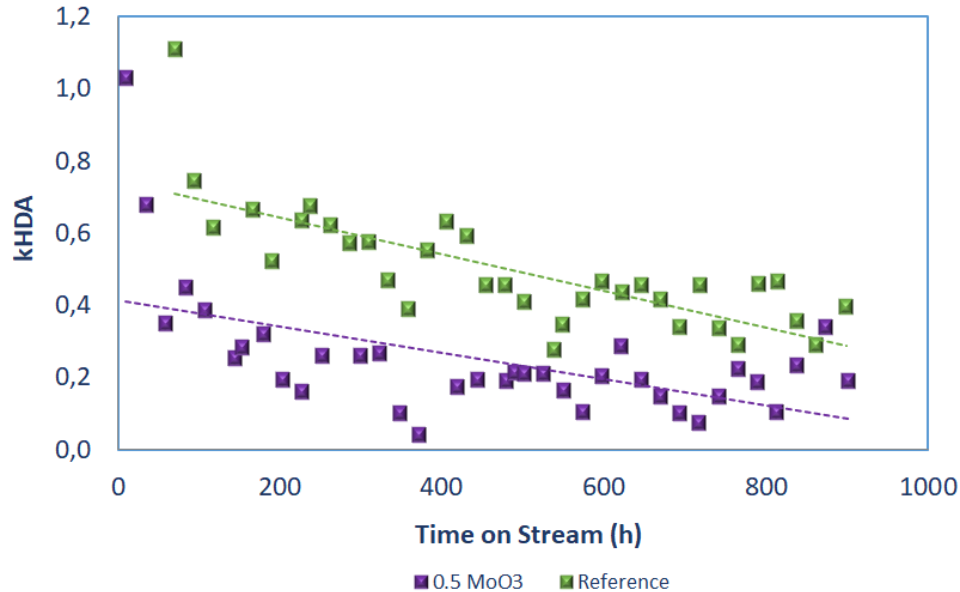


**Figure 65. Global reactor reaction rate coefficients evolution with time on stream for HDA reactions for catalysts with different metal contents.**

### 3.1.1. Activity loss rate coefficients

For reactions with catalyst deactivation, there is a dependence of the kinetic performance on the deactivation. Thus, the apparent reaction rate coefficients calculated so far are indeed the combination of kinetics and deactivation. Therefore, to dissociate both phenomena for cracking reactions, the data of the calculated rate constants as a function of the time on stream were fitted (Appendix 5) to the exponential decay model presented in chapter 3 (Equation 19). The alpha ( $\alpha$ ) parameter accounts for the activity loss rate either by inhibition or permanent deactivation of the catalyst. The c parameter represents the residual activity of the spent catalysts. The coefficients for both catalysts are presented in Table 20. The results indicate that the activity loss was faster for the catalyst with the stronger hydrogenation function. A higher residual activity (~50% higher with respect to the 0.5MoO<sub>3</sub> catalyst) was found for this catalyst.

## Chapter 4-Impact of metal content on the deactivation of a bifunctional hydrocracking catalyst

---

**Table 20. Activity loss rate coefficients ( $\alpha$ ) and residual activities ( $c$ ), calculated with an exponential decay model for catalysts with different metal contents.**

<b>Catalyst</b>	<b><math>\alpha</math></b>	<b><math>c</math></b>
	(1/day)	
0.5 MoO <sub>3</sub>	0.23	2.7
Reference	0.39	4.3

### 3.2. Spent catalysts characterization

This section presents the characterization results of the spent catalysts with the two different metal contents. Samples were collected from three different locations in the reactors, first reactor inlet (Bed In), second reactor inlet (Middle bed) and second reactor outlet (Bed Out). All the samples were submitted to an extraction with toluene in a soxhlet extractor to remove the physically adsorbed hydrocarbons. The washing procedure and the characterization techniques were described in chapter 2 (Section 2.3.4).

#### 3.2.1. Elemental analysis

The carbon content of the spent samples is presented in Figure 66. Contrary to what was expected, the carbon deposition was lower for the catalyst with a lower metal content. This behavior can be attributed to the higher nitrogen concentration (less  $k_{HDN}$  values) in the reactant environment with this catalyst, which inhibits cracking reactions and, consequently, the polymerization reactions to form coke. The latter was confirmed by the values of the N/C ratio and coke nitrogen content displayed in Figure 67 and Figure 68, respectively. The nitrogen was higher for the spent catalysts with lower molybdenum. It means that the contribution to the coke formation from nitrogen precursors plays a more important role for this catalyst in comparison with the reference one. For both catalysts, carbon content along the reactor increased from the inlet to the outlet; meanwhile, the N/C values decreased. Both facts agree with the concentration nitrogen profile, which decreases along the length of the reactor.

## Chapter 4-Impact of metal content on the deactivation of a bifunctional hydrocracking catalyst

---

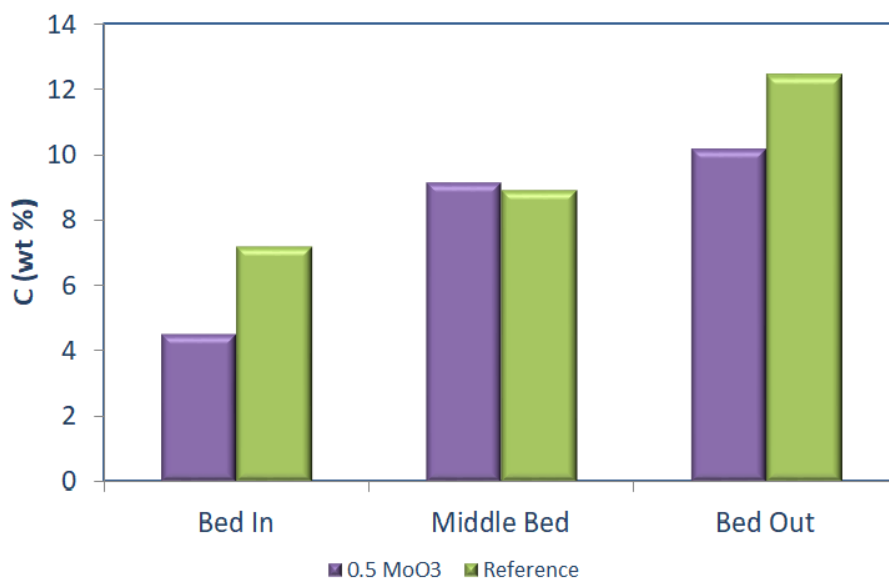


Figure 66. Carbon contents of the spent catalysts with different metal contents. Samples taken at different reactor locations.

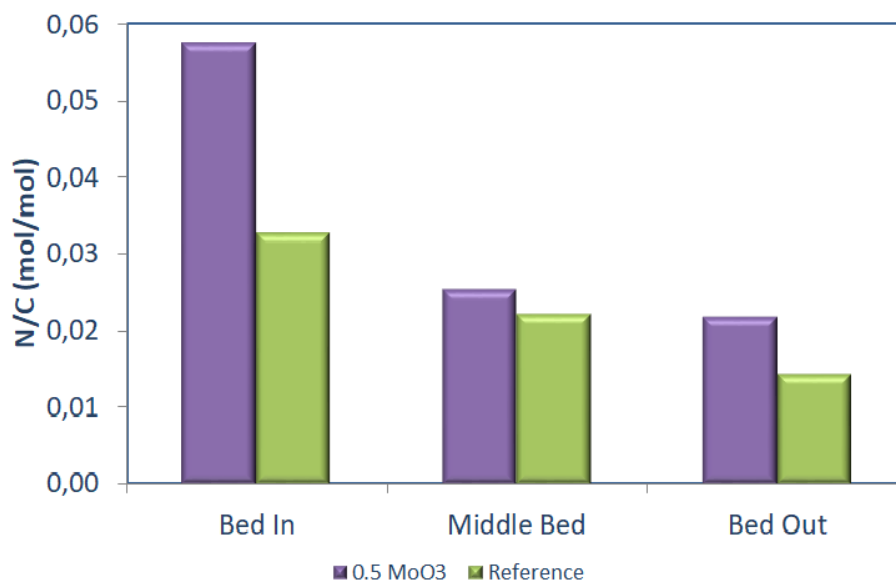
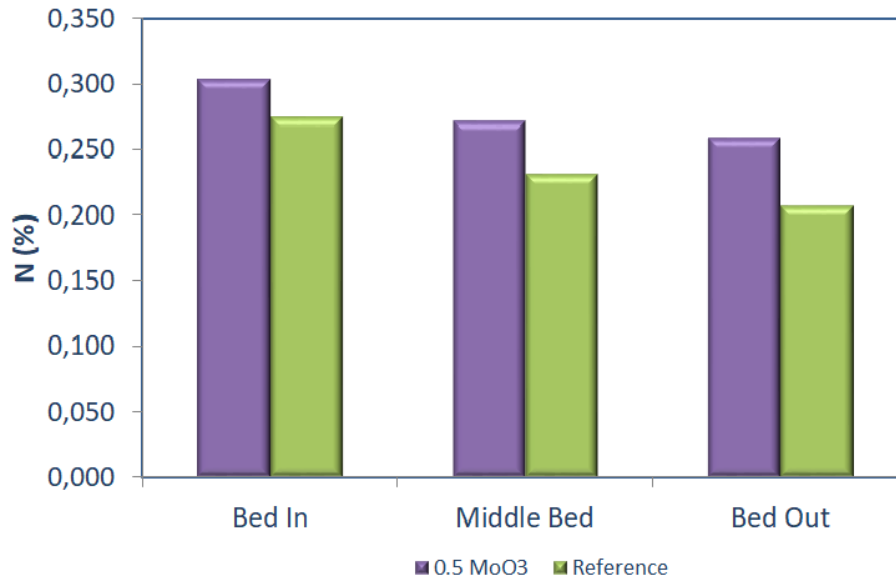


Figure 67. N/C ratio of the spent catalysts with different metal contents. Samples taken at different reactor locations.

## Chapter 4-Impact of metal content on the deactivation of a bifunctional hydrocracking catalyst

---



**Figure 68. Nitrogen content of the spent catalysts with different metal content. Samples taken at different reactor locations.**

Results of the H/C ratio of the coke in the spent catalysts are shown in Figure 69. A lower H/C ratio (indicating a more aromatic character of the coke deposit) was observed for the carbon deposits formed on the reference catalyst than for the one with half of the molybdenum content. It can be related to the higher cracking kinetic rate of the reference catalyst. This enhances the polymerization reactions of the coke precursors, forming more condensed structures with lower H/C ratios. The H/C ratio (Figure 69) diminished along the catalytic bed.

## Chapter 4-Impact of metal content on the deactivation of a bifunctional hydrocracking catalyst

---

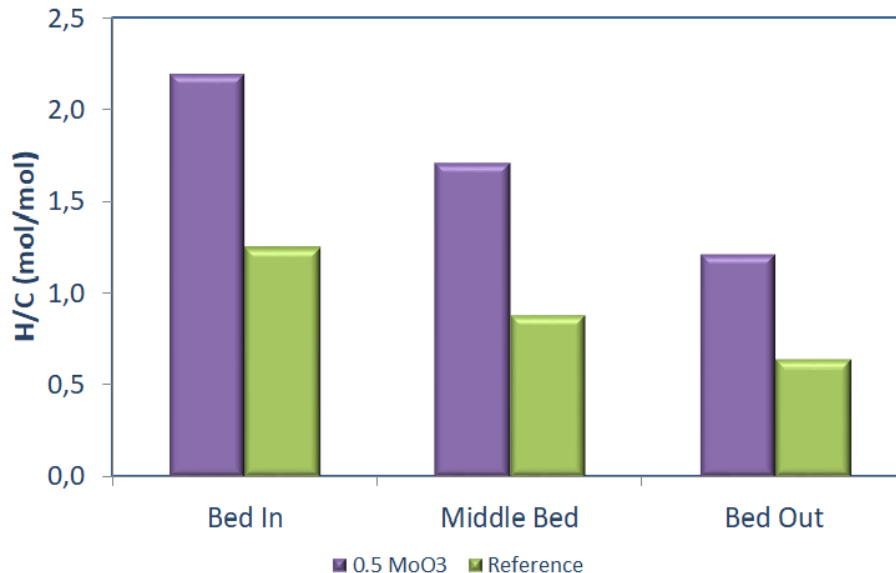


**Figure 69. Hydrogen/Carbon ratio of the spent catalysts with different metal content. Samples taken at different reactor locations.**

### 3.2.2. Textural Analysis

Catalysts were also analyzed by nitrogen adsorption-desorption isotherms. The surface area (S) and pore volume (V) with respect to the fresh catalyst are presented in Table 21. The area and volume losses for each catalyst show a direct correlation with its carbon deposition. Thus, the most significant modifications of the textural properties of the catalyst were found for the reference catalyst.

A more pronounced decrease of surface and pore volume was found at the bed outlet, in agreement with the higher carbon content. In the same sense, for both catalysts, the loss in textural properties was more pronounced for the samples obtained at the reactor outlet, where the carbon deposition was also superior.

## Chapter 4-Impact of metal content on the deactivation of a bifunctional hydrocracking catalyst

Table 21 also shows the ratio between the hysteresis area of each spent catalyst and the corresponding fresh catalyst, following the methodology described in chapter 2 (Section 2.4). The higher the value, the higher the extent of catalyst deactivation. The data showed a higher deactivation rate with the reference catalyst than with the one containing less molybdenum. The reactor outlet values were also higher than at the reactor inlet for the two spent catalysts.

**Table 21. Characterization of spent catalysts with different metal contents: Surface area (S), total pore volume (V) and the ratio of hysteresis area (HA) of the spent catalyst relative to the fresh catalyst.**

Catalyst	S/S <sub>fresh</sub>		V/V <sub>fresh</sub>		$\frac{HA_{Spent\ Catalyst}}{HA_{Fresh\ Catalyst}}$	
	Bed Inlet	Bed Outlet	Bed Inlet	Bed Outlet	Bed Inlet	Bed Outlet
	(%)	(%)	(%)	(%)		
0.5 MoO <sub>3</sub>	82	78	85	79	1.13	1.28
Reference	82	71	78	69	1.33	1.49

### 3.2.3. Thermo-gravimetric Analysis

TGA analysis were done to characterize the coke deposits on the spent catalysts. The first time-derivative of weight loss as a function of temperature is illustrated in Figure 70. The first peak, around 100°C, corresponds to H<sub>2</sub>O desorption, the second one (280-330°C) corresponds mainly to SO<sub>2</sub> release and the last peak is associated with the combustion of the coke deposits [214,234]. In Table 22, the percentage of the mass loss within the range of temperature corresponding to coke deposition is presented. These values agree with the carbon content from elemental analysis (see Figure 66).

## Chapter 4-Impact of metal content on the deactivation of a bifunctional hydrocracking catalyst

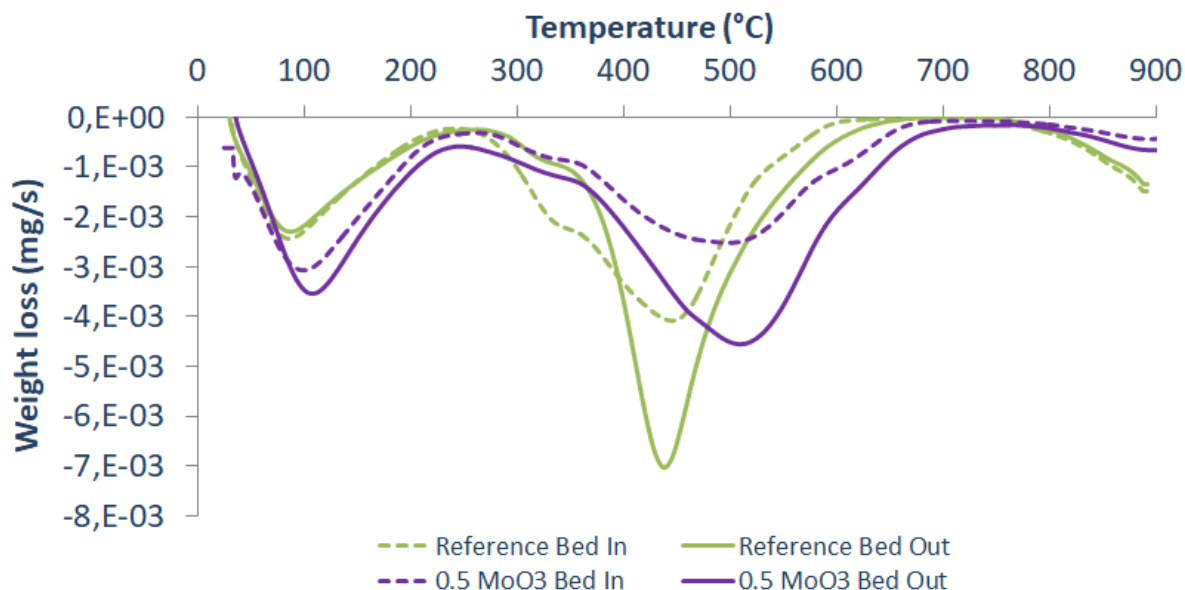


**Figure 70. TGA profiles of bed inlet and bed outlet samples from the spent catalyst with different metal content. Dotted line=First reactor effluent, continuous line=Total effluent.**

The maximum weight loss temperature is an indicator of the nature of coke; the higher this temperature, the more difficult to combust the coke is. It is often associated with a lower H/C ratio of the coke deposits. However, the coke deposits on the catalyst with less metal concentration required a higher temperature to combust (Figure 70 and Table 22), although its H/C ratio is higher (Figure 69). This behavior suggests that the high-temperature peaks for this catalyst were related to the higher nitrogen content of its coke deposits (Figure 68). This is in agreement with the work of Zeuthen et al. [143], who characterized some aged hydroprocessing catalysts by temperature-programmed oxidation and identified that the strongly adsorbed organic-nitrogen species are oxidized at temperatures around 500°C.

## Chapter 4-Impact of metal content on the deactivation of a bifunctional hydrocracking catalyst

---

**Table 22. Estimation of CO<sub>2</sub> mass loss of the coke deposit and maximum peak temperature from TGA profiles for spent catalysts with different metal content.**

<b>Catalyst</b>	<b>CO<sub>2</sub> mass loss (wt %)</b>	<b>Maximum Peak Temperature (°C)</b>
0.5 MoO <sub>3</sub> Bed In	7.8	495
0.5 MoO <sub>3</sub> Bed Out	10.3	510
Reference Bed In	11.2	445
Reference Bed Out	16.6	440

### 3.2.4. Model molecule tests

The residual activity of the (de)/hydrogenation function and the acid function of the spent catalysts were characterized by toluene hydrogenation and heptane hydroconversion, respectively. Figure 71 illustrates the first-order rate constant of the spent catalysts relative to the corresponding fresh catalyst ( $k_{\text{Hydro fresh}}$ ) for both studied catalysts during toluene hydrogenation ( $k_{\text{Hydro}}$ ). Figure 72 is dedicated to n-heptane constants ( $k_{\text{Crack}}$ ). These values reveal that, despite its lower initial activity, the catalysts with the lower metal content retained more hydrogenation activity than the reference catalyst, which lost around 80% of its original activity. The above is a consequence of the more substantial inhibition of the coke formation by nitrogen compounds in the case of the catalyst presenting the lowest MoO<sub>3</sub> content. The activity loss (inverse of Figure 71) of the metal function increased along the catalytic bed for both samples.

## Chapter 4-Impact of metal content on the deactivation of a bifunctional hydrocracking catalyst

---

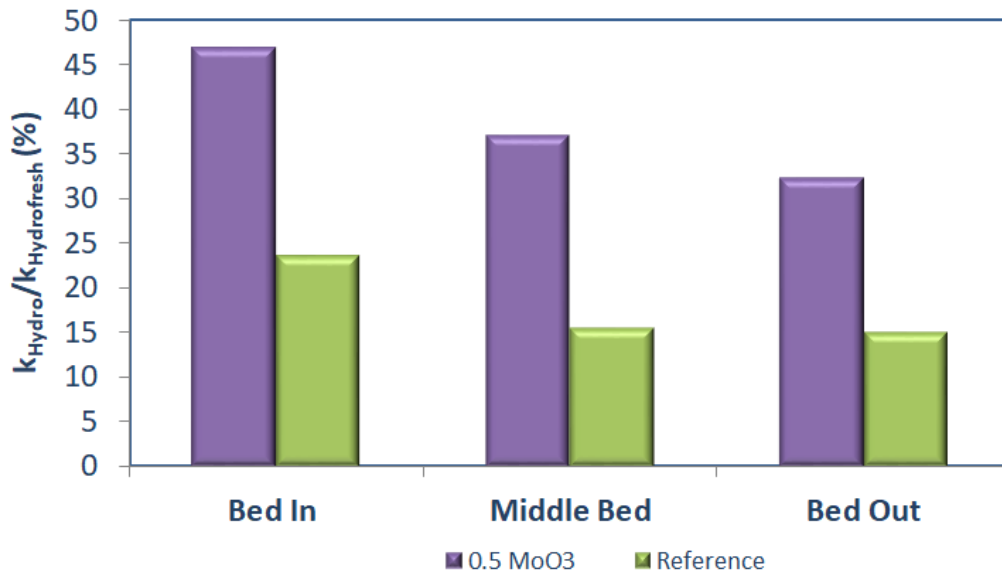


**Figure 71. Residual catalytic hydrogenation activity of the spent catalysts relative to the fresh catalysts, evaluated by toluene hydrogenation. Samples taken at different reactor locations.**

Regarding the cracking activity results (Figure 72), it was noticeable that this function was severely deactivated in both cases. All the residual activities were below 5% in relation to the fresh catalyst. For the catalyst with lower molybdenum content, the differences along the reactor were negligible. However, the reference catalyst had a significantly higher residual cracking activity (in absolute and relative terms) at the bed outlet. It could be related to the difference in nitrogen content of the carbon deposits. The reference catalyst had a significantly lower N/C ratio at the bed outlet. It seems that the nitrogen in the coke is the main cause of the decrease in residual cracking activity.

## Chapter 4-Impact of metal content on the deactivation of a bifunctional hydrocracking catalyst

---

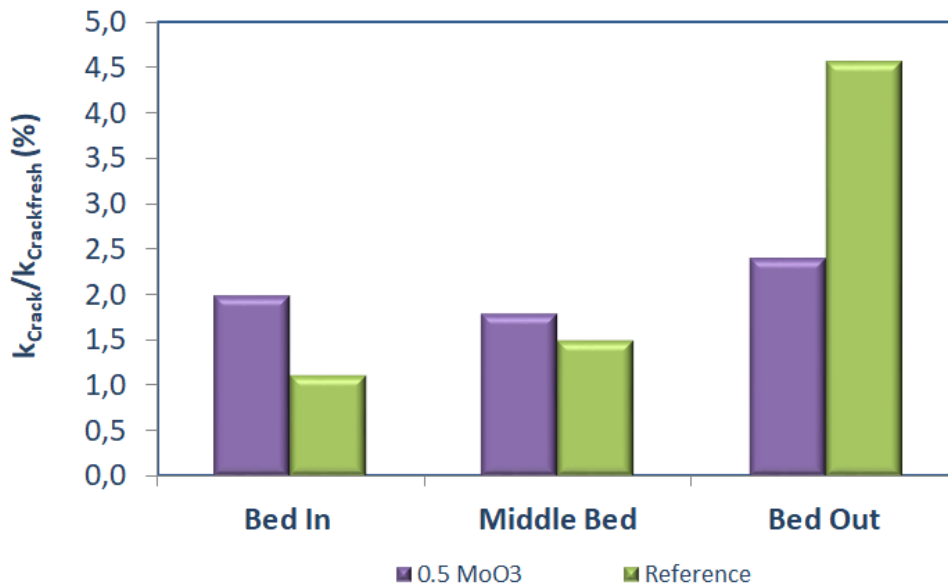


**Figure 72. Residual catalytic hydrogenation activity of the spent catalysts relative to the fresh catalyst, evaluated by isomerization/cracking of n-heptane at 360°C. Samples taken at different reactor locations.**

The selectivity to i-heptane is presented in Figure 73. The selectivity was higher for the fresh reference catalyst, meaning that the ratio between the metal and acid sites (M/A) was better balanced in that case. The tendency was the opposite for the spent samples, with higher i-heptane selectivity for the catalyst with half of the metal content. Thus, for this catalyst, it can be said that the hydrogenation sites better balanced the acid sites.

## Chapter 4-Impact of metal content on the deactivation of a bifunctional hydrocracking catalyst

---

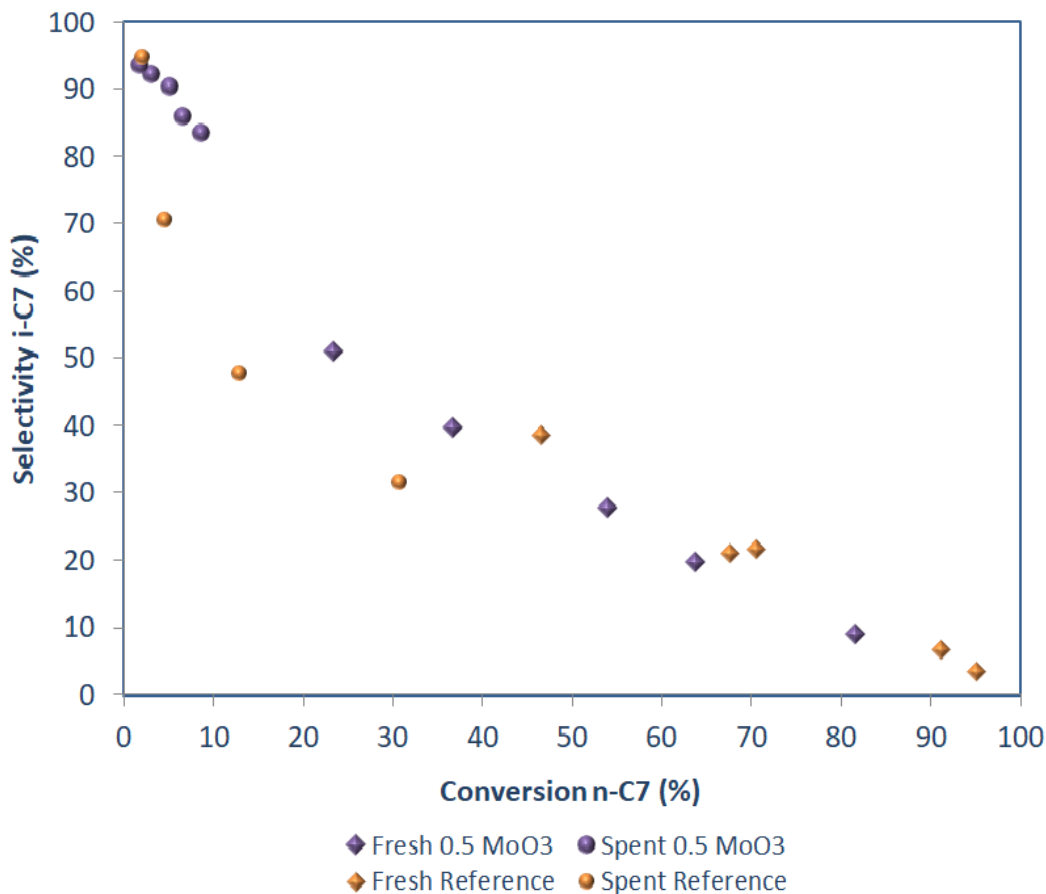


**Figure 73. Selectivity to i-C<sub>7</sub> Vs. conversion n-C<sub>7</sub>, obtained by n-heptane hydroconversion at different temperatures.**

### 4. DISCUSSION

The classical bifunctional hydrocracking mechanism [51,110,111,235] considers an initial dehydrogenation of alkanes on the metal sites to the corresponding alkenes. These alkenes are desorbed from the metal sites and diffuse to the acid sites, where they are protonated to carbenium ions. These carbocations undergo skeletal isomerization and cracking; their products are desorbed as alkenes which are finally hydrogenated to small alkanes on metal sites. For optimum performance, the activities of these two functions have to be balanced. Here the impact of the metal content, responsible for the hydrogenation activity, on catalyst deactivation was

## Chapter 4-Impact of metal content on the deactivation of a bifunctional hydrocracking catalyst

---

studied. To do so, one NiMo reference catalyst and another with half of the molybdenum content were submitted to the same deactivation conditions in a pilot unit with a real feedstock containing 120 ppmw of organic nitrogen.

On fresh catalysts, a consequent reduction of the hydrogenation activity as the molybdenum content decreased (Figure 57, a) was observed. Furthermore, the decrease in the metal content had a negative impact on the activity of the cracking function (Figure 57, b). It agrees with other authors [102], who established that at low metal/acid (M/A) ratios, there is a limitation of the bifunctional process by (de)-hydrogenation steps. This means that the metal sites are not sufficiently abundant to provide olefins for all the acid sites, so the maximum activity of the cracking function cannot be exploited. A decrease in the overall activity of the catalyst is then observed.

During the pilot plant deactivation experiments, the performance revealed lower reaction rate coefficients for HDN (Figure 64) and HDA (Figure 65) reactions with the catalyst with 50% of molybdenum. The lower the HDN reactions, the higher the nitrogen compounds concentration along the catalytic bed. This higher concentration has a determinant repercussion on the catalytic performance since nitrogen derivatives are known to be inhibitors of the metal sites [131–133,236]. Nitrogen is preferentially strongly adsorbed on acid sites [119,149,219,231] and thus inhibited them [233]. The remaining adsorbed nitrogen compounds are converted to coke with a longer time on stream, deactivating the acid sites permanently [16–18]. Both facts decrease cracking activity [8,10] and coke deposition from aromatics [197]. The decline of the HDA reaction rate produces an increase in aromatics concentration along the reactor. If there are sufficiently available acid sites, they undergo addition, dehydrogenation, and hydrogen

## Chapter 4-Impact of metal content on the deactivation of a bifunctional hydrocracking catalyst

---

transfer reactions to grow into large polyaromatic molecules, i.e., coke precursors [10,125]. For the catalyst with low molybdenum, nitrogen inhibition/deactivation controls the coke formation on top of the aromatics since less coke was deposited on this catalyst. It is because there are not enough acid sites to convert the more abundant aromatic species.

The data also displayed that the catalyst with low metal oxide had a lower residual cracking activity than the reference catalyst (Figure 63). Considering what has been stated, it is clear that these results from the low hydrogenation function and the more pronounced nitrogen inhibition/deactivation from the higher nitrogen concentration. On the other hand, the fit of the cracking reaction rate coefficients based on the exponential decay function (Table 17) showed a faster deactivation rate for the reference catalyst. This could be related to the faster deactivation of the hydrogenation function for the reference catalyst (Figure 64), which causes the nitrogen content to increase rapidly with time, and thus a higher inhibition of the cracking function was observed during the pilot test. The higher deactivation rate is consistent with the higher coke deposition measured on the spent samples of this catalyst and the ratio of the hysteresis areas between spent and fresh catalysts (Table 21).

The catalyst samples with the lower molybdenum concentration presented higher nitrogen contents than the reference catalyst (Figure 67 and Figure 68). It agrees with the fact that with this catalyst, there was a more nitrogen-rich atmosphere in the reactor. Thus, the strong interaction of the organic nitrogen compounds with the acid sites has a more pronounced contribution in the catalyst with low metal content. Accordingly, for the reference catalyst where there was a higher amount of coke with less nitrogen, the more significant contribution came from aromatic compounds (more cracking activity). This can also explain the lower H/C ratio (Figure 69) of these samples.

## Chapter 4-Impact of metal content on the deactivation of a bifunctional hydrocracking catalyst

---

Regarding the residual activities of the spent samples, it was observed that the loss of hydrogenating activity was more pronounced for the reference catalyst (Figure 71). Since no meaningful differences were observed in sintering or depromotion between the spent samples (Appendix 10), this behavior was attributed to higher coke build-up with the reference catalyst. The smaller decrease of the hydrogenating activity for the catalyst with less molybdenum is related to the higher inhibition of the (de)hydrogenation reactions by the nitrogen compounds, which inhibit the coke deposition on the metal surface.

The residual cracking activity (Figure 72) was minimal for both samples. The catalysts with half of the reference metal oxide retained slightly more cracking activity than the reference catalysts except for the bed outlet samples. This may be due to higher coke deposition on the acid sites of the lower metal content sample, which, as observed in Figure 68, has higher nitrogen content. The same behavior may not be observed in the samples from the other reactor positions since the difference in nitrogen content in the coke is smaller and also because cracking occurs in a more significant proportion as one moves up the bed. The ratio between the residual cracking activity of the catalyst with lower molybdenum content with respect to the reference catalyst is around 50%, which agrees with the ratio obtained between the two residual activities with the exponential decay model (Table 17). Despite the reduction in the hydrogenating function for the  $0.5\text{MO}_3$  catalyst, the results of selectivity to i-heptane (Figure 73) showed that the M/A ratio was higher for this catalyst indicating a better balance of the acid sites by the metal sites. This is because of the more pronounced deactivation of the metal function and, at the same time, a higher residual cracking activity for the reference spent catalyst.

## Chapter 4-Impact of metal content on the deactivation of a bifunctional hydrocracking catalyst

---

In general, it can be said that the assessment of the impact of the change of one of the functions of the bifunctional catalysts cannot be studied independently, but the effects must be rather considered in a coupled way. In the literature, it is said that when there is a reduction in the hydrogenating function, for samples with the same acid function, there is a greater coke formation on the catalyst, which leads to a rapid deactivation [102–104]. However, this study showed that this is not entirely true for nitrogen-rich reaction systems. In this case, it was observed that the decrease in the hydrogenating function causes an indirect decrease in the acid function of the catalyst. This provoked a modification on the M/A ratio, so the spent catalyst showed a better balance. Consequently, less coke generation was observed with a lower aromatic character but with higher nitrogen content. Therefore, the deactivation was lower for the catalyst with a weaker hydrogenating function.

### 5. CONCLUSIONS

- The balance between the metal and the acid functions determines the rate-limiting step of the bifunctional reaction mechanism. Consequently, when there is a reduction in the metal content, the rate-limiting step is the (de)/hydrogenation reactions that constituted the initial step of the mechanism. Therefore, the entire process is limited, and the global catalyst activity decreases.
- In hydrocracking of feedstocks with high nitrogen content, the decrease of the metal content of a bifunctional catalyst causes a substantial increase in the concentration of nitrogen compounds in the catalytic bed. This increase determines the performance of the catalyst by significantly reducing the available acid sites. Thus, there is a modification in the M/A ratio

## Chapter 4-Impact of metal content on the deactivation of a bifunctional hydrocracking catalyst

---

favoring a better balance of the spent catalyst resulting in a lower coke deposition.

Therefore, there is a lower deactivation rate.

- The interplay between HDN and cracking in VGO hydroprocessing leads to perverse effects, i.e., an improvement of the M/A balance when reducing the metal content, via the mechanism explained above. The direct effect of the reduction of the metal content and its indirect consequence, which is an increase in the acid sites inhibition by nitrogen, have an antagonistic influence on the deactivation behavior. The balance between both effects is expected to subtly depend on the properties of both the feed and the catalyst. This study provides a methodology for studying this complex system and a framework for interpreting the results, but one should be careful in generalizing the trends observed in this work, because they may depend on the system under consideration.

# General conclusion and perspectives

---

### GENERAL CONCLUSIONS AND PERSPECTIVES

The purpose of this work was to understand the loss of activity of a hydrocracking catalyst during the processing of VGO at representative operating conditions. The different causes of deactivation that are generally reported in the literature for this type of feedstock, i.e., poisoning by nitrogen compounds and coke formation, were explored. The challenge was to determine the individual role of these causes and the relationship between them on the loss of activity of a catalyst consisted of nickel-molybdenum sulfide particles dispersed on a carrier containing USY zeolite (NiMoP/USY).

The initial step of the thesis consisted of a variables screening from which it was possible to establish that the two operating conditions having the strongest impact on deactivation were temperature and space velocity. The first one because at high temperatures, coke precursors are formed faster and deactivate the catalysts through carbon deposition. The latter one because the lower the residence time, the lower the conversion of HDN and aromatics hydrogenation. Consequently, there is an increase in the concentration of coke precursors along the reactor, i.e., aromatics and nitrogen compounds (these are also inhibitors).

The results obtained from the variables screening led to establish a set of operating conditions to favor catalyst deactivation within the ranges typically used in hydrocracking processes. This set of conditions constituted an accelerated (30 days) deactivation protocol that yielded aged catalysts with textural properties, amount and nature of coke deposits and residual activity comparable to spent industrial catalysts. Thus, this methodology allowed a representative, fast and insightful way to evaluate the deactivation phenomena for VGO hydrocracking catalysts.

## General Conclusions and Perspectives

---

By using this experimental protocol, the deactivation causes for both the acid and the metal functions were studied. The acid function presented a drastic activity loss compared to the metal function. For the acid function organic nitrogen was found to play a fundamental role in the deactivation phenomena. These compounds are strongly chemisorbed on the acid sites due to their basic character, producing an initial inhibition. Then, they produce an irreversible deactivation since the adsorbed organic nitrogen compounds that remain on the catalyst surface produce coke before being desorbed. Concerning metal sites, nitrogen compounds have just an inhibitory effect on the metal function. The observed organic nitrogen impact on the reaction rates follows this order: Cracking>>HDN>HDA>HDS. The HDS activity was less affected as desulfurization can proceed via direct desulfurization (DDS), which does not rely on hydrogenation sites, strongly inhibited by nitrogen. The permanent deactivation of the metal function was mainly due to nickel depromotion. The aromatic coke formation plays a more important role in catalyst deactivation (both functions) with the increase of time on stream and far away from the reactor inlet, as explained later.

After understanding the importance of the feed nitrogen concentration on the deactivation rate, the impact of the feedstock properties on catalyst deactivation, i.e., the role of nitrogen and aromatic content as well as the boiling range, was evaluated. It was found that combining a feedstock with higher aromatics concentration and a lower nitrogen content creates an imbalance in the ratio M/A, with a low number of metal sites in relation to the acid sites. Consequently, there is poor hydrogenation of the unsaturated coke precursors species produced on the acid sites, which undergo polymerization and condensation reactions forming the coke deposits on the catalyst surface, thus promoting its deactivation. This combination has an effect that outweighs the effect of differences in the feedstock's molecular weight and boiling range. For a similar type of feed with a similar final boiling point, the total nitrogen and aromatics contents significantly impacted the resulting catalyst deactivation. As a matter of fact, the key

## General Conclusions and Perspectives

---

parameters are both the content but mostly the type of nitrogen compounds as they are at the origin of the inhibition of hydrogenation and cracking activities; but even more important, they determine the number of acid sites available for the reactions. It was observed that the presence of refractory compounds like carbazole (neutral), benzocarbazole (neutral), and acridine(basic), as well as nitrogen molecules with high molecular weight and a high degree of alkyl substitution, have a stronger negative impact on the catalyst activity, mainly in the cracking function. Concerning the aromatics, it was noted that the more aromatic structures are condensed, the higher the coke formation on the catalyst surface and consequently, the higher the activity loss.

The mechanisms leading to deactivation depend on the nitrogen concentration profile, which decreases along the reactor. This profile determines the number of available acid sites along the reactor and consequently the ratio of metal/acid sites (M/A). The balance in this ratio determines the amount and the type of formed coke. The lower the ratio, the lower the hydrogenation of intermediate unsaturated coke precursors species produced on the acid sites, and consequently, the higher the coke production rate. A lower balance also leads to a coke presenting a lower hydrogen content and, as a result, a more aromatic (less reactive) structure. Since the metal/acid balance decreases from the bed inlet to the bed outlet (due to less inhibition by organic nitrogen at the bed outlet), the bed outlet contains a higher amount of coke, which a more aromatic structure. The formed coke can originate from the organic nitrogen compounds or other coke precursors, like aromatic compounds. The N/C ratio values of the coke deposits from the spent catalyst decreased along the reactor, whereas the amount of deposited coke increased, as already mentioned. It means that the role of aromatics in coke formation becomes more significant towards the reactor outlet.

Regarding the catalyst deactivation evolution with time on stream, the catalyst was strongly deactivated during the first days on-stream. Then, the reaction rate coefficients reached almost constant values. This behavior follows the classical evolution of coke deposition, which is mainly

## General Conclusions and Perspectives

---

produced at the beginning of the test runs. These coke deposits are preferentially formed on the acid sites because of the rapid and strong chemisorption of nitrogen on these sites on one side and due to aromatics condensation and polymerization on the other side. The coke aromaticity increased with catalyst aging because as reactions to form coke progress, dehydrogenation occurs. The N/C ratio decreased over time due to the preferential adsorption of the nitrogen compounds on acid sites. These adsorbed compounds form coke precursors and, consequently, the coke deposits in the early stages of the operation. Subsequent coke results from the condensation/polymerization reactions of the unsaturated intermediates formed preferentially from aromatic structures, thus provoking a reduction in the N/C ratio. The model molecule tests also illustrated an activity decrease in both functions for the more aged samples, especially in the case of the cracking function. It could be related to the fact that coke on metal initially increases with time and then remains constant, while coke on the acid sites increases during the whole run.

Finally, the effect of the metal content on the deactivation of the bifunctional hydrocracking catalysts was examined. It was observed that in hydrocracking of feedstocks with high nitrogen concentration, the decrease of the metal content causes a substantial increase in nitrogen compounds in the catalytic bed. This increase determines the performance of the catalyst by significantly reducing the available acid sites. Thus, there is a modification in the M/A ratio favoring a better balance of the spent catalyst resulting in a lower coke deposition and consequently a lower deactivation rate than with the catalyst with higher metal content. The coke deposited on the catalyst with low metal oxide content had a higher nitrogen concentration and a higher H/C ratio than the reference catalyst. Both features are related to the more nitrogen-rich atmosphere in the reactor and the consequent strong interaction with the acid sites. It leads to a higher contribution of the nitrogen on the coke formation and lower cracking/hydrogenation activities, inducing less polymerized structures with more hydrogen per carbon atom.

## General Conclusions and Perspectives

---

In general, it was noted that the assessment of the impact of the change of one of the functions of the bifunctional catalysts cannot be studied independently, but rather the effects must be considered in a coupled way.

Concerning the perspectives of this work, a better understanding of the role of nitrogen compounds could be achieved by subjecting the catalyst to accelerated deactivation conditions with hydrotreated feeds at lower nitrogen levels. In this study, the deactivation mechanisms were dominated by the high nitrogen content making it difficult to decouple the impact of the aromatics coke precursors on the catalyst deactivation.

It might also be useful to compare the deactivation at iso-conversion conditions (instead of constant operating conditions). It could provide a more accurate assessment because the type of molecules to which the catalyst would be subjected would be similar. The way to obtain the same conversion should be by adjusting the LSHV rather than temperature since the temperature can shift the deactivation mechanisms toward the thermal cracking regime.

Additionally, performing deactivation tests by varying more significantly the content of nitrogenous and aromatic compounds would allow acquiring much more insight on the effect of these feed properties on the extent of deactivation. The above should be combined with a detailed characterization of these compounds in both feeds and products to follow the different species' evolution during deactivation. This information would allow further kinetic studies to construct a more specific mechanism for the deactivation by these compounds and establish the interaction between these two types of molecules.

Due to the impact of the catalyst porosity on the diffusion of the reactants, intermediates, and products, it would be interesting to evaluate its effect on deactivation, especially the effect of decreased pore size. It would enhance the confinement effects increasing the residence time of the reactants inside the pores, which would increase the coke formation and subsequent

## General Conclusions and Perspectives

---

deactivation. This may help understanding the deactivation mechanisms that occur when the pore diameter is reduced by coke deposition during time on stream. Finally, all these proposals should converge to the construction of a predictive deactivation model that considers the physicochemical properties of the feedstock as well as the catalyst characteristics. This deactivation model could be integrated into existing models of the hydrocracking process in order to guide the design of future catalytic formulations and to optimize the operation of the industrial plant by extending the catalyst lifetime.

### • References

- [1] Speight JG. Refining Processes. In: *The Refinery of the Future*. Elsevier; 2011, p. 39–80.
- [2] Ancheyta Juárez J. Deactivation of heavy oil hydroprocessing catalysts: Fundamentals and modeling. Hoboken New Jersey: Wiley; 2016.
- [3] Eni, World Oil Review. Volume 1-2020.
- [4] Worldwide Refinery Processing Review. Second Quarter 2017. Hydrocarbon Publishing Company.
- [5] Hydrocarbon Publishing Company. Worldwide refinery processing review; 2017.
- [6] M. Rashidzadeh A. Ahmad, S. Sadighi. Studying of Catalyst Deactivation in a Commercial Hydrocracking Process (ISOMAX). *Journal of Petroleum Science and Technology* 2011;1(1):46–54.
- [7] S.T. Sie. Consequences of catalyst deactivation for process design and operation. *Applied Catalysis A: General* 2001(212):129–51.
- [8] Sau M, Basak K, Manna U, Santra M, Verma RP. Effects of organic nitrogen compounds on hydrotreating and hydrocracking reactions. *Catalysis Today* 2005;109(1-4):112–9. <https://doi.org/10.1016/j.cattod.2005.08.007>.
- [9] Scherzer J, Gruia AJ. *Hydrocracking science and technology*. New York: Marcel Dekker; 1996.
- [10] Speight JG. *The refinery of the future*. 1st ed. Amsterdam, Boston, Heidelberg: Elsevier; Gulf Professional Publishing; 2011.
- [11] Toulhoat H, Raybaud P (eds.). *Catalysis by transition metal sulphides: From molecular theory to industrial application*. Paris: Éd. Technip; 2013.
- [12] Furimsky E. *Catalysts for upgrading heavy petroleum feeds*. Amsterdam, Boston, Paris: Elsevier; 2007.

## References

---

- [13] Ancheyta J, Speight JG. Hydroprocessing of heavy oils and residua. Boca Raton: CRC Press; 2007.
- [14] Leprince P. Petroleum refining. Petroleum refining 2001.
- [15] Sánchez-Delgado RA. Organometallic Modeling of the Hydrodesulfurization and Hydrodenitrogenation Reactions. Cham: Springer International Publishing; 20.
- [16] NAG N. Hydrodesulfurization of polycyclic aromatics catalyzed by sulfided CoO-MoO<sub>3</sub>/gamma-Al<sub>2</sub>O<sub>3</sub>: The relative reactivities. *Journal of Catalysis* 1979;57(3):509–12. [https://doi.org/10.1016/0021-9517\(79\)90016-2](https://doi.org/10.1016/0021-9517(79)90016-2).
- [17] Weisser O, Landa S. Sulphide Catalysts, Their Properties and Applications. Kent: Elsevier Science; 2014.
- [18] D. R. Kilanowski, H. Teeuwen, V. H. J. De Beer, B. C. Gates, G. C. A. Schuit, and H. Kwart. Hydrodesulfurization of thiophene, benzothiophene, dibenzothiophene, and related compounds catalyzed by sulfided CoO-MoO<sub>3</sub>/gamma-Al<sub>2</sub>O<sub>3</sub>: Low-pressure reactivity studies. *Journal of Catalysis*:129–37.
- [19] K.F. MC Carty and G. L. Schrader. Deuterodesulfurization of Thiophene: An Investigation of the Reaction Mechanism. *Journal of Catalysis* 1987, 1987:261–9.
- [20] *Advances in catalysis: And related subjects*. New York: Acad. Press; 1998.
- [21] Topsøe H, Knudsen KG, Byskov LS, Nørskov JK, Clausen BS. Advances in deep desulfurization. In: *Science and Technology in Catalysis 1998, Proceedings of the Third Tokyo Conference on Advanced Catalytic Science and Technology*. Elsevier; 1999, p. 13–22.
- [22] Anderson JR, Boudart M. *Catalysis*. Berlin, Heidelberg: Springer Berlin Heidelberg; 1996.
- [23] Ruetter, F, Ludeña E. Molecular orbital calculations of the hydrodesulfurization of thiophene over a Mo-Co catalyst. *Journal of Catalysis* 1981;67(2):266–81. [https://doi.org/10.1016/0021-9517\(81\)90286-4](https://doi.org/10.1016/0021-9517(81)90286-4).

## References

---

- [24] Rong C, Qin X. Quantum chemical study of MoS<sub>2</sub> hydro desulfurization catalysts. *Journal of Molecular Catalysis* 1991;64(3):321–35. [https://doi.org/10.1016/0304-5102\(91\)85141-N](https://doi.org/10.1016/0304-5102(91)85141-N).
- [25] LIPSCH J. The CoO-MoO<sub>3</sub>-Al<sub>2</sub>O<sub>3</sub> catalyst I. Cobalt molybdate and the cobalt oxide molybdenum oxide system. *Journal of Catalysis* 1969;15(2):163–73. [https://doi.org/10.1016/0021-9517\(69\)90020-7](https://doi.org/10.1016/0021-9517(69)90020-7).
- [26] Overend J. Chemistry of Catalytic Processes (Gates, Bruce C; Katzer, James R; Schuit, G. C. A; ed.s). *J. Chem. Educ.* 1979;56(7):A242. <https://doi.org/10.1021/ed056pA242.2>.
- [27] Houalla M, Nag NK, Sapre AV, Broderick DH, Gates BC. Hydrodesulfurization of dibenzothiophene catalyzed by sulfided CoO-MoO<sub>3</sub>/γ-Al<sub>2</sub>O<sub>3</sub>: The reaction network. *AIChE J.* 1978;24(6):1015–21. <https://doi.org/10.1002/aic.690240611>.
- [28] Sapre AV, Broderick DH, Fraenkel D, Gates BC, Nag NK. Hydrodesulfurization of benzo[b]naphtho[2,3-d]thiophene catalyzed by sulfided CoO-MoO<sub>3</sub>/γ-Al<sub>2</sub>O<sub>3</sub>: The reaction network. *AIChE J.* 1980;26(4):690–4. <https://doi.org/10.1002/aic.690260426>.
- [29] KWART H. Hydrodesulfurization of thiophenic compounds: The reaction mechanism. *Journal of Catalysis* 1980;61(1):128–34. [https://doi.org/10.1016/0021-9517\(80\)90347-4](https://doi.org/10.1016/0021-9517(80)90347-4).
- [30] Songhal L G. Hydrodesulfurization of sulfur heterocyclic compounds Reaction mechanisms. *Journal of Catalysis* 1981;67(2):446–56. [https://doi.org/10.1016/0021-9517\(81\)90304-3](https://doi.org/10.1016/0021-9517(81)90304-3).
- [31] Topsøe H. In situ Mössbauer emission spectroscopy studies of unsupported and supported sulfided Co-Mo hydrodesulfurization catalysts: Evidence for and nature of a Co-Mo-S phase. *Journal of Catalysis* 1981;68(2):433–52. [https://doi.org/10.1016/0021-9517\(81\)90114-7](https://doi.org/10.1016/0021-9517(81)90114-7).
- [32] Perot G. The reactions involved in hydrodenitrogenation. *Catalysis Today* 1991;10(4):447–72. [https://doi.org/10.1016/0920-5861\(91\)80033-6](https://doi.org/10.1016/0920-5861(91)80033-6).
- [33] Furimsky E. Deactivation of hydroprocessing catalysts. *Catalysis Today* 1999;52(4):381–495. [https://doi.org/10.1016/S0920-5861\(99\)00096-6](https://doi.org/10.1016/S0920-5861(99)00096-6).

## References

---

- [34] Spessard GO. Introduction to organic chemistry (Streitwieser, Andrew Jr; Heathcock, Clayton H.). *J. Chem. Educ.* 1977;54(6):A294. <https://doi.org/10.1021/ed054pA294.2>.
- [35] Girgis MJ, Gates BC. Reactivities, reaction networks, and kinetics in high-pressure catalytic hydroprocessing. *Ind. Eng. Chem. Res.* 1991;30(9):2021–58. <https://doi.org/10.1021/ie00057a001>.
- [36] Prado GHC, Rao Y, Klerk A de. Nitrogen Removal from Oil: A Review. *Energy Fuels* 2017;31(1):14–36. <https://doi.org/10.1021/acs.energyfuels.6b02779>.
- [37] Minh Tuan Nguyen. Support acidity effects of NiMo sulfide catalysts in hydrodenitrogenation of quinoline, indole and Coker Gas Oil. Lyon, France: Université Claude Bernard-Lyon I; 2016.
- [38] Schulz H, Schon M, Rahman NM. Chapter 6 Hydrogenative Denitrogenation of Model Compounds as Related to the Refining of Liquid Fuels. In: *Catalytic Hydrogenation*. Elsevier; 1986, p. 201–255.
- [39] Bej SK, Dalai AK, Adjaye J. Comparison of Hydrodenitrogenation of Basic and Nonbasic Nitrogen Compounds Present in Oil Sands Derived Heavy Gas Oil. *Energy Fuels* 2001;15(2):377–83. <https://doi.org/10.1021/ef0001484>.
- [40] Minh Tuan Nguyen. Support acidity effects of NiMo sulfide catalysts in hydrodenitrogenation of quinoline, indole and Coker Gas Oil: Université de Lyon; 2016.
- [41] Landau MV. Deep hydrotreating of middle distillates from crude and shale oils. *Catalysis Today* 1997;36(4):393–429. [https://doi.org/10.1016/S0920-5861\(96\)00233-7](https://doi.org/10.1016/S0920-5861(96)00233-7).
- [42] Grange P. Catalytic Hydrodesulfurization. *Catalysis Reviews* 1980;21(1):135–81. <https://doi.org/10.1080/03602458008068062>.
- [43] Satterfield CN, Cocchetto JF. Reaction network and kinetics of the vapor-phase catalytic hydrodenitrogenation of quinoline. *Ind. Eng. Chem. Proc. Des. Dev.* 1981;20(1):53–62. <https://doi.org/10.1021/i200012a008>.

## References

---

- [44] C. Moreau, R. Durand, N. Zmimita, and P. Geneste. Hydrodenitrogenation of Benzo(f)quinoline and Benzo(h)quinoline over a Sulfided NiO-MoO<sub>3</sub>-Al<sub>2</sub>O<sub>3</sub> Catalyst. *Journal of Catalysis* 1988, 1988:411–7.
- [45] Lapinas AT, Klein MT, Macris A, Lyons JE, Gates BC. Catalytic hydrogenation and hydrocracking of fluoranthene: reaction pathways and kinetics. *Ind. Eng. Chem. Res.* 1987;26(5):1026–33. <https://doi.org/10.1021/ie00065a029>.
- [46] Sapre AV, Gates BC. Hydrogenation of aromatic hydrocarbons catalyzed by sulfided cobalt oxide-molybdenum oxide/.alpha.-aluminum oxide. Reactivities and reaction networks. *Ind. Eng. Chem. Proc. Des. Dev.* 1981;20(1):68–73. <https://doi.org/10.1021/i200012a010>.
- [47] Neurock M, Libanati C, Nigam A, Klein MT. Monte carlo simulation of complex reaction systems: molecular structure and reactivity in modelling heavy oils. *Chemical Engineering Science* 1990;45(8):2083–8. [https://doi.org/10.1016/0009-2509\(90\)80080-X](https://doi.org/10.1016/0009-2509(90)80080-X).
- [48] Le Page J-F, Cosyns J, Courty P. *Applied heterogeneous catalysis: Design, manufacture, use of solid catalysts*. Paris: Ed.Technip; 1987.
- [49] Dufresne P, Bigeard PH, Billon A. New developments in hydrocracking: low pressure high-conversion hydrocracking. *Catalysis Today* 1987;1(4):367–84. [https://doi.org/10.1016/0920-5861\(87\)80005-6](https://doi.org/10.1016/0920-5861(87)80005-6).
- [50] Wisner WH, Singh S, Qader SA, Hill GR. Catalytic Hydrogenation of Multiring Aromatic Coal Tar Constituents. *Ind. Eng. Chem. Prod. Res. Dev.* 1970;9(3):350–7. <https://doi.org/10.1021/i360035a017>.
- [51] Weitkamp J. Catalytic Hydrocracking—Mechanisms and Versatility of the Process. *ChemCatChem* 2012;4(3):292–306. <https://doi.org/10.1002/cctc.201100315>.
- [52] Bouchy C, Hastoy G, Guillon E, Martens JA. Fischer-Tropsch Waxes Upgrading via Hydrocracking and Selective Hydroisomerization. *Oil & Gas Science and Technology - Rev. IFP* 2009;64(1):91–112. <https://doi.org/10.2516/ogst/2008047>.

## References

---

- [53] Ancheyta J, Sánchez S, Rodríguez MA. Kinetic modeling of hydrocracking of heavy oil fractions: A review. *Catalysis Today* 2005;109(1-4):76–92. <https://doi.org/10.1016/j.cattod.2005.08.015>.
- [54] Satterfield CN, Roberts GW. Kinetics of thiophene hydrogenolysis on a cobalt molybdate catalyst. *AIChE J.* 1968;14(1):159–64. <https://doi.org/10.1002/aic.690140127>.
- [55] Kilanowski DBG. Kinetics of hydrodesulfurization of benzothiophene catalyzed by sulfided Co-Mo/Al<sub>2</sub>O<sub>3</sub>. *Journal of Catalysis* 1980;62(1):70–8. [https://doi.org/10.1016/0021-9517\(80\)90421-2](https://doi.org/10.1016/0021-9517(80)90421-2).
- [56] Kabe T, Ishihara A, Zhang Q. Deep desulfurization of light oil. Part 2: hydrodesulfurization of dibenzothiophene, 4-methyldibenzothiophene and 4,6-dimethyldibenzothiophene. *Applied Catalysis A: General* 1993;97(1):L1-L9. [https://doi.org/10.1016/0926-860X\(93\)80059-Y](https://doi.org/10.1016/0926-860X(93)80059-Y).
- [57] Edvinsson R, Irandoust S. Hydrodesulfurization of dibenzothiophene in a monolithic catalyst reactor. *Ind. Eng. Chem. Res.* 1993;32(2):391–5. <https://doi.org/10.1021/ie00014a016>.
- [58] Satterfield CN, Yang SH. Catalytic hydrodenitrogenation of quinoline in a trickle-bed reactor. Comparison with vapor phase reaction. *Ind. Eng. Chem. Proc. Des. Dev.* 1984;23(1):11–9. <https://doi.org/10.1021/i200024a003>.
- [59] Miller JC. Competition, Predation, and Catchnet Differentiation among Net-Spinning Caddisflies (Trichoptera). *Oikos* 1984;43(1):117. <https://doi.org/10.2307/3544253>.
- [60] Massoth FE. Catalytic functionalities of supported sulfides VI. The effect of H<sub>2</sub>S promotion on the kinetics of indole hydrogenolysis. *Journal of Catalysis* 1990;122(2):256–70. [https://doi.org/10.1016/0021-9517\(90\)90280-W](https://doi.org/10.1016/0021-9517(90)90280-W).
- [61] Qader SA, Hill GR. Hydrocracking of Gas Oil. *Ind. Eng. Chem. Proc. Des. Dev.* 1969;8(1):98–105. <https://doi.org/10.1021/i260029a017>.

## References

---

- [62] El-Kady, F.Y.A., Menoufy, M.F., Hassan, H.A. Effect of the reaction temperature and pressure on the hydroisomerization of n-heptane. *Indian Journal of Technology* 1983, 1983:293–9.
- [63] Baltanas MA, Vansina H, Froment GF. Hydroisomerization and hydrocracking. 5. Kinetic analysis of rate data for n-octane. *Ind. Eng. Chem. Prod. Res. Dev.* 1983;22(4):531–9. <https://doi.org/10.1021/i300012a004>.
- [64] Steijns M, Froment GF. Hydroisomerization and hydrocracking. 3. Kinetic analysis of rate data for n-decane and n-dodecane. *Ind. Eng. Chem. Prod. Res. Dev.* 1981;20(4):660–8. <https://doi.org/10.1021/i300004a014>.
- [65] C. A. Bernardo and D. L. Trimm. *Rev. Port. Quim.* 1977, 1977:369.
- [66] Stangeland BE. A Kinetic Model for the Prediction of Hydrocracker Yields. *Ind. Eng. Chem. Proc. Des. Dev.* 1974;13(1):71–6. <https://doi.org/10.1021/i260049a013>.
- [67] Da Novaes LR, Pacheco ME, Salim VMM, Resende NS de. Accelerated deactivation studies of hydrotreating catalysts in pilot unit. *Applied Catalysis A: General* 2017;548:114–21. <https://doi.org/10.1016/j.apcata.2017.06.040>.
- [68] Ancheyta J, Angeles MJ, Macías MJ, Marroquín G, Morales R. Changes in Apparent Reaction Order and Activation Energy in the Hydrodesulfurization of Real Feedstocks. *Energy Fuels* 2002;16(1):189–93. <https://doi.org/10.1021/ef0101917>.
- [69] Ferdous D, Dalai AK, Adjaye J. Hydrodenitrogenation and Hydrodesulfurization of Heavy Gas Oil Using NiMo/Al<sub>2</sub>O<sub>3</sub> Catalyst Containing Boron: Experimental and Kinetic Studies. *Ind. Eng. Chem. Res.* 2006;45(2):544–52. <https://doi.org/10.1021/ie050094r>.
- [70] Pacheco ME, Martins Salim VM, Pinto JC. Accelerated Deactivation of Hydrotreating Catalysts by Coke Deposition. *Ind. Eng. Chem. Res.* 2011;50(10):5975–81. <https://doi.org/10.1021/ie1023595>.

- [71] Roussel M, Norsic S, Lemberon J-L, Guisnet M, Cseri T, Benazzi E. Hydrocracking of n-decane on a bifunctional sulfided NiW/silica–alumina catalyst: effect of the operating conditions. *Applied Catalysis A: General* 2005;279(1-2):53–8. <https://doi.org/10.1016/j.apcata.2004.10.011>.
- [72] Ward JW. Hydrocracking processes and catalysts. *Fuel Processing Technology* 1993;35(1-2):55–85. [https://doi.org/10.1016/0378-3820\(93\)90085-1](https://doi.org/10.1016/0378-3820(93)90085-1).
- [73] Deldari H. Suitable catalysts for hydroisomerization of long-chain normal paraffins. *Applied Catalysis A: General* 2005;293:1–10. <https://doi.org/10.1016/j.apcata.2005.07.008>.
- [74] Yan TY. Effect of metal on zeolite catalysts for extinction hydrocracking. *Ind. Eng. Chem. Res.* 1990;29(10):1995–8. <https://doi.org/10.1021/ie00106a003>.
- [75] *Advances in Catalysis*. San Diego, CA, USA: Elsevier Science; 2016.
- [76] Rigutto MS, van Veen R, Huve L. Zeolites in Hydrocarbon Processing. In: *Introduction to Zeolite Science and Practice*. Elsevier; 2007, 855-XXVI.
- [77] Vázquez MI, Escardino A, Aucejo A, Corma A. Hydrocracking of n -heptane. Study of NiO-MoO<sub>3</sub> catalysts supported on a HY ultrastable zeolite. *Can. J. Chem. Eng.* 1986;64(2):272–7. <https://doi.org/10.1002/cjce.5450640217>.
- [78] Feeley O, Sachtler W. Oxidative redispersion of metals in Y zeolites effect of ammonia on Pd/HY rejuvenation. *Applied Catalysis* 1990;67(1):141–50. [https://doi.org/10.1016/S0166-9834\(00\)84437-1](https://doi.org/10.1016/S0166-9834(00)84437-1).
- [79] Cui Q, Zhou Y, Wei Q, Tao X, Yu G, Wang Y et al. Role of the Zeolite Crystallite Size on Hydrocracking of Vacuum Gas Oil over NiW/Y-ASA Catalysts. *Energy Fuels* 2012;26(8):4664–70. <https://doi.org/10.1021/ef300544c>.
- [80] Carsten Wivel, Roberto Candia, Bjerne S.Clausen, SteenMørup, HenrikTopsøe. On the catalytic significance of a Co-Mo-S phase in Co-Mo/Al<sub>2</sub>O<sub>3</sub> hydrodesulfurization catalysts:

- Combined in situ Mossbauer emission spectroscopy and activity studies. *Journal of Catalysis* 1981;68(2):453–63. [https://doi.org/10.1016/0021-9517\(81\)90115-9](https://doi.org/10.1016/0021-9517(81)90115-9).
- [81] Raybaud P, Hafner J, Kresse G, Kasztelan S, Toulhoat H. Structure, Energetics, and Electronic Properties of the Surface of a Promoted MoS<sub>2</sub> Catalyst: An ab Initio Local Density Functional Study. *Journal of Catalysis* 2000;190(1):128–43. <https://doi.org/10.1006/jcat.1999.2743>.
- [82] Topsøe H, Clausen BS, Topsøe N-Y, Nørskov JK, Ovesen CV, Jacobsen CJH. The Bond Energy Model for Hydrotreating Reactions: Theoretical and Experimental Aspects. *Bull. Soc. Chim. Belges* 1995;104(4-5):283–91. <https://doi.org/10.1002/bscb.19951040415>.
- [83] Bertrand Guichard. Vieillissement des catalyseurs d'hydrodesulfuration: méthodologie d'étude et simulation de l'évolution du site actif. Lyon: l'UNIVERSITÉ CLAUDE BERNARD - LYON 1; 2007.
- [84] Kolboe S. Catalytic hydrodesulfurization of thiophene. VII. Comparison between thiophene, tetrahydrothiophene, and n -butanethiol. *Can. J. Chem.* 1969;47(2):352–5. <https://doi.org/10.1139/v69-050>.
- [85] Raybaud P. Understanding and predicting improved sulfide catalysts: Insights from first principles modeling. *Applied Catalysis A: General* 2007;322:76–91. <https://doi.org/10.1016/j.apcata.2007.01.005>.
- [86] Song C. An overview of new approaches to deep desulfurization for ultra-clean gasoline, diesel fuel and jet fuel. *Catalysis Today* 2003;86(1-4):211–63. [https://doi.org/10.1016/S0920-5861\(03\)00412-7](https://doi.org/10.1016/S0920-5861(03)00412-7).
- [87] Breyse M, Djega-Mariadassou G, Pessayre S, Geantet C, Vrinat M, Pérot G et al. Deep desulfurization: reactions, catalysts and technological challenges. *Catalysis Today* 2003;84(3-4):129–38. [https://doi.org/10.1016/S0920-5861\(03\)00266-9](https://doi.org/10.1016/S0920-5861(03)00266-9).

## References

---

- [88] Brémaud M, Vivier L, Pérot G, Harlé V, Bouchy C. Hydrogenation of olefins over hydrotreating catalysts. *Applied Catalysis A: General* 2005;289(1):44–50. <https://doi.org/10.1016/j.apcata.2005.04.014>.
- [89] Lauritsen J, Helveg S, Lægsgaard E, Stensgaard I, Clausen B, Topsøe H et al. Atomic-Scale Structure of Co–Mo–S Nanoclusters in Hydrotreating Catalysts. *Journal of Catalysis* 2001;197(1):1–5. <https://doi.org/10.1006/jcat.2000.3088>.
- [90] Topsøe H. The role of Co–Mo–S type structures in hydrotreating catalysts. *Applied Catalysis A: General* 2007;322:3–8. <https://doi.org/10.1016/j.apcata.2007.01.002>.
- [91] Lauritsen JV, Bollinger MV, Lægsgaard E, Jacobsen KW, Nørskov JK, Clausen BS et al. Atomic-scale insight into structure and morphology changes of MoS<sub>2</sub> nanoclusters in hydrotreating catalysts. *Journal of Catalysis* 2004;221(2):510–22. <https://doi.org/10.1016/j.jcat.2003.09.015>.
- [92] Vanderbilt. Soft self-consistent pseudopotentials in a generalized eigenvalue formalism. *Phys Rev B Condens Matter* 1990;41(11):7892–5. <https://doi.org/10.1103/PhysRevB.41.7892>.
- [93] Corma A, Martínez A. Zeolites in refining and petrochemistry. In: *Zeolites and Ordered Mesoporous Materials: Progress and Prospects*. Elsevier; 2005, p. 337–366.
- [94] Maxwell IE. Zeolite catalysis in hydroprocessing technology. *Catalysis Today* 1987;1(4):385–413. [https://doi.org/10.1016/0920-5861\(87\)80006-8](https://doi.org/10.1016/0920-5861(87)80006-8).
- [95] Dik PP, Danilova IG, Golubev IS, Kazakov MO, Nadeina KA, Budukva SV et al. Hydrocracking of vacuum gas oil over NiMo/zeolite-Al<sub>2</sub>O<sub>3</sub>: Influence of zeolite properties. *Fuel* 2019;237:178–90. <https://doi.org/10.1016/j.fuel.2018.10.012>.
- [96] Ding L, Zheng Y, Zhang Z, Ring Z, Chen J. HDS, HDN, HDA, and hydrocracking of model compounds over Mo-Ni catalysts with various acidities. *Applied Catalysis A: General* 2007;319:25–37. <https://doi.org/10.1016/j.apcata.2006.11.016>.

- [97] Vogt ET, Whiting GT, Dutta Chowdhury A, Weckhuysen BM. Zeolites and Zeotypes for Oil and Gas Conversion. In: Elsevier; 2015, p. 143–314.
- [98] Loewenstein W. The Distribution of Aluminium in the Tetra-Hedra of Silicates and Aluminates. *American Mineralogist* 1954, 1954:92–6.
- [99] Marcilly C. *Acido-basic catalysis*. Paris: Ed. Technip; 20052006.
- [100] Primo A, Garcia H. Zeolites as catalysts in oil refining. *Chem Soc Rev* 2014;43(22):7548–61. <https://doi.org/10.1039/C3CS60394F>.
- [101] Guisnet M. “Ideal” bifunctional catalysis over Pt-acid zeolites. *Catalysis Today* 2013;218-219:123–34. <https://doi.org/10.1016/j.cattod.2013.04.028>.
- [102] Giannetto GE, Perot GR, Guisnet MR. Hydroisomerization and hydrocracking of n-alkanes. 1. Ideal hydroisomerization PtHY catalysts. *Ind. Eng. Chem. Prod. Res. Dev.* 1986;25(3):481–90. <https://doi.org/10.1021/i300023a021>.
- [103] Guisnet M, Alvarez F, Giannetto G, Perot G. Hydroisomerization and hydrocracking of n-heptane on Pth zeolites. Effect of the porosity and of the distribution of metallic and acid sites. *Catalysis Today* 1987;1(4):415–33. [https://doi.org/10.1016/0920-5861\(87\)80007-X](https://doi.org/10.1016/0920-5861(87)80007-X).
- [104] Alvarez F, Ribeiro FR, Perot G, Thomazeau C, Guisnet M. Hydroisomerization and Hydrocracking of Alkanes. *Journal of Catalysis* 1996;162(2):179–89. <https://doi.org/10.1006/jcat.1996.0275>.
- [105] Denayer JF, Baron GV, Vanbutsele G, Jacobs PA, Martens JA. Evidence for Alkylcarbenium Ion Reaction Intermediates from Intrinsic Reaction Kinetics of C6–C9n-Alkane Hydroisomerization and Hydrocracking on Pt/H–Y and Pt/USY Zeolites. *Journal of Catalysis* 2000;190(2):469–73. <https://doi.org/10.1006/jcat.1999.2756>.
- [106] Kinger G, Vinek H. n-Nonane hydroconversion on Ni and Pt containing HMF1, HMOR and HBEA. *Applied Catalysis A: General* 2001;218(1-2):139–49. [https://doi.org/10.1016/S0926-860X\(01\)00629-9](https://doi.org/10.1016/S0926-860X(01)00629-9).

- [107] Sullivan R. F., MEYER JA. Catalyst Effects on Yields and Product Properties in Hydrocracking. In: Ward JW, Qader SA, editors. Hydrocracking and Hydrotreating. WASHINGTON, D. C.: AMERICAN CHEMICAL SOCIETY; 1975, p. 28–51.
- [108] SULLIVAN RF, SCOTT JW. The Development of Hydrocracking. In: Ward JW, Qader SA, editors. Hydrocracking and Hydrotreating. WASHINGTON, D. C.: AMERICAN CHEMICAL SOCIETY; 1975, p. 293–313.
- [109] Barbier J, Corro G, Zhang Y, Bournville JP, Franck JP. Coke formation on bimetallic platinum/rhenium and platinum/iridium catalysts. *Applied Catalysis* 1985;16(2):169–77. [https://doi.org/10.1016/S0166-9834\(00\)84470-X](https://doi.org/10.1016/S0166-9834(00)84470-X).
- [110] Weisz PB. Polyfunctional Heterogeneous Catalysis. In: Elsevier; 1962, p. 137–190.
- [111] Batalha N, Pinard L, Bouchy C, Guillon E, Guisnet M. n-Hexadecane hydroisomerization over Pt-HBEA catalysts. Quantification and effect of the intimacy between metal and protonic sites. *Journal of Catalysis* 2013;307:122–31. <https://doi.org/10.1016/j.jcat.2013.07.014>.
- [112] Zečević J, Vanbutsele G, Jong KP de, Martens JA. Nanoscale intimacy in bifunctional catalysts for selective conversion of hydrocarbons. *Nature* 2015;528(7581):245–8. <https://doi.org/10.1038/nature16173>.
- [113] Francis J, Guillon E, Bats N, Pichon C, Corma A, Simon LJ. Design of improved hydrocracking catalysts by increasing the proximity between acid and metallic sites. *Applied Catalysis A: General* 2011;409-410:140–7. <https://doi.org/10.1016/j.apcata.2011.09.040>.
- [114] Zhang A, Nakamura I, Aimoto K, Fujimoto K. Isomerization of n-Pentane and Other Light Hydrocarbons on Hybrid Catalyst. Effect of Hydrogen Spillover. *Ind. Eng. Chem. Res.* 1995;34(4):1074–80. <https://doi.org/10.1021/ie00043a008>.

## References

---

- [115] Sato K, Iwata Y, Miki Y, Shimada H. Hydrocracking of Tetralin over NiW/USY Zeolite Catalysts: For the Improvement of Heavy-Oil Upgrading Catalysts. *Journal of Catalysis* 1999;186(1):45–56. <https://doi.org/10.1006/jcat.1999.2546>.
- [116] Lugstein A, Jentys A, Vinek H. Hydroconversion of n-heptane over bifunctional HZSM5 zeolites influence of the metal concentration and distribution on the activity and selectivity. *Applied Catalysis A: General* 1998;166(1):29–38. [https://doi.org/10.1016/S0926-860X\(97\)00236-6](https://doi.org/10.1016/S0926-860X(97)00236-6).
- [117] Weitkamp J, Ernst S. Factors Influencing the Selectivity of Hydrocracking in Zeolites. In: Barthomeuf D, Derouane EG, Hölderich W, editors. *Guidelines for Mastering the Properties of Molecular Sieves*. Boston, MA: Springer US; 1991, p. 343–354.
- [118] Cheng K, van der Wal LI, Yoshida H, Oenema J, Harmel J, Zhang Z et al. Impact of the Spatial Organization of Bifunctional Metal-Zeolite Catalysts on the Hydroisomerization of Light Alkanes. *Angew Chem Int Ed Engl* 2020;59(9):3592–600. <https://doi.org/10.1002/anie.201915080>.
- [119] Vogelaar BM, Eijsbouts S, Bergwerff JA, Heiszwolf JJ. Hydroprocessing catalyst deactivation in commercial practice. *Catalysis Today* 2010;154(3-4):256–63. <https://doi.org/10.1016/j.cattod.2010.03.039>.
- [120] Forzatti P. Catalyst deactivation. *Catalysis Today* 1999;52(2-3):165–81. [https://doi.org/10.1016/S0920-5861\(99\)00074-7](https://doi.org/10.1016/S0920-5861(99)00074-7).
- [121] Gualda G, Toulhoat H. Etude de la desactivation des catalyseurs d'hydrotraitement par cokage. *Synthèse bibliographique. Rev. Inst. Fr. Pét.* 1988;43(4):567–94. <https://doi.org/10.2516/ogst:1988036>.
- [122] Bartholomew CH. Mechanisms of catalyst deactivation. *Applied Catalysis A: General* 2001;212(1-2):17–60. [https://doi.org/10.1016/S0926-860X\(00\)00843-7](https://doi.org/10.1016/S0926-860X(00)00843-7).

## References

---

- [123] Moulijn J, van Diepen A, Kapteijn F. Catalyst deactivation: is it predictable? *Applied Catalysis A: General* 2001;212(1-2):3–16. [https://doi.org/10.1016/S0926-860X\(00\)00842-5](https://doi.org/10.1016/S0926-860X(00)00842-5).
- [124] Haber J, Block JH, Delmon B. Manual of methods and procedures for catalyst characterization (Technical Report). *Pure and Applied Chemistry* 1995;67(8-9):1257–306. <https://doi.org/10.1351/pac199567081257>.
- [125] Scherzer J, Gruia AJ. *Hydrocracking science and technology*. New York: Marcel Dekker; 1996.
- [126] J.A. Moulijn, A.E. van Diepen, F. Kapteijn. Catalyst deactivation: is it predictable? What to do? *Applied Catalysis A: General* 2001(212):3–16.
- [127] Dufresne P, Quesada A, Mignard S. Influence of Nitrogen Feed Content On The Performances of A Zeolite Hydrocracking Catalyst. In: *Catalysts in Petroleum Refining 1989, Proceedings of the Conference on Catalysts in Petroleum Refining*. Elsevier; 1989, p. 301–315.
- [128] Park YC, Rhee H-K. The role of nickel in pyridine hydrodenitrogenation over NiMo/Al<sub>2</sub>O<sub>3</sub>. *Korean J. Chem. Eng.* 1998;15(4):411–6. <https://doi.org/10.1007/BF02697131>.
- [129] Breyse M, Furimsky E, Kasztelan S, Lacroix M, Perot G. HYDROGEN ACTIVATION BY TRANSITION METAL SULFIDES. *Catalysis Reviews* 2002;44(4):651–735. <https://doi.org/10.1081/CR-120015483>.
- [130] Furimsky E, Massoth FE. Hydrodenitrogenation of Petroleum. *Catalysis Reviews* 2005;47(3):297–489. <https://doi.org/10.1081/CR-200057492>.
- [131] Kraus H, Prins R. The Effect of Phosphorus on Oxidic NiMo(CoMo)/ $\gamma$ -Al<sub>2</sub>O<sub>3</sub> Catalysts: A Solid State NMR Investigation. *Journal of Catalysis* 1997;170(1):20–8. <https://doi.org/10.1006/jcat.1997.1728>.

## References

---

- [132] Hrabar A, Hein J, Gutiérrez OY, Lercher JA. Selective poisoning of the direct denitrogenation route in o-propylaniline HDN by DBT on Mo and NiMo/ $\gamma$ -Al<sub>2</sub>O<sub>3</sub> sulfide catalysts. *Journal of Catalysis* 2011;281(2):325–38. <https://doi.org/10.1016/j.jcat.2011.05.017>.
- [133] Ho T. Poisoning effect of ethylcarbazole on hydrodesulfurization of 4,6-diethyldibenzothiophene. *Journal of Catalysis* 2004;222(2):450–60. <https://doi.org/10.1016/j.jcat.2003.12.010>.
- [134] Chen J, Ring Z. HDS reactivities of dibenzothiophenic compounds in a LC-finer LGO and H<sub>2</sub>S/NH<sub>3</sub> inhibition effect. *Fuel* 2004;83(3):305–13. <https://doi.org/10.1016/j.fuel.2003.08.009>.
- [135] Sano Y, Choi K-H, Korai Y, Mochida I. Effects of nitrogen and refractory sulfur species removal on the deep HDS of gas oil. *Applied Catalysis B: Environmental* 2004;53(3):169–74. <https://doi.org/10.1016/j.apcatb.2004.05.014>.
- [136] Dorbon M, Bernasconi C. Nitrogen compounds in light cycle oils: identification and consequences of ageing. *Fuel* 1989;68(8):1067–74. [https://doi.org/10.1016/0016-2361\(89\)90077-X](https://doi.org/10.1016/0016-2361(89)90077-X).
- [137] Laredo G. Nitrogen compounds characterization in atmospheric gas oil and light cycle oil from a blend of Mexican crudes. *Fuel* 2002;81(10):1341–50. [https://doi.org/10.1016/S0016-2361\(02\)00047-9](https://doi.org/10.1016/S0016-2361(02)00047-9).
- [138] Furimsky E. Chemical Origin of Coke Deposited on Catalyst Surface. *Ind. Eng. Chem. Prod. Res. Dev.* 1978;17(4):329–31. <https://doi.org/10.1021/i360068a008>.
- [139] Satterfield CN, Modell M, Hites RA, Declerck CJ. Intermediate Reactions in the Catalytic Hydrodenitrogenation of Quinoline. *Ind. Eng. Chem. Proc. Des. Dev.* 1978;17(2):141–8. <https://doi.org/10.1021/i260066a006>.

- [140] Wiwel P, Hinnemann B, Hidalgo-Vivas A, Zeuthen P, Petersen BO, Duus JØ. Characterization and Identification of the most Refractory Nitrogen Compounds in Hydroprocessed Vacuum Gas Oil. *Ind. Eng. Chem. Res.* 2010;49(7):3184–93. <https://doi.org/10.1021/ie901473x>.
- [141] Adkins BD, Milburn DR, Goodman JP, Davis BH. Mechanism for coking of coal liquefaction catalysts involving basic nitrogen compounds, sodium and catalyst acid sites. *Applied Catalysis* 1988;44:199–222. [https://doi.org/10.1016/S0166-9834\(00\)80054-8](https://doi.org/10.1016/S0166-9834(00)80054-8).
- [142] Muegge B, Massoth FE. Comparison of Hydrotreating Catalyst Deactivation by Coking with Vacuum Gas Oil Vs. Anthracene. In: *Catalyst Deactivation 1991, Proceedings of the 5th International Symposium*. Elsevier; 1991, p. 297–304.
- [143] Zeuthen P, Blom P, Massoth FE. Characterization of nitrogen on aged hydroprocessing catalysts by temperature-programmed oxidation. *Applied Catalysis* 1991;78(2):265–76. [https://doi.org/10.1016/0166-9834\(91\)80111-9](https://doi.org/10.1016/0166-9834(91)80111-9).
- [144] Zeuthen P, Blom P, Muegge B, Massoth FE. Temperature-programmed sulfidation and oxidation of Ni-Mo/alumina catalysts and reaction with ammonia. *Applied Catalysis* 1991;68(1):117–30. [https://doi.org/10.1016/S0166-9834\(00\)84097-X](https://doi.org/10.1016/S0166-9834(00)84097-X).
- [145] Zeuthen P, Cooper BH, Clark FT, Arters D. Characterization and Deactivation Studies of Spent Resid Catalyst from Ebullating Bed Service. *Ind. Eng. Chem. Res.* 1995;34(3):755–62. <https://doi.org/10.1021/ie00042a007>.
- [146] Absi-Halabi M, Stanislaus A, Trimm DL. Coke formation on catalysts during the hydroprocessing of heavy oils. *Applied Catalysis* 1991;72(2):193–215. [https://doi.org/10.1016/0166-9834\(91\)85053-X](https://doi.org/10.1016/0166-9834(91)85053-X).
- [147] Kaernbach W, Kisielow W, Warzecha L, Miga K, Klecan R. Influence of petroleum nitrogen compounds on hydrodesulphurization. *Fuel* 1990;69(2):221–4. [https://doi.org/10.1016/0016-2361\(90\)90178-S](https://doi.org/10.1016/0016-2361(90)90178-S).

## References

---

- [148] Dong D, Jeong S, Massoth FE. Effect of nitrogen compounds on deactivation of hydrotreating catalysts by coke. *Catalysis Today* 1997;37(3):267–75. [https://doi.org/10.1016/S0920-5861\(97\)00022-9](https://doi.org/10.1016/S0920-5861(97)00022-9).
- [149] Celis-Cornejo CM, Pérez-Martínez DJ, Orrego-Ruiz JA, Baldovino-Medrano VG. Identification of Refractory Weakly Basic Nitrogen Compounds in a Deeply Hydrotreated Vacuum Gas Oil and Assessment of the Effect of Some Representative Species over the Performance of a Ni–MoS<sub>2</sub>/Y-Zeolite–Alumina Catalyst in Phenanthrene Hydrocracking. *Energy Fuels* 2018;32(8):8715–26. <https://doi.org/10.1021/acs.energyfuels.8b02045>.
- [150] Laredo S GC, los Reyes H J de, Luis Cano D J, Jesús Castillo M J. Inhibition effects of nitrogen compounds on the hydrodesulfurization of dibenzothiophene. *Applied Catalysis A: General* 2001;207(1-2):103–12. [https://doi.org/10.1016/S0926-860X\(00\)00620-7](https://doi.org/10.1016/S0926-860X(00)00620-7).
- [151] Kirker, Garry W, Mizrahi, Sadi Shih, Stuart S. Hydrocracking process for producing a high density jet fuel(U.S. Patent No. 5.000.839).
- [152] Voge, H. H., Good, G. M., and B. S. Greensfelder. (ed.). "Catalytic Cracking of Pure Compounds and Petroleum Fractions."; 1951.
- [153] Thakur DS, Thomas MG. Catalyst deactivation during direct coal liquefaction: a review. *Ind. Eng. Chem. Prod. Res. Dev.* 1984;23(3):349–60. <https://doi.org/10.1021/i300015a005>.
- [154] Wang W, Cai X, Hou H, Dong M, Li Z, Liu F et al. Different Mechanisms of Coke Precursor Formation in Thermal Conversion and Deep Hydroprocessing of Vacuum Residue. *Energy Fuels* 2016;30(10):8171–6. <https://doi.org/10.1021/acs.energyfuels.6b01488>.
- [155] Voorhies A. Carbon Formation in Catalytic Cracking. *Ind. Eng. Chem.* 1945;37(4):318–22. <https://doi.org/10.1021/ie50424a010>.
- [156] Trimm DL. Catalyst design for reduced coking (review). *Applied Catalysis* 1983;5(3):263–90. [https://doi.org/10.1016/0166-9834\(83\)80156-0](https://doi.org/10.1016/0166-9834(83)80156-0).

- [157] Barbier J. Deactivation of reforming catalysts by coking - a review. *Applied Catalysis* 1986;23(2):225–43. [https://doi.org/10.1016/S0166-9834\(00\)81294-4](https://doi.org/10.1016/S0166-9834(00)81294-4).
- [158] Magnoux P, Rabeharitsara A, Cerqueira HS. Influence of reaction temperature and crystallite size on HBEA zeolite deactivation by coke. *Applied Catalysis A: General* 2006;304:142–51. <https://doi.org/10.1016/j.apcata.2006.02.040>.
- [159] C.A. Querini, N.S. Figoli and J.M. Parera. Hydrocarbons reforming on Pt-Re-/Al<sub>2</sub>O<sub>3</sub>-Cl coked in a commercial reactor. *Applied Catalysis* 1989, 1989:249–62.
- [160] Augustine S. The effect of Re, S, and Cl on the deactivation of Pt/ $\gamma$ -Al<sub>2</sub>O<sub>3</sub> reforming catalysts. *Journal of Catalysis* 1989;115(1):217–32. [https://doi.org/10.1016/0021-9517\(89\)90020-1](https://doi.org/10.1016/0021-9517(89)90020-1).
- [161] Argyle M, Bartholomew C. Heterogeneous Catalyst Deactivation and Regeneration: A Review. *Catalysts* 2015;5(1):145–269. <https://doi.org/10.3390/catal5010145>.
- [162] Sahoo SK, Ray SS, Singh ID. Structural characterization of coke on spent hydroprocessing catalysts used for processing of vacuum gas oils. *Applied Catalysis A: General* 2004;278(1):83–91. <https://doi.org/10.1016/j.apcata.2004.09.028>.
- [163] AMEMIYA M, Korai Y, Mochida I. Catalyst Deactivation in Distillate Hydrotreating (Part 2) Raman Analysis of Carbon Deposited on Hydrotreating Catalyst for Vacuum Gas Oil. *J. Jpn. Petrol. Inst.* 2003;46(2):99–104. <https://doi.org/10.1627/jpi.46.99>.
- [164] Koizumi N, Urabe Y, Inamura K, Itoh T, Yamada M. Investigation of carbonaceous compounds deposited on NiMo catalyst used for ultra-deep hydrodesulfurization of gas oil by means of temperature-programmed oxidation and Raman spectroscopy. *Catalysis Today* 2005;106(1-4):211–8. <https://doi.org/10.1016/j.cattod.2005.07.172>.
- [165] Eijsbouts S. On the flexibility of the active phase in hydrotreating catalysts. *Applied Catalysis A: General* 1997;158(1-2):53–92. [https://doi.org/10.1016/S0926-860X\(97\)00035-5](https://doi.org/10.1016/S0926-860X(97)00035-5).

- [166] T. M. Tri, J-P Candy, P. Gallezot, J. Massardier, M. Primet, J.C. Védrine and B. Imelik. Pt-Mo bimetallic catalysts supported on Y-zeolite I. Characterization of the catalysts. *Journal of Catalysis* 1983;79(2):396–409. [https://doi.org/10.1016/0021-9517\(83\)90333-0](https://doi.org/10.1016/0021-9517(83)90333-0).
- [167] Bergeret G, Gallezot P, Imelik B. X-ray study of the activation, reduction, and reoxidation of palladium in Y-type zeolites. *J. Phys. Chem.* 1981;85(4):411–6. <https://doi.org/10.1021/j150604a020>.
- [168] Homeyer ST, Sachtler W. Design of Metal Clusters in Nay Zeolite. In: *Zeolites: Facts, Figures, Future Part A - Proceedings of the 8th International Zeolite Conference*. Elsevier; 1989, p. 975–984.
- [169] Topsøe H, Clausen BS. Active sites and support effects in hydrodesulfurization catalysts. *Applied Catalysis* 1986;25(1-2):273–93. [https://doi.org/10.1016/S0166-9834\(00\)81246-4](https://doi.org/10.1016/S0166-9834(00)81246-4).
- [170] Candia, R., Topsøe, H., Clausen, B. (ed.); 1984.
- [171] Freeman GB, Heink J, Long NJ, Davis BH. Coal liquefaction catalysts. The growth of cobalt sulfide particles during use at 450°C. *Applied Catalysis* 1986;23(2):309–26. [https://doi.org/10.1016/S0166-9834\(00\)81301-9](https://doi.org/10.1016/S0166-9834(00)81301-9).
- [172] Makishima H, Tanaka Y, Kato Y, Kure S, Shimada H, Matsubayashi N et al. Characterization of Ni · W/A12O3-SiO2 aromatics saturation catalysts used in a one-year commercial HDS run. *Catalysis Today* 1996;29(1-4):267–71. [https://doi.org/10.1016/0920-5861\(95\)00283-9](https://doi.org/10.1016/0920-5861(95)00283-9).
- [173] Eijsbouts S, Heinerman J, Elzerman H. MoS2 structures in high activity hydrotreating catalysts. II. Evolution of the active phase during the catalyst life cycle. Deactivation model. *Applied Catalysis A: General* 1993;105(1):69–82. [https://doi.org/10.1016/0926-860X\(93\)85134-B](https://doi.org/10.1016/0926-860X(93)85134-B).

## References

---

- [174] Guichard B, Roy-Auberger M, Devers E, Legens C, Raybaud P. Aging of Co(Ni)MoP/Al<sub>2</sub>O<sub>3</sub> catalysts in working state. *Catalysis Today* 2008;130(1):97–108. <https://doi.org/10.1016/j.cattod.2007.09.007>.
- [175] K.P. de Jong, H.P.C.E. Kuipers and J.A.R. van Veen. *Catalyst deactivation* 1991, 1991:28.
- [176] Stohl FV, Stephens HP. A comparative study of catalyst deactivation in integrated two-stage direct coal liquefaction processes. *Ind. Eng. Chem. Res.* 1987;26(12):2466–73. <https://doi.org/10.1021/ie00072a014>.
- [177] Ternan M, Furimsky E, Parsons BI. Coke formation on hydrodesulphurization catalysts. *Fuel Processing Technology* 1979;2(1):45–55. [https://doi.org/10.1016/0378-3820\(79\)90030-4](https://doi.org/10.1016/0378-3820(79)90030-4).
- [178] Richardson SM, Nagaishi H, Gray MR. Initial Coke Deposition on a NiMo/γ-Al<sub>2</sub>O<sub>3</sub> Bitumen Hydroprocessing Catalyst. *Ind. Eng. Chem. Res.* 1996;35(11):3940–50. <https://doi.org/10.1021/ie950761o>.
- [179] Gualda G, Kasztelan S. Initial Deactivation of Residue Hydrodemetallization Catalysts. *Journal of Catalysis* 1996;161(1):319–37. <https://doi.org/10.1006/jcat.1996.0190>.
- [180] Wiwel, P., Zeuthen, P., Jacobsen, A.C., Bartholomew, C.H., Butt, J.B. *Catalyst deactivation* 1991, 1991:257–66.
- [181] Hydrocarbon Publishing Company. *Worldwide Refinery Processing Review* 2017(2Q).
- [182] Argyle M, Bartholomew C. Heterogeneous Catalyst Deactivation and Regeneration: A Review. *Catalysts* 2015;5(1):145–269. <https://doi.org/10.3390/catal5010145>.
- [183] Y. Tanaka, H. Shimadab, N. Matsubayashib, A. Nishijima, M. Nomura. Accelerated deactivation of hydrotreating catalysts: comparison to long-term deactivation in a commercial plant. *Catalysis Today* 1998(45):319–25.

## References

---

- [184] Juraidan M, Al-Shamali M, Qabazard H, Kam EKT. A Refined Hydroprocessing Multicatalyst Deactivation and Reactor Performance Model Pilot-Plant Accelerated Test Applications. *Energy Fuels* 2006;20(4):1354–64. <https://doi.org/10.1021/ef0504265>.
- [185] Delmon B. Characterization of catalyst deactivation: Industrial and laboratory time scales. *Applied Catalysis* 1985;15(1):1–16. [https://doi.org/10.1016/S0166-9834\(00\)81482-7](https://doi.org/10.1016/S0166-9834(00)81482-7).
- [186] Bernard Delmon. Characterization of catalyst deactivation: Industrial and laboratory time scales. *Applied Catalysis* 1985(15):1–16.
- [187] Al Bazzaz H, Kang J-L, Chehadeh D, Bahzad D, Wong DS-H, Jang S-S. Robust Predictions of Catalyst Deactivation of Atmospheric Residual Desulfurization. *Energy Fuels* 2015;29(11):7089–100. <https://doi.org/10.1021/acs.energyfuels.5b01841>.
- [188] Jarullah AT, Mujtaba IM, Wood AS. Whole Crude Oil Hydrotreating from Small-Scale Laboratory Pilot Plant to Large-Scale trickle-Bed Reactor: Analysis of Operational Issues through Modeling. *Energy Fuels* 2012;26(1):629–41. <https://doi.org/10.1021/ef201406r>.
- [189] Rodríguez E, Félix G, Ancheyta J, Trejo F. Modeling of hydrotreating catalyst deactivation for heavy oil hydrocarbons. *Fuel* 2018;225:118–33. <https://doi.org/10.1016/j.fuel.2018.02.085>.
- [190] Odile Dujardin. *Étude Des Phénomènes De Desactivation*. Paris: Université Pierre et Marie Curie; 1992.
- [191] N.S. Figoli, J.N. Beitramini, C.A. Querini and J.M. Parera. Accelerated deactivation tests in naphta reforming. *Applied Catalysis* 1986(26):39–45.
- [192] Weissman JG, Edwards JC. Characterization and aging of hydrotreating catalysts exposed to industrial processing conditions. *Applied Catalysis A: General* 1996;142(2):289–314. [https://doi.org/10.1016/0926-860X\(96\)00020-8](https://doi.org/10.1016/0926-860X(96)00020-8).

- [193] Ahmed HS, Shaban SA, Menoufy MF, El Kady FY. Effect of catalyst deactivation on vacuum residue hydrocracking. *Egyptian Journal of Petroleum* 2013;22(3):367–72. <https://doi.org/10.1016/j.ejpe.2013.10.006>.
- [194] Edward Furimsky, Franklin E. Massoth. Deactivation of hydroprocessing catalysts. *Catalysis Today* 1999;52:381–495.
- [195] Calvin H. Bartholomew. Mechanisms of catalyst deactivation. *Applied Catalysis A: General* 2001(212):17–60.
- [196] Mugge, B.D. and Massoth, F.E. Proc. 5th Int. Symp. Catalyst Deactivation (Surface Science and Catalysis): Mugge, B.D. and Massoth, F.E., 1991. In: C.H. Bartholomew and J.B. Amsterdam; 1991.
- [197] B.D. Muegge and F.E. Massoth. Basic studies of deactivation of hydrotreating catalysts with anthracene. *Fuel Processing Technology* 1991(29):19–30.
- [198] J. Bartholdy, P. Zeuthen, F.E. Massoth. Temperature-programmed oxidation studies of aged hydroprocessing catalysts. *Applied Catalysis A: General* 1995(129).
- [199] Sie ST. Advantages, Possibilities, and Limitations of Small-Scale Testing of Catalysts for Fixed-Bed Processes. In: Ward JW, Qader SA, editors. *Hydrocracking and Hydrotreating*. WASHINGTON, D. C.: AMERICAN CHEMICAL SOCIETY; 1975, p. 6–41.
- [200] Mederos FS, Ancheyta J, Chen J. Review on criteria to ensure ideal behaviors in trickle-bed reactors. *Applied Catalysis A: General* 2009;355(1-2):1–19. <https://doi.org/10.1016/j.apcata.2008.11.018>.
- [201] Servia A. Using modeling to select catalyst dilution methods for mass transfer intensification in lab gas–liquid fixed-bed reactors. *Oil Gas Sci. Technol. – Rev. IFP Energies nouvelles* 2020;75:74. <https://doi.org/10.2516/ogst/2020071>.
- [202] Ferrari AC, Robertson J. Interpretation of Raman spectra of disordered and amorphous carbon. *Phys. Rev. B* 2000;61(20):14095–107. <https://doi.org/10.1103/PhysRevB.61.14095>.

- [203] Arancon R, Saab M, Morvan A, Bonduelle-Skrzypczak A, Taleb A-L, Gay A-S et al. Combined Experimental and Theoretical Molecular Approach of the Catalytically Active Hydrotreating MoS<sub>2</sub> Phases Promoted by 3d Transition Metals. *J. Phys. Chem. C* 2019;123(40):24659–69. <https://doi.org/10.1021/acs.jpcc.9b08437>.
- [204] D. Ferdous, A. K. Dalai<sup>1</sup> and J. Adjaye. Hydrodenitrogenation and Hydrodesulphurization of Heavy Gas Oil Using NiMo/Al<sub>2</sub>O<sub>3</sub> Catalyst Containing Phosphorus: Experimental and Kinetic Studies. *The Canadian Journal of Chemistry Engineering* 2005, October, 2005:855–64.
- [205] Michael J. Girgis/Bruce C. Gates. Reactivities, reaction networks, and kinetics in high-pressure catalytic hydroprocessing.
- [206] Kanda W, Siu I, Adjaye J, Nelson AE, Gray MR. Inhibition and Deactivation of Hydrodenitrogenation (HDN) Catalysts by Narrow-Boiling Fractions of Athabasca Coker Gas Oil. *Energy Fuels* 2004;18(2):539–46. <https://doi.org/10.1021/ef034063p>.
- [207] Bandyopadhyay R, Upadhyayula S. Thermodynamic analysis of diesel hydrotreating reactions. *Fuel* 2018;214:314–21. <https://doi.org/10.1016/j.fuel.2017.10.015>.
- [208] Ho TC. Hydrodenitrogenation property–reactivity correlation. *Applied Catalysis A: General* 2010;378(1):52–8. <https://doi.org/10.1016/j.apcata.2010.01.045>.
- [209] P. Dufresne, P.H. Bigeard, A. Billon. New Developments In Hydrocracking:Low Pressure High-Conversion Hydrocracking,. *Catalysis Today* 1987(1):367-364.
- [210] B. C. Gates, Henrik Topsoe. Reactivities in deep catalytic hydrodesulfurization: challenges, opportunities, and the importance of 4-methyldibenzothiophene and 4,6-dimethyldibenzothiophene. *Polyhedron* 1997;16(18):3213–3217.
- [211] Logadóttir Á, Moses PG, Hinnemann B, Topsøe N-Y, Knudsen KG, Topsøe H et al. A density functional study of inhibition of the HDS hydrogenation pathway by pyridine,

- benzene, and H<sub>2</sub>S on MoS<sub>2</sub>-based catalysts. *Catalysis Today* 2006;111(1-2):44–51.  
<https://doi.org/10.1016/j.cattod.2005.10.018>.
- [212] MAITY S, Ancheyta J, ALONSO F, VAZQUEZ J. Study of accelerated deactivation of hydrotreating catalysts by vanadium impregnation method. *Catalysis Today* 2008;130(2-4):405–10. <https://doi.org/10.1016/j.cattod.2007.10.009>.
- [213] Sámano V, Rana MS, Ancheyta J. An easy approach based on textural properties to evaluate catalyst deactivation during heavy oil hydrotreating. *Catalysis Communications* 2020;133:105823. <https://doi.org/10.1016/j.catcom.2019.105823>.
- [214] M.A. Callejas, M.T. Martínez, T. Blasco, E. Sastre. Coke characterisation in aged residue hydrotreating catalysts by solid-state <sup>13</sup>C-NMR spectroscopy and temperature-programmed oxidation. *Applied Catalysis A: General* 2001(218):181–8.
- [215] C.L. Li, O. Novaro, E. Muñoz, J.L. Boldú, X. Bokhimi, J.A. Wang, T. López, R. Gómez. Coke deactivation of Pd/H-mordenite catalysts used for C<sub>5</sub>/C<sub>6</sub> hydroisomerization. *Applied Catalysis A: General* 2000(199):211–20.
- [216] Anderson JR, Boudart M (eds.). *Catalysis: Science and technology*. Berlin, New York: Springer-Verlag; 1996.
- [217] Pirngruber GD, Maury S, Daudin A, Alspektor PY, Bouchy C, Guillon E. Balance between (De)hydrogenation and Acid Sites: Comparison between Sulfide-Based and Pt-Based Bifunctional Hydrocracking Catalysts. *Ind. Eng. Chem. Res.* 2020;59(28):12686–95. <https://doi.org/10.1021/acs.iecr.0c01680>.
- [218] Scherzer J, Gruia AJ. *Hydrocracking science and technology*. New York: Marcel Dekker; 1996.
- [219] C.H. Bartholomew. Mechanisms of catalyst deactivation. *Applied Catalysis A: General* 2001, 2001:17–60.

- [220] Furimsky E (ed.). *Catalysts for upgrading heavy petroleum feeds*. Amsterdam: Elsevier; 2007.
- [221] Speight JG. *The chemistry and technology of petroleum*. 3rd ed. New York: Marcel Dekker; 1999.
- [222] Muegge BD, Massoth FE. Basic studies of deactivation of hydrotreating catalysts with anthracene. *Fuel Processing Technology* 1991;29(1-2):19–30. [https://doi.org/10.1016/0378-3820\(91\)90014-4](https://doi.org/10.1016/0378-3820(91)90014-4).
- [223] Guillemant J, Albrieux F, Oliveira LP de, Lacoue-Nègre M, Duponchel L, Joly J-F. Insights from Nitrogen Compounds in Gas Oils Highlighted by High-Resolution Fourier Transform Mass Spectrometry. *Anal Chem* 2019;91(20):12644–52. <https://doi.org/10.1021/acs.analchem.9b01702>.
- [224] Castañeda LC, Muñoz J, Ancheyta J. Comparison of approaches to determine hydrogen consumption during catalytic hydrotreating of oil fractions. *Fuel* 2011;90(12):3593–601. <https://doi.org/10.1016/j.fuel.2010.11.047>.
- [225] Le Maître J, Paupy B, Hubert-Roux M, Marceau S, Rüger C, Afonso C et al. Structural Analysis of Neutral Nitrogen Compounds Refractory to the Hydrodenitrogenation Process of Heavy Oil Fractions by High-Resolution Tandem Mass Spectrometry and Ion Mobility–Mass Spectrometry. *Energy Fuels* 2020;34(8):9328–38. <https://doi.org/10.1021/acs.energyfuels.0c01160>.
- [226] Nguyen M-T, Pirngruber GD, Chainet F, Albrieux F, Tayakout-Fayolle M, Geantet C. Molecular-Level Insights into Coker/Straight-Run Gas Oil Hydrodenitrogenation by Fourier Transform Ion Cyclotron Resonance Mass Spectrometry. *Energy Fuels* 2019;33(4):3034–46. <https://doi.org/10.1021/acs.energyfuels.8b04432>.

- [227] Shin S, Sakanishi K, Mochida I, Grudoski DA, Shinn JH. Identification and Reactivity of Nitrogen Molecular Species in Gas Oils. *Energy Fuels* 2000;14(3):539–44. <https://doi.org/10.1021/ef990136m>.
- [228] Absi-Halabi M SA. Coke formation on Ctz during hydroprocessing. *Applied Catalysis* 1991;72:193–215.
- [229] Hauser A, Stanislaus A, Marafi A, Al-Adwani A. Initial coke deposition on hydrotreating catalysts. Part II. Structure elucidation of initial coke on hydrodematallation catalysts. *Fuel* 2005;84(2-3):259–69. <https://doi.org/10.1016/j.fuel.2004.08.010>.
- [230] Myers, T.E., Lee, F.S., Myers, B.L., Fleisch, T.H., Zajac, G.W. Resid catalyst deactivation in expanded-bed service. *AIChE Symposium Series* 1989, 1989:21–31.
- [231] Khalil I, Celis-Cornejo CM, Thomas K, Bazin P, Travert A, Pérez-Martínez DJ et al. In Situ IR-ATR Study of the Interaction of Nitrogen Heteroaromatic Compounds with HY Zeolites: Experimental and Theoretical Approaches. *ChemCatChem* 2020;12(4):1095–108. <https://doi.org/10.1002/cctc.201901560>.
- [232] Mendes PSF, Silva JM, Ribeiro MF, Daudin A, Bouchy C. Bridging the gap between academic and industrial hydrocracking: On catalyst and operating conditions' effects. *Catal. Sci. Technol.* 2020;10(15):5136–48. <https://doi.org/10.1039/D0CY00568A>.
- [233] Mendes PS, Silva JM, Ribeiro MF, Bouchy C, Daudin A. Quantification of the available acid sites in the hydrocracking of nitrogen-containing feedstocks over USY shaped NiMo-catalysts. *Journal of Industrial and Engineering Chemistry* 2019;71:167–76. <https://doi.org/10.1016/j.jiec.2018.11.019>.
- [234] C.A. Querini N.S. Figoli, J.M. Parera. Hydrocarbons reforming on Pt-Re-S/Al<sub>2</sub>O<sub>3</sub>-Cl coked in a commercial reactor. *Applied Catalysis* 1989(52).

## References

---

- [235] Coonradt HL, Garwood WE. Mechanism of Hydrocracking. Reactions of Paraffins and Olefins. Ind. Eng. Chem. Proc. Des. Dev. 1964;3(1):38–45. <https://doi.org/10.1021/i260009a010>.
- [236] IEEE Global Telecommunications Conference and Exhibition. Communications for the Information Age. IEEE; 1988.

**APPENDICES**

**APPENDIX 1** ..... 219

**APPENDIX 2** ..... 219

**APPENDIX 3** ..... 220

**APPENDIX 4** ..... 222

**APPENDIX 5** ..... 224

**APPENDIX 6** ..... 226

**APPENDIX 7** ..... 226

**APPENDIX 8** ..... 227

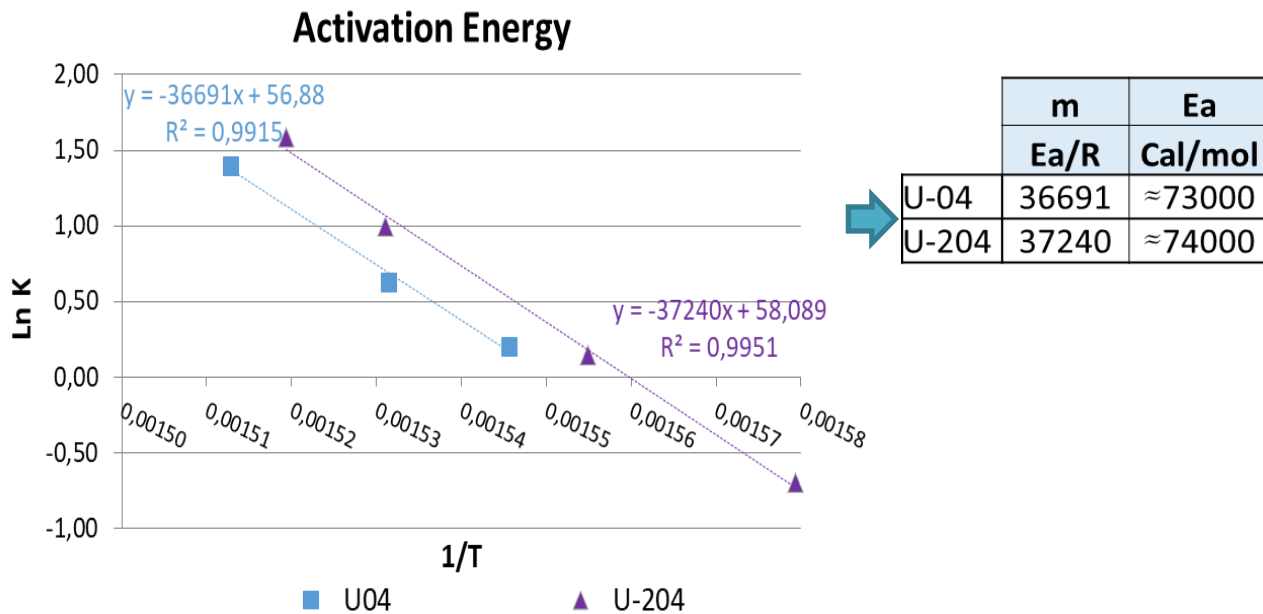
**APPENDIX 9** ..... 228

**APPENDIX 10** ..... 232

**Appendix 1.** Mass balances for pilot plant validation.

Test	P	T reaction	Feed Flow	H <sub>2</sub> Flow	H <sub>2</sub> Flow (Stripping)	H <sub>2</sub> mass inlet	Mass liquid product	Mass total gas	Mass balance	Error	
#	bar	°C	g/h	SL/h	SL/h	g	g	g	g	%	
1	140	374	32,8	45	5,00	36	228	65	5	1,84	valid
2	140	374	32,9	45	5,00	45	287	80	7	1,82	valid
3	140	380	32,7	45	5,00	45	279	91	2	0,55	valid
4	140	388	32,7	46	5,00	46	263	116	-7	-1,77	valid

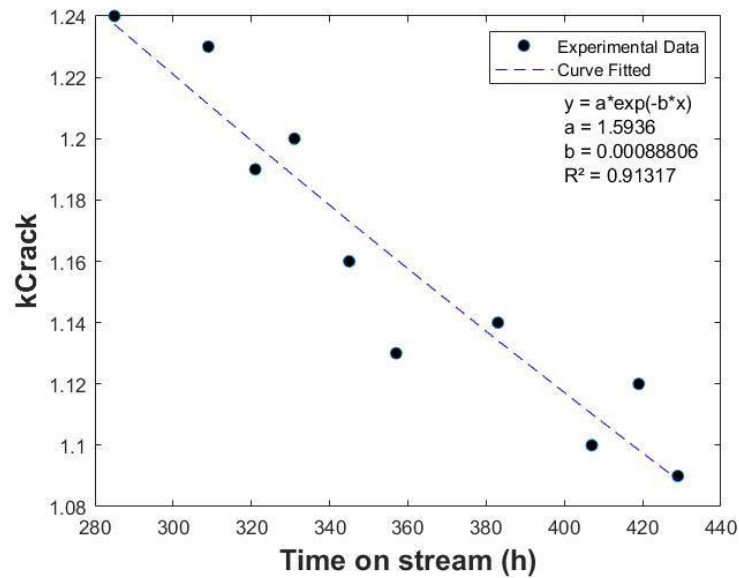
**Appendix 2.** Activation energy based on experimental data from U-04 (Catalyst volume 50 cm<sup>3</sup>) and U-204 (Catalyst volume 200 cm<sup>3</sup>).



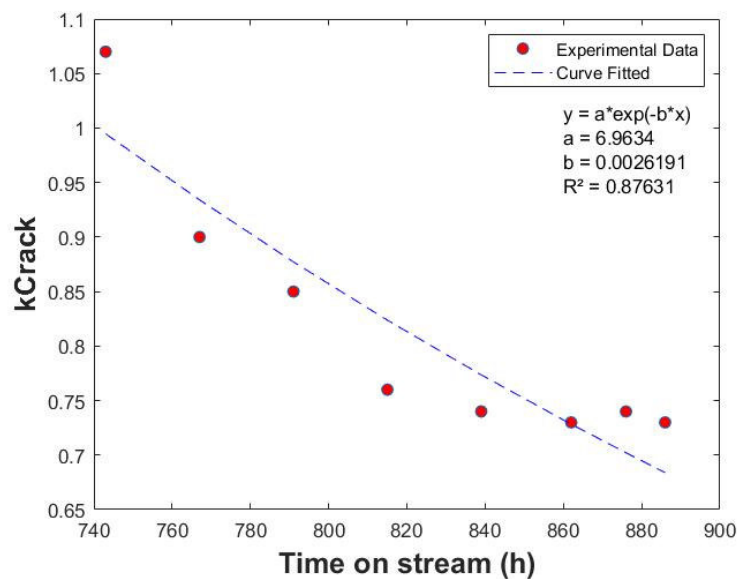
**Appendix 3.** Activity loss rate coefficients. Fitting of an exponential decay function to the experimental data of cracking constant as function of time on stream during the variables screening test.

- Exponential function:  $k_{\text{crack}} = k_{\text{crack}}^{\text{fresh}} \exp(-\alpha \cdot \text{TOS}) = y(x) = a \exp(-bx)$

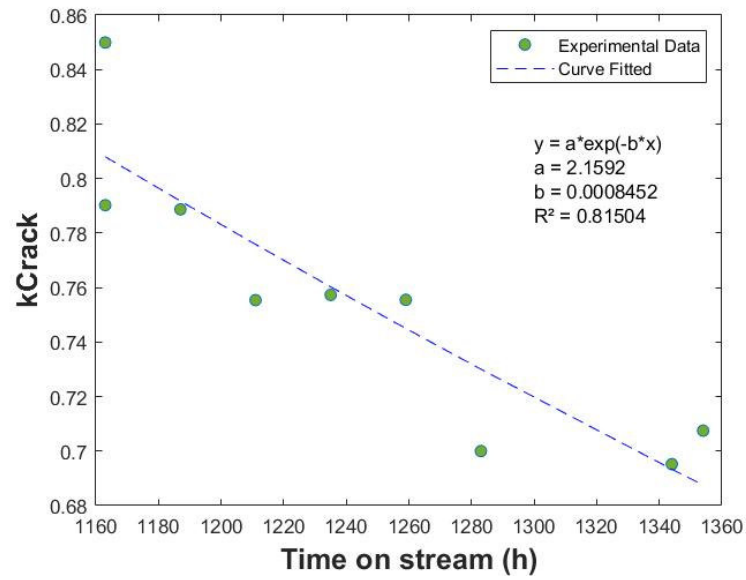
**a) Exponential fit for reference case (T=403°C, LHSV=2h<sup>-1</sup>, P=14MPa H<sub>2</sub>/HC=1500NL/L).**



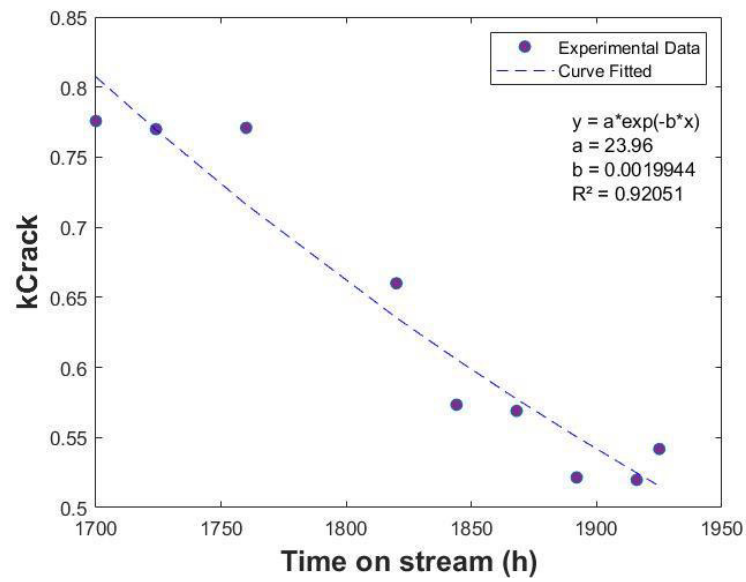
**b) Exponential fit for reference case after temperature change.**



c) Exponential fit for reference case after H<sub>2</sub>/HC change.

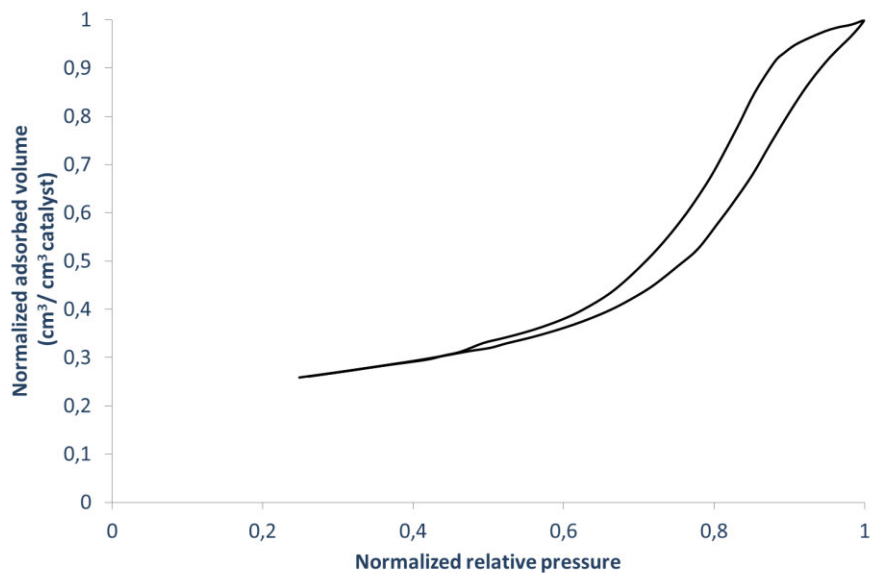


d) Exponential fit for reference case after LHSV change.

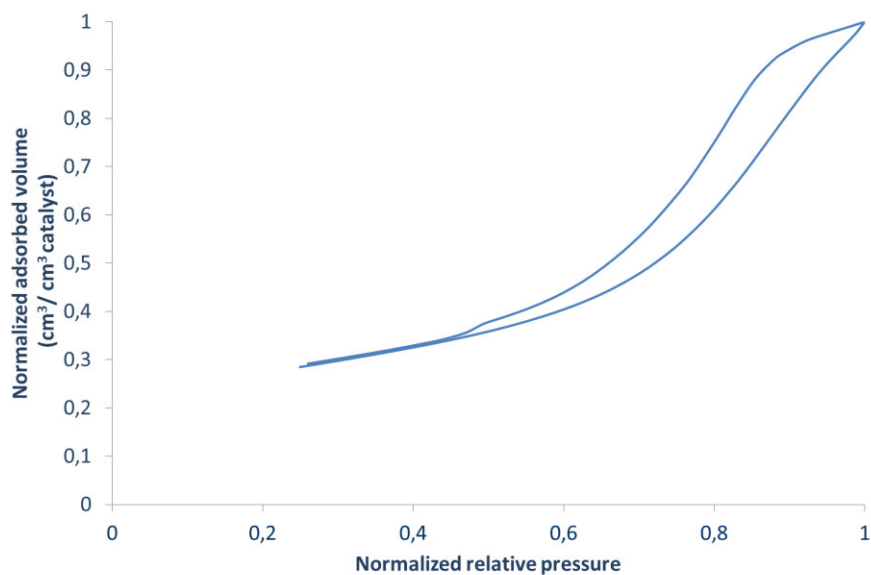


**Appendix 4.** Calculation of adsorption and desorption areas from isotherms, for ratio hysteresis area determination. Spent catalyst samples from, reference and deactivation test.

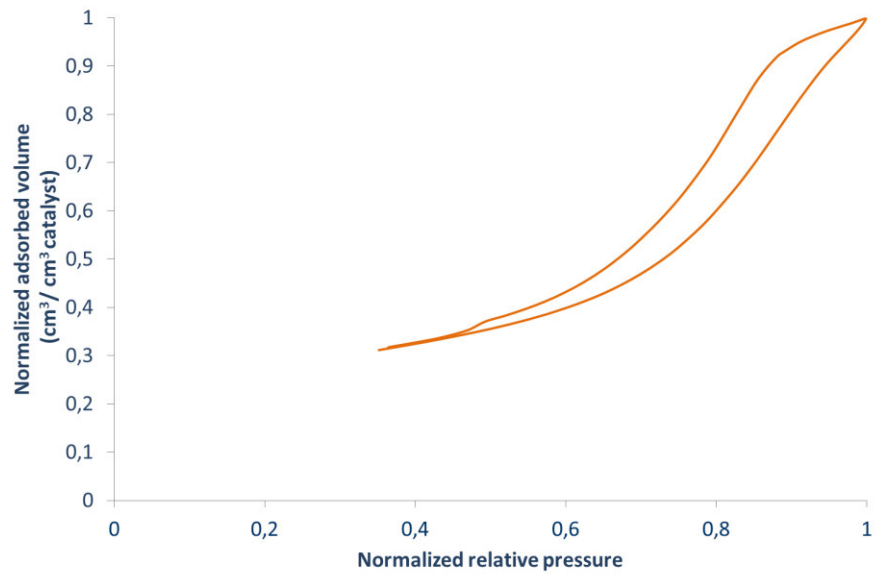
**a) Fresh catalyst.**



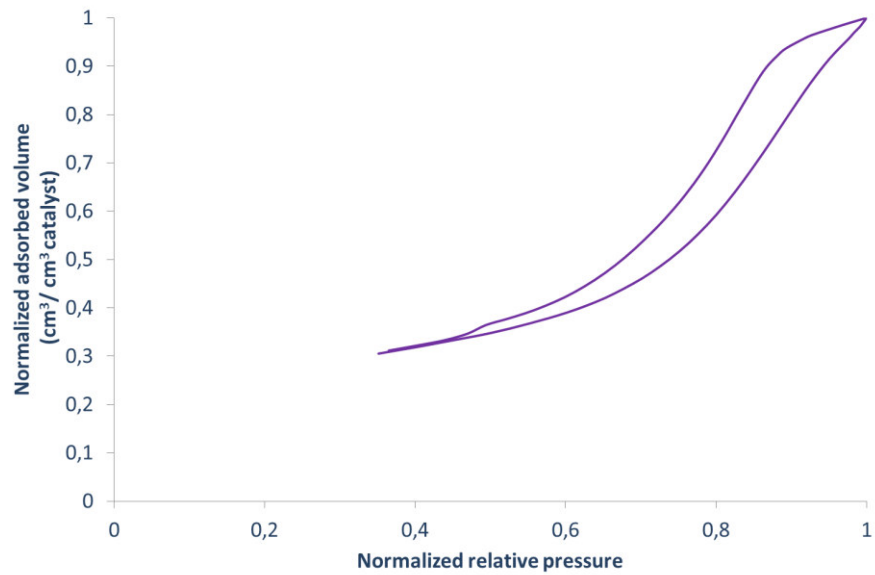
**b) Spent catalyst from reference test-Bed inlet.**



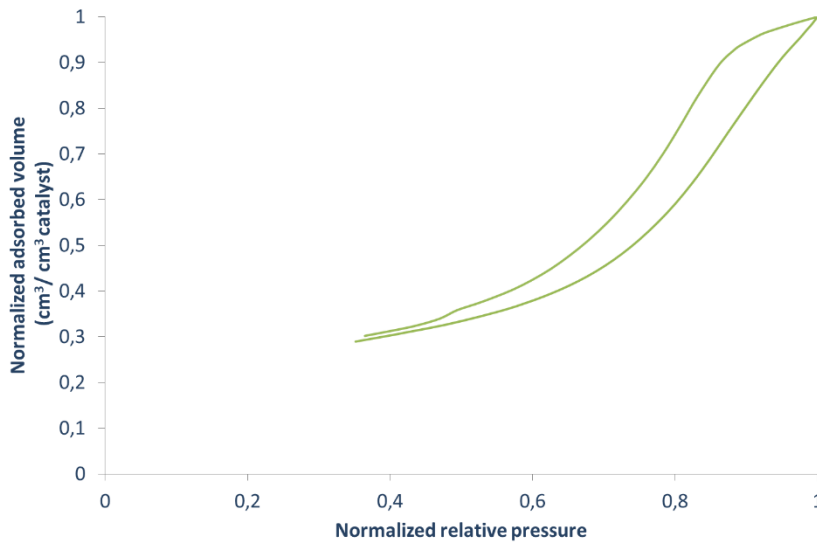
c) Spent catalyst from reference test-Bed outlet.



d) Spent catalyst from deactivation test-Bed Inlet.



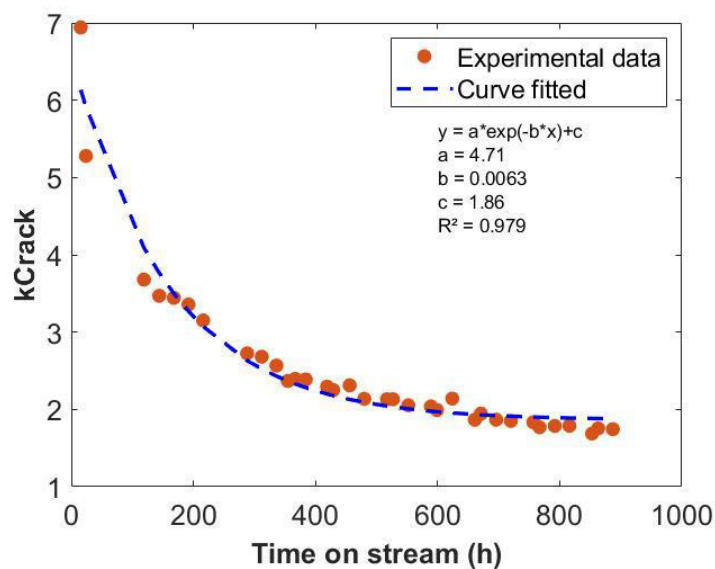
e) Spent catalyst from deactivation test-Bed Outlet.



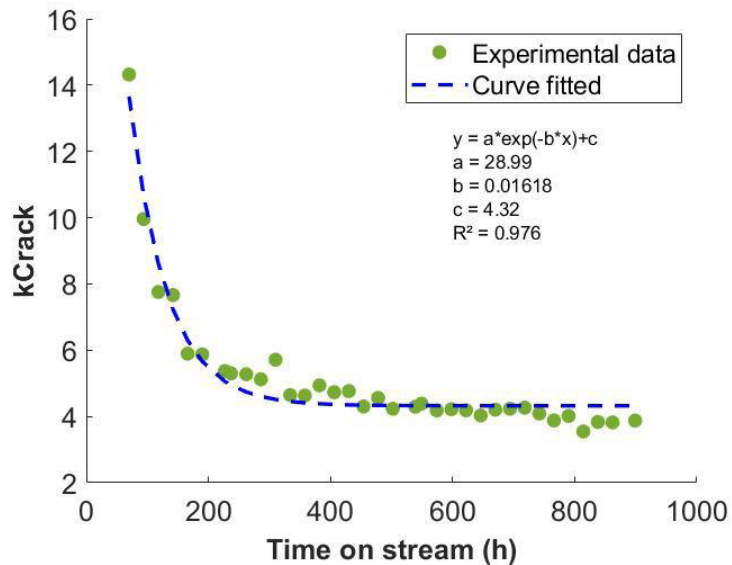
**Appendix 5.** Activity loss rate coefficients. Fitting of an exponential decay function to the experimental data of cracking constant as function of time on stream during the test with different feedstocks (Feed A and Feed B).

$k_{crack} = A \cdot \exp(-a \cdot TOS) + c$ , Where:  $(A+c)$  corresponds to the kinetic constant of the fresh catalyst,  $t=0$ , and corresponds to the residual activity of the spent catalyst.

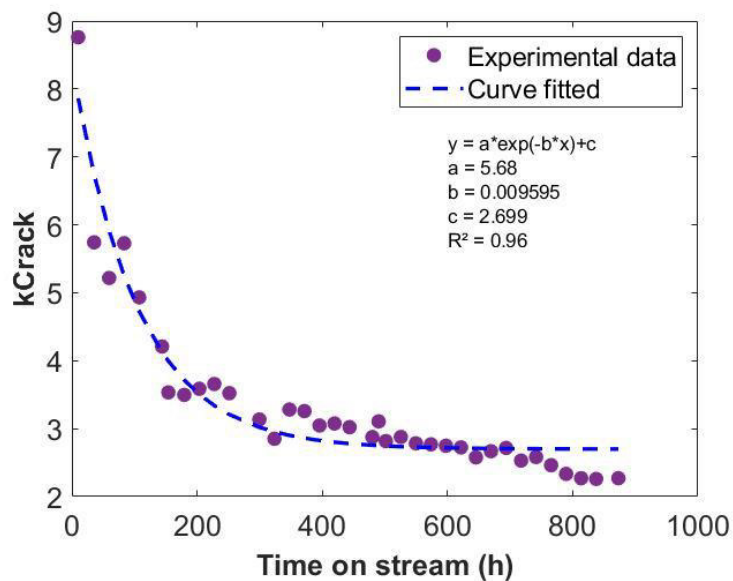
a) Exponential decay model for test with feed A during 30 days.



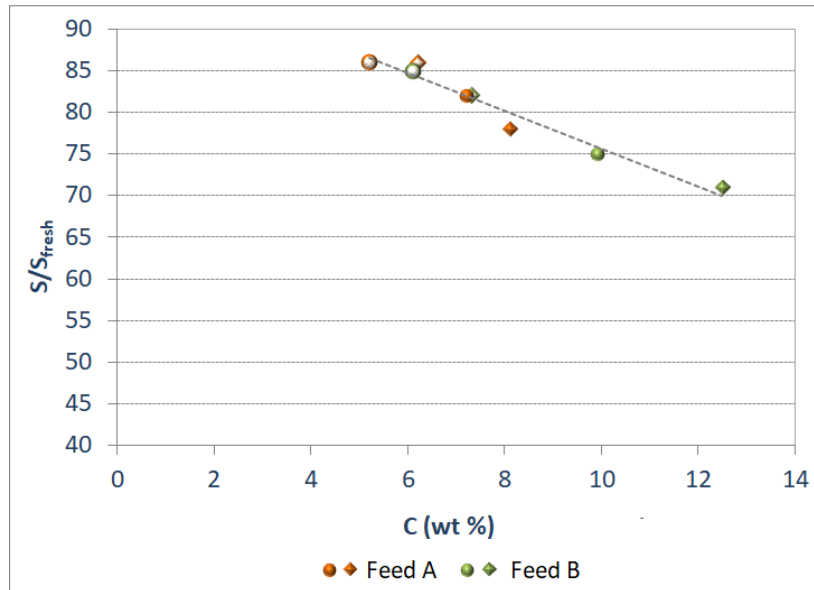
b) Exponential decay model for test with feed B during 30 days/ Reference catalyst.



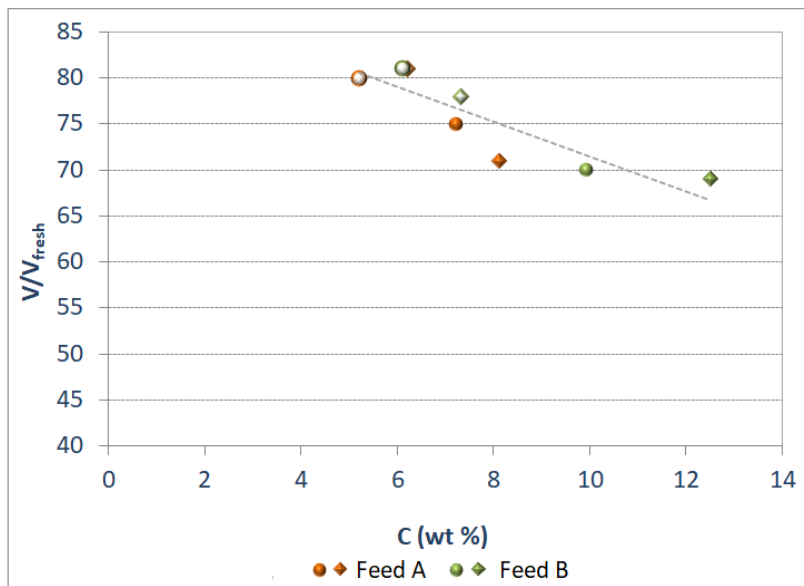
c) Exponential decay model for test with the 0.5 MoO<sub>3</sub> catalyst.



**Appendix 6.** Characterization of spent catalyst: loss of surface area (S) as function of carbon deposition. Open symbols= first reactor effluent, full symbols= second reactor effluent. Circle=6 days tests, Diamond= 30 days tests.

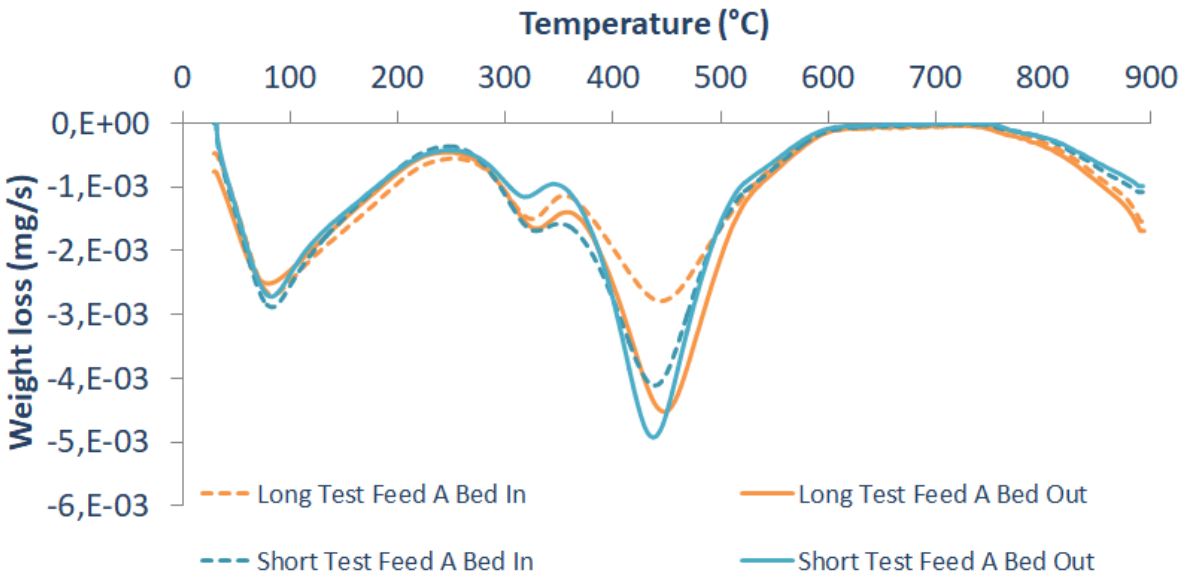


**Appendix 7.** Characterization of spent catalyst: loss of pore volume (V) as function of carbon deposition. Open symbols= first reactor effluent, full symbols= second reactor effluent. Circle=6 days tests, Diamond= 30 days tests.

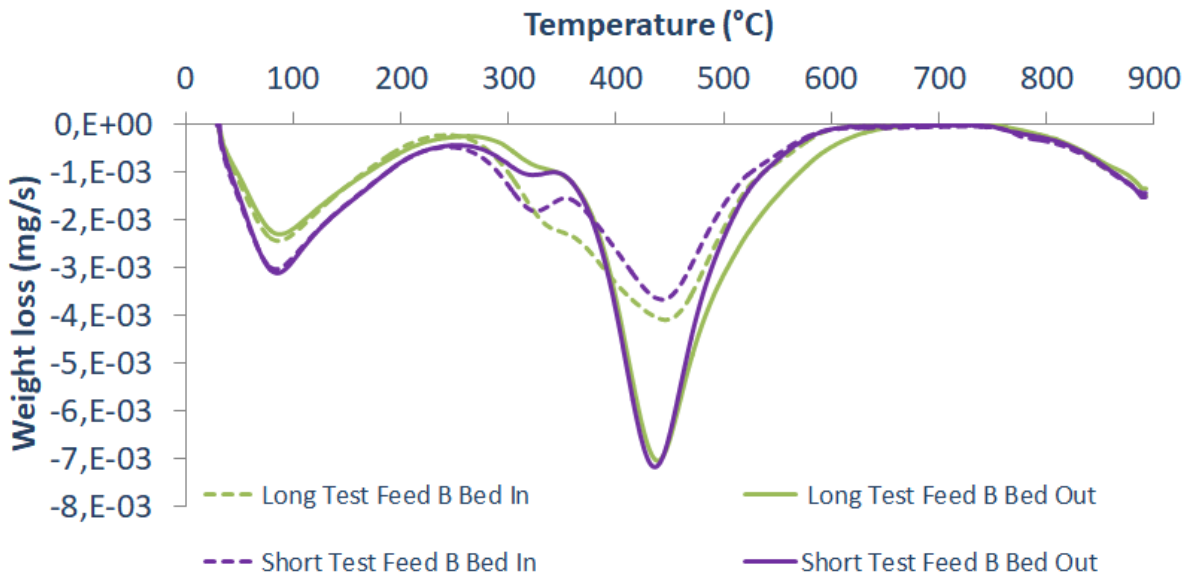


**Appendix 8.** TGA profiles of bed inlet and bed outlet samples from the deactivation test.  
 a) Long and short term tests with Feed A b) Long and short term tests with feed B.

**a) Long and short term tests with Feed A.**

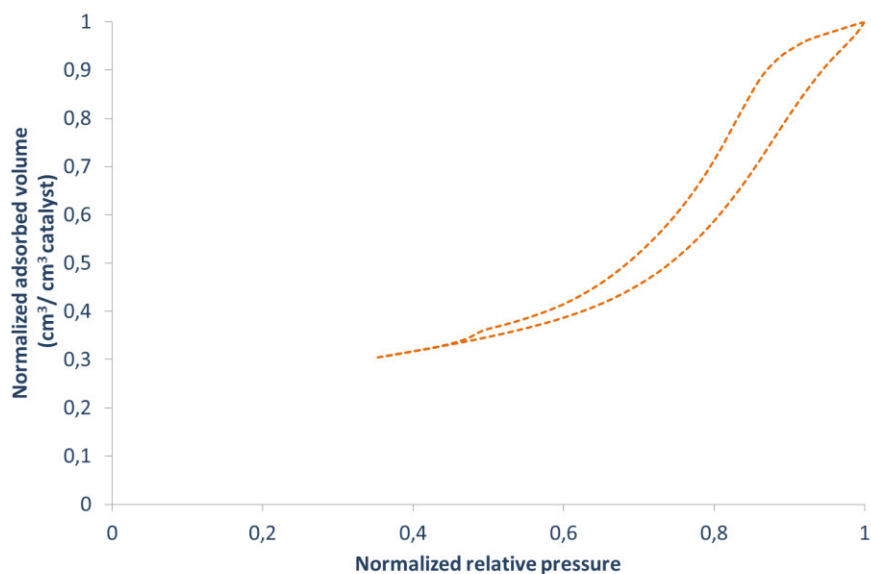


**b) Long and short term tests with feed B.**

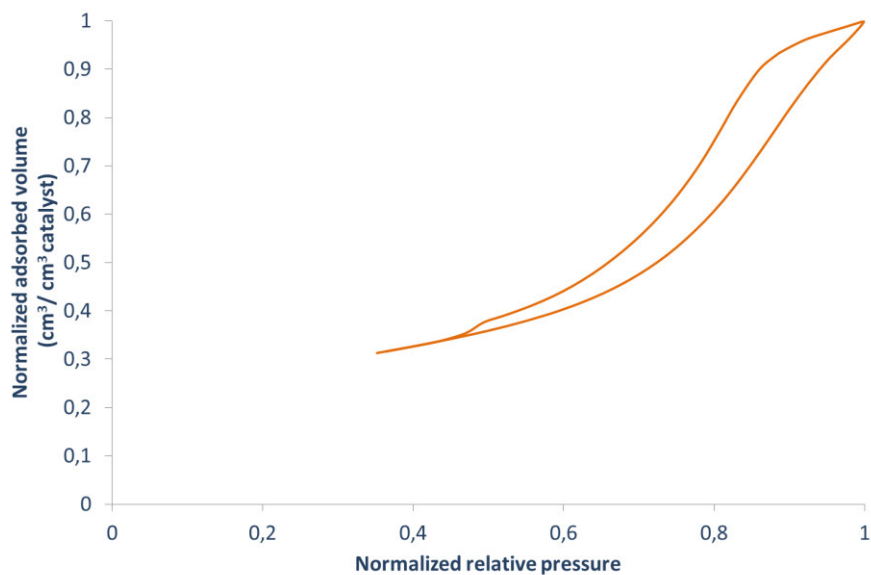


**Appendix 9.** Calculation of adsorption and desorption areas from isotherms, for ratio hysteresis area determination. Spent catalyst samples from tests with different feedstocks. (Fresh catalyst: appendix 1 a)).

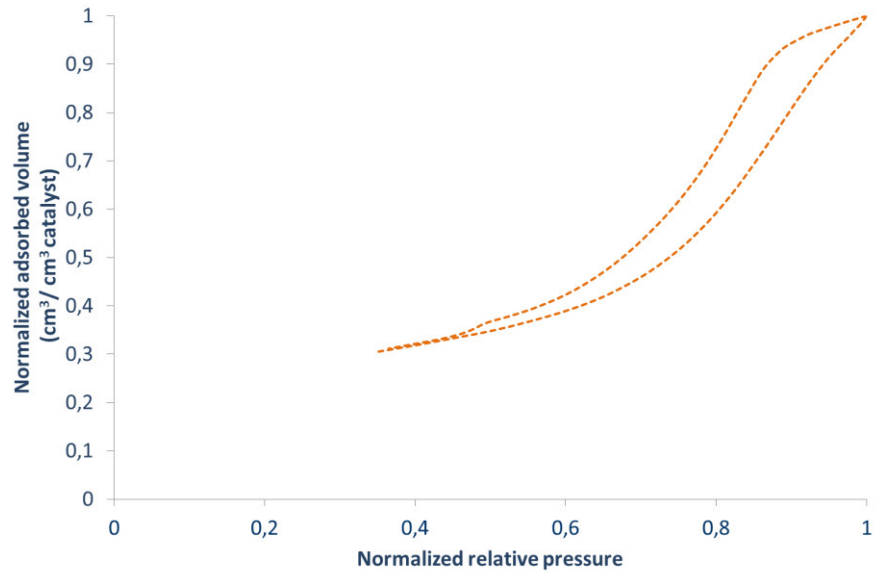
**a) Spent catalyst from short-term test (6 days) with feed A. Bed Inlet.**



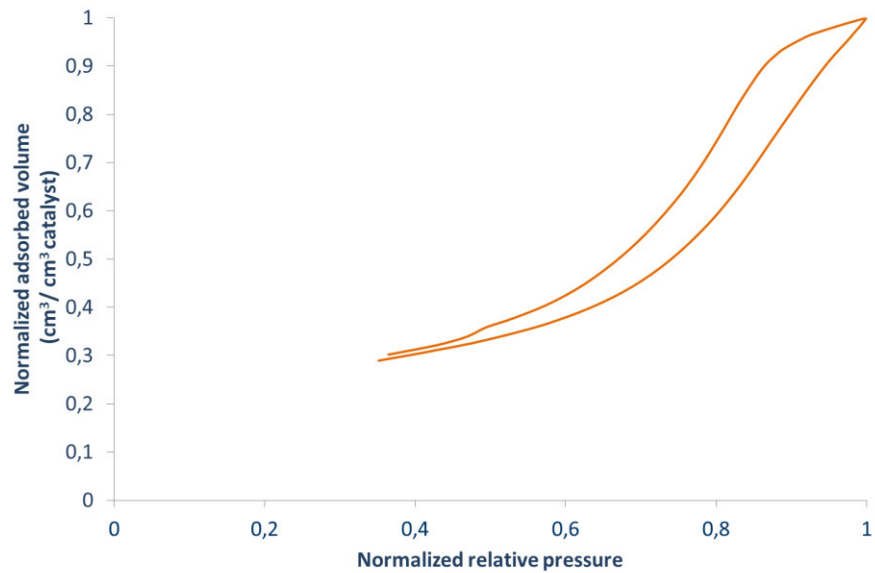
**b) Spent catalyst from short-term test (6 days) with feed A. Bed Outlet.**



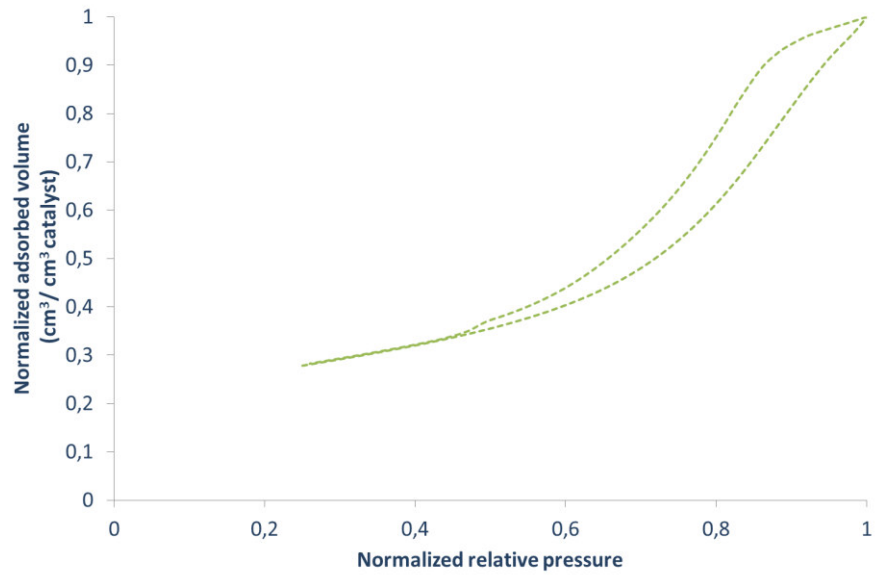
c) Spent catalyst from long-term test (30 days) with feed A. Bed Inlet.



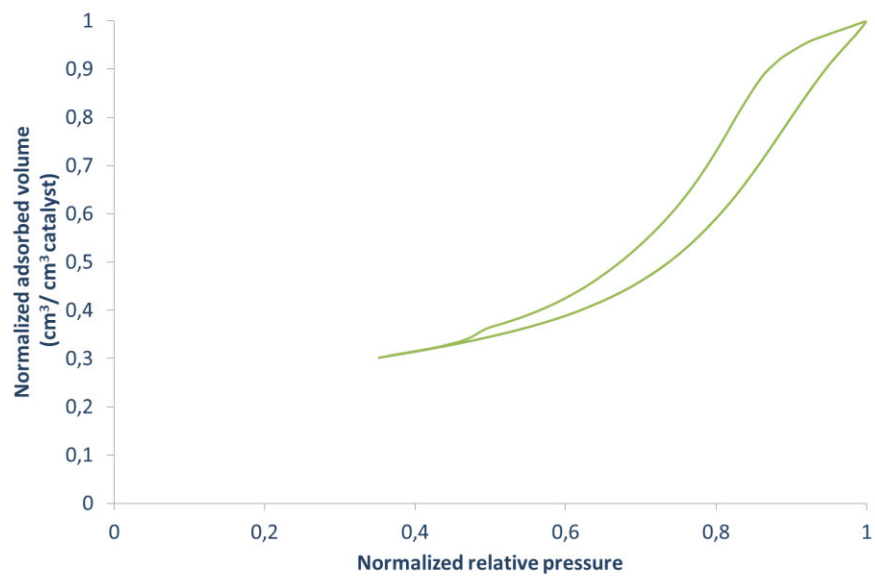
d) Spent catalyst from long-term test (30 days) with feed A. Bed Outlet.



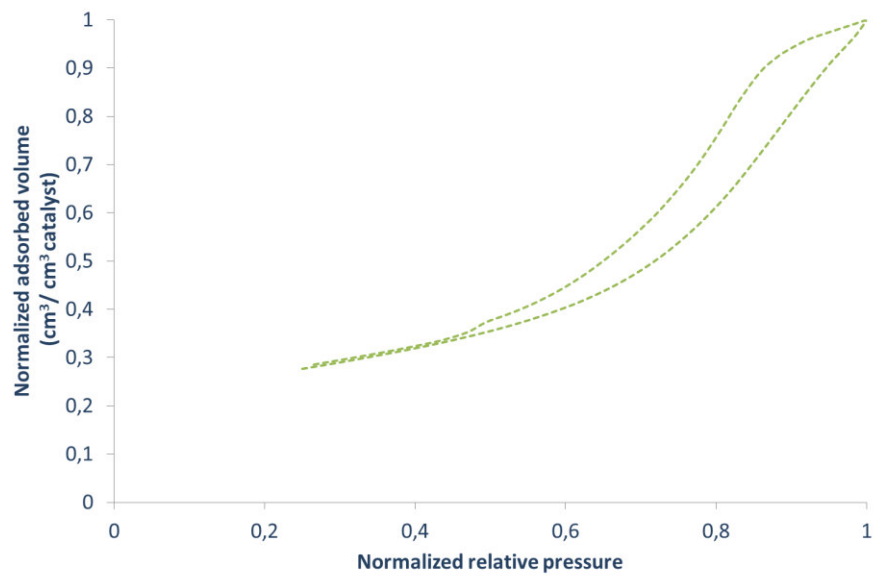
e) Spent catalyst from short-term test (6 days) with feed B. Bed Inlet.



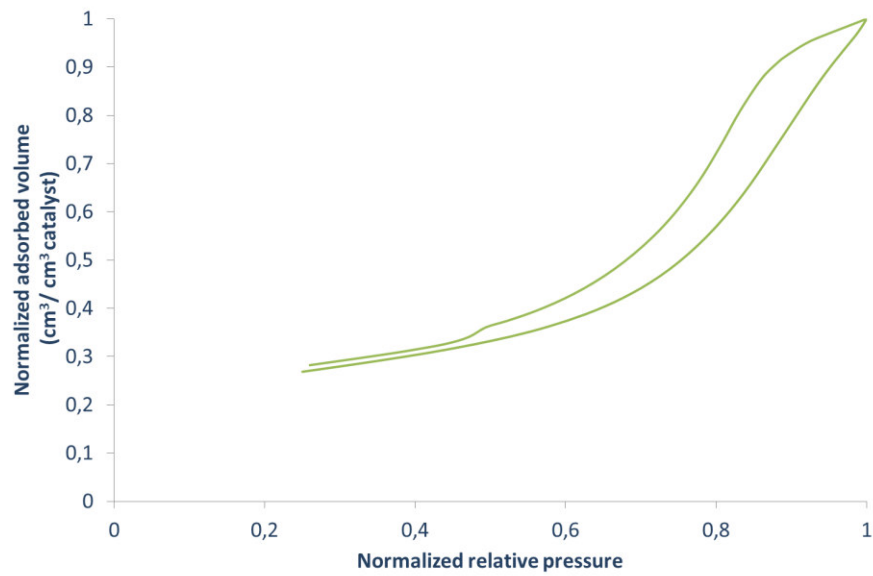
f) Spent catalyst from short-term test (6 days) with feed B. Bed Outlet.



**g) Spent catalyst from long-term test (30 days) with feed B. Bed Inlet.**



**h) Spent catalyst from long-term test (30 days) with feed B. Bed Outlet.**



**Appendix 10.** Average stacking size and dispersion measured by TEM and Ni/Mo ratio in MoS<sub>2</sub> particles measured by EDX for spent catalysts with different metal content.

	<b>Slab length (nm)</b>	<b>Dispersion</b>	<b>Ni/Mo</b>
<b>0.5 MoO<sub>3</sub> Bed In</b>	4.1±1.3	0.24	0.12±0.07
<b>0.5 MoO<sub>3</sub> Bed Out</b>	3.8±1.2	0.26	0.17±0.06
<b>Reference Catalyst</b>	4.6±1.5	0.22	0.14±0.21
<b>Reference Catalyst</b>	4.6±1.7	0.20	0.16±0.08